JOINT TRANSPORTATION
RESEARCH PROGRAM
INDIANA DEPARTMENT OF TRANSPORTATION
AND PURDUE UNIVERSITY

Updating Physical and Chemical Characteristics of Fly Ash for Use in Concrete

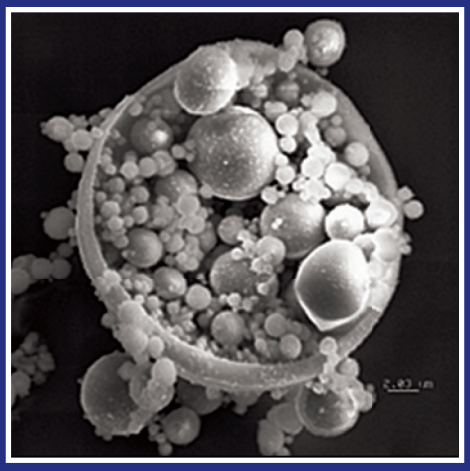
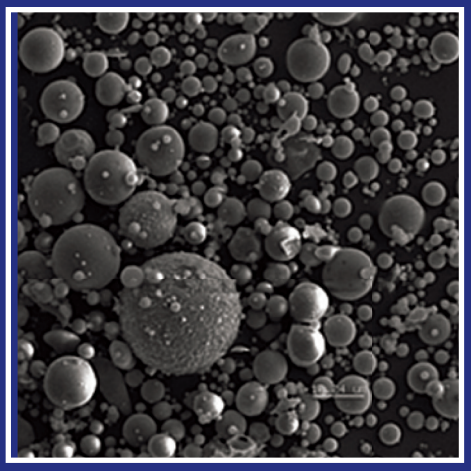
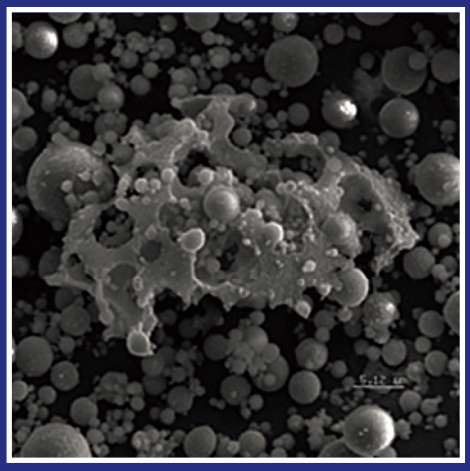

Prasanth Tanikella

Jan Olek

SPR-3020 • Report Number: FHWA/IN/JTRP-2017/11 • DOI: 10.5703/1288284315213

RECOMMENDED CITATION

Tanikella, P., & Olek, J. (2017). *Updating physical and chemical characteristics of fly ash for use in concrete* (Joint Transportation Research Program Publication No. FHWA/IN/JTRP-2017/11). West Lafayette, IN: Purdue University. https://doi.org/10.5703/1288284315213

AUTHORS

Prasanth Tanikella
Graduate Research Assistant
Lyles School of Civil Engineering
Purdue University

Jan Olek, PhD, PE
Professor of Civil Engineering
Lyles School of Civil Engineering
Purdue University
(765) 464-5015
olek@purdue.edu
Corresponding Author

JOINT TRANSPORTATION RESEARCH PROGRAM

The Joint Transportation Research Program serves as a vehicle for INDOT collaboration with higher education institutions and industry in Indiana to facilitate innovation that results in continuous improvement in the planning, design, construction, operation, management and economic efficiency of the Indiana transportation infrastructure. https://engineering.purdue.edu/JTRP/index_html

Published reports of the Joint Transportation Research Program are available at: http://docs.lib.purdue.edu/jtrp/

NOTICE

TECHNICAL REPORT STANDARD TITLE PAGE

1. Report No.	2. Government Accession No.	3. Recipient's Catalog No.
FHWA/IN/JTRP-2017/11		

4. Title and Subtitle	5. Report Date
Updating Physical and Chemical Characteristics of Fly Ash for Use in Concrete	December 2017
	6. Performing Organization Code

7. Author(s)	8. Performing Organization Report No.
Prasanth Tanikella and Jan Olek	FHWA/IN/JTRP-2017/11

9. Performing Organization Name and Address	10. Work Unit No.
Joint Transportation Research Program Purdue University 550 Stadium Mall Drive West Lafayette, IN 47907-2051	
	11. Contract or Grant No. SPR-3020

12. Sponsoring Agency Name and Address	13. Type of Report and Period Covered
Indiana Department of Transportation State Office Building 100 North Senate Avenue Indianapolis, IN 46204	Final Report
	14. Sponsoring Agency Code

15. Supplementary Notes

Prepared in cooperation with the Indiana Department of Transportation and Federal Highway Administration.

16. Abstract

When incorporated in concrete mixtures, fly ashes are known to influence both its fresh and hardened properties. An accurate and quick technique to predict the extent of this influence based on the characteristics of fly ash would be highly beneficial in terms of field applications. The current study was an attempt to quantify the effects of fly ashes on the properties of pastes as a function of: (a) the mean particle size of the fly ash particles, (b) their fineness and (c) their chemical composition. In addition, since the type and the amount of glass present in the fly ash significantly affect its reactivity, this property was also included in the investigation.

Twenty different fly ashes (both, ASTM Class C and Class F), obtained from power plants in and around Indiana, were characterized during the Phase 1 of the study. The information collected included: physical characteristics, chemical composition and the amount and type of glass present. Phase 2 of the study consisted of evaluation of various properties of binary paste systems (portland cement with 20% of cement of fly replacement). The evaluated properties included: the set time, the heat of hydration, the strength activity index, the non-evaporable water content and the amount of calcium hydroxide formed at different ages.

These results obtained from both phases of the study were used to build statistical models for prediction of previously evaluated properties for any hypothetical fly ash with similar characteristics. The models included only the most significant variables, i.e., those which were found to most strongly affect any specific property. The variables to be included in the model were selected based on the adjusted R2 values.

As a result of the modeling process, it was found that the sets of statistically significant variables affecting the properties consisted of both physical and chemical characteristics of the fly ash and that the combination of these variables was unique for each property evaluated. When applied to a set of results from two additional (not previously used) fly ashes, the models provided the following residuals of predicted properties:

(a) Initial set time – 100 minutes for Class F ashes and over 300 minutes for Class C ashes
(b) Peak heat of hydration – 0.7 W/kg
(c) Time of peak heat – 375 minutes
(d) Total heat of hydration – 96 J/kg
(e) Calcium hydroxide content at various ages – 0.25% for early ages (1 and 3 days) and 0.5% for later ages (7 and 28 days)
(f) Non-evaporable water content – 0.7% for early ages (1 and 3 days) and 5% for later ages (28 days)
(g) Strength activity index – range of 1% in Class C ashes and 1% to 2% in Class F ashes (from 7 days to 28 days)

Phase 3 of the study consisted of evaluating the same set of properties but using ternary paste systems (cement and two different fly ashes). The goal for this study was to ascertain the applicability of the weighted sum of the models chosen for the binary paste systems to predict the properties of ternary binder systems. In addition, the analysis as to which of the chosen variables has the maximum effect on the properties was performed. It was found that the properties of the ternary binder systems were not additive in nature, except for strength activity index at 28 days. Lastly, the percent influence of each of the chosen independent variables, which affect the mentioned properties, was calculated along with the unexplained variation (error percentage). The error percentages varied for each of the properties, with set time having the maximum error (almost 50%).

17. Key Words	18. Distribution Statement
fly ash, strength activity index, statistical modeling, physical and chemical characteristics, SPR-3020	No restrictions. This document is available to the public through the National Technical Information Service, Springfield, VA 22161.

19. Security Classif. (of this report)	20. Security Classif. (of this page)	21. No. of Pages	22. Price
Unclassified	Unclassified	112	

Form DOT F 1700.7 (8-69)

EXECUTIVE SUMMARY

UPDATING PHYSICAL AND CHEMICAL CHARACTERISTICS OF FLY ASH FOR USE IN CONCRETE

Introduction

When incorporated in concrete mixtures, fly ashes are known to influence both their fresh and hardened properties. An accurate and quick technique to predict the extent of this influence, and one which takes into account the physical and chemical characteristics of fly ash, would be highly beneficial in terms of field applications. The current study was an attempt to quantify the effects of fly ashes on the properties of pastes as a function of the mean particle size of the fly ash particles, their fineness, and their chemical composition. In addition, since both the type and the amount of glass present in the fly ash significantly affect its reactivity, this property was also included in the investigation.

Findings

Twenty different fly ashes (ASTM Class C and Class F) obtained from power plants in and around Indiana were characterized during Phase 1 of the study. The information collected included physical characteristics, chemical composition, and the amount and type of glass present. Phase 2 of the study consisted of the evaluation of various properties of binary paste systems (prepared by replacing 20% by weight of cement with one type of fly ash). The evaluated properties included the set time, heat of hydration, strength activity index, non-evaporable water content, and amount of calcium hydroxide formed at different ages.

The results obtained from these two phases of the study were used to build statistical models for prediction of previously evaluated properties for any hypothetical fly ash with similar characteristics. The models included only the most significant variables—that is, those which were found to most strongly affect any specific property. The variables to be included in the model were selected based on the adjusted R^2 values.

As a result of the modeling process, it was found that the sets of statistically significant variables affecting the properties consisted of both physical and chemical characteristics of the fly ash, and that the combination of these variables was unique for each property evaluated.

Phase 3 of the study consisted of evaluating the same set of properties but using ternary paste systems (cement and two different fly ashes). The goal for this study was to ascertain the applicability of the weighted sum of the models chosen for the binary paste systems to predict the properties of ternary binder systems. In addition, an analysis to determine which of the chosen variables had the maximum effect on the properties was performed. It was found that the properties of the ternary binder systems were not additive in nature, except for strength activity index at 28 days. Lastly, the percent of influence of each of the chosen independent variables that affected the mentioned properties was calculated, along with the unexplained variation (error percentage). The error percentages varied for each of the properties, with set time having the maximum error (almost 50%).

The statistical studies resulted in a conclusion that both the physical and the chemical characteristics of fly ash affect the properties of the pastes containing ashes at all the ages. The sets of variables affecting various binder properties were unique for each of the properties evaluated. However, the variable which was found to have the most significant effect on almost all properties was the specific surface area of the fly ash grains.

The Indiana Department of Transportation personnel as well as the contractors using state-approved fly ashes in their mixtures can use the models developed in this study for preliminary performance prediction purposes. In addition, a complete database of all pertinent characteristics of fly ashes from INDOT's approved sources has been prepared and is available (as a supplement to this report titled *Fly Ash Handbook* (FAH) and available for download at https://doi.org/10.5703/1288284315213) for quality control and modeling purposes.

Implementation

Based on the data on fly ash characteristics collected in this study and the results of the laboratory experiments performed, the following implementation suggestions are offered:

- The results from the paste study and fly ash database compiled in the *Fly Ash Handbook* (FAH) developed over the course of this research can be used as a source of baseline information when performing a comparative assessment of potential influences of changes in the quality of the fly ash on the properties of concrete.
- Since the report contains a detailed evaluation of how fly ash characteristics influence properties of both binary and ternary paste systems, the data contained in the FAH can be consulted and used along with the statistical models for prediction of previously evaluated properties for any hypothetical fly ash with similar characteristics.
- Requirements related to the need for conducting trial batches in cases involving change of the fly ash source set forth in section 500 of INDOT's specification should consider allowing a contractor to continue the production if the source of a new pozzolans can be verified (using data supplied in the FAH) as being similar to the old source in terms of physical and chemical characteristics.
- Consider initiation of a field trial project to assess the benefits of using ternary mixtures (i.e., portland cement and two fly ashes) and to verify if a blend of good and lesser quality fly ash may produce concrete of a quality comparable to concrete utilizing only high-quality fly ash. If successful, such approach may offer a very effective way of dealing with the seasonal shortages of high-quality fly ash and reduce the cost of construction while improving the quality of concrete.

The benefits of this research include the following:

- Generation of a comprehensive set of information about essential physical and technical characteristics of 20 fly ashes (13 Class C and 7 Class F) available for use in concretes supplied to INDOT.
- Identification of a group of fly ashes with comparable common characteristics, thus providing INDOT engineers with a decision-making tool for potential substitution of sources.
- Development of easy-to-navigate electronic FAH (a supplemental file to this report, available for download at https://doi.org/10.5703/1288284315213) as a tool for engineers to quickly check the physical and chemical characteristics of fly ashes investigated in this project. The FAH offers the benchmark data which can be used for relative assessment of fly ashes from alternative sources with respect to their suitability for use on INDOT projects.
- Development of a statistical model for prediction of both fresh and hardened properties of binary (cement plus one fly ash) and ternary (cement plus two fly ashes) cementitious systems based on the characteristics of fly ashes included in the FAH.

CONTENTS

LIST OF TABLES

LIST OF FIGURES

1. INTRODUCTION

Fly ash, a by-product of combustion of coal in the electric power plants can possess both cementitious and pozzolanic properties (depending on the type of coal burnt). Growing environmental concerns regarding the disposal of fly ashes, combined with the restrictions on the emissions of carbon dioxide during the burning process of the portland cement clinker material lead to an increased usage of fly ash as a replacement material for cement in concrete mixtures. Extensive research on fly ash for the past few decades has shown that it can replace up to 50% of portland cement. In addition to reduction of the cost of the binder, the usage of fly ash provides additional benefit of improving the later age strengths, reducing permeability and increasing durability.

Fly ash is a very complex material, which contains both crystalline and amorphous phases. The chemical composition of fly ash is found to depend on the type of feed coal used in the combustion process (*1*). The physical characteristics of the fly ash particles are influenced primarily by the composition of the feed coal, pulverizing and combustion conditions and fly ash collection method. The variability in fly ashes is such that no two ashes sampled from different power plants share exactly the same properties. Hence, a classification system of the fly ash is needed.

Fly ash is typically divided into different classes based on its chemical composition. The most abundantly found compounds in fly ashes are oxides of silicon, calcium, iron, magnesium, sodium, potassium and sulfur. Apart from these, quite a few of fly ashes also contain a significant amount of unburnt carbon. Different standards across the world recognize different classes of fly ashes, but most of them use a similar set of parameters as a basis for classification. In the USA, the ASTM C 618 standard (*2*) recognizes two classes of ashes. These are Class C ash and Class F ash. The ashes are distinguished primarily based on the sum of the oxides of silicon, aluminum and iron (SAF). If SAF is found to be less than 70%, the material is classified as Class C ash and if SAF is more than 70%, the material is called a Class F ash. There are other physical and chemical requirements for the inclusion of an ash into a specific class, which are also listed in the standard.

1.1 Problem Statement and Research Hypothesis

The usage of fly ash in the cement industry has improved drastically over the past two decades. A replacement of up to 25% of the cement in the binder system with fly ash is a very common practice. Even higher replacements (up to 50%) are actively studied as a part of so-called high volume fly ash binders (*3*). In most cases, the current use of fly ash in cement concrete is based on experience and intuition. A streamlined approach of selecting fly ashes focused on meeting certain performance characteristics of concrete can potentially be developed if a tool existed, to link properties of the ashes with properties of concrete. This research project is intended to evaluate the physic-chemical properties of twenty different ashes (containing both Class C and Class F ashes) and use them to build statistical models to predict the properties of binary (cement + fly ash) and ternary (cement + two different fly ashes) paste systems.

It is hypothesized that the properties of the paste systems containing fly ash(es), depend directly on the fundamental physical and chemical characteristics of fly ash. The goal of the project is to statistically verify the importance of certain characteristics of fly ash in the behavior of pastes. If any of the characteristics of the fly ash were found to have a significant role in the paste's behavior, statistical models using these variables would be developed to predict the properties of the paste systems based on these variables. The project also intends to verify if the properties of ternary paste systems are linear combinations of the properties of the binary paste systems.

1.2 Research Objectives, Scope and Methodology

The primary objectives of this research was to build statistical models to predict the properties of binary paste systems (initial time of set, heat of hydration, calcium hydroxide and non-evaporable water content, and rate of strength gain) and inspect whether they can be combined linearly to predict the properties of the ternary paste systems. The synergistic effects due to the addition of two different fly ashes over the addition of a single fly ash were also assessed.

The main tasks of the project were as follows:

1. Review of the existing literature regarding typical characteristics of fly ashes and their performance in paste systems.
2. Obtaining samples of fly ashes and determining all the relevant characteristics.
3. Developing a test plan for evaluating the binary paste systems, including selecting the mixture proportion, water-binder ratio, sample preparation techniques, and curing methods.
4. Testing of binary mixtures to obtain the data set for subsequent statistical analysis, followed by identification of variables most influencing the pre-selected properties (performance characteristics).
5. Development of statistical models for prediction the properties of the binary paste systems for fly ash with similar characteristics.
6. Identification of testing techniques to statistically evaluate the linearity of the properties of ternary paste systems; preparation of the test plan for assessing the properties of ternary paste systems and testing the paste systems to obtain the statistical data.
7. Analysis of the test results and building statistical models to predict the properties of ternary paste systems. Development of a procedure to predict the characteristics of ashes (and their percentages) needed to obtain specific properties, assuming the properties are found to be linearly additive.

The flow chart of the study methodology is shown in Figure 1.1.

1.3 Organization of Contents

This report is divided into seven chapters. Chapter 1 described the problem statement, the research objectives, scope of the project and the study methodology.

Chapter 2 presents a review of the existing literature on the characterization of fly ashes and on how each of the characteristics of fly ash affects the hydration of cement + fly ash paste systems. A section on the effect of fly ashes on properties of ternary paste systems (cement + two different fly ashes) is also included. A short review of the fractional factorial experimental design is included.

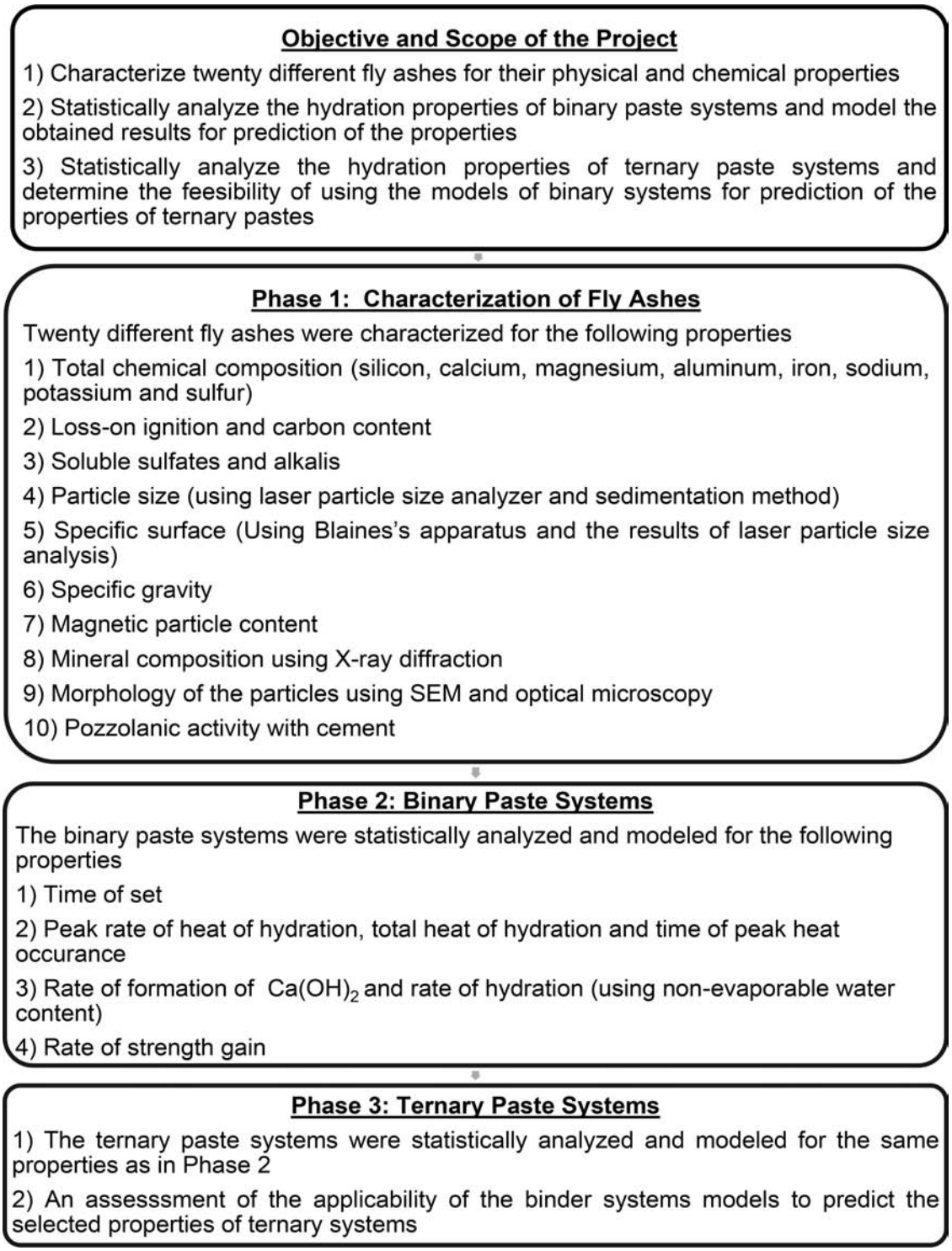

Figure 1.1 Flow chart of the study methodology.

Details and description of the methods of examination employed in the current study for the characterization of fly ashes and for the evaluation of binary paste systems are provided in chapter 3.

The fly ash characterization results and their analysis are presented in chapter 4. Chapter 5 contains the test results for binary paste systems and their utilization in development of statistical models. A similar evaluation and analysis of the ternary paste systems using the results obtained from the statistical modeling of the binary paste systems is discussed in chapter 6.

The overall summary of the research finding is presented in chapter 7.

2. LITERATURE REVIEW

2.1 Introduction

This literature review chapter is divided into three parts. The first part focuses on the prior studies on the fly ash characterization and morphology, which was also the focus of the first phase of the current study. This includes a brief review of the physical and the chemical characteristics of fly ashes and the typical reported ranges for each of the chemical components.

The second part presents a review of prior studies on the effects of the characteristics of fly ash on the properties of the paste systems with blended (portland cement + fly ash) binders.

The third part describes the details of the statistical method, which was used in the study of ternary binder systems (the orthogonal array technique, also known as Taguchi method).

2.2 Fly Ash Characterization Techniques

Fly ash is a very complex material with a highly variable physical characteristics and chemical composition. Its characteristics depend on various parameters including the type of feed coal from which is it obtained (*4*), the location in the coal seam from which it is produced (*5*), the temperature at which it is burnt (*1*) and the type of fly ash collection system at the coal plants and. Hence, there is a definite need to characterize and standardize the characteristics of fly ashes for its use in cement concrete.

ASTM C 311 standard (*6*) describes the test methods of sampling and testing of fly ashes including both their physical properties and the chemical characteristics. The main chemical components of fly ash that need to be evaluated, include: silicon dioxide, aluminum oxide, iron oxide, calcium oxide, magnesium oxide, sulfur trioxide, sodium oxide and potassium oxide. In addition, the loss on ignition, the moisture content, the available alkali contents and the ammonia contents should also be measured and reported. The physical tests include testing for density and fineness. Although not a part of the standard requirement, the particle size distribution (typically using a laser particle size analyzer) and Blaine's fineness (according to ASTM C 204) (*7*) test results are also occasionally reported as they influence the reaction rates, water demand and fresh properties of concrete.

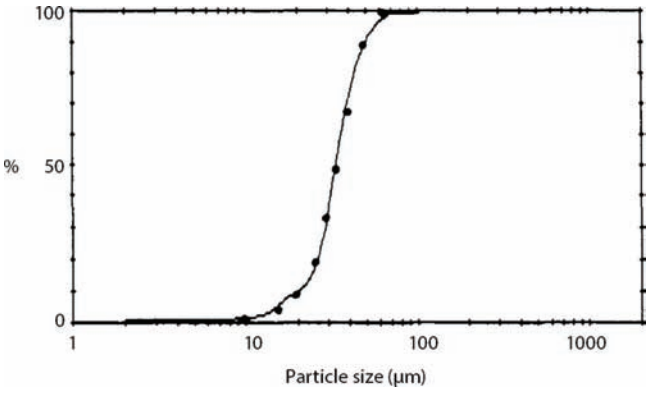

Figure 2.1 Comparison of particle size distribution using laser particle size analyzer (solid line) and particle size distribution using Andreasen Pipette sedimentation method (*9*).

The properties of fly ash related to its performance in cement pastes, which (all evaluated according to their respective standards) typically include: the drying shrinkage of mortar bars, soundness of paste, air entraining ability, strength activity index with Portland cement, the effectiveness of fly ash in controlling alkali-silica reaction and sulfate resistance.

2.2.1 Physical Characteristics (Particle Size Distribution and Fineness) of Fly Ash

The reactivity of fly ash depends a lot on its particle size distribution and fineness. In fact, it was observed that pozzolanic reactivity of fly ash depends directly on the amount of particles present below 10 μm size (*8*).

Diamond (*9*) studied the particle size distribution (PSD) of 14 fly ashes using the laser particle size analyzer and the Andreasen pipette analysis. The results of the study revealed that most of the ashes did not contain a significant amount of particles over 100 μm and under 1 μm. Figure 2.1 shows a typical particle size distribution of a fly ash utilized in the study. The x-axis represents the particle size in microns (on a log scale) and the y-axis represents the percentage of particles below the given size. The solid line indicates the PSD results from the laser particle size analyzer and the dots represent the data points obtained from the Andreasen pipette analysis. For most of the fly ashes, the two sets of results showed a good agreement. However, a few discrepancies were observed at very low particle sizes (< 5 μm) and also at larger particle sizes (> 50 μm).

Kulaots et al. (*10*) studied the size distribution of fly ash particles and found that a large amount of particles have a diameter smaller than 106 μm. A marginal distinction was seen in the size distribution of Class C and Class F ashes. Very few particles existed above the 106 μm in both Class C and Class F ashes. Figure 2.2 and Figure 2.3 show respectively, the particle size distributions of Class F and Class C evaluated in this

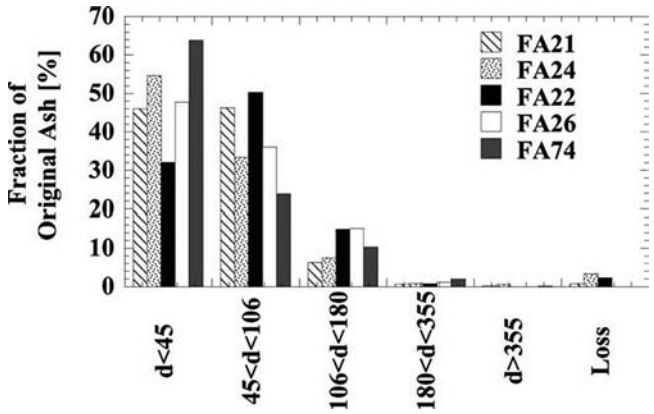

Figure 2.2 Particle size distribution of Class F ashes used in the study (sizes in microns) (*10*).

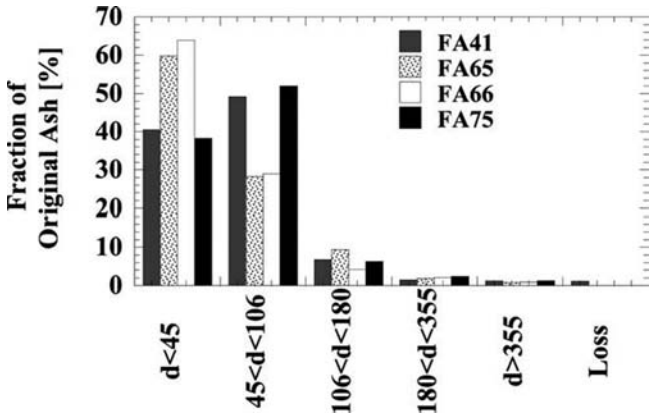

Figure 2.3 Particle size distribution of Class C ashes used in the study (sizes in microns) (*10*).

study. The fly ashes FA21, FA22, FA24, FA26 and FA74 are Class F ashes while the fly ashes FA41, FA65, FA66 and FA75 are Class C ashes. On comparing the plots in these figures, it can be observed that the Class F ashes were marginally coarser than Class C ashes.

A further study into the nature of the large sized particles using scanning electron microscope (SEM) revealed that a significant fraction of the large grains contained unburnt carbon particles. However, relatively bigger amounts of the carbon particles were also a part of the lower sized fractions. Figure 2.4 and Figure 2.5 show the distribution of the carbon particles in various size fractions of Class F and Class C ashes.

In order to measure the fineness of cementitious materials, different methods such as sieving, sedimentation, Blaine's apparatus and the laser diffraction can be used. Frias et al. (*11*) studied the specific surface areas of various pozzolanic materials using Blaine's method and the laser diffraction method. It was found that the laser diffraction technique was a more convenient experimental technique (as compared to Blaine's apparatus) since porosity data were not necessary for calculating the results. The contention was that Blaine's method might not work for materials containing porous grains, especially for fly ashes, as the results are affected by

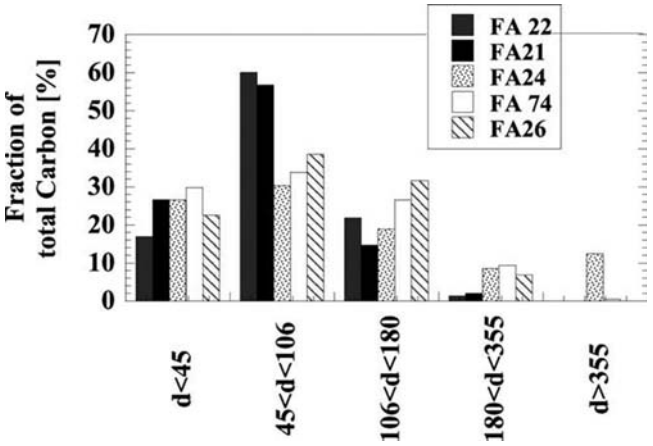

Figure 2.4 Carbon distribution in different fractions of Class F fly ashes (*10*).

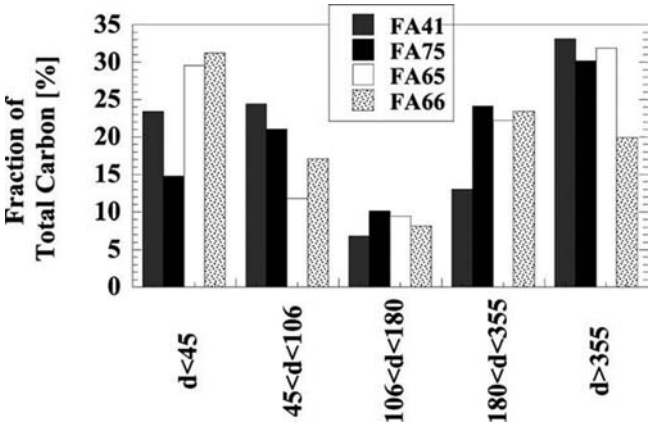

Figure 2.5 Carbon distribution in different fractions of Class C ashes (*10*).

TABLE 2.1
Chemical requirements for Class F and Class C ashes listed in ASTM C 618 (*2*).

Chemicals	Class F	Class C
Silicon dioxide + aluminum oxide + iron oxide, min (%)	70	50
Sulfur trioxide, max (%)	5	5
Moisture content, max (%)	3	3
Loss on ignition, max (%)	6	6

unburned carbon particles, which tend to be highly porous.

2.2.2 Chemical Characteristics of Fly Ash

According to ASTM C 618 standard (*2*), the coal fly ash is classified into two classes: Class C and Class F (see Table 2.1). This classification is based on the chemical composition of the material. The chemical requirements specified by ASTM C 618 include: minimum

TABLE 2.2
X-ray techniques for glass content determination (*16*).

Technique	Used for
QXRD Method	Mineral dusts, portland cement, coal ashes, slags, glass-ceramics
Amorphous Intensity Method	Glass-ceramics
Amorphous Hump Method	Pozzolans
Amorphous-Crystalline Method	Polymers
Differential Intensity Method	Polymers

limit for the sum of silicon, alumina and iron oxides, maximum limit for the sulfate content, maximum limit for the moisture content and the maximum limit for loss on ignition. However, the only difference between Class C and Class F ashes is the content of the sum of the oxides (minimum 70% for Class F ashes and 50% for Class C ashes). This difference in the sum of the silicon, aluminum and iron oxides is also usually reflected in the amount of calcium oxide present in the fly ash, as this is the only other major oxide present in the fly ash apart from the above-mentioned oxides. It should be noted that the Canadian specifications dealing with fly ashes (CSA – A 23.5) recognizes three types of fly ash, depending on the calcium oxide (CaO) content. These classes are Class F (CaO content less than 8% by mass), Class I (CaO content between 8% and 20% by mass) and Class H (CaO content more than 20% by mass).

In the report submitted to Indiana Department of Highways by Diamond (*12*), fourteen different fly ashes collected across Indiana were characterized for their physical and chemical characteristics. Twelve out of the fourteen ashes were Class F ashes. Most of the ashes were found to be similar in their chemical composition and this was attributed to the use of same type of coal as a feed material in electric power plants. The combined oxide contents of silicon, aluminum and iron were found to be around 90% for all the Class F ashes, with some exceptions. The iron oxide contents were in the range of 16% to 24%. Very low calcium oxide (CaO) content, typically around 1% to 2% was observed in the ashes. In addition, a very consistent amount of alkali content was found (K_2O about 2.5% and Na_2O about 0.5%). Most of the alkalis were completely insoluble. These alkalis were deemed to contribute very slowly to the concentration of ions in the concrete pore solution. Very low contents of SO_3, typically below 2%, were found in all the ashes. The amount of magnetic particles found in all the ashes was high, as the ashes contained high amounts of iron oxides. The fly ashes showed a great variation in the carbon contents. All the above characteristics of fly ashes had exceptions in a few of the ashes.

On the other hand, the two Class C ashes presumably had very high contents of calcium oxide and an extremely low amount of carbon. The magnesium oxide content in one of the Class C ashes was unusually high.

To sum it up, all the Class F ashes derived from the plants using the same coal seemed to be very consistent in their chemical characteristics. The two Class C ashes showed minor differences in their characteristics.

In another study by Diamond and Lopez-Flores (*13*) two Class F ashes and three Class C ashes were characterized extensively and the properties of these ashes were found very similar to the fly ashes in the earlier studies by Diamond (*12*).

Hubbard et al. (*14*) studied various ashes obtained from coal plants in the UK. A careful study of the tables comprising of the physical and chemical characteristics of the ashes revealed that they were very consistent within their respective classes. However, minor variations were always seen and no two ashes were exactly the same.

2.2.3 X-ray Diffraction Analysis of Fly Ash

Apart from the above-mentioned chemical characteristics, the glass content present in fly ash was found to play a major in the performance of paste systems incorporating these ashes (*15*). The presence of the amorphous phase in the fly ash was explored extensively by Hemmings and Berry (*16*), using X-ray diffraction techniques, infrared and Raman spectroscopy, Gamma-ray spectroscopy, nuclear magnetic resonance, thermal analysis and acid dissolution techniques. The experimental techniques for the quantification of the amount of glass present in fly ashes were also explored by Hooton, as mentioned by Roode et al (*15*). Table 2.2 summarizes different X-ray techniques which can be used to quantitatively measure the glass content in various materials (*15*). The glass present in the fly ash is revealed in the X-ray pattern as a broad glass hump (see Figure 2.6).

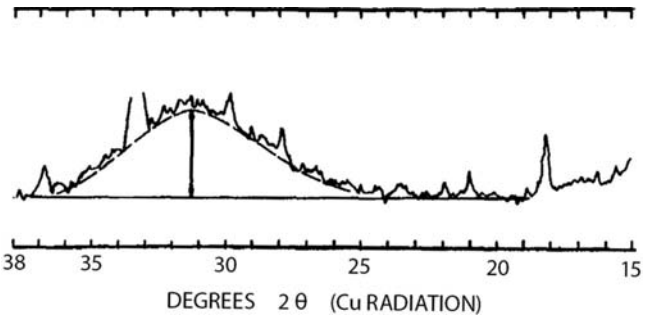

Figure 2.6 Glass hump in the X-ray pattern of a fly ash (*17*).

In a study on the quantification of the glass content in the fly ash (*18*), it was noted that the amount of glass had a profound effect on the hydration related properties and products of paste systems containing fly ash. It was also found that the glass composition varied from particle to particle and that the behavior and that the composition of the glass also varied.

Other research (*17*) noted that the proportion of the glass present in the fly ash is related to the area under the glass hump in the X-ray patterns and that the 2-Theta angle of the peak of the glass hump was linearly related to the analytical CaO contents in low calcium ashes. The 2-Theta angle remained constant for the high calcium ashes.

2.2.4 Morphology of the Fly Ash

The morphology of fly ashes was discussed extensively in a previous study by Diamond (*12*). He observed that most of the fly ash particles were spherical with the diameter in the range of 0.5 μm to 100 μm. The surfaces of the spheres were typically smooth. A small population of hollow particles (cenospheres) and many thin-walled hollow particles (plerospheres) were observed, along with a few irregularly shaped particles. In addition, numerous clusters of particles were also found.

Finally, it was found that there was a clear distinction between iron-rich magnetic spheres (which contained very little glass) and non-magnetic spheres, which often contained mostly glass.

2.3 Binary Paste Systems Containing Cement and Fly Ash

The effects of fly ashes on the properties of the binary (plain portland cement + fly ash) paste systems containing fly ashes have been extensively studied in the past (*19*). Depending on the type and the amount of fly ash present in the system, its effect on properties can vary.

Most of the characteristics of fly ashes listed in Section 2.2 affect one or more properties of the paste system. However, which of the parameters of the fly ash have a relatively higher effect, is not clearly understood. The subsequent sections identify all characteristics of fly ashes (independent variables) that affect the chosen properties of the paste systems (initial time of set, heat of hydration, calcium hydroxide content and non-evaporable water content, and the rate of strength gain) as these properties were examined in the current study. The remainder of this section reviews, in more detail, the main "fly ash characteristics-paste properties" relationships reported in the literature.

2.3.1 Effect of Physical Characteristics of Fly Ash on Pastes

Kiattikomol et al. (*19*) performed a series of tests on the initial time of set of binary pastes containing cement and fly ashes with Blaine's fineness ranging from 2300 cm^2/g to 12300 cm^2/g. They observed that the initial set time gradually deceased with the increase in fineness of fly ash. However, all the setting times were within the limit specified by ASTM C 150 (*20*). The same study also explored the effect of fineness and the median particle size of fly ash on the strength activity index. It was observed that as the fineness was increased (and the median particle size was reduced), the strength activity index at any age increased.

A similar investigation conducted by Sybertz and Weins (*21*), showed that an increase in the fineness resulted in an acceleration of pozzolanic reaction (measured in terms of calcium hydroxide content). This was observed in some fly ashes even before 28 days, but clear improvements were observed only after 28 days. The same study also reported a significant decrease in the late ages in strength activity index with a reduction in the median particle size.

Fajun et al. (*22*) studied the effect of fly ash fineness on the heat of hydration and found that an increase the fineness of the pozzolana added results in a delay in the time for the formation of the peak heat of hydration. In addition, the increase in fineness also results in a reduction in the height of peak heat of hydration. They explained the above process by suggesting that the fly ash acts like a "calcium-sink." The calcium in the solution is removed by the abundant aluminum associated with fly ashes as an Aft phase preferentially forms on the surface of the fly ash. This depresses the concentration of calcium ions in the solution during the early stages of hydration, leading to a retardation of the formation of calcium rich phases on the surfaces on the clinker materials. As a result of this process, a longer induction period is observed in paste systems with pozzolana which delays the occurrence of the peak heat of hydration.

2.3.2 Effects of Aluminum Oxide and Sulfate Content of Fly Ash on Pastes

A significant difference in the rate of reaction of alumina present in the fly ash and the added sulfates was found in the study of two fly ashes (Class C and Class F) by Ma and Brown (*23*). Specifically, a reaction between alumina-containing phases in fly ash and the added sulfates was observed to occur in the Class C fly ash. This reaction resulted in the formation of ettringite, even at early ages. However, this reaction was found to be limited in Class F ashes, due to their low lime contents. This reaction had a significant impact on the calorimetric curve of Class C fly ashes when they were hydrated by themselves. The hydration products formed by both classes of fly ashes were also found to be significantly different.

It was also found that the increase in the sulfate contents leads to a deleterious effect in the compressive strength, as there is a higher amount of ettringite formed in the system.

A study on the heat release in plain portland cement pastes, with the increase in the amount of sulfate (*24*)

revealed that, at lower levels of sulfate there is an increase in the peak heat of hydration for the second peak (aluminate peak). However, with a further increase in the sulfate content, this peak is gradually suppressed and delayed. In addition, a slight increase in the total heat of hydration was observed with an increase in the sulfate content. Hence, a profound effect was seen due to the effect of the presence of aluminate and sulfate in the binder systems on heat of hydration of pastes.

2.3.3 Effects of Magnesium Oxide Content of Fly Ash on Pastes

According to ACI 232.2R-96 (*25*), the content of the crystalline MgO (periclase) found in fly ashes is usually more than 2%. However, some fly ashes may have a much higher periclase contents (as high as 80%) of the MgO. This periclase, unlike the periclase in cement, is not a free MgO and typically is nonreactive when exposed to water or basic solution at normal temperatures. However, typically the remaining MgO (noncrystalline fraction) is reactive and has a role to play in the hydration reaction.

Zheng et al. (*26*) performed a series of tests on concrete containing plain portland cement calcined with various levels of MgO (0 to 5% at increments of 1%). The MgO resulting from the above process can be considered as free MgO, which is reactive. The two tests performed on these cements were initial and final time of set and heat of hydration. It was observed that with the increase in the MgO content, the initial and final time of set gradually increased (see Table 2.3). In Table 2.3, the number associated with the sample number (e.g., F-2) represents the percentage of magnesium oxide added to the sample (2% MgO).

In addition, the heat of hydration at early ages (within first 5 hours) was very large compared to the plain cement paste, which gradually reduced at later ages. There was a significant delay in the occurrence of the peak heat of hydration. The main hypothesis for the above findings was based on the solubility products of the two hydroxides ($Mg(OH)_2$ and $Ca(OH)_2$). The $Mg(OH)_2$ has a much lower solubility product and hence precipitates in the liquid phase of hydrating cement before $Ca(OH)_2$, thus reducing the concentration of the $(OH)^-$ ions in the solution. Therefore, more time is needed to reach the maximum $Ca(OH)_2$ saturation ratio. Hence, an increase in the free MgO content leads to the delay in the initiation of the peak, a prolonged induction period and retardation in the acceleration period, which leads to the increase of the set time of these cements.

TABLE 2.3
Set time of MgO-type expansive cements.

	Sample No.				
	F-0	**F-2**	**F-3**	**F-4**	**F-5**
Initial setting time	2:43	3:11	4:00	5:35	6:00
Final setting time	4:46	5:00	5:26	6:45	7:44

2.3.4 Effects of Loss on Ignition of Fly Ash on Pastes

Tests on concrete containing fly ash with varying loss on ignition values indicated that the increase in the loss on ignition leads to an increase in the water demand and a consequent reduction of the compressive strength (*27*). The loss on ignition of fly ash gives an approximate estimate of the unburnt carbon content present in the fly ash. The unburnt carbon particles, which are porous in nature, absorb water, which is not released for hydration. Class F fly ashes in general inclined to have a higher water demand compared to Class C ashes due to their higher loss on ignition. Furthermore, an increase in the replacement level is cement by fly ash, increased the water demand.

It was also observed by Langan et al. (*28*), that a higher loss on ignition of the fly ash tends to retard the hydration process as the amount of available water is reduces, thus prolonging the induction period.

2.4 Ternary Paste Systems

Ternary paste systems containing a mixture of both high and low calcium fly ashes were tested for synergistic effects in terms of strength gain (*29*). The strength of ternary systems was calculated by adding measured strengths of binary binder systems (P_{Bi} and P_{Bj}) scaled to reflect the proportions of fly ash in the binary systems of fly ash "i" and "j" in the ternary system. The synergistic effect of using two different fly ashes in the ternary system was evaluated by calculating the so-called synergistic action (SA) parameter as shown below.

$$SA = P_{(Ti+j)}\left(W_i P_{Bi} + W_j P_{Bj}\right) \quad (1)$$

where, SA = synergistic action (in MPa)

i, j = fly ash type

$P_{(Ti+j)}$ = measured compressive strength of the ternary paste

P_{Bi}, P_{Bj} = measured compressive strengths of the corresponding binary pastes

W_i, W_j = proportion (by weight) of the fly ashes i and j in ternary blend

The SA values were plotted against the strength gain (SG) values in order to evaluate the synergistic action in ternary blends. SG is the additional strength gained by the fly ash-cement paste system as compared to the normalized strength of the reference plain cement paste.

$$SG_i = R_i - \left(R_c \frac{c_{cem}}{c_{poz}}\right) \quad (2)$$

where, SG = strength gain of the ternary binder

R_i = the compressive strength of the fly ash-cement binder system

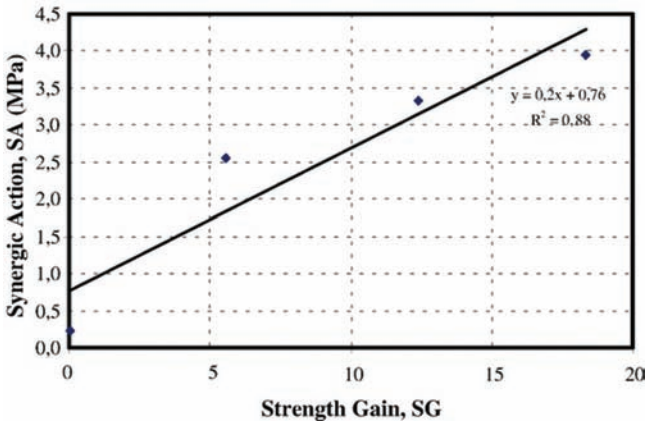

Figure 2.7 Strength gain (SG) versus synergistic action (SA) in ternary cements (*29*).

R_c = the compressive strength of the reference cement binder

C_{cem} = the proportions of cement in the binder

C_{poz} = the proportion of the pozzolan in each mixture

It was observed that the synergistic action bore a linear relationship with the strength gain of the ternary binder. Figure 2.7 shows a plot between the synergistic action and strength gain at various ages, 2 days, 7 days, 28 days and 90 days.

2.5 Model Selection Techniques

When a large number of independent variables are used to statistically model and predict a dependent variable, the model containing all the independent variables need not be the "best model," which yields the best predictions. Hence, it is necessary to evaluate all the sets of independent variables and select the most influencing independent variables.

Model selection techniques are statistical procedures which allow for identification subsets of independent variables (i.e., predictors) with highest influence on the dependent (i.e., response) variables. These sets of independent variables, when used to develop statistical models to predict the dependent variables, yield the most accurate predictions.

A number of statistical parameters are available to evaluate the sets of independent variables in order to select the best model. However, each of them have trade-offs with respect to the accuracy of selection and the complexity of the calculations. All the statistical model evaluation procedures using these parameters are also different in their approach in reaching the conclusion about the best model. (The explanation for the all the parameters is out of the scope of this study).

A few of the available statistical parameters to evaluate the sets of independent variables in the modeling process are R^2, adjusted R^2, Mallow's C_p, Akaike's Information Criterion (AIC) and Schwarz's Bayesian Information Criterion (BIC).

The fit of the model can be evaluated using R^2 while the importance of the variables present in the model is indicated by adjusted R^2 and the other parameters mentioned above. These two parameters (R^2 and adjusted R^2) have been clearly defined in Section 5.1.

2.6 Experimental Design Techniques

The advantage of using a full factorial design approach when planning the experiment lies in the fact that it helps to generate large number of data points which, in turn, help in the process of analysis and assessing the properties of a given system. However, in most cases it is practically not feasible to perform the tests based on a full factorial design due to economical, time and other constraints. Hence, an experimental design called fractional factorial design is often used. This design yields only a part of the full factorial design data, but requires less experimentation. The quality of the acquired data is such that, it represents the most important features of the problem studies.

Srinivasan et al. (*30*) successfully implemented a fractional factorial design called the Orthogonal Array Technique (also known as Taguchi Method) to develop a rapid-set high-strength cement by varying the fineness of the mixture and by supplying three different additives to the binder systems, namely, alkali carbonate, alkali sulfate and mixture of alkali carbonates. Table 2.4 shows the factors and factor levels used in the experimentation. Table 2.5 shows the orthogonal array used for the experimental design. The analysis was performed using the software called "ANOVA by Taguchi Method" (ATM) and the percentage of the effect of each of the factors was reported.

TABLE 2.4
Factors and their levels of the experiment (*30*).

	Levels		
Factors	**1**	**2**	**3**
(A) OPC/high-alumina cement/ anhydrous calcium sulfate	70:20:10	75:15:10	80:15:5
(B) Fineness of the cement (cm^2/g)	5000	5500	6000
(C) Additive type	alkali carbonate (AC)	alkali sulfate (AS)	mixture of alkali carbonates (MAC)

TABLE 2.5
Orthogonal array for $L_9(3^4)$ (*30*).

Experiment Number	Columns			
	A	B	C	E
1	1	1	1	1
2	1	2	2	2
3	1	3	3	3
4	2	1	2	3
5	2	2	3	1
6	2	3	1	2
7	3	1	3	2
8	3	2	1	3
9	3	3	2	1

A detailed explanation on the orthogonal arrays is given in Section 6.1.1.

Note: Each of the elements in the symbol $L_9(3^4)$ refer to:

(1) L – Orthogonal array.

(2) 9 – The number of experiments to be performed.

(3) 3– The number of factor levels for each of the factors.

(4) 4 – The number of factors affecting the dependent variable (A, B, C and e).

3. EXPERIMENTAL METHODS FOR CHARACTERIZATION OF FLY ASHES AND TESTING OF PASTE SYSTEMS

3.1 Materials Used in the Study

3.1.1 Fly Ash

The project utilized a set of twenty different fly ashes obtained from electric power plants in and around Indiana, USA. The set comprised of thirteen ASTM Class C and seven ASTM Class F ashes. Ten of the thirteen Class C ashes and five of the seven Class F ashes were on the Indiana Department of Transportation's (INDOT) list of approved materials. The ashes were obtained directly from the suppliers. Table 3.1 shows the summary of the basic information for all fly ashes used in the study, including the name of the supplier, name of the source plant (used as a label for the fly ash) and their respective ASTM C 618 classification (*2*).

The samples were transported in airtight containers to the laboratory at Purdue University and sub sampled for testing. A data sheet comprising of the physical and chemical characteristics of the ashes was also obtained for all but two (Joppa and Miller) of the materials at the time of delivery. The complete set of the available data is included in the *Fly Ash Handbook* (FAH) which can be downloaded as a separate file from https://doi.org/10.5703/1288284315213. An example of the data sheet provided by the fly ash supplier is given in Appendix A. That appendix also contains Table A.1, which provides the overall summary of selected physical and chemical characteristics of all fly ashes used in this study.

3.1.2 Portland Cement

The cement used for testing in the study was portland cement Type I which conformed to ASTM C 150 (*20*). The cement in the study was supplied by Buzzi Unicem, cement plant located in Greencastle, IN, USA. The data sheet for the cement is shown in Figure 3.1.

TABLE 3.1
Fly ash supplier details and names of the fly ashes.

No.	Supplier	Source	Class	Name
1	Headwaters Resources	Baldwin Power Plant, MI	C	Baldwin*
2		Edwards Power Plant	C	Edwards*
3		Hennepin Power Station	C	Hennepin*
4		Schahfer Power Plant Unit 15, IN	C	Schahfer*
5		Vermilion Power Plant	C	Vermilion*
6	Holcim Inc.	Miller Plant, AL	C	Miller*
7	Lafarge North America	Joliet Power Station, IL	C	Joliet*
8		Will County Power Plant	C	Will County*
9		Kenosha Plant, WI	C	Kenosha
10		Rockport, IL	C	Rockport
11	Mineral Resource Technologies	Petersburg Power Plant, IN	F	Petersburg*
12		Trimble County Power Station. Bedford, KY	F	Trimble
13		Rush Island Power Plant	C	Rush Island
14		Mill Creek Power Station	F	Mill Creek
15		Labadie Power Plant, MO	C	Labadie*
16		Joppa Station, IL	C	Joppa*
17	Fly Ash Direct	Zimmer Power Station, Moscow, IL	F	Zimmer*
18		Miami Fort Unit #8, North Bend, OH	F	Miami 8*
19		Elmer Smith Station, Owensboro, KY	F	Elmersmith*
20		Miami Fort Unit #7, North Bend, OH	F	Miami 7*

*= INDOT's list of approved materials.

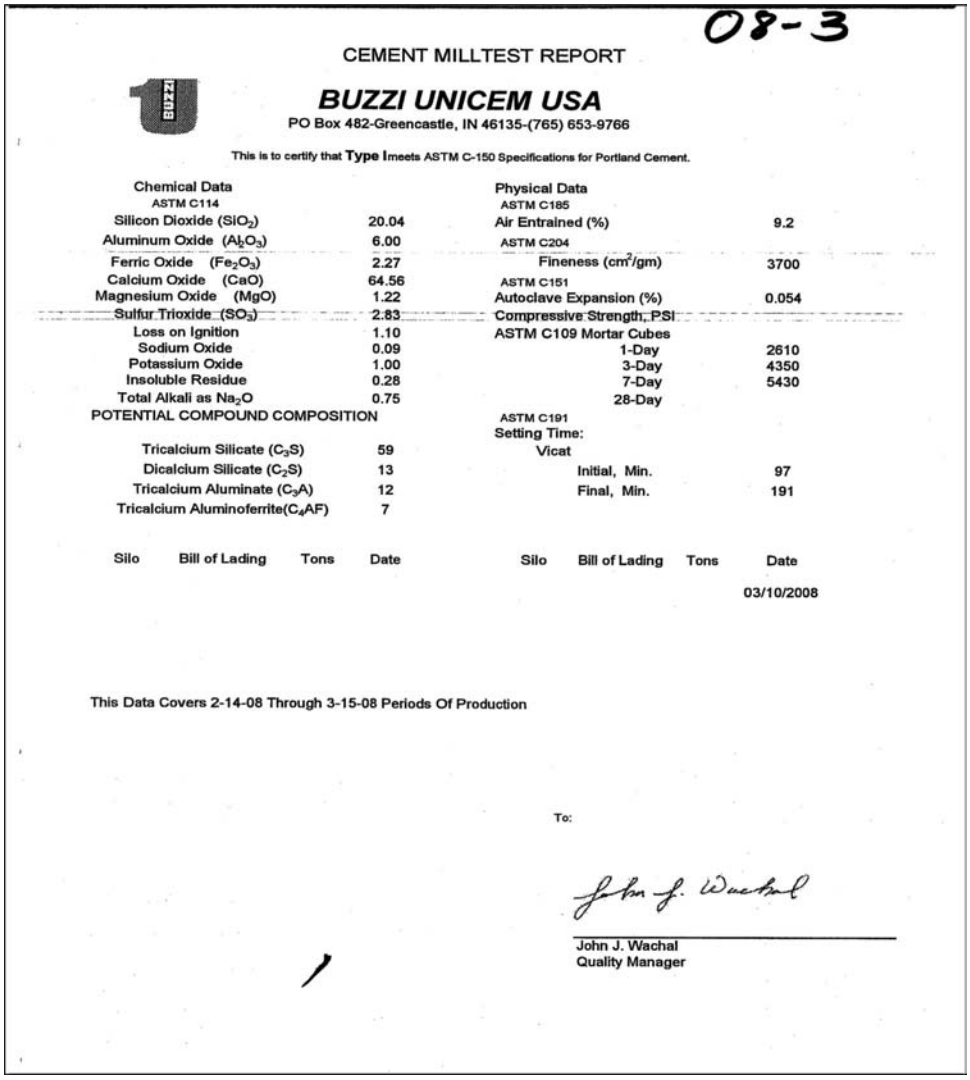

08-3

CEMENT MILLTEST REPORT

BUZZI UNICEM USA

PO Box 482-Greencastle, IN 46135-(765) 653-9766

This is to certify that **Type I** meets ASTM C-150 Specifications for Portland Cement.

Chemical Data ASTM C114	
Silicon Dioxide (SiO_2)	20.04
Aluminum Oxide (Al_2O_3)	6.00
Ferric Oxide (Fe_2O_3)	2.27
Calcium Oxide (CaO)	64.56
Magnesium Oxide (MgO)	1.22
Sulfur Trioxide (SO_3)	2.83
Loss on Ignition	1.10
Sodium Oxide	0.09
Potassium Oxide	1.00
Insoluble Residue	0.28
Total Alkali as Na_2O	0.75
POTENTIAL COMPOUND COMPOSITION	
Tricalcium Silicate (C_3S)	59
Dicalcium Silicate (C_2S)	13
Tricalcium Aluminate (C_3A)	12
Tricalcium Aluminoferrite(C_4AF)	7

Physical Data ASTM C185	
Air Entrained (%)	9.2
ASTM C204	
Fineness (cm^2/gm)	3700
ASTM C151	
Autoclave Expansion (%)	0.054
Compressive Strength, PSI	
ASTM C109 Mortar Cubes	
1-Day	2610
3-Day	4350
7-Day	5430
28-Day	
ASTM C191	
Setting Time:	
Vicat	
Initial, Min.	97
Final, Min.	191

Silo	Bill of Lading	Tons	Date	Silo	Bill of Lading	Tons	Date
							03/10/2008

This Data Covers 2-14-08 Through 3-15-08 Periods Of Production

To:

John J. Wachal
Quality Manager

Figure 3.1 Datasheet for Type I portland cement.

3.1.3 Graded Sand

The ASTM C778 (*31*) graded sand was obtained from the Ottawa, Illinois, USA source. The specific gravity of the sand was 2.65.

3.2 Fly Ash Characterization

All fly ashes obtained for the study were subjected to a rigorous testing process to evaluate their physical and chemical characteristics. The results of the tests performed were analyzed, documented and were further used in developing statistical models for predicting properties of the paste systems containing fly ash(es). The properties evaluated included the following (NOTE: (1) = information provided by the fly ash supplier; (2) = parameters determined in the laboratory at Purdue University):

- Total chemical analysis[1][2] (contents of silicon, calcium, magnesium, aluminum, iron, sodium, potassium and sulfur)
- Loss on ignition[1]
- Content of soluble sulfates and alkalis[2]
- Particle size[2]
- Specific surface (Using Blaine's apparatus[1] and laser particle size analyzer)[2]
- Specific gravity[1]
- Magnetic particle content[2]
- Mineral composition using X-ray diffraction[2]
- Morphology of the particles using SEM and optical microscopy[2]

The above properties were selected for testing as they are required by ASTM C 618 standard (*2*) or because they were considered to have a potential influence on the performance of the pastes containing these ashes.

3.2.1 Total Chemical Analysis and Loss on Ignition

As mentioned earlier, the chemical analyses of fly ashes were provided by the suppliers. These analyses were performed using X-ray fluorescence technique.

All fly ash samples were analyzed on an ignited weight basis. Loss on Ignition was performed by the supplier in accordance with ASTM C 311 (*6*).

3.2.2 Soluble Sulfur and Soluble Alkalis

To determine the content of soluble sulfates and alkalis, 25 g of fly ash was added to 250 ml of de-ionized water contained in a 500 ml volumetric flask. The flask was then shaken continuously by hand for 15 minutes while the temperature of the solution was maintained at about 23°C. Upon completion of the shaking, the fly ash suspension was filtered through a Whatman filter paper without rinsing. The SO_4^{2-} concentration of the solution was then determined by ion chromatography method, using a Dionex BioLC with IONPAC® AS4A analytical column. The results were expressed as percentages of soluble sulfate.

The Na^+ and K^+ concentrations were determined by atomic absorption through flame emission, using a Varian Spectra AA-20 using flame emission instrument. The percentage of the total alkali content of each fly ash that was soluble was calculated according to ASTM C 311 (*6*). The results were expressed as percentages of soluble Na_2O, K_2O and combined alkalis (as equivalent% Na_2O).

3.2.3 Particle Size Distribution, Specific Surface Area and Fineness

3.2.3.1 Particle size distribution and specific surface area by laser diffractometry. The particle size distribution, the approximate surface area values and median particle sizes of each fly ash was determined at two different laboratories (Purdue University and Boral Material Technologies Inc.) using a laser particle size analyzer. Based on the data obtained, a cumulative size distribution for each fly ash was plotted. The mean particle size was calculated by using the obtained data of the size distribution, by taking a weighted average of the amount of particles at various intervals obtained from the laser particle size analyzer. However, the reported values from the equipment are slightly lower than the manually calculated values (using the particle size distribution data obtained from the equipment).

A discrepancy was observed between particle size distributions obtained from the laser analyzers by the two laboratories, which was resolved using the sedimentation analysis. The sedimentation test was performed using the "Andreasen Pipette Analysis" as shown in Figure 3.2. The procedure for the sedimentation analysis is explained in Section 3.2.3.2.

3.2.3.2 Particle size distribution using sedimentation analysis. The analysis involved dispersing fly ash particles (about 1% by volume of the final suspension) for two minutes in a medium consisting of water mixed with 9.8 g/l of dispersing agent (sodium hexametaphosphate. The suspension was then transferred to the Andreasen pipette and the fly ash particles were allowed to settle under gravity in a water column. Right before the start of the measurement the suspension was agitated manually by shaking the pipette and its contents vigorously for one minute. Following the shaking, the pipette was placed on the table and left undisturbed. A 10 ml aliquots of the solution were drawn at a depth of 20 cm (from the initial surface of water) at specific time intervals, dried at 100°C and weighed to 1/1000 of a gram. The dried sample would contain particles equal to or below a certain diameter, calculated using the Stokes law:

Figure 3.2 Andreasen pipette (Source: www.gargscientific.com/lg196-58.jpg).

$$h = \frac{2(\rho_s - \rho_1)}{9\mu} g R^2 t \qquad (3)$$

where:

h = the depth from the surface of the solution at which aliquot is taken

ρ_s = the density of the solid particles (fly ash)

ρ_l = the density of the liquid (water with dissolved sodium hexametaphosphate)

g = the gravitational acceleration

R = the maximum radius of the particles in the sample

t = the time of sampling

μ = viscosity of the solution

A sample was also taken immediately after the suspension was prepared as a representative of all the sizes. A cumulative size distribution curve was plotted using the dried weights' information after the correction for the weight of the dispersing agent.

3.2.3.3 Specific surface area using Blaine's method. The Blaine's air-permeability apparatus was also used to obtain the specific surface area values of fly ashes. The experiment was performed as specified in ASTM C 204 (*7*). Before the fly ashes were tested, the calibration of the air permeability apparatus was performed using the NIST Standard Reference Material 114p (Portland Cement Fineness Standard.

3.2.4 Content of Magnetic Particles

In order to determine the content of magnetic particles, about 20 g of fly ash was weighed out and placed into a beaker with 100 mL of water. The beaker was placed over a magnetic stirrer after a Teflon-coated bar magnet was added to the solution. The solution was stirred for 5 minutes at moderate velocity and then turned off. All magnetic particles stuck on the magnet were carefully brushed off and collected. The operation was then repeated as many times as required, until no further magnetic particles were found attached to the magnet. The remaining suspension was then filtered, dried, and reweighed. The weight percentage of the particles removed was calculated and reported as the content of magnetic particles for each fly ash.

While it is well known that all fly ashes contain certain amount of magnetic particles, the results obtained from the test for some fly ashes seemed erroneous, mainly for some Class C fly ashes, as no magnetic particles were detected. It could be because very small proportions of magnetic particles were present in these ashes and errors introduced during the procedure were comparable to the magnetic particle content itself.

3.2.5 X-Ray Diffraction Analysis

X-ray diffraction analysis of fly ash powders was performed using Siemens D-500 diffractometer. The source of radiation used was CuKα with the tube powered to 50 kV and 30 mA. The random powder mount specimens were scanned from 5° to 65° of 2-Theta (2θ) values at 0.02° step size.

The sample preparation (considered standard for this research) was the randomly oriented powder mount technique. A 1/8 inch (~3 mm) thick aluminum holder with a 5/8 (~15 mm) inch diameter circular hole was covered with a piece of stick pad paper of proper size. The paper was covered, in turn, with a glass slide. The glass slide was taped in place and the mount was inverted. The dry, powdered fly ash sample (ground to pass the 200-mesh sieve) was placed inside the exposed well after passing it through the sieve. The powder mass was compacted lightly with the edge of the spatula and trimmed. A slight excess of powder was added to the surface, and a second glass slide was taped to the aluminum frame. The sample was again inverted and the original glass slide and paper were carefully removed with the aid of a razor blade, leaving the plane face of randomly oriented compacted fly ash powder ready to be exposed to the X-ray beam.

Interpretation of patterns for the presence of crystalline components was carried out by the usual methods, involving assignment of each of the peaks present to one (or sometime more than one) of the crystalline substances which may be present.

In addition to information on the crystalline components present (that was derived from the peaks), the glass that is also normally present produces a very broad band of intensity that shifts the background upward over a range of 2-Theta angles. The angle 2θ at which its maximum occurs provides an indication of the basic structure of the glass. Class F fly ashes are known to generally yield band maximum near about 24° 2-Theta (Cu radiation), the position of the main SiO_2 peak. With the increasing calcium oxide content, Class C fly ash has a maxima moving progressively upward in position and shows a maximum at about 32° 2θ (Cu radiation), which is the position of the main peak for the compound $C_{12}A_7$ (*17*).

3.2.6 Scanning Electron Microscopy

The morphologies of fly ash particles were examined using an ASPEX® Personal SEM.

The particular fly ash samples were sprinkled onto a copper tape mounted on aluminum stubs and then coated with palladium for 3 minutes, using a Hummer 6.2 Sputtering System. The samples were imaged in the secondary mode at various magnifications.

All the fly ash samples were examined initially at a lower magnification, typically from 400× to 1000× according to the fineness of the fly ash, to assess the general morphology characteristics. Any specific features found during this scan were later focused on, at a higher magnification if necessary, at times as high as 3000×. Approximately 10–20 micrographs were taken for each fly ash and a set of four individual micrographs were selected for inclusion in this report. The basis for selection was the representativeness of the features depicted, rather than photographic excellence. Besides the SEM images, the EDX analysis was also carried out on some specific particles to confirm the probable chemical composition of the particles.

3.2.7 Glass Content

The glass content in the fly ashes was empirically estimated by precisely measuring the area under the glass hump in the X-ray diffraction pattern. The area was measured from 15° to the point where the curve flattens (approximately 45–50° of 2-Theta). The area under the curve before 15° was neglected as it involves an elevation in the base intensity not due to the presence of glass. To estimate the area accurately, it is necessary to discard the area of the crystalline peaks and nullify the effects of the noise in the intensity measurements. In a bid to measure the area under the glass hump, a simple methodology was adopted, which is described in the flow chart shown in Figure 3.3.

The process of measuring the area under the glass hump involved three steps.

1. The first step involved elimination of all the peaks due to crystalline phases from the glass-containing part of the X-ray diffraction pattern. This was accomplished by manually selecting a series of equally spaced points that were located on the "hump" line and at the base of the individual peaks. In addition to eliminating the peaks, the process also reduced the noise in the background as the

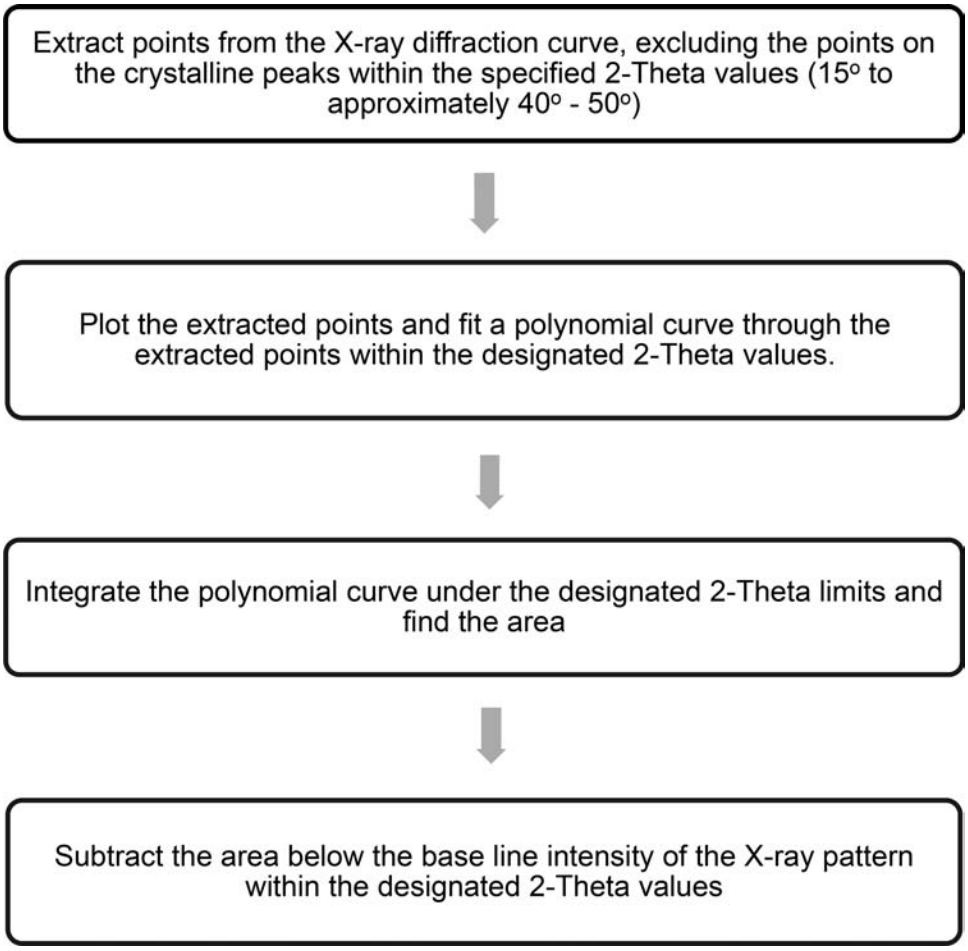

Figure 3.3 Flowchart describing the process of estimating the area under the glass hump in the X-ray diffraction pattern.

points were chosen manually and had a higher spacing than the collected data points. A software called "xyExtract" was used to extract the data points to help draw a continuous X-ray diffraction pattern. The procedure to use the software for this purpose is described below.

xyExtract: The software requires as an input a BITMAP image of the X-ray pattern as shown in Figure 3.4. The initial and final points of both the x and y axes are chosen precisely by pointing the mouse cursor on the axes' end points (see points A and B in Figure 3.5). The cursor is then placed on the X-ray pattern and points are selected at equal intervals (approximately 1 point for 1°), to cover the entire glass hump and the flat baseline intensity following the glass hump as shown in Figure 3.5 (points 1 to 4). The coordinates of these points are then displayed in Microsoft® Windows Notepad and are plotted using Microsoft® Excel.

2. Once the plot was prepared, a polynomial curve of 6^{th} order was fitted through the points. The motive behind choosing the order polynomial as six was the high R^2 values obtained for all the patterns and six is also is the limitation on the order of the polynomial for trend lines in Microsoft® Excel. While plotting the curves and fitting a trend line, the tabs to display R^2 and to display the trend-line polynomial equation on the graphs were checked. This equation was modified later to measure the area underneath the curve as it was observed that the equation obtained from the above process cannot be used to obtain the areas as the number of decimal points for the coefficients in the polynomial equation were insufficient for an accurate integration procedure.

   It was also observed that a single equation could not define the complete X-ray pattern with a high value of R^2. Hence, the pattern of the glass hump was split into two at the peak value of the hump. Subsequently, two different equations were used to define the complete pattern, Equation 1 for the points before the peak and Equation 2 for the points after the peak as shown in Figure 3.6.

3. A software called "LAB Fit" was used for the purpose of estimating the coefficients of the 6^{th} order polynomial trend-line more accurately, up to 8 decimal places after the decimal point. The extracted points were used as the input for the program and the output after the fitting process would yield the same equations as mentioned above, with a more accurate estimation of the coefficients for the polynomial equation. The curve was split into two parts, before the peak and after the peak, namely equation 1 and equation 2 respectively.

   Finally, a software named "Sicyon Calculator" was used to estimate the area under the curve, by integrating the polynomial equation between the previously mentioned range of 2-Theta values (minimum 15° and max 40°–55°). The input for this program is the polynomial equation and the output after running the program would be a value of the area under the curve. The area under base line of the curve is

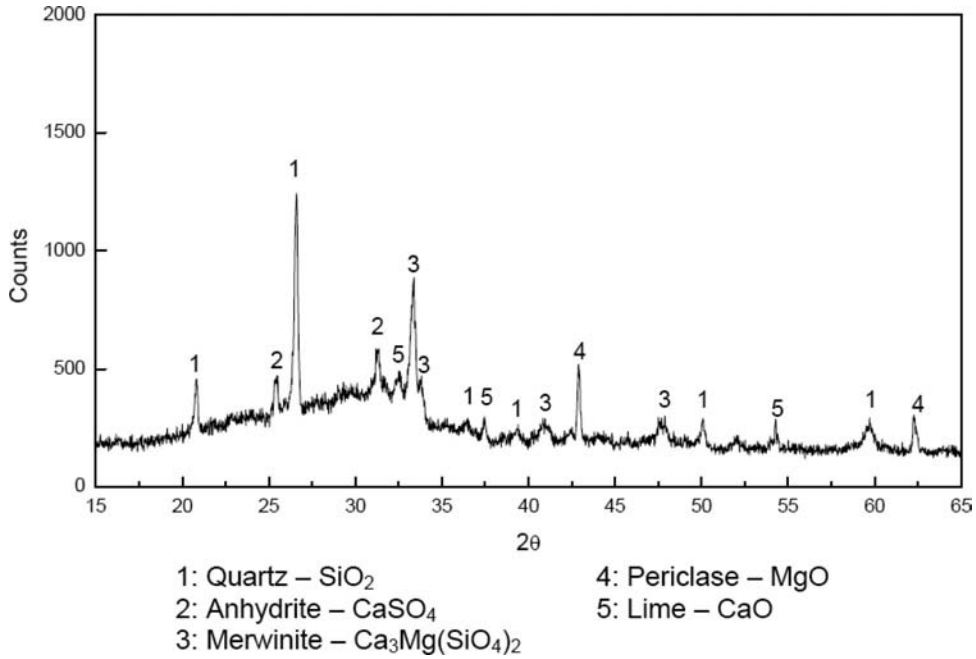

Figure 3.4 BITMAP image of the X-ray pattern for Baldwin fly ash (numbers on peaks represent various crystalline phases).

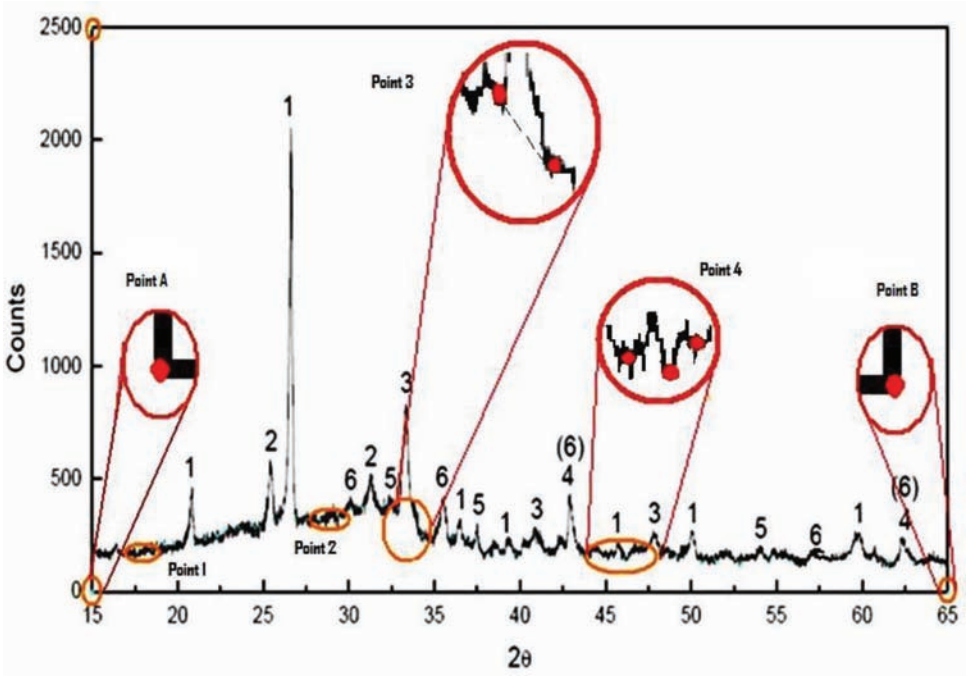

Figure 3.5 Extraction of points using "xyExtract."

deducted from this value obtained from the integration of the polynomial curve. Figure 3.7 depicts the areas evaluated under the glass hump.

3.3 Mixing Procedure and the Experimental Techniques for Evaluating Pastes

This section describes in detail, the experimental techniques used to characterize the hydration related properties of fly ashes namely, the time of set, parameters describing the heat of hydration, the rate of strength gain, rate of formation of calcium hydroxide and the non-evaporable water content of the pastes at different ages (1, 3, 7, and 28 days). The mixing process in preparing specimen for each of the test is also mentioned. The statistical modeling of all the measured properties is described in Chapter 5. The tests were selected based on their importance in the field applications of the binder

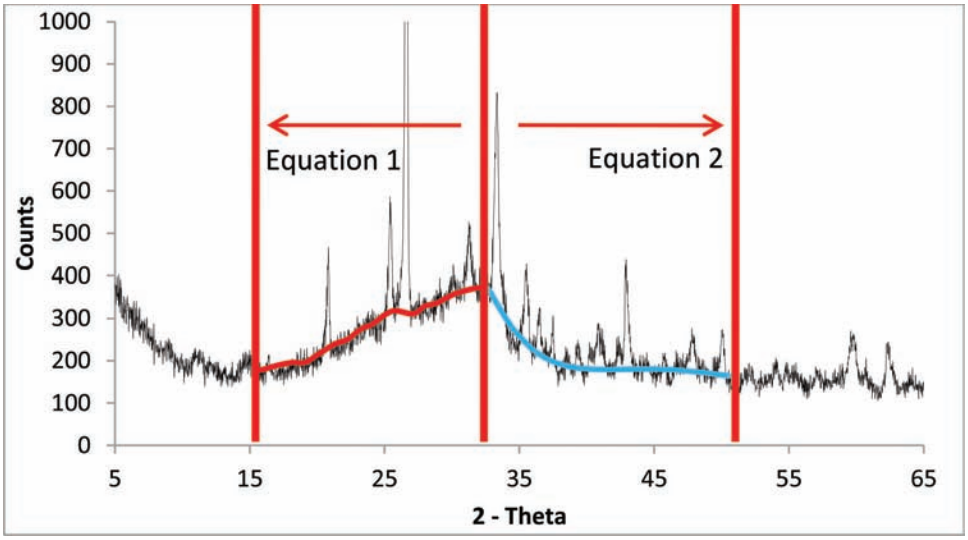

Figure 3.6 Plotting of extracted points in Excel for Baldwin fly ash—Equations 1 and 2.

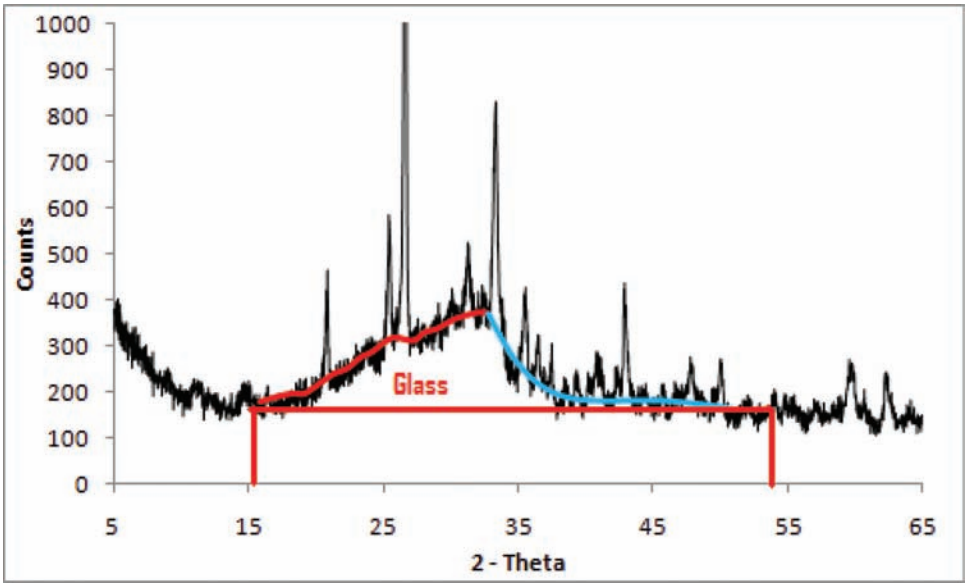

Figure 3.7 Area of the glass hump evaluated with the deduction of the crystalline fraction of the curve between the angles 15° and 54° for Baldwin fly ash.

systems more particularly, the time of set, the rate of strength gain and the heat of hydration.

3.3.1 Initial Time of Set

The initial time of set was performed using the Vicat apparatus in accordance with ASTM C 191 (*32*). This testing method for setting time is the most widely used commercially; both mechanical and automated Vicat testing apparatus' are used. However, all the experiments in this study were carried out using a mechanical Vicat testing apparatus. The experiment was performed on cement (control mix), twenty different binary paste systems in duplicates and nine sets of ternary paste systems in duplicates. The binary and ternary pastes contained 20% of the cement replaced with fly ash(es) by weight and the water/binder ratio was selected based on the normal consistency of the binder measured in accordance with the standard, ASTM C 187 (*33*). A dry mixing by hand of fly ash(es) and cement prior to mixing with water was performed to homogenize the binder and break any lumps if present. The paste specimens were left in the curing room for 30 minutes before they were taken out and allowed to set at room temperature. The initial time of set was measured as mentioned in ASTM C 191 (*32*).

3.3.2 Rate of Strength Gain

The compressive strength of 2-inch cubes of neat cement mortars (control mix), binary binder mortars and ternary binder mortars were measured at different

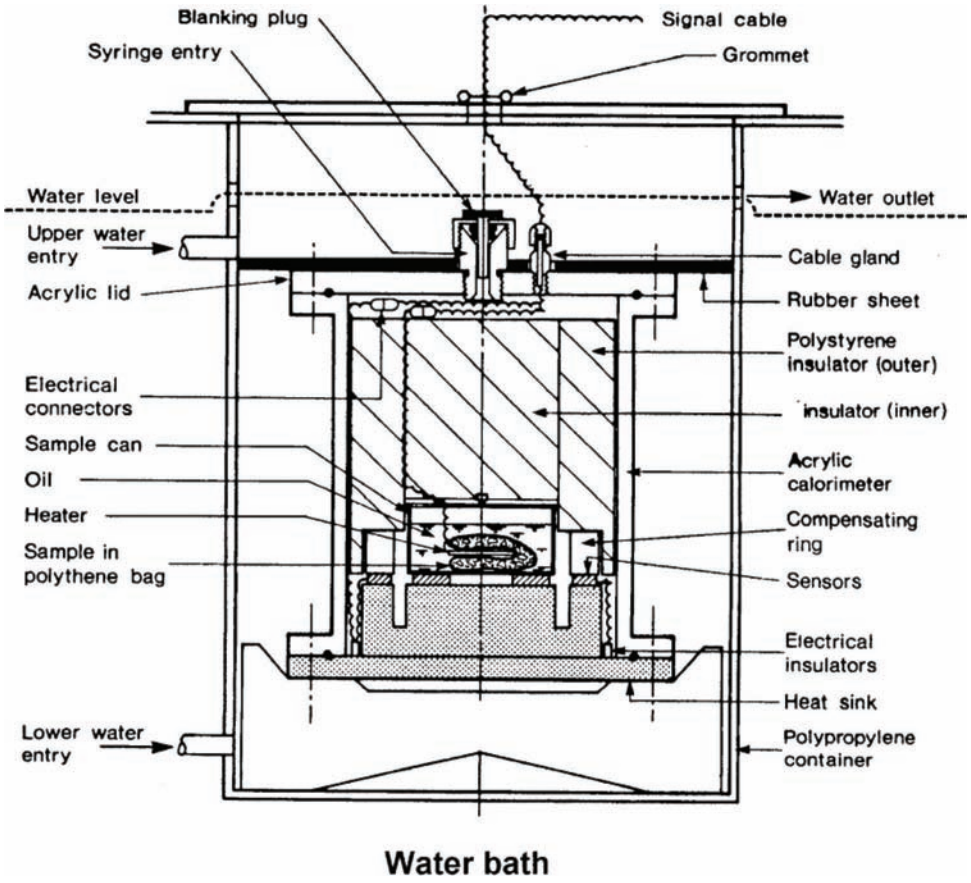

Figure 3.8 A labeled sectional view of the calorimeter (*35*).

ages (1 day, 3 days, 7 days, and 28 days). Three cubes each for a binder system and age were tested. All the specimens were prepared, cured in the molds for a day, de-molded and cured until their age in the moist room at 23°C. The samples were tested according to ASTM C 311 (*6*). Graded Ottawa sand as mentioned in the standard ASTM C778 (*31*) was used to prepare the mortar cubes. The binary and ternary paste systems contained cement binders, where 20% of the cement was replaced by fly ash(es) by weight. The water/binder ratio was selected according to the specified flow of the mortars, which was performed using a flow table according to ASTM C 1437 (*34*). While the flow of the control mix was determined with 242 ml of water, the water content of the paste systems was fixed to obtain a flow of control ± 5.

3.3.3 Heat of Hydration

The heat of hydration, which can be directly related to the rate of temperature rise inside the concrete, was measured in this study using an isothermal calorimeter.

3.3.3.1 Test setup. The calorimeter consists of a large stainless steel tank containing water at constant temperature (maintained at 21°C). An acrylic cylinder inside this steel tank, submerged in the water, contains a sample holder (sample can) within. The sample can contains the paste wrapped in a polythene bag. The sectional view of the calorimeter is shown in Figure 3.8.

The acrylic cylinder is seated on an aluminum heat sink and is bolted to it. An acrylic lid is attached to the upper flange of the cylinder. This is sealed using an 'O' ring, which makes the acrylic cylinder, water-tight. The lid is designed in such a way that it can be detached from the cylinder in order to facilitate the placement of the sample holder inside the acrylic cylinder.

Two sets of wires run through this acrylic lid, one of which connects the heater to the power supply and the other is a link between the data-logging equipment and the heat sensors. The lid is equipped with two male-female wire connectors, which facilitate the complete detachment of the lid with the acrylic cylinder.

The cylindrical sample can as shown in Figure 3.9 and Figure 3.10 is made from aluminum, has a very tight fitting lid, sealed with an "O" ring. It contains vegetable oil in measured quantities, to distribute the heat to the heaters uniformly. A thin aluminum plate is fitted on the aluminum lid, which has a small electrical heater attached on its underside. This electrical heater is used for the calibration of the equipment. Two electrical wires extending from this heater are connected to a two pin female socket mounted on the lid. These wires

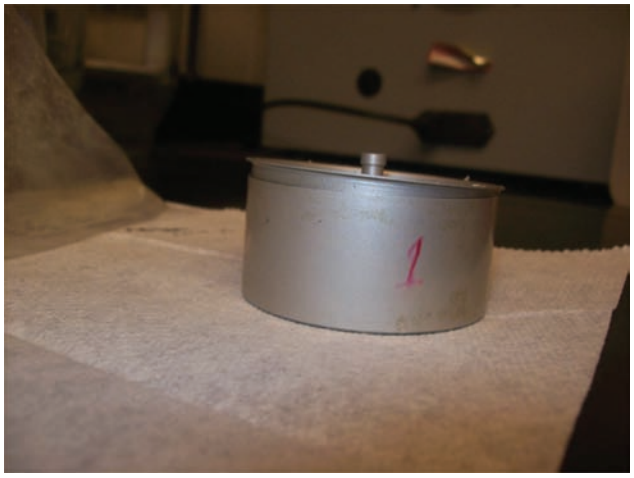

Figure 3.9 The aluminum sample holder closed with the lid.

Figure 3.10 Sample holder filled with oil and the lid on which the heater is mounted.

are used to supply power to the electrical heater on the aluminum plate. The sample holder is allowed to take up to 60 grams of sample weight however; the compensating ring around the sample holder is designed to match a sample weight of 30 grams.

The sample holder sits on electrical heat sensors, around which a compensating ring is placed concentrically. This ring is used to absorb all the heat generated inside by the sample. This compensating ring also sits on a set of four heat sensors, which detect the amount of heat transferred to the ring from the sample can. The presence of the ring practically eliminates all the external factors, which affect the measured signal.

Polystyrene insulators are positioned inside the acrylic body of the calorimeter to minimize the thermal air movements. Figure 3.11 shows, the position of the insulators inside the acrylic cylinder.

The sides and the bottom of the steel tank are fitted with insulators, to prevent ant heat loss from the sample. The temperature of the water inside the tank is maintained by an inbuilt heating system in the bath.

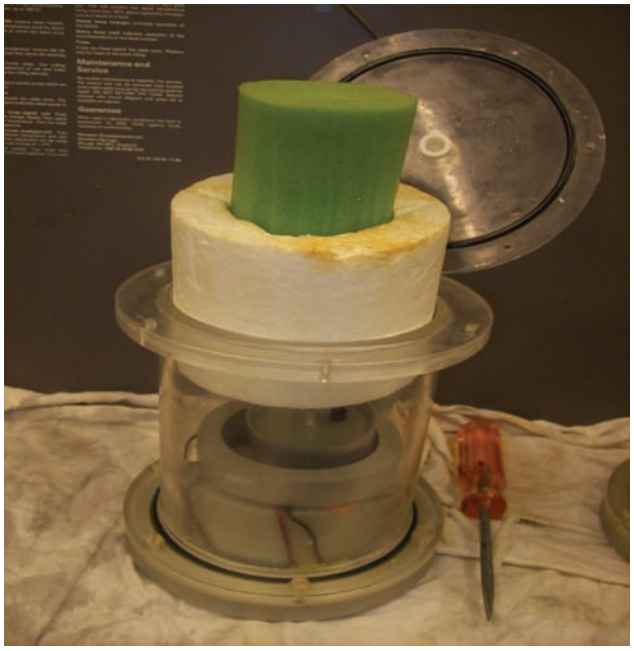

Figure 3.11 Insulators (polystyrene and sponge) inside the calorimeter.

However it relies on the water pumped from a reservoir bath (see Figure 3.12) placed next to it, through a heat exchanger, for its cooling.

A calorimeter interface module acts as a link between the calorimeter and the data logging equipment. The data from the calorimeter is collected using the data logger. This interface also has a control unit using which the heating of the sample for its calibration can be performed.

3.3.3.2 Experimental procedure. The heat of hydration experiments were performed on plain cement pastes (control), binary paste systems and ternary paste systems. The fly ash pastes were prepared by replacing 20% by weight of the cement by one fly ash (binary paste) or two different fly ashes at certain proportions (ternary pastes). All the pastes contained water at a constant water to binder ratio of 0.41. The experimental procedure is described below. All the pastes were mixed following the procedure recommended by the manufacturer of the calorimeter. The details of the procedure are provided below.

The control cement paste was prepared by taking 30 grams of cement powder in a plastic bag as shown in the Figure 3.13, which was dry-mixed by hand by constant grinding and shaking to break any lumps present. 12.3 ml of water was then directly added to the cement in the bag. The bag was then constantly shook and squished by hand until the color and texture of the paste was uniform. The bag was then folded into half, a knot was tied at the open end and the extra piece of the plastic bag was cut away. The final form of the paste in the bag, which is placed inside the calorimeter, is shown in the Figure 3.14.

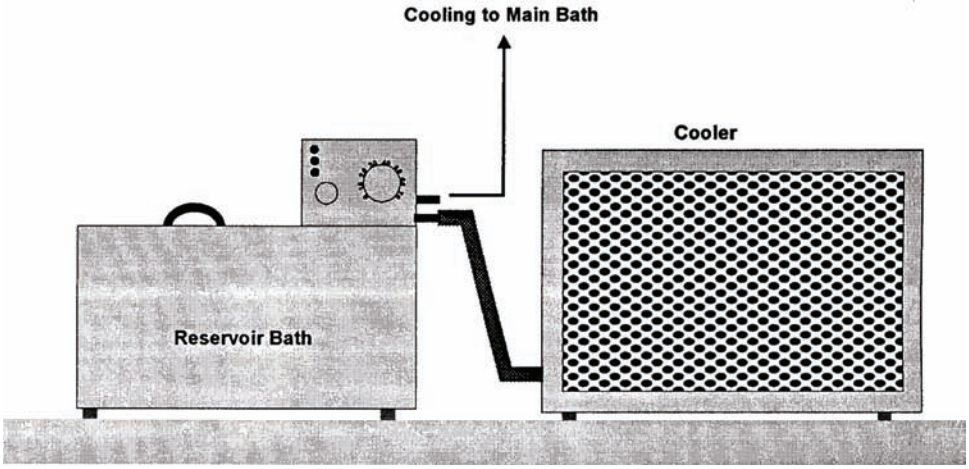

Figure 3.12 Cooling system and the reservoir bath of cold water in the calorimeter (*35*).

Figure 3.13 Dry powders taken in a plastic bag.

Figure 3.14 Folded plastic bag with a knot, to be placed inside the sample holder.

In the case of fly ash pastes, 24 grams of cement and 6 grams of fly ash(es) powder were taken in a plastic bag and were dry-mixed by hand, until the color appeared uniform. 12.3 ml of water was then added to the sample, the paste was mixed by shaking, and squishing until the color and texture of the paste was uniform.

The plastic bag containing the paste was then wrapped around the aluminum plate fixed on the lid of the sample can, inside the sample can (Figure 3.15). This plate was attached to the lid of an aluminum sample holder. The lid with the attached plate was then placed carefully on the sample holder without spilling the oil inside the sample holder. The sample holder was placed inside the ceramic container containing the heat sensors inside it, and was wrapped with polystyrene and sponge. The ceramic container was placed in a water bath maintained at a constant temperature of 21°C using a thermostat.

The data was acquired in terms of the resulting voltage change, which can be recalculated into the

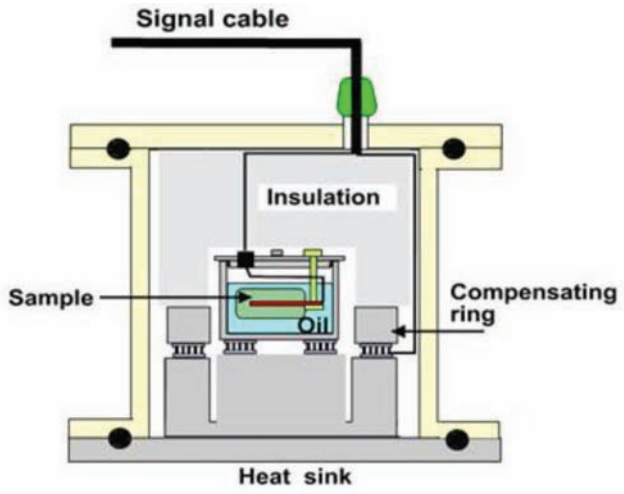

Figure 3.15 Plastic bag with paste folded inside the sample can (*35*).

amount of released energy in Joules (see Section 5.3.2). The calibration of equipment was done after testing every sample where heat is supplied to the sample and the resultant increase in the voltage is noted.

The data was collected using a CR10-X data-logger system at 30-second intervals. A graph (calorimeter curve) was plotted between energy released per unit time per unit mass (mW/g) against time for all the pastes.

3.3.3.3 Variables of the heat of hydration curve

3.3.3.3.1 Peak heat of hydration. The peak heat of hydration was directly read off from the calorimeter curve in terms of the energy released per unit time per unit mass (mW/g). This does not include the initial rapid evolution of heat, as it is practically not possible to measure all the heat evolved in the initial stages when the testing apparatus is being setup.

3.3.3.3.2 Time of occurrence of peak heat of hydration. The time of the occurrence of the peak heat of hydration (in minutes) was also read off from the calorimeter curve.

3.3.3.3.3 Total heat of hydration. The total heat of hydration after 3 days (4320 minutes) in terms of Joules was calculated by finding the area under the calorimeter curve. This period was selected for the total heat evolution as the heat released after 3 days is relatively insignificant and is constant for all the pastes. In the measurement of the total heat of hydration, the first 60 minutes where there is an abrupt increase in the heat of hydration was not considered. This was assumed, as the initial part of the calorimeter curve cannot be completely captured due to the time lag between the time of contact of water with the binder and the time at which the heat measurements commence.

3.3.4 Thermo-Gravimetric Analysis (TGA)

The amount of calcium hydroxide formed and the non-evaporable water content in a hydration reaction were measured using thermo-gravimetric analysis. The test is based on the fact that, calcium hydroxide when heated to a certain temperature decomposes into calcium oxide and water which when evaporates reflects in a reduction of the mass of the sample. The amount of non-evaporable water was also found out by this technique. The procedure for the estimation of the non-evaporable water content was developed by Barneyback (*36*) and is currently used here.

The sample was prepared by hand mixing, where 20% of the cement by weight was replaced by fly ash. The powders were initially dry mixed while breaking any lumps in them, until the powder looks uniform in color. Water was then added to the binder at a ratio 0.41, and then mixed with a glass rod for about 3 minutes. The sample was then covered with a plastic sheet to avoid any losses due to evaporation. The sample was then cured until the age of testing, by keeping it constantly submerged under water.

A piece of the sample was then ground using a mortar and pestle to a size finer than 200 microns. A sample size about 40 $\pm$ 4 mg was then ignited to 1000°C at a rate of 10°C per minute.

The data was then processed to obtain the results of the amount of non-evaporable water, calcium hydroxide content, calcium carbonate content and loss on ignition by percentage weight of the ignited sample.

3.3.4.1 Amount of non-evaporable water. The amount of non-evaporable water in the binary and ternary paste systems at various ages (1, 3, 7 and 28 days) were found as a percentage of the ignited weight of the sample. This was done by igniting the sample to 1000°C and measuring the weight loss between 105°C and 1000°C.

3.3.4.2 Amount of calcium hydroxide. The amount of calcium hydroxide formed during the hydration process of binary and ternary paste systems was found as a percentage of the ignited sample weight at different ages (1, 3, 7 and 28 days). This was done by measuring the weight loss of the sample between 450°C and 580°C. In addition, the carbonation of the sample was also taken into account by measuring the amount of calcium carbonate formed. This was done by measuring the weight loss of the sample between 580°C and approximately 800°C. This amount of calcium carbonate was stoichiometrically converted into the calcium hydroxide according to the following equation.

$$Ca(OH)_2 + CO_2 \rightarrow CaCO_3 + H_2O \quad (4)$$

4. RESULTS OF FLY ASH CHARACTERIZATION

As mentioned in Sections 3.1 and 3.2, twenty different fly ashes were characterized for their physical and chemical characteristics. All physical and chemical characteristics of each of the fly ashes, along with their X-ray diffraction patterns and the scanning electron microscopy images are provided in the *Fly Ash Handbook* (FAH) available as a supplemental file at https://doi.org/10.5703/1288284315213. An example of these summaries (one for Class C fly ash and one for Class F fly ash) are provided in Appendix C.

4.1 Results of Physical and Chemical Characteristics of Fly Ash

A summary of all physical and chemical characteristics of the fly ashes obtained from their testing in the laboratory (Boral Material Technologies Inc.) is provided in Table 4.1 for Class C ashes and Table 4.2 for Class F ashes.

The standard chemical and physical characteristics listed in these tables include, Silicon dioxide content (SiO_2)%, Aluminum oxide content (Al_2O_3)%, Iron oxide content (Fe_2O_3)%, Sum of SiO_2, Al_2O_3 and Fe_2O_3 (SAF)%, Calcium oxide (CaO)%, Magnesium oxide (MgO)%, Sulfur trioxide (SO_3)%, Sodium oxide

TABLE 4.1
Physical and chemical characteristics of Class C fly ashes.

Source Plant	Baldwin	Edwards	Hennepin	Joliet	Joppa	Kenosha	Labadie	Miller	Rush Island	Rockport	Schahfer	Vermilion	Will County
SiO_2, %	35.06	33.15	40.36	32.12	35.75	37.78	37.03	36.38	34.23	43.65	41.90	39.13	32.30
Al_2O_3, %	19.39	19.21	19.38	17.88	18.01	20.11	19.28	18.74	16.91	21.76	19.32	18.77	18.55
Fe_2O_3, %	6.25	10.11	5.91	6.41	6.36	5.87	6.46	6.03	6.86	6.58	6.76	6.19	6.47
SAF, %	60.70	62.47	65.65	56.41	60.12	63.76	62.77	61.15	58.00	71.99	67.98	64.09	57.32
CaO, %	25.23	24.28	21.80	26.98	26.23	23.35	24.26	24.62	27.66	16.98	20.29	23.92	26.97
MgO, %	5.90	4.92	4.93	5.83	5.01	5.52	4.86	5.64	5.51	3.55	4.29	4.55	5.78
SO_3, %	1.55	2.73	1.43	2.45	1.72	1.11	2.13	1.97	2.40	0.98	1.42	1.40	2.61
Na_2O, %	1.93	1.38	1.57	3.70	1.99	1.80	1.54	1.73	2.02	1.24	1.35	1.50	2.82
K_2O, %	0.47	0.38	0.64	0.34	0.49	0.58	0.61	0.53	0.36	1.28	0.73	0.62	0.37
Alkalies (as Na_2O), %	2.24	1.63	1.99	3.92	2.31	2.18	1.94	2.08	2.26	2.08	1.83	1.91	3.06
LOI, %	0.49	0.43	0.61	0.49	0.35	0.38	0.25	0.44	0.17	0.90	0.44	0.43	0.35
meansize, μm	21.99	15.08	16.88	14.48	18.37	17.35	16.69	24.93	20.77	32.2	18.89	13.85	14.85
Blaines, cm^2/g	6102	7306	5125	5356	4371	4452	6269	4851	5924	4354	6428	5536	5907
Spsurface, cm^2/g	15492	22075	16457	19776	17597	16577	16503	17089	17477	11963	14679	17928	19646
Magnetic particles, %	0.00	3.34	0.07	0.00	0.31	0.00	2.89	0.00	0.00	3.50	2.7	0.12	0.00
Glass, ratio	1.28	1.694	1.309	1	1.286	1.355	1.64	1.13	1.077	1.54	1.656	1.298	1.292
Total, %	95.78	96.16	96.02	95.71	95.56	96.12	96.17	95.64	95.95	96.02	96.06	96.08	95.87

(Na_2O)%, Potassium oxide (K_2O)%, Total alkalis as Na_2O%, Loss on ignition%, Mean particle size (Mean size) μm, Blaine's fineness (Blaines) cm^2/g and Specific surface area using laser particle size analyzer (LPSA Specific surface) cm^2/g. The tables also include the Glass content (expressed as a ratio of the area under the hump of the fly ash to the area under the hump of the fly ash having the lowest area, Joliet fly ash). These tables are shown in Table 4.1 and in Table 4.2.

The chemical composition of fly ashes shown in these tables was evaluated in the laboratory (Boral Material Technologies Inc.); however, there is a slight difference in the chemical composition reported from this laboratory analysis and the analysis reported by the individual fly ash suppliers (provided in the *Fly Ash Handbook* (FAH) which is available as a supplemental file at https://doi.org/10.5703/1288284315213.).

4.1.1 Summary of Chemical Characteristics and Glass Content in Fly Ashes

Among the 13 Class C fly ashes studied in this project, many but not all have very similar chemical compositions. The general compositional pattern can be described as follows:

(a) A combined content of silicon, aluminum and iron oxides was in the range of 56% to 65%. Two fly ashes have a relatively higher content of 68% and 72% (Schahfer and Rockport respectively). The fly ash Rockport was deemed to be Class C, even though the percentage of the sum of the oxides is higher than 70% as the sum of the oxide content reported by the fly ash supplier was less than 70% (see Appendix A). This fly ash might have been the only fly ash reported as an intermediate Class C fly ash (CI) according to the Canadian Standards.

(b) The iron oxide contents of almost all the Class C fly ashes varied very little from the typical content of 6% with one exception (Edwards, 10%).

(c) Typical CaO contents ranged from about 20% to 27% for most Class C fly ashes. However, CaO contents were found to be as low as 17% (Rockport) and as high as 28% (Rush Island).

(d) The contents of Na_2O were found to be between 1.2% to 2% for all the Class C fly ashes except for Joliet (3.7%) and Will County (2.82%). The content of K_2O typically falls into the range of 0.3% to 0.6% with exception of Rockport with a content of about 1.3%. For all the Class C fly ashes, both alkalis turn out to be almost complete insoluble.

(e) The sulfate contents of Class C fly ashes appear to be not very high, with the highest value being 2.7% (Edwards) and the lowest 1.0% (Rockport). The maximum allowable sulfate value according to ASTM C 618 (*2*) is 5% for Class C fly ash.

(f) The contents of MgO appeared in the normal range of 4% to 6% for all the Class C fly ashes, although the 3.5% MgO content of Rockport fly ash seemed low for a Class C fly ash.

(g) The values for loss on ignition of almost all the Class C fly ashes were typically below 0.5% or a little higher (0.61% for Hennepin), except only one case which was quite high for a Class C fly ash (0.90% for Rockport).

TABLE 4.2
Physical and chemical characteristics of Class F fly ashes.

Source Plant	Elmersmith	Miami 7	Miami 8	Mill Creek	Petersburg	Trimble	Zimmer
SiO_2, %	41.60	55.89	55.52	47.48	43.82	46.91	38.66
Al_2O_3, %	17.74	29.45	26.02	19.99	21.74	21.08	18.96
Fe_2O_3, %	22.02	4.96	4.62	18.52	25.29	19.90	24.90
SAF, %	81.36	90.30	86.16	85.99	90.85	87.89	82.52
CaO, %	9.31	1.25	3.98	5.42	1.86	2.50	4.94
MgO, %	0.90	0.85	1.44	1.05	0.88	0.86	4.81
SO_3, %	1.71	0.21	0.45	1.12	0.54	0.99	3.07
Na_2O, %	0.80	0.36	0.88	0.60	0.67	0.73	0.44
K_2O, %	2.31	2.79	2.54	2.97	2.46	1.97	1.52
Alkalies (as Na_2O), %	2.32	2.20	2.55	2.55	2.29	2.03	1.44
LOI, %	2.37	2.31	2.43	1.38	1.39	1.89	1.48
meansize, μm	33.24	30.41	31.58	26.35	28.37	27.35	26.1
Blaines, cm^2/g	3092	4088	3600	3739	2391	3253.00	3782
Spsurface, cm^2/g	6344	12592	13012	10295	9849	8857.00	11308
Magnetic particles, %	32.99	3.68	4.18	24.90	37.72	26.39	35.32
Glass, ratio	1.476	2.881	2.485	1.517	1.488	2.13	1.4
Total, %	96.39	95.76	95.45	97.15	97.26	94.94	97.30

(h) Typical glass ratios for all the Class C fly ashes were ranging from 1 to 1.694. There were no unusual values in any of the fly ashes

The seven Class F fly ashes also appeared to share some common chemical composition characteristics although again, several exceptions were present. The values were quite distinct from those of the Class C ashes. Compositions for Class F fly ashes studied here are summarized as follows:

(a) The combined content of silicon, aluminum and iron oxides ranged from 81% to 91%. According to ASTM C 618 (*2*), the Class F fly ash requirement for combined silicon, aluminum and iron oxides was not less than 70%.
(b) With respect to iron oxide content, 5 out of the 7 Class F fly ashes had iron oxide contents within the range of 18% to 25%. However, the other 2 Class F fly ashes (Miami 7 and Miami 8, both from the same plant, showed much lower contents of iron oxide, both close to 5%. These two fly ashes had relatively high contents of silica (about 56%) and aluminum oxide (29% for Miami 7 and 26% for Miami 8, compared to the typical content of around 20% for Class F fly ashes in this study).
(c) The CaO contents appeared reasonable for almost all Class F fly ashes here except for Elmersmith, for which the CaO content was 9%. This CaO content is considered rather high for a Class F fly ash. The XRD pattern for this fly ash includes a clear peak for CaO, which is not common in Class F fly ashes.
(d) The combined alkali contents seem consistent for almost all the Class F fly ashes in this study. The only exception was Zimmer, with a relatively low content of 1.4% compared to a typical alkali content of around 2.3%.
(e) Contrary to alkali contents, the sulfate contents of different Class F fly ashes varied over a broad range. A single fly ash, Zimmer had an unusually high content (3.1%), the while others were below 1.7%. The lowest sulfate content was 0.21%, for Miami 7.
(f) The contents of MgO appeared to be consistently around 0.9% for almost all the Class F fly ashes with a single exception. Similar to the sulfate content, the magnesium content of Zimmer was far higher than usual, 4.8% compared to 0.9% for other Class F fly ashes studied here.
(g) The loss on ignition values of all the Class F fly ashes in this study ranged between 1.4% and 2.4%.
(h) The glass ratios for all the Class F ashes ranged from 1.4 to 2.881, and were typically higher than the ratios observed in Class C ashes (~1.0–1.7). Two of the ashes, Miami 7 and Miami 8, a glass ratio substantially higher than the rest of the Class F fly ashes (2.9 and 2.5 respectively).

4.1.2 Summary of the Physical Characteristics of Fly Ashes

The particle size distribution (PSD) curves for Class C and Class F fly ashes in this study were characteristically different from each other. Figure 4.1 shows the particle size distribution curves for a set of three typical Class C fly ashes and a set of three typical Class F ashes (as indicated on the graph). It can be clearly observed that the two different classes of ashes form a band of PSDs within their classes.

For Class C fly ashes, the percentage of particles smaller than 1 μm was typically less than 5%. The mean particle size for the Class C ashes ranged from 15 to 22 μm, with two exceptions of 32.2 μm for Rockport and 25 μm for Miller. The specific surface area evaluated using Blaine's method, ranged between 4000 cm^2/g and 7000 cm^2/g.

For Class F fly ashes, the percentage of particles smaller than 1 μm appeared to be slightly less than those for Class C fly ashes, approximately 2% for all Class F fly ashes. The mean particle size for the Class F fly ashes was 30 $\pm$ 4 μm. The higher mean particle size was translated into a higher specific surface are in Class F ashes, which ranged approximately from 2000 cm^2/g to 4000 cm^2/g.

To sum up, it appeared that the fly ashes were consistent in their physical properties within their own class. The Class C ashes were significantly finer than the Class F ashes.

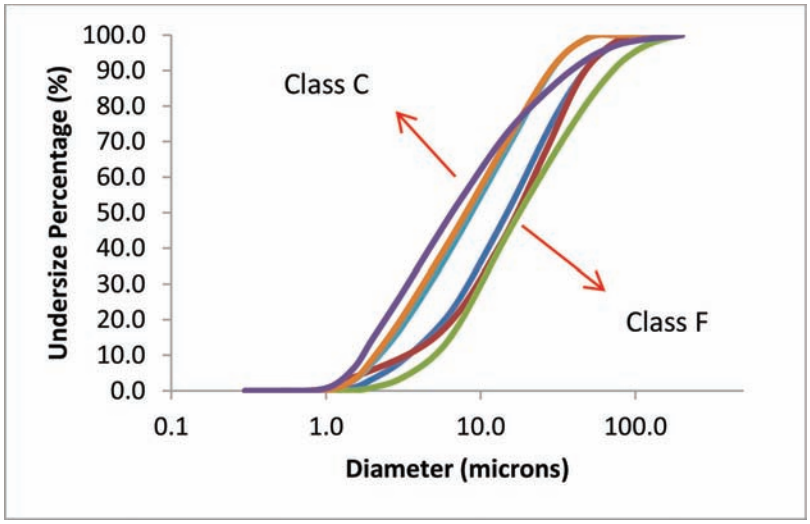

Figure 4.1 Particle size distribution for Class C and Class F ashes.

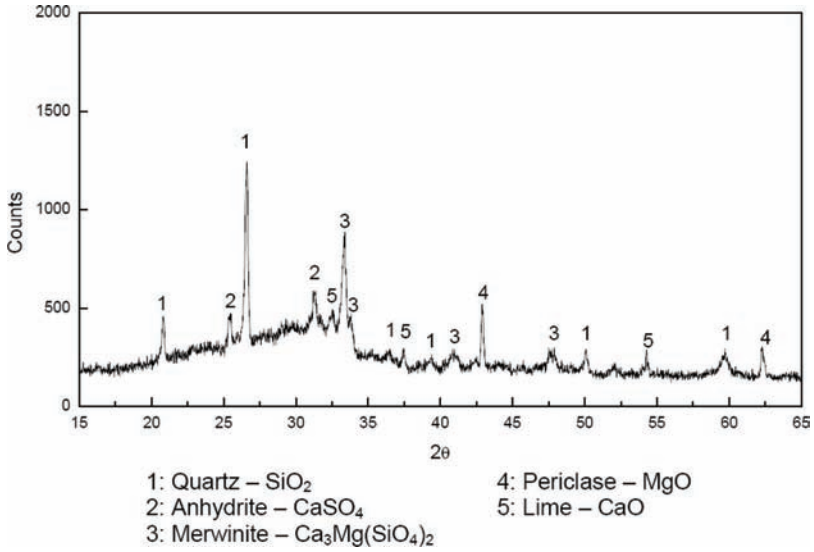

Figure 4.2 Typical XRD curve for Class C fly ash (Baldwin).

4.2 Summary of the X-ray Diffraction Patterns for Fly Ashes

A typical X-ray diffraction curve for Class C ashes (Baldwin) is shown in Figure 4.2. Two different patterns (typical pattern, five out of seven and exception pattern, two out of seven) were observed within Class F ashes (shown in Figure 4.3 and Figure 4.4 respectively).

As can be seen from the above figures, the crystalline components studied in Class C and Class F fly ashes were different from each other, but most of them shared common characteristics within their classification. Typically, Class C ashes contained quartz, anhydrite, merwinite, periclase and lime, while typical Class F ashes contained quartz, anhydrite, mullite, magnetite, hematite and lime. Two of the Class F fly ashes, which were both obtained from the same coal plant (Miami 7 and Miami 8), were found to contain lesser number of crystalline components (quartz and mullite only) as compared to the rest of the Class F ashes. These two fly ashes were seen to contain lower amount of magnetic particles as compared to the rest of the Class F fly ashes and slightly higher amount of particles as compared to Class C fly ashes.

The X-ray diffraction patterns for all the fly ashes are presented in the *Fly Ash Handbook* (FAH) which is available as a supplemental file at https://doi.org/10.5703/1288284315213.

4.3 Summary of the Morphological Characteristics of Fly Ashes

Figure 4.5, Figure 4.6, Figure 4.7 and Figure 4.8 show the SEM micrographs of typical Class C ashes. There were wide ranges of sizes of spherical particles found in Class C ashes. Many of these spherical particles were found to be

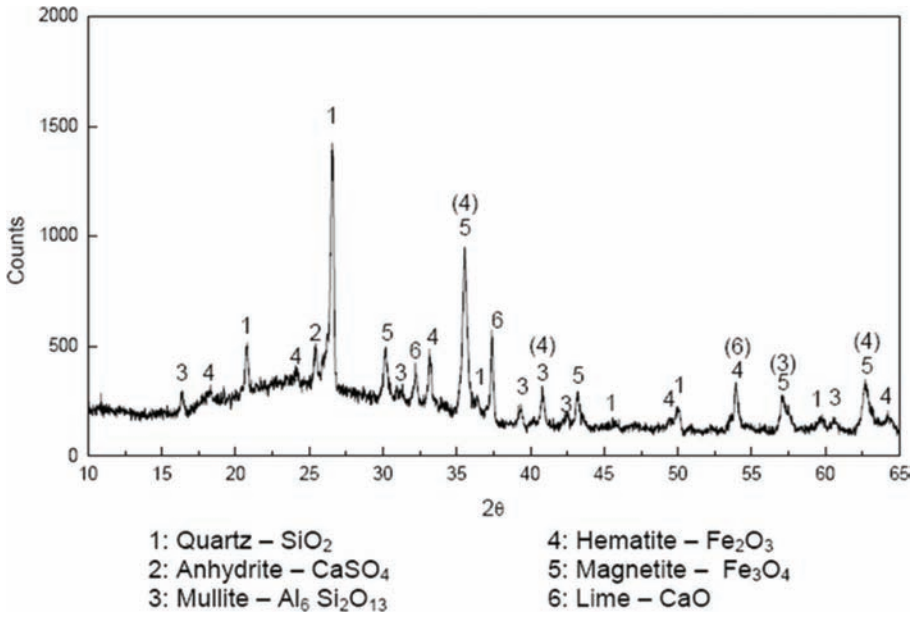

Figure 4.3 Typical XRD pattern for Class F fly ash (Elmersmith).

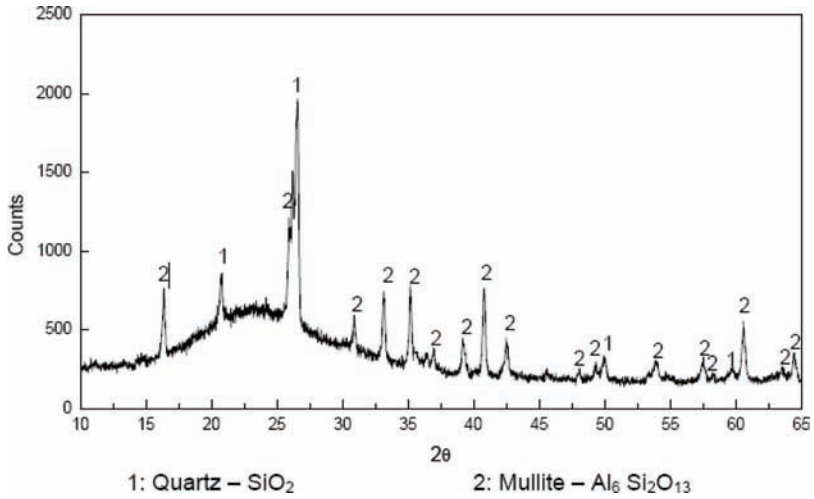

Figure 4.4 XRD pattern (exception) for Class F fly ash (Miami 7).

hollow. The hollow shells mainly were composed of silica and alumina as examined using EDX. Quite a few irregularly shaped particles were also seen, which predominantly were composed of sulfates, magnesium or sodium.

Figure 4.9, Figure 4.10, Figure 4.11 and Figure 4.12 show the SEM micrographs of typical Class F ashes. There was a large variation in the sizes of spherical particles found in Class F ashes. Many of these spherical particles were found to be hollow. There were also a few rugged particles found in these ashes. These rugged particles were mainly composed of magnetic particles. Quite a few irregularly shaped particles were also seen, which predominantly were the unburnt carbon particles. A higher number of unburnt carbon particles were seen in these SEM pictures as compared to Class C ashes, which is consistent with the higher LOI values for Class F ashes.

A set of typical micrographs at various magnifications were provided for each of the twenty fly ashes in the *Fly Ash Handbook* (FAH) which is available as a separate file at https://doi.org/10.5703/1288284315213.

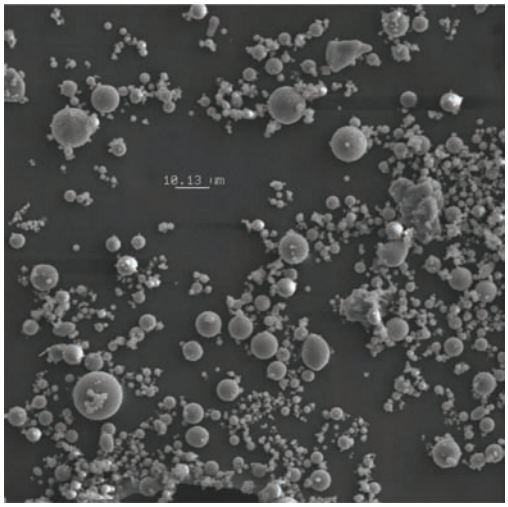

Figure 4.5 SEM micrograph of Labadie fly ash at a magnification of 600x.

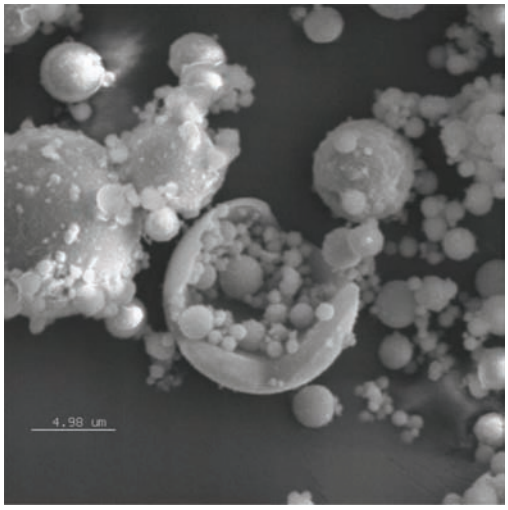

Figure 4.6 SEM micrograph of Kenosha fly ash at a magnification of 2000x.

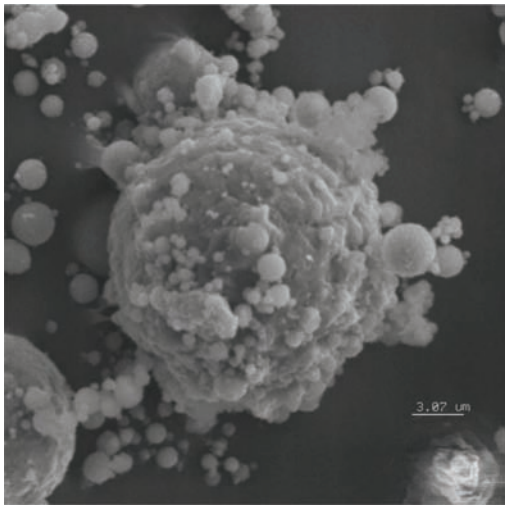

Figure 4.7 SEM micrograph of Will County fly ash at a magnification of 2000x.

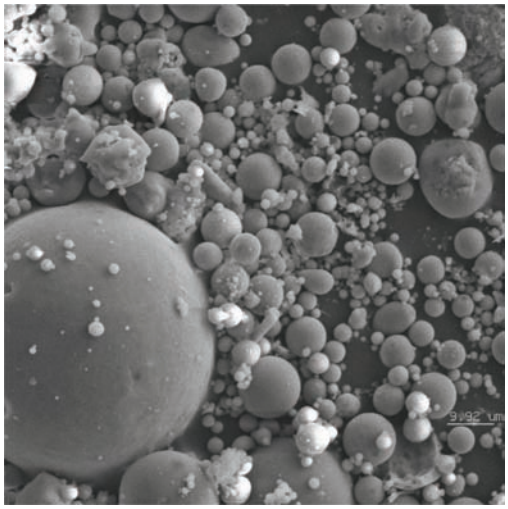

Figure 4.8 SEM micrograph of Rush Island fly ash at a magnification of 600x.

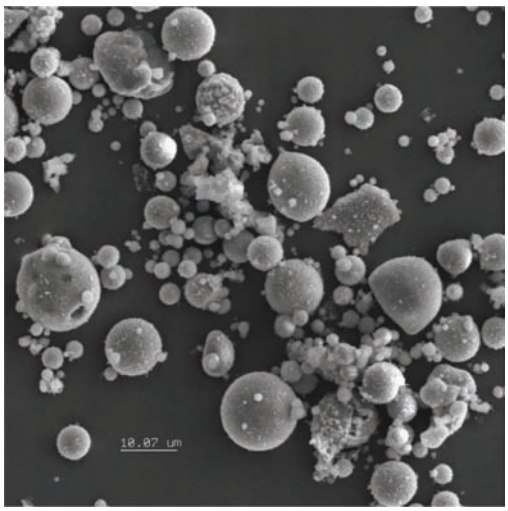

Figure 4.9 SEM micrograph of Zimmer fly ash at a magnification of 600x.

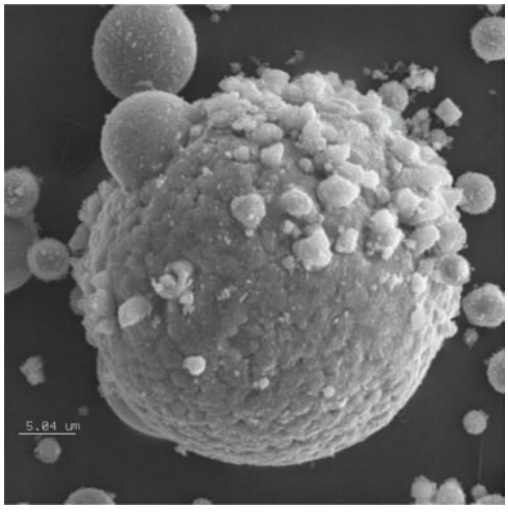

Figure 4.10 SEM micrograph of Elmersmith fly ash at a magnification of 1000x.

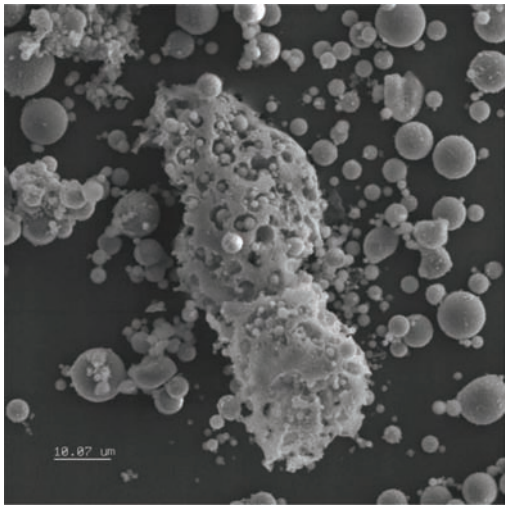

Figure 4.11 SEM micrograph of Petersburg fly ash at a magnification of 600x.

Figure 4.12 SEM micrograph of Mill Creek fly ash at a magnification of 2000x.

5. STATISTICAL ANALYSIS OF LABORATORY RESULTS FOR BINARY PASTE SYSTEMS

5.1 Selection of Statistical Parameters

This section describes the basis for selection of parameters used in statistical analysis of the properties of binary paste systems consisting of Type I portland cement and one fly ash. These binary cement + fly ash pastes will from now on be referred to as fly ash pastes.

In total, thirteen Class C fly ash pastes and seven Class F fly ash pastes were prepared. In addition, plain cement paste was also prepared and used as a reference material. All pastes were tested for the following properties: the initial set time, the rate of strength gain, the heat of hydration, the non-evaporable water content at various ages and the calcium hydroxide content at various ages. The details of the procedures used have been previously described in Chapter 3. All the test results were statistically analyzed and modeled using "Statistical Analysis Software" (SAS).

Linear regression models were built based on the variables, which yielded the best fit. The parameter chosen to explain the fit of the model was "Adjusted R^2". The motivation behind choosing this parameter over the usual parameter, R^2 is explained following the brief description of these two parameters (R^2 and adjusted R^2) in the following sections, Section 5.1.1 and Section 5.1.2, respectively.

5.1.1 R-Square (R^2)

The term R^2, also known as the coefficient of determination, is used to indicate the goodness of fit of statistical models, which are used to predict the outcomes from a given set of variables. In that sense, R^2 represents the amount of variability in the data set accounted for by the model. It other words, R^2 is a measure of how accurate the models predictions are. The value of R^2 lies between 0 and 1. The most generalized mathematical definition of this parameter is

$$R^2 = 1 - \frac{SS_{err}}{SS_{total}} \quad (5)$$

where, R^2 is the coefficient of determination

SS_{err} is the error sum of squares $= \sum_i (y_i - \hat{y})^2$

SS_{total} is the total sum of squares $= \sum_i (y_i - f_j)^2$

The data used to calculate R^2 consists of several values of the dependent variable (y_i), each of which has a corresponding predicted value of f_i. The symbol $\hat{y}$ represents the mean of all the observations.

Increasing the number of variables in the regression model can only increase the value of R^2 because an increase in the number of independent variables reduces the term SS_{err} while for a given set of responses the SS_{total} will always remain the same.

However, a few words of caution are always mentioned when R^2 is used to explain the variability in the model. The most significant drawback of using this parameter is that, R^2 does not point out if the independent variables are the true cause of the changes in the dependent variables. It also does not readily indicate existence of possible transformations, which can be used in order to improve the predictability of the model. One way to tackle the above-mentioned shortcomings is to use the so-called statistic "Adjusted R^2".

5.1.2 Adjusted R^2 (adj-R^2)

Since all the physical and chemical characteristics of fly ashes used in the models as independent variables, their number was relatively high (ten) and close to the number of data points (13 for Class C and 7 for Class F). As the number of independent variables in the model starts to approach the number of data points, the percentage of variation explained (accounted for) by the model increases. However, this does not mean that the predictability of the model is also increasing. In fact,

regression models in which the number of independent variables is close to the number of data points usually have a very high R^2 but a very low significance (p-value). To counteract the negative effects of the increased number of variables on the significance of the model, another statistic, "adjusted R^2", is used. The mathematical definition of this parameter is

$$\text{adj} - R^2 = 1 - \frac{SS_{err}(df_{total})}{SS_{total}(df_{error})} \quad (6)$$

where, df_{total} is the total degrees of freedom of the model and

df_{error} is the error degrees of freedom of the model

The adj-R^2 parameter can be interpreted as the amount of useful information added to the model by the inclusion of an additional variable. However, it is to be noted that adj-R^2 is never better than R^2; they can at the most be equal. The addition of an extra independent variable to the model could only render a higher or the same R^2 for the model but never a smaller R^2. However, this can also lead to a decrease in the adj-R^2, if the added variable does not statistically contribute to the prediction of the outcome. Thus, adj-R^2 can effectively be used to justify the inclusion of an additional variable in the regression model.

Hence, in the course of the modeling process employed in this study, the adj-R^2 parameter was used to select the "best model". In this context, the "best model" is to be interpreted as the model containing the set of independent variables that affect the dependent variable; the most (see Section 5.2). It should be mentioned that the variables used in the models were not selected based on the adj-R^2 alone; rather the theoretical significance of the inclusion of the variables in the models was also considered.

5.1.3 p-Value

This parameter is defined as the probability of obtaining a result at least as extreme as the one that was actually observed, assuming the null hypothesis is true. The lower the p-value, the less likely the result is and hence it is more statistically significant. The result of a test of significance is either a statistically "significant result" or a "not significant result".

In the current modeling process, the p-value for the model and the individual variables was assumed as 0.1, thus corresponding to a 10% chance of an outcome, that extreme, given a null hypothesis (*37*).

5.2 Procedure for Statistical Modeling

Statistical linear regression models were built for the properties (dependent variables) of binary binder systems, in order to predict these properties for any fly ash (similar to those used in the study) based on the fly ash's fundamental physical and chemical characteristics. The fundamental characteristics on which the models were built (independent variables) are listed in Table 5.1. This table also lists the abbreviations used to label these variables in the models.

The selected independent variables were all known to play a role in the outcome of the dependent variables and the effects are mentioned in Chapter 2.

Separate experimental designs and modeling procedures were adopted respectively for the binary and the ternary paste systems. This is because the number of data points (cement + fly ash, binary combinations) available for the binary models was 20 (13 Class C ashes and 7 Class F ashes), whereas the number of data points (cement + fly ash + fly ash, ternary combinations) or the number of possible combinations of fly ashes in ternary paste systems were 180 (number of combinations of choosing two fly ashes out of twenty when the proportion of the two chosen ashes is a constant, is $20C_2 = 180$). Performing the number of experiments for as many combinations of ternary binder systems is not practically feasible. Hence, a different experimental design (fractional factorial design) was used which allowed to reduce the number of experiments in the ternary systems to nine.

The aim of the modeling process was to use statistical linear regression analysis to identify the best set of independent variables, which affect a dependent variable (property of the binder) of both binary and ternary paste systems, the most.

The modeling process was not a straightforward linear regression analysis, as it was assumed that the single model to predict the properties for the entire suite of fly ashes might not be feasible. The reasons are as follows.

1. The set of fly ashes used in the study contain two different kinds of ashes, ASTM Class C ashes and ASTM Class F ashes. The ashes were markedly different in their fundamental physical and chemical compositions and hence, it is likely that their behavior in concrete might be different.
2. The available number of data points for modeling the set of ashes is similar to the number of independent (predictor) variables available to explain the variations in the dependent variables. More so, the number of predictor variables is greater than the number of data points available for Class F ashes.

To counteract the above two challenges, the following modeling methodology was adopted.

A linear regression analysis was performed on the dependent variables using Statistical Analysis Software (SAS), which included all the twenty data points. The "best set of variables" (which constitute the "best model") found to affect the dependent variable was chosen based on the highest adj-R^2 of the models. All the data points were in turn predicted using the same models (using the same "best set of variables") built for the dependent variable for the thirteen data points of Class C ashes and seven data points of Class F ashes separately. A plot of the observed and the predicted data values, each for the results obtained for all the data points of Class C and Class F ashes was

plotted. If the prediction of the observed points is accurate, the points on this graph lie close to the 45° line drawn from the origin. The above-mentioned technique is clearly described in the form of a flow chart, Figure 5.1. The trustworthiness of the predictions can be evaluated by using the p-value of the model. Nevertheless, all the regression models were tested by obtaining the dependent variable data for new fly ashes and were validated.

The number and set of variables used to predict the dependent variables (model containing the "best set of variables," referred to as the "best model") were kept the same for the models of both the classes and at three (with a maximum of four in special cases) for the following reasons.

1. As the number of data points in the models was small (13 for Class C ashes and 7 for Class F ashes), an increase

TABLE 5.1
Independent variables used in the modeling process and their abbreviations.

	Variables	Abbreviations
Physical Properties	Mean particle size	meansize
	Specific surface area measured using Blaine's apparatus	blaines
	Specific surface area measured using laser particle size analyzer	spsurface
Chemical Properties	Calcium oxide content	cao
	Sum of silicon, aluminum and iron oxide contents	SAF
	Magnesium oxide content	mgo
	Aluminum oxide content	alumina
	Sulfate content	sulfate
Physico-chemical Properties	Loss on ignition	carbon
	Glass content measured using X-ray diffraction	glass

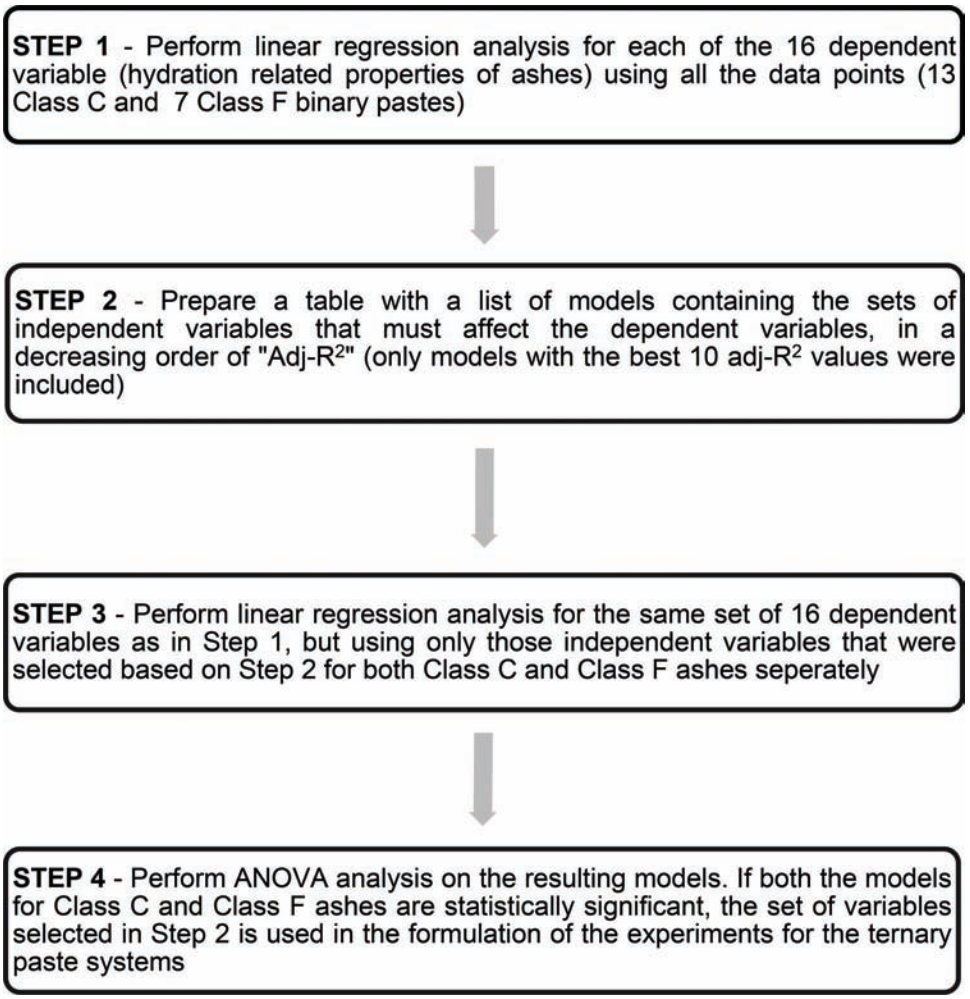

Figure 5.1 Flowchart depicting the statistical analysis procedure.

in the number of variables used to describe the variation in the dependent variable would lead to a good fit in the data, but an insignificant model. This would reflect in the ability of the model to predict the dependent variable for a new fly ash, which was not used as a data point in the modeling process.

2. The same set of variables were adopted in the models used to predict the dependent variables in both Class C and Class F ashes because the models which were used to predict the properties of the ternary paste systems are based on a linear relationship between the two binary paste models. In addition, the experimental design for modeling the ternary paste systems (see Chapter 6) involves the use of the variables used in binary paste regression models.
3. An increase in the number of variables used to predict the properties usually leads to

    i. A larger number of experiments, which need to be performed for the ternary paste systems based on the experimental design.
    ii. The added variable being rendered insignificant compared to the original set of variables.

The statistical modeling of various properties (dependent variables) of binary paste systems is explained in the following sections. The analysis of the data includes a table containing the sets of variables of linear regression models, sorted in terms of adjusted R^2, and the chosen model with three/four independent variables is highlighted (if present). A table with the predictions of the original data points is included along with a graph showing the deviations of the predictions from the observed values.

5.3 Analysis of Results for the Dependent Variables

From here on in Chapter 5, the property of a fly ash refers to the property of binary paste prepared using cement, of which 20% by weight is replaced by the fly ash.

5.3.1 Initial Time of Set

The initial time of setting has been determined for all the binary paste systems containing cement and a fly ash using the Vicat needle test as explained in Section 3.3.1. The initial setting time of the fly ash-cement binders will be referred to as the setting time of the fly ash or ash from here on. Table 5.2 has the complete list of the initial setting times of all the ashes classified in an increasing order of the setting time. The water required for consistency is also mentioned along with the water to binder ratio. The water of consistency for all the ashes except the fly ash with the highest setting time (Joliet) was found to be lower than that of cement. The water for consistency for Class F ashes was found to be slightly higher than most of Class C ashes. However, no clear trends or differences were observed within the classes of ashes or between the classes. There was also no correlation observed between the water of consistency and the initial setting time. All the above-mentioned inferences can be clearly visualized in Figure 5.2. In addition, Figure 5.3 shows the setting time comparison of all the ashes.

In Figure 5.3, the first thirteen bars represent the time of set for the suite of Class C ashes, the next seven bars represent the time of set for Class F ashes and the last bar represents the setting time of the reference cement. The initial setting times of all the ashes was found to lie between 1 hour and 4.5 hours. This wide range was seen in Class C ashes whereas the setting times of the Class F ashes had a narrower range. Joliet, a Class C ash was found to have the highest setting time of 4.2 hours while Miller, another Class C ash was found to have the lowest setting time of 1.3 hours. The lowest setting time of Class F ashes was 2.5 hours, that of Mill Creek ash and the highest setting time of Class F ashes was that of Petersburg, 3.4 hours.

Eight of the 13 Class C ashes were found to have a lower setting time than the setting time of reference cement, while four of the remaining five Class C ashes had a higher setting time. One ash (Kenosha) was found to have a flash set.

Six out of the seven Class F ashes were found to have a setting time higher than the reference cement, while the setting time of the remaining one fly ash was marginally smaller than the reference cement.

It can be stated, that Class F ashes tend to delay the initial setting time, whereas Class C ashes could act either way, leading to an increase or a decrease in the setting time.

This suggests that there is a clear-cut difference in the behavior of the fly ash initial time of set based on the Class. As we know that fly ashes are differentiated into two classes based on their chemical composition (the sum of silicon, aluminum and iron oxides and the amount of sulfates), we can now expect at least a few of these variables to be present in the regression model for predicting the setting time of ashes.

5.3.1.1 Selection of variables for statistical modeling. Statistical linear regression models were built for the initial setting time of the binary paste systems using all data points given in Table 5.2 except the fly ash, which had a flash set (Kenosha) and the reference cement paste itself. The independent variables considered when constructing the regression models, are mentioned in Table 5.1. A SAS code was written, which investigated all the possible combinations of independent variables to construct the regression models. A template of the SAS code is given in Appendix B. The program uses all independent variables and the dependent variable (setting time). The output of the program consists of a table containing the list of combinations of independent variables forming linear regression models, sorted according to the adj-R^2 values. The values of the R^2 are also listed in the table for each model.

TABLE 5.2
Initial setting times and water of consistency of all the ashes.

Fly Ash	Consistency (ml)	Water/Binder	Setting Time (hrs)	Class
Miller	161.2	0.248	1.27	C
Schahfer	160.7	0.247	1.67	C
Hennepin	162	0.249	1.78	C
Joppa	156.9	0.241	2.23	C
Vermilion	159.7	0.246	2.23	C
Edward	165	0.254	2.27	C
Mill Creek	164.7	0.253	2.52	F
Will County	163.1	0.251	2.52	C
Rockport	164	0.252	2.54	C
Elmer Smith	167	0.257	2.86	F
Zimmer	165.2	0.254	0.25	F
Rush Island	163	0.251	3.06	C
Trimble	163.9	0.252	3.20	F
Miami # 7	167.7	0.258	3.30	F
Miami # 8	167.1	0.257	3.38	F
Petersburg	167.2	0.257	3.40	F
Baldwin	162.2	0.250	3.46	C
Labadie	165.8	0.255	3.80	C
Joliet	183	0.282	4.17	C
Kenosha	163.7	0.252	FLASH SET	C
Cement	172	0.265	2.73	—

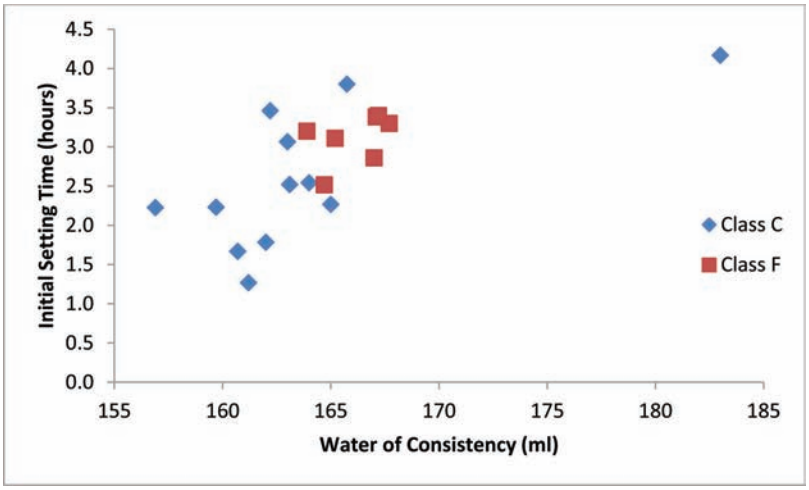

Figure 5.2 Setting time Vs consistency for all the fly ashes.

The best ten regression models based on adj-R^2 values for initial setting time are listed in Table 5.3.

It was observed that the R^2 and the adj-R^2 values for the regression models of setting time are low (maximum adjusted $R^2 = 0.2447$). The reasons for the low values of adj-R^2 lie in the measurement procedure of the setting time. The possible reasons are listed below.

1. It is possible that there are small lumps of cement of fly ash particles present in the paste, how much ever dry mixing of the binder was done, as the process is manual.
2. The mixing process using the Hobart mixer presents a range of issues, including in-homogeneity of the paste, if the paste is not properly scraped from the base of the mixer.
3. The above two reasons lead to a variation in the penetration measurements over the surface of the setting time sample, even at the same instant of measurement.
4. Setting time is calculated by linearly interpolating between times at penetrations before and after 25. This could lead to an additional error in the estimation of the setting time at the penetration of 25, as the rate of setting might not be constant over time.
5. The behavior of Class C and Class F ashes could be significantly different leading to a detrimental effect on the adj-R^2 for the model consisting of both the Classes of ashes.

The variables, which were selected in the regression model 1, the model with the highest adj-R^2, are sulfate content, alumina content and the glass content as

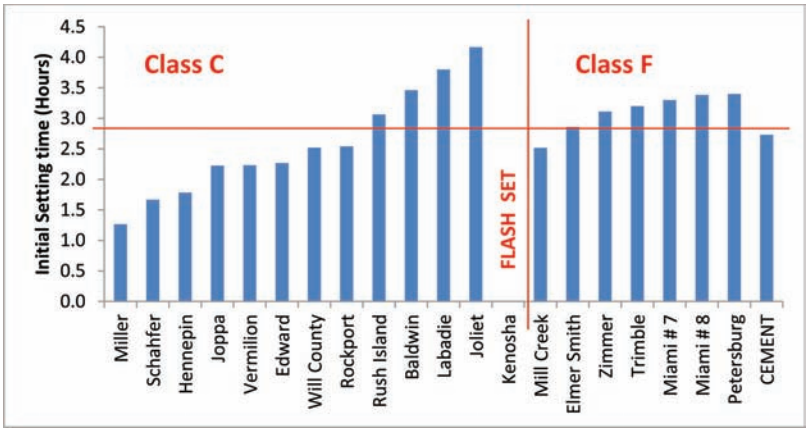

Figure 5.3 Initial setting times for all the binary paste systems along with the setting time of the reference cement paste.

TABLE 5.3
Best ten regression models for initial setting time.

Number of Variables in the Model	Adjusted R^2	R^2	Variables in the Model
3	0.2447	0.3706	sulfate, alumina, glass
5	0.2298	0.4437	sulfate, SAF , mgo, alumina, glass
2	0.223	0.3093	sulfate, alumina
7	0.2189	0.5226	spsurface, meansize, sulfate, carbon, SAF, alumina, glass
1	0.217	0.2605	sulfate
7	0.2099	0.5172	spsurface, meansize, sulfate, carbon, cao, alumina, glass
6	0.2095	0.473	spsurface, sulfate, SAF, mgo, alumina, glass
4	0.2089	0.3847	sulfate, SAF, mgo, alumina
2	0.2032	0.2917	sulfate, carbon
5	0.2008	0.4228	spsurface, sulfate, SAF, mgo, alumina

shown in Table 5.3. It was observed that the best model contained only three variables, which suggests that these are the factors having a maximum effect on the setting time. As we look into the other models with similar adj-R^2 in Table 5.3, the variables sulfate and alumina are recurring in all the models and hence it can be inferred that the variables sulfate and alumina have the most significant effect on the initial time of set. All the models, which contain the physical characteristics of fly ash as dependent variables, spsurface, meansize and blaines have a very large number of variables in them. This clearly suggests that the initial time of set depends more on the chemical composition rather than the physical characteristics of the fly ash. This also is evident in some of the models containing four dependent variables as most of the models comprise of the chemical characteristics of the fly ash. The sets of variables in the models containing 3 or 4 variables, also include cao, SAF and mgo.

Considering Model 1, the dependence of initial setting time on sulfate ions and alumina is justified as the sulfate ions in the pore solution control the rate of reaction of calcium aluminates present in the binder. Sulfates are present in the cement and fly ash mainly in the form of gypsum, hemihydrate and anhydrite. As soon as water is added to the binder, sulfates react with the aluminate and ferrite phases to produce Aft phase. A further reaction of this phase with aluminate and ferrite phases form the AFm phase. These phases form in the early stages of hydration process, after which they become spectator phases. The amount of glass present in the fly ash was also found to be an important contributor to the setting time of fly ash.

5.3.1.2 Linear regression for binary pastes containing class C ashes. Linear regression analysis was performed on the initial setting time of binary paste systems containing Class C ashes, using the model with the three chosen dependent variables sulfate, alumina and glass. The ANOVA table along with the regression coefficients and the p-values are shown in Table 5.4.

The sign of the coefficients in the parameter estimate column indicates the effect of the variables on the dependent variable. As expected, the sign of the coefficient of sulfate was positive, indicating that the increase in the amount of sulfate leads to an increase in the setting time of the binder. The signs of alumina and glass were negative, which implies that the increase in the amounts of either of the variables leads to a decrease in the setting time of the binder.

The p-values of the model and the individual variables, which denote the significance of the model and

each of these variables respectively, were all greater than 0.1. This means that that model predictions are not very accurate and a significant amount of the variation in the setting time is not explained by the model. In addition, the error in the parameter estimates for all the parameters were comparable to the parameter estimates themselves, which also suggests that the prediction is not accurate. This could be due to various possible reasons as listed before in Section 5.3.1.1.

However, 7 of the 12 predictions obtained from model 1 for Class C ashes were within 30 minutes of the observed setting time of the ashes. According to ASTM C 191 (*32*), two different set times measured by a single operator in the same laboratory conditions were found to have a maximum variation of 34 minutes. The remaining five ashes whose setting time prediction differed from the observed setting time by more than 30 minutes lie at the extremes of the range of the setting time of all the Class C ashes. It can therefore be inferred that the model predicts well for the setting time lying between 1.7 and 3 hours, while any value of setting time not lying in this range cannot be predicted accurately. Table 5.5 shows the observed and predicted setting times of all the Class C ashes (except Kenosha fly ash, which had a flash setting) along with their sulfate, alumina and glass contents. The residuals and the squared residuals of the model are also included.

Figure 5.4 shows a plot between observed and the predicted setting times of all the Class C ashes. It can be seen that there is a higher deviation of the predicted setting time from the observed setting time at lower values of the setting time, whereas most of the higher setting times are predicted well.

TABLE 5.4
Regression analysis for setting time of binary pastes with Class C ashes.

Source	DF	Sum of Squares	Mean Square	F Value	p-Value
Model	3	3.269	1.089	1.65	0.2543
Error	8	5.292	0.6615		
Total	11	8.561			
		R^2	0.3818		
		adj-R^2	0.15		
Variable	**DF**	**Parameter Estimate**	**Standard Error**	**t-Value**	**p-Value**
Intercept	1	4.456	4.112	1.08	0.3101
sulfate	1	1.178	0.644	0.183	0.1048
alumina	1	-0.085	0.235	-0.36	0.7267
glass	1	-0.583	0.619	-0.94	0.3738

5.3.1.3 Linear regression models for binary pastes containing class F ashes. Linear regression models were built for binary paste systems containing Class F ashes. The number of data points used for the modeling process was seven. The three chosen independent variables sulfate, alumina and glass were used for building the models. The ANOVA table along with the regression coefficients and the p-values are shown in Table 5.6.

The inferences from the p-values and the adj-R^2 for this regression model and the sign of the coefficient for the independent variable alumina, were incoherent. While we expect a negative sign for the coefficient for alumina, the observed sign for the coefficient was positive. It was also seen that the errors for the parameter estimates were very high compared to the estimates. None of the independent variables was significant, including the model itself. Even though the adj-R^2 for the model was higher than that of the model for Class C ashes, its prediction for any new fly ash is not reliable. Table 5.7 shows the predicted and observed values of setting times for binary binder containing Class F ashes. Figure 5.5 shows the plot of the observed and predicted values of the setting time for the pastes with Class F ashes.

The plot (Figure 5.5) shows a fair equality between the observed and the predicted setting times for Class F ashes. However, none of the variables was even close to being significant and the p-value for the model was also very high. Hence, even though the model had a relatively higher adj-R^2 than the model for Class C

TABLE 5.5
Observed and predicted setting times (hours) of Class C ashes.

Fly Ash	Observed Set Time	Predicted Set Time	Residual	Squared Residual
Miller	1.27	2.81	-1.5514	2.40683
Schahfer	1.66	2.41	-0.74929	0.56144
Hennepin	1.78	1.67	0.11195	0.01253
Joppa	2.22	2.25	-0.02676	0.00072
Vermilion	2.23	2.36	-0.13045	0.01702
Edwards	2.26	2.71	-0.4497	0.20223
Will County	2.52	2.62	-0.10557	0.01114
Rockport	2.54	2.24	0.30079	0.09048
Rush Island	3.06	2.45	0.61475	0.37792
Baldwin	3.46	2.38	1.07499	1.15561
Labadie	3.8	3.20	0.59975	0.3597
Joliet	4.16	3.86	0.31093	0.09668

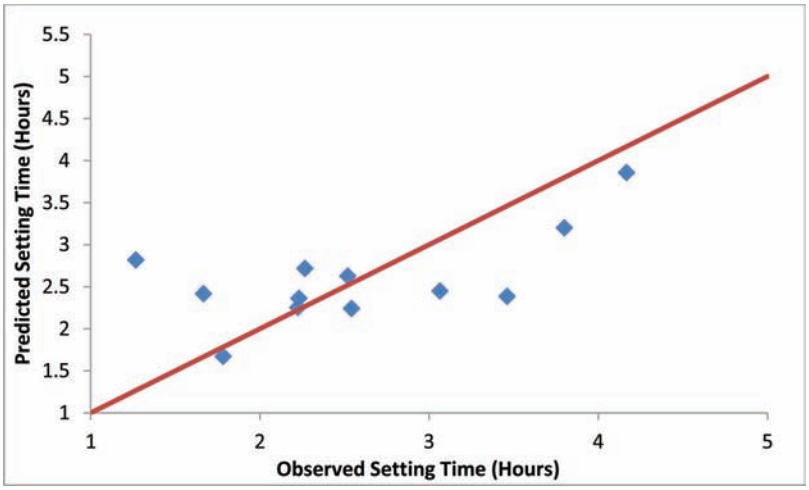

Figure 5.4 Plot of predicted Vs observed values of setting times for Class C ashes.

TABLE 5.6
Regression analysis for setting time of binary pastes with Class F ashes.

Source	DF	Sum of Squares	Mean Square	F Value	p-Value
Model	3	0.44358	0.14786	1.63	0.3487
Error	3	0.27189	0.09063		
Total	6	0.71547			
		R^2	0.62		
		adj-R^2	0.24		
Variable	**DF**	**Parameter Estimate**	**Standard Error**	**t-Value**	**p-Value**
Intercept	1	1.26093	0.99826	1.26	0.2958
sulfate	1	0.46946	0.25233	1.86	0.1598
alumina	1	0.07325	0.0769	0.95	0.4111
glass	1	-0.0845	0.53944	-0.16	0.8855

TABLE 5.7
Observed and predicted setting times (minutes) of Class F ashes.

Fly Ash	Observed Set Time	Predicted Set Time	Residual	Squared Residual
Millcreek	2.5	2.9	-0.4	0.16
Elmersmith	2.9	2.7	0.2	0.04
Trimble	3.2	3.1	0.1	0.01
Miami 7	3.3	3.4	-0.1	0.04
Miami 8	3.4	3.3	0.1	0.01
Petersburg	3.4	3.1	0.3	0.09
Zimmer	3.5	3.5	0	0

ashes, this model cannot be utilized to predict the set time of any Class F ash.

5.3.1.4 Model verification. Two fly ashes (NIP 1 – Class C ash and NIP 1A – Class F ash) not used in building the above models were used to test the accuracy and predictability of the models. The sulfate content, alumina content and the glass content of the fly ashes are given in Table 5.8. The observed and predicted set times for the test ashes are shown in Table 5.9.

From Table 5.9, it is clear that the predictions of the model are not very accurate as the difference between the observed and predicted set times are close to 100 minutes for Class F ash and more than 300 minutes for Class C ash. This was expected, as the p-values of both the models were greater than 0.1 and the model predictions were found to not be reliable.

5.3.2 Heat of Hydration

The heat of hydration tests were performed on the binary paste systems as explained in Section 3.3.3. To obtain the heat of hydration curve in its final form (Figure 5.6), the data, which was obtained in terms of millivolts at every 30-second intervals, was processed as explained below (*35*).

It is assumed that the calorimeter is in a stable temperature conditions with the sample holder at T_i and the heat sink at T_o.

Now, as heat (dW) is released in the system during a short time interval (*dt*), there is an increase in the temperature of the sample holder, above that of the heat sink.

$$T = T_i - T_o \tag{7}$$

If the thermal capacity of the sample holder is u, then internal heat absorption rate is given by

$$u\frac{DT}{dt} \tag{8}$$

The remainder of the heat leaks only by conduction (and not convection or radiation), considering the set up. This rate of heat loss is proportional to the temperature T, i.e.,

Rate of heat loss = pT

where, p is a constant.

From the heat balance equation,

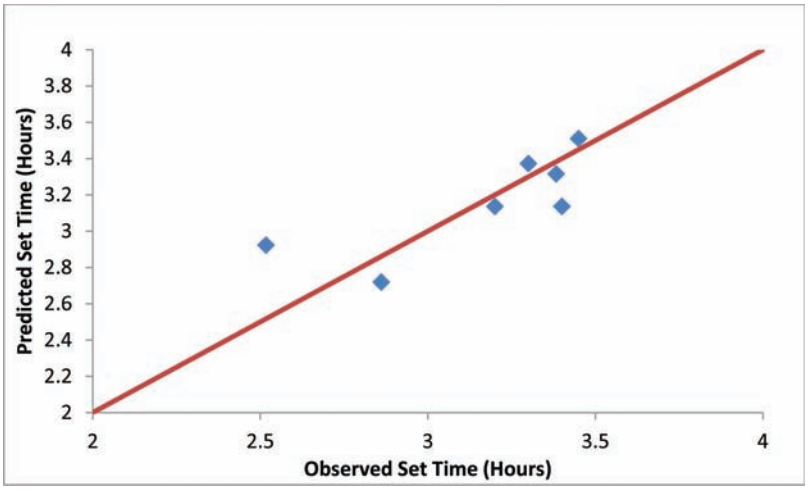

Figure 5.5 Plot of predicted Vs observed values of setting times for Class F ashes.

TABLE 5.8
Characteristics of the test fly ashes used for model verification.

Fly Ash	Sulfate (%)	Alumina (%)	Glass
NIP 1	3.13	23	2.5545
NIP 1A	5.98	15.2	0.92388

TABLE 5.9
Observed and predicted set times (minutes) for the test ashes.

Fly Ash	Class	Observed Settime (min)	Predicted Settime (min)	Residual (min)	Squared Residual (min^2)
NIP 1	F	155	252	97	9400
NIP1A	C	215	580	365	133363

$$\frac{dW}{dt} = pT + u\frac{dT}{dt} \tag{9}$$

The EMF produced due to the temperature change T is proportional to the temperature change, i.e.,

$$E = gT, \tag{10}$$

where g is a constant.

Therefore,

$$\frac{dW}{dt} = p\frac{E}{g} + \frac{dE}{dt}\frac{u}{g} \tag{11}$$

which can be written as,

$$\frac{dW}{dt} = K_1.E + K_2.\frac{dE}{dt} \tag{12}$$

where, K_1 and K_2 are constants for the calorimeter. The above equation is called Tian-Calvet equation.

We can rearrange the equation to the following format,

$$\frac{dE}{dt} = -\frac{K_1}{K_2}E + \frac{dW/dt}{K_2} \tag{13}$$

which will give a straight line when plotted between, $\frac{dE}{dt} = -\frac{K_1}{K_2}E + \frac{dW/dt}{K_2}$

These values of K_1 and K_2 can be obtained by providing a constant supply of heat to the sample and measuring the voltage response. This is called the calibration curve of the paste, which is a straight line.

Once the values of K_1 and K_2 are known, the output heat (in milli-Watts) can be calculated at every time interval, by making use of the Tian-Calvet equation. A plot between output heat and time is called the calorimetric curve. A typical calorimetric curve for fly ash-cement binary paste systems is shown in Figure 5.6.

The data for the voltage was collected at intervals of 30 second intervals. The data for peak rate of heat of hydration (peakheat) and the time of the peak heat of hydration (timepeak) for the binary paste systems and the control mix were directly read-off from their respective calorimetric curves. The total heat of hydration (totalheat) in Joules, (collected within the period from 60 minutes after the addition of water to the binder to 3 days) old sample was found by the summation of the data points. From here on, the peak rate of heat of hydration will be referred to as peak heat of hydration.

5.3.2 1 Peak heat of hydration (peakheat). The values of peak heat of hydration for binary paste systems are shown in the Table 5.10. All the values are in mW/g. As already mentioned, the values of the peak heat of hydration for the binary paste systems were obtained directly from their respective heat of hydration curves.

The peak heat of hydration for the plain cement paste was found to be 3.831 W/kg. Figure 5.7 shows a

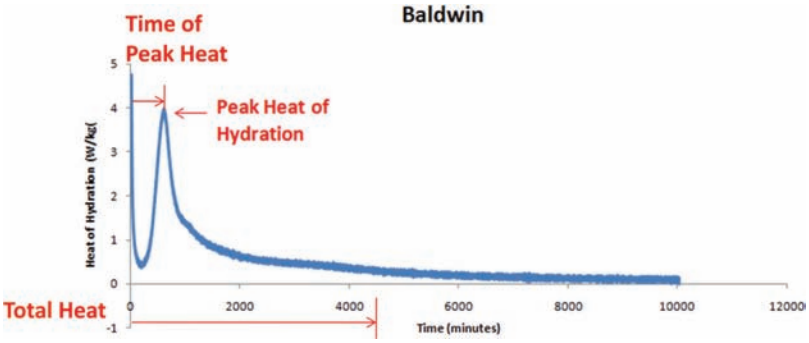

Figure 5.6 A typical calorimeter curve (Baldwin fly ash).

TABLE 5.10
Peak heat of hydration for all the fly ashes.

Fly Ash	Class	Peakheat (W/kg)	Fly Ash	Class	Peakheat (W/kg)
Kenosha	C	2.189	Baldwin	C	3.976
Edwards	C	2.346	Labadie	C	4.028
Vermilion	C	2.596	Rush Island	C	4.222
Joliet	C	2.808	Petersburg	F	2.783
Miller	C	2.876	Mill Creek	F	3.5
Schahfer	C	2.879	Miami 7	F	3.63
Will County	C	3.214	Elmersmith	F	3.695
Hennepin	C	3.4698	Miami 8	F	3.891
Joppa	C	3.561	Zimmer	F	3.961
Rockport	C	3.582	Trimble	F	4.34

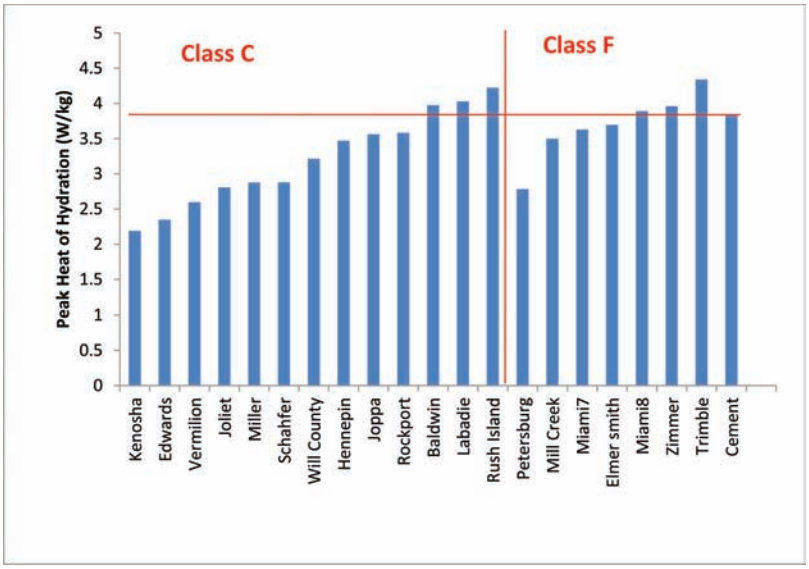

Figure 5.7 Comparison of peak heat of hydration for all the paste systems.

comparison of the peak heat of hydration for all the fly ashes. In this figure, the first 12 bars represent the peak heat of hydration for the binary paste systems containing Class C ashes. The next seven bars represent Class F ashes and the last bar represents the same data for a paste containing plain cement.

It is clear from the bar plot that most of the ashes tend reduce the peak heat of hydration as compared to plain cement paste. Three out of twelve Class C ashes and three out of seven Class F ashes showed a relative increase in the peak heat of hydration. Class F ashes in general tend to have a higher peak heat of hydration compared to Class C ashes. The highest value of the peak heat was 4.34 W/kg, and was obtained for Class F ash. The lowest value of peak heat was 2.189 W/kg, obtained for Kenosha, a Class C ash. It is interesting to

note that this fly ash experienced a flash set. However, no correlation was noticed between peak heat of hydration and setting time for all the ashes, as shown in Figure 5.8. Nevertheless, a slight indication of an increase in the setting time with the increase in the peak heat of hydration can be observed.

In general, Class F ashes had higher values of the peak heat of hydration when compared to Class C ashes. The range of the values were larger for Class C ashes (varying from 2.189 W/kg to 4.222 W/kg), while the range of values for Class F ashes were smaller, (ranging from 2.783 W/kg to 4.34 W/kg).

A clear distinction between Class C and Class F ashes can be seen here, where Class C ashes tend to reduce the peak heat of hydration, while Class F ashes could act either way.

5.3.2.1.1 Selection of variables for statistical modeling. Statistical linear regression models were built for the peak heat of hydration of the binary paste systems using all the data points given in Table 5.10. The independent variables considered when constructing the regression models are mentioned in Table 5.1. A SAS code was written, which investigated all the possible combinations of independent variables to construct the regression models. A template of the code is given in Appendix B. The program uses all the independent variables and the dependent variable (*peakheat*) as inputs. The output of the program consists of a table containing the list of combinations of independent variables forming linear regression models, sorted according to the adj-R^2 values. The values of the R^2 are also listed in the table for each model.

The best ten regression models for peak heat of hydration based on adj-R^2 are listed in Table 5.11.

Using the information in the above table, it can be inferred that both physical and chemical characteristics of fly ashes affect the peak heat of hydration. As can be seen from the above table, the best ten models do not contain a model with three variables. However, the variables chosen to build the linear regression models for Class C and Class F ashes were spsurface, SAF and glass. This was the three variables set (best model), which resulted in the model with the highest adj-R^2 (0.203) and R^2 (0.3289) among all the three variable models considered. It can be seen from the table that these three variables were amongst the most frequently occurring variables in all the ten models (cao, being the other frequently occurring variable).

It was also observed earlier that SAF and cao have a very high correlation. Hence, a model consisting of both these variables could render the two variables, insignificant. The inclusion of the variable SAF clearly indicated the differences in the peak heat of hydrations between the two classes, the low-calcium and high calcium ashes.

The R^2 and adj-R^2 for the best model were low. This could be because of the differences in the behavior of Class C and Class F ashes (see Figure 5.7). It can also be seen that the variables, which affect the peak heat of hydration (SAF and cao) are considerably different for the two classes of ashes (see Tables 4.1 and 4.2)

5.3.2.1.2 Linear regression models for binary pastes containing class c ashes. Linear regression analysis was performed on the peak heat of hydration of binary paste systems containing Class C ashes, using the model with the three chosen dependent variables spsurface, SAF and glass. Table 5.12 shows the results of the model (R^2, adj-R^2 and parameter estimates along with the p values for the model and the variables) ANOVA analysis.

The sign of the coefficients in the parameter estimate column indicates the effect of the variables on the dependent variable. The sign of the coefficient of spsurface was negative, indicating that the increase in the surface area of the fly ashes leads to a decrease in the peak heat of hydration of the binder. It was found earlier by Fajun et al. (*22*), that fly ash particles act as a Ca^{+2} ion sink. The Ca^{+2} ions present in the solution react with the abundantly available aluminum from fly ashes to preferentially form an Aft phase on the surface of fly ash. This reaction reduces the formation of calcium rich surfaces on the surface of cement particles,

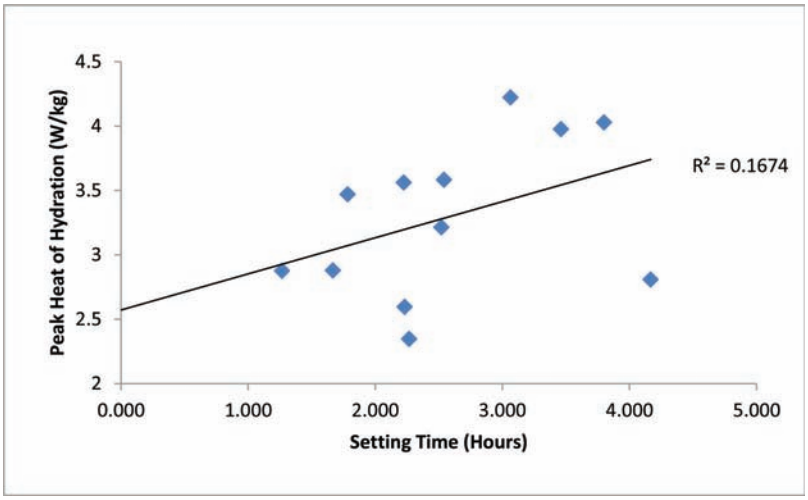

Figure 5.8 Correlation between peak heat of hydration and setting time for all the ashes.

TABLE 5.11
Best ten regression models for peak heat of hydration.

Model Number	Number of Variables in the Model	Adjusted R^2	R^2	Variables in the model
1	6	0.3455	0.5522	blaines, spsurface, sulfate, SAF, cao, glass
2	4	0.3399	0.4789	spsurface, SAF, cao, glass
3	5	0.3348	0.5099	blaines, spsurface, SAF, cao, glass
4	5	0.3265	0.5037	blaines, spsurface, sulfate, SAF, cao
5	5	0.3209	0.4996	spsurface, sulfate, SAF, cao, glass
6	6	0.3121	0.5293	blaines, spsurface, meansize, SAF, cao, glass
7	5	0.3119	0.493	spsurface, meansize, SAF, cao, glass
8	5	0.3104	0.4918	spsurface, SAF, cao, mgo, glass
9	6	0.3102	0.528	blaines, spsurface, SAF, cao, mgo, glass
10	7	0.3067	0.5621	blaines, spsurface, sulfate, carbon, SAF, cao, glass

TABLE 5.12
Regression analysis for peak heat of hydration of binary pastes with Class C ashes.

Source	DF	Sum of Squares	Mean Square	Model F Value	Model p-Value
Model	3	2.92053	0.97351	3.916092	0.0484
Error	9	2.23733	0.2485922		
Total	12	5.15786			
		R^2	0.5662		
		adj-R^2	0.4216		
Variable	**DF**	**Parameter Estimate**	**Standard Error**	**Variable t-Value**	**Variable p-Value**
Intercept	1	17.7175	4.5007	3.93661	0.0034
spsurface	1	-0.000291	0.0000865	-3.36416	0.0084
SAF	1	-0.16808	0.0576	-2.91806	0.0172
glass	1	0.6817	0.4268	1.597235	0.1447

resulting in a longer induction period and thus reducing the rate of reaction at early ages. The lengthening of the induction period could also be a result of a chemisorption of Ca^{+2} ions on the fly ash surface.

The sign of SAF was negative, which indicates that the increase in the amounts of SAF (decrease in CaO content) leads to a decrease in the peak heat of hydration of the binder. The amount of glass present in the fly ash had a positive sign, which suggests that an increase in the glass content leads to an increase in the peak heat of hydration.

The p-value of the model was less than 0.1, indicating that the model produces reliable predictions. The p-values for spsurface and SAF were below 0.1, indicating that these are two most influencing variables. In addition, the p-value for glass was greater than 0.1, which means that the effect of glass content on the peak heat of hydration was not as significant as the other variables.

Table 5.13 shows the observed and predicted values of peak heat of hydrations for all the Class C ashes. The residuals and the squared residuals of the model are also included.

It can be seen from Table 5.13 that ten out of thirteen ashes had a prediction within 0.3 W/kg of the observed peakheat of hydrations, which was about the same as the standard deviation for the peak heat of hydration obtained from the experiments. In addition, the remaining three ashes were the ones with extreme values of the peak heat. Figure 5.9 shows the plot of a relationship between the observed and predicted peak heat of hydration for all the Class C ashes. It can be noted that the three points not predicted well lie at either extremes of the set of points.

5.3.2.1.3 Linear regression models for binary pastes containing class F ashes. Linear regression analysis was performed on the peak heat of hydration of binary paste systems containing Class F ashes, using the same three dependent variables, spsurface, SAF and glass, which were previously used for Class C ashes. Table 5.14 shows the results of the model (R^2, adj-R^2 and parameter estimates along with the p values for the model and the variables) ANOVA analysis.

The sign of the coefficients in the parameter estimate column indicates the effect of the variables on the dependent variable. The sign of the coefficient of spsurface was negative, indicating that the increase in the surface area of the fly ashes leads to a decrease in the peak heat of hydration of the binder. This was similar to the results obtained for Class C ashes.

TABLE 5.13
Observed and predicted peak heat of hydration of Class C ashes.

ID	Observed Peakheat (W/kg)	Predicted Peakheat (W/kg)	Residual (W/kg)	Squared Residual (W^2/kg^2)
Kenosha	2.189	3.105	-0.916	0.8381
Edwards	2.346	1.954	0.3922	0.1538
Vermilion	2.596	2.617	-0.021	0.0005
Joliet	2.808	3.168	-0.36	0.1294
Miller	2.876	3.24	-0.364	0.1327
Schahfer	2.879	3.152	-0.273	0.0747
Will County	3.214	3.252	-0.038	0.0014
Hennepin	3.47	3.705	-0.235	0.0553
Joppa	3.561	3.373	0.1883	0.0355
Rockport	3.582	3.189	0.3931	0.1546
Baldwin	3.976	3.884	0.0922	0.0085
Labadie	4.028	3.487	0.5406	0.2923
Rush Island	4.222	3.621	0.6006	0.3607

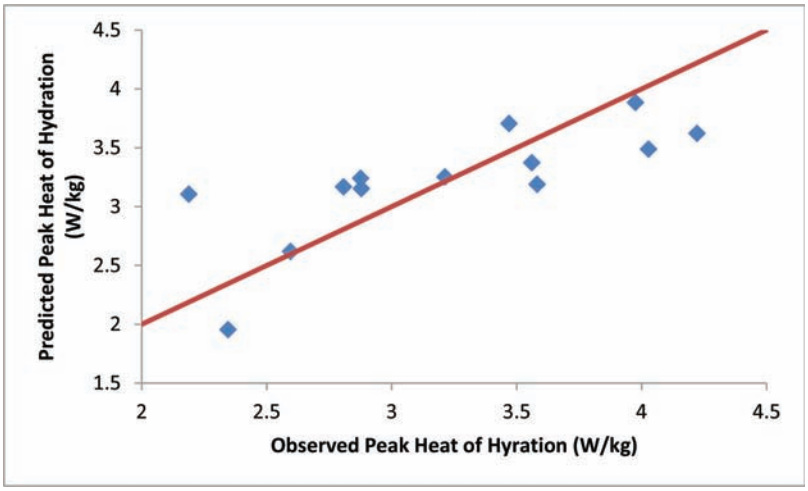

Figure 5.9 Plot showing the variations in the predicted and observed peak heat of hydration for all the Class C ashes.

TABLE 5.14
Regression analysis for peak heat of hydration of binary pastes with Class F ashes.

Source	DF	Sum of Squares	Mean Square	Model F Value	Model p-Value
Model	3	0.74725	0.249083	1.15	0.4564
Error	3	0.6514	0.217133		
Total	6	1.39864			
		R^2	0.5343		
		adj-R^2	0.0685		
Variable	**DF**	**Parameter Estimate**	**Standard Error**	**Variable t-Value**	**Variable p-Value**
Intercept	1	11.39065	4.9644	2.294467	0.1055
spsurface	1	-2.64E-05	0.000105	-0.2527	0.8168
SAF	1	-0.09952	0.06179	-1.61062	0.2057
glass	1	0.61193	0.42775	1.430579	0.2479

The sign of SAF was also negative indicating that the increase in the amounts of SAF (decrease in CaO content) leads to a decrease in the peak heat of hydration of the binder. The amount of glass present in the fly ash had a positive sign, which is also an indicator that an increase in the glass content leads to an increase in the peak heat of hydration.

When evaluated by the ANOVA procedure, the p-value of the model was greater than 0.1, indicating that the model does not produce reliable predictions.

The p-values for spsurface, SAF and glass were all above 0.1, indicating that the regression model used is incapable of predicting the peak heat of hydration. It would not be productive to attempt to evaluate the relation between observed and predicted peak heat of hydration for Class F ashes. However, for the completeness of the presentation, Table 5.15 is presented which shows the observed and predicted peak heat of hydrations of all the Class F ashes. The residuals and the squared residuals of the model are also included.

It can be seen from Table 5.15, that six out of seven ashes have a prediction within 0.3 W/kg of the observed peak heat of hydration. The remaining one ash is the one with extreme value of the peak heat. However, these predictions do not give any inference about the predictions of the peak heat of hydration for any other new Class F fly ash, as the model is not reliable, even though the residuals are relatively smaller.

Figure 5.10 shows the plot of the observed and predicted peak heat of hydration for all the Class F ashes. It can be observed that the one point not predicted well lies at the extreme of the set of points.

5.3.2.1.4 Model verification. Two fly ashes (NIP 1 – Class C ash and NIP 1A – Class F ash) not included in the set of fly ashes utilized for development of the above models were used to test their accuracy with respect to the predictability of the peak heat of hydration. The specific surface (spsurface), SAF content and the glass content of the fly ashes are given in the Table 5.16. The observed and predicted values of peak heat of hydration values for these ashes are shown in Table 5.17.

From Table 5.17, it can be seen that the residual of the prediction of peak heat of hydration for the Class F model was higher than the residuals obtained for all the Class F ashes used in developing the model. This was expected as the p-value of the model was just much larger than 0.1. The value for predicted peak heat of hydration for Class C ash (NIP 1A) could not be calculated as the value for spsurface of NIP 1A was unavailable. Nevertheless, the expected residual for this model would have been lower than that of Class F ash as the p-value for the model was smaller than 0.1.

TABLE 5.16
Characteristics of the test fly ashes used for model verification.

Fly Ash	Spsurface (cm^2/cm^3)	SAF (%)	Glass
NIP 1	20978	87	2.5545
NIP 1A	—	58.1	0.92388

TABLE 5.15
Observed and predicted peak heat of hydration of Class F ashes.

ID	Observed Peakheat (W/kg)	Predicted Peakheat (W/kg)	Residual (W/kg)	Squared Residual (W^2/kg^2)
Petersburg	2.783	3	-0.217	0.04707
Millcreek	3.5	3.49	0.0104	0.00011
Miami 7	3.63	3.835	-0.205	0.04208
Elmersmith	3.695	4.03	-0.335	0.11196
Miami 8	3.891	3.993	-0.102	0.01045
Zimmer	3.961	3.737	0.2245	0.05039
Trimble	4.34	3.716	0.624	0.38935

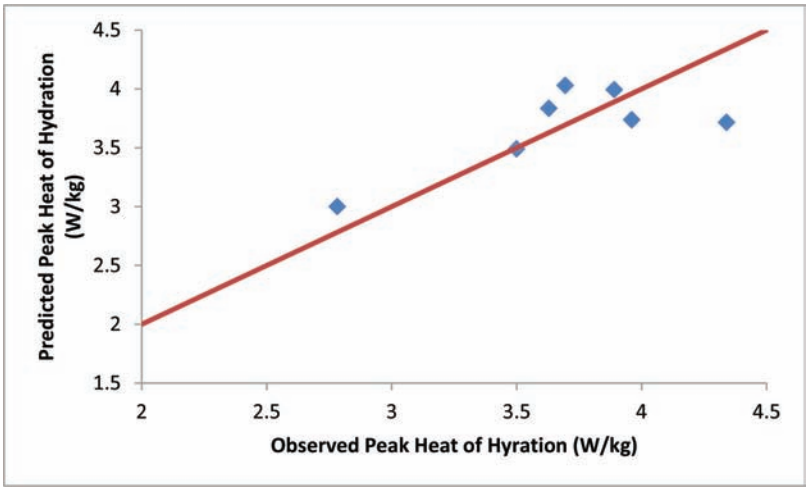

Figure 5.10 Plot showing the variations in the predicted and observed peak heat of hydration for all the Class F ashes.

5.3.2.2 Time of peak heat of hydration (timepeak). The values of time of peak heat of hydration for binary paste systems are shown in the Table 5.18. These values were scaled off directly from their respective calorimeter curves.

The time of peak heat of hydration for the plain cement paste was found to be 449 minutes. Figure 5.11 shows a comparison of the time of peak heat of hydration for all the fly ashes. In this figure, the first 13 bars represent the time of peak heat of hydration for the binary paste systems containing Class C ashes. The next seven bars represent Class F ashes and the last bar represents the same data for a paste containing plain cement.

It is clear from the bar plot that all the ashes but one ash (Class F, Miami 8) tend to delay the occurrence of the peak heat of hydration as compared to plain cement paste. Eight out of thirteen Class C ashes show a higher delay in the time of peak heat of hydration compared to all the Class F ashes. The highest value of the observed time of peak heat was 784 minutes. This was observed for Kenosha, a Class C ash. It is however interesting to note that the use of this fly ash resulted in a flash setting. In addition, this particular fly ash had the lowest value of peak heat of hydration amongst all the ashes. The lowest value of time of peak heat of hydration was observed for a Class F ash, Miami 8. As already mentioned, this was the only fly ash, which advanced the occurrence of the peak heat of hydration when compared to the plain cement paste. No correlation was observed between time of peak heat of hydration and setting time of ashes or between the time of peak heat of hydration and peak heat of hydration itself.

TABLE 5.17
Observed and predicted peak heat of hydration (W/kg) for the test ashes.

Fly Ash	Class	Observed Peakheat	Predicted Peakheat	Residual	Squared Residual
NIP 1	F	3.0242	3.70418	0.68	0.462375
NIP1A	C	3.0929	—	—	—

TABLE 5.18
Time of peak heat of hydration for the fly ashes used in the study.

Fly Ash	Class	Time of Peakheat (min)	Fly Ash	Class	Time of Peakheat (min)
Baldwin	C	604	Schahfer	C	557.5
Edwards	C	484	Vermilion	C	534.5
Hennepin	C	632.5	Will County	C	594.5
Joliet	C	496.5	Elmer smith	F	581.5
Joppa	C	637.5	Miami 7	F	477
Kenosha	C	784	Miami 8	F	440
Labadie	C	635	Mill Creek	F	560
Miller	C	520	Petersburg	F	487.5
Rockport	C	506	Trimble	F	562
Rush Island	C	623	Zimmer	F	587

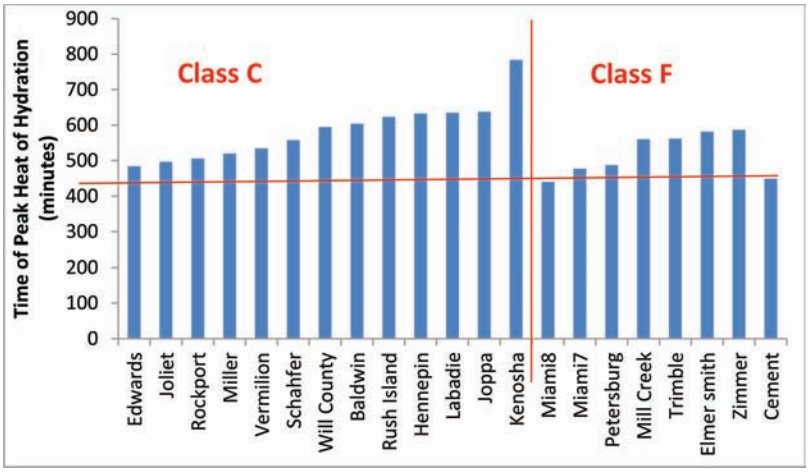

Figure 5.11 Comparison of time of peak heat of hydration for all paste systems.

5.3.2.2.1 Selection of variables for statistical modeling. Statistical linear regression models were built for the time of peak heat of hydration of the binary binder systems using all the points mentioned in Table 5.18. The independent variables looked at to develop the regression models are mentioned in Table 5.1. A SAS code was written which investigated all the possible combinations of independent variables to construct the regression models. A template of the code is given in Appendix B. The program uses all independent variables and the dependent variable (time of peak heat of hydration – timepeak). The output of the program consists of a table containing the list of combinations of independent variables forming linear regression models, sorted according to the adj-R^2 values. The values of the R^2 are also listed in the table for each model.

The best ten regression models (based on adj-R^2) are listed in Table 5.19.

Using the information in Table 5.19, it can be inferred that both physical and chemical characteristics of fly ashes affect the time of peak heat of hydration, the most important variables being blaines, spsurface, meansize, sulfate, mgo and alumina (as listed in Model 1).

The R^2 and adj-R^2 for the above listed models were relatively higher compared to the set time models and the models for peak heat of hydration. This could be because there was no clear distinction observed in the ranges of the time of peak heat of Class C and Class F ashes and hence a single regression model (developed using the data points of both the classes of ashes) could easily explain most of the variations in all the data points. The similarities in the behavior of the two classes can be seen in Figure 5.11. The variables SAF and cao were also not found to be significantly influencing the independent variable, as they did not appear in most of the models listed in Table 5.19.

The variables chosen to build the linear regression models for Class C and Class F ashes were spsurface, meansize and mgo. This was the three variables set which had the best adj-R^2 (0.4021) and R^2 (0.4965) among all the three variable models considered.

From the chosen best model with three variables, it was clear that the physical properties of fly ash influence the time of peak heat of hydration more than their chemical properties (it will be seen in Section 5.3.2.2.2 that the variable mgo was not significant compared to the other two). This is in contrary to the set of chosen variables for setting time, which were all chemical characteristics of fly ash. This suggests that the rate of reaction after the initial induction period depends mostly on the physical characteristics of the fly ash (spsurface and meansize).

5.3.2.2.2 Linear regression models for binary pastes containing class C ashes. Linear regression analysis was performed on the time of peak heat of hydration of binary paste systems containing Class C ashes, using the model with the three chosen dependent variables spsurface, meansize and mgo. Table 5.20 shows the results of the model (R^2, adj-R^2 and parameter estimates along with the p-values for the model and variables) ANOVA analysis.

The sign of the coefficients in the parameter estimate column indicates the effect of the variables on the dependent variable. The sign of the coefficient of spsurface was negative, indicating that the increase in the surface area of the fly ashes leads to a decrease in the time of peak heat of hydration of the binder. This can be attributed to the delay in the nucleation of $Ca(OH)_2$ by the suppression of the increase in the concentration of Ca^{+2} ions in solution as they are absorbed on the surface of fly ashes. As the Ca^{+2} ions concentration in the liquid phase goes lower, it delays the nucleation and crystallization of CH and CSH. Thus, the amount of surface area plays an important role in the delay of the occurrence of the time of peak heat of hydration.

In a similar way, the reduction in the mean particle size of fly ash increases the specific surface area, leading to an acceleration of the hydration reaction. Thus, the negative sign of the variable, meansize is also justified.

The presence of the variable mgo in the model is not quite justified, however the presence of mgo was found to reduce the hydration kinetics (LEA's Chemistry of

TABLE 5.19
Best ten regression models for time of peak heat of hydration.

Model Number	Number of Variables in the Model	Adjusted R^2	R^2	Variables in the Model
1	6	0.4358	0.6140	blaines, spsurface, meansize, sulfate, mgo, alumina
2	5	0.4332	0.5824	spsurface, meansize, sulfate, mgo, alumina
3	5	0.4299	0.5799	blaines, spsurface, meansize, sulfate, mgo
4	4	0.4282	0.5486	spsurface, meansize, sulfate, mgo
5	5	0.4121	0.5668	spsurface, meansize, sulfate, SAF, mgo
6	5	0.4112	0.5661	spsurface, meansize, sulfate, cao, mgo
7	6	0.4042	0.5923	spsurface, meansize, sulfate, cao, mgo, alumina
8	3	0.4021	0.4965	spsurface, meansize, mgo
9	6	0.4019	0.5908	blaines, spsurface, meansize, sulfate, SAF, mgo
10	7	0.4016	0.6221	blaines, spsurface, meansize, sulfate, carbon, mgo, alumina

Cement and Concrete, Hewlett). Nevertheless, the p-value of the variable suggests that its effect is not significant compared to the other two variables.

The R^2 and the adj-R^2 for the model for Class C ashes was slightly better than for the model including both the classes, thus giving a better fit.

The p-value of the model was greater than 0.1 indicating that the model does not produce reliable predictions. The p-value for spsurface was below 0.1 indicating that this is the most influencing variable. In addition, the p-values for meansize and mgo were greater than 0.1, which means that the effect of these variables on the time of peak heat of hydration is not as significant compared to the specific surface area.

Table 5.21 shows the observed and predicted values of time of peak heat of hydrations for all Class C ashes. The residuals and the squared residuals of the model are also included.

It can be seen from Table 5.21 that ten out of thirteen ashes have a prediction within 10% of the observed time of peak heat of hydration which was observed as the variation in a data point (by experimenting). In addition, the remaining three ashes are the ones with extreme values of the time of peak heat. This model can be used to predict the time of peak heat of hydration for Class C ashes provided they lie within 500 to 600 minutes.

Figure 5.12 shows the plot of the observed and predicted time of peak heat of hydration for all the Class C ashes. It can be observed that two of the three points not predicted well lie at either extremes of the set of points.

5.3.2.2.3 Linear regression models for binary pastes containing class F ashes. Linear regression analysis was performed on the time of peak heat of hydration of binary binder systems containing Class F ashes, using the model with the three chosen dependent variables spsurface, meansize and mgo. Table 5.22 shows the results of the model (R^2, adj-R^2 and parameter estimates along with the p-values for the model and variables) ANOVA analysis.

The sign of the coefficients in the parameter estimate column indicates the effect of the variables on the dependent variable. The sign of the coefficient of spsurface was negative, indicating that the increase in the surface area of the fly ashes leads to a decrease in the time of peak heat of hydration of the paste. This was similar to the results obtained for Class C ashes.

TABLE 5.20
Regression analysis for time of peak heat of hydration of binary pastes with Class C ashes.

Source	DF	Sum of Squares	Mean Square	Model F Value	Model p-Value
Model	3	32170	10723.33	2.087605	0.1722
Error	9	46230	5136.667		
Total	12	78400			
		R^2	0.4103		
		adj-R^2	0.2138		
Variable	**DF**	**Parameter Estimate**	**Standard Error**	**Variable t-Value**	**Variable p-Value**
Intercept	1	967.784	320.706	3.017667	0.0145
spsurface	1	-0.0301	0.01356	-2.21976	0.0533
meansize	1	-10.1287	6.0826	-1.66519	0.1302
mgo	1	63.35305	35.31955	1.793711	0.1064

TABLE 5.21
Observed and predicted time of peak heat of hydration (minutes) of Class C ashes.

ID	Observed Timepeak (min)	Predicted Timepeak (min)	Residual (min)	Squared Residual (min^2)
Edwards	484	461.5	22.505	506.49
Joliet	496.5	594.5	-98.01	9605
Rockport	506	506	-0.03	0
Miller	520	557.5	-37.6	1413.6
Vermilion	534.5	575.5	-40.99	1679.8
Schahfer	557.5	606	-48.58	2359.8
Hennepin	581.5	613	-31.7	1004.8
Will County	594.5	591.5	2.992	8.95
Baldwin	604	652	-47.98	2301.6
Rush Island	623	580	43.195	1865.8
Labadie	635	609	25.698	660.37
Joppa	637.5	569	68.679	4716.9
Kenosha	784	642	141.8	20107

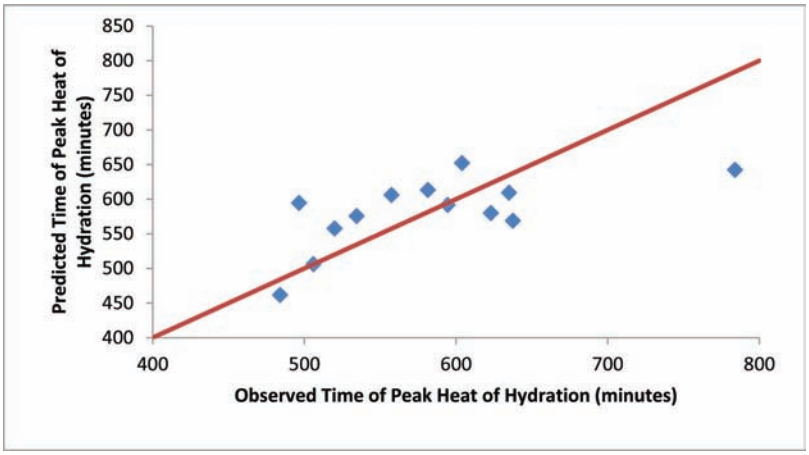

Figure 5.12 Plot showing the variations in the predicted and observed time of peak heat of hydration for all Class C ashes.

TABLE 5.22
Regression analysis for time of peak heat of hydration of binary pastes with Class F ashes.

Source	DF	Sum of Squares	Mean Square	F Value	p-Value
Model	3	15061	5020.333	7.18	0.0698
Error	3	2096.225	698.7417		
Total	6	17157.23			
		R^2	0.8778		
		adj-R^2	0.7556		
Variable	**DF**	**Parameter Estimate**	**Standard Error**	**t-Value**	**p-Value**
Intercept	1	1010.563	145.6373	6.938902	0.0061
spsurface	1	-0.0145	0.00489	-2.96524	0.0597
meansize	1	-12.4914	4.3973	-2.8407	0.0656
mgo	1	13.5769	8.4427	1.608123	0.2062

The signs of remaining variables are also the same as what was observed for Class C ashes.

The R^2 and adj-R^2 for the model was very high and hence the predictions were very accurate. The p-value of the model was less than 0.1 indicating that the model produces very reliable predictions. The p-values for spsurface and meansize were above 0.1 indicating that the regression model is dependent mainly on these two variables. The variable mgo was not found to be significant.

Table 5.23 shows the observed and predicted time of peak heat of hydrations of all the Class F ashes. The residuals and the squared residuals of the model are also included.

It can be seen from Table 5.23 that all of the seven ashes have a prediction within 10% (which was observed as the variation on multiple tests on similar samples) of the observed time of peak heat of hydration. This model can be used to predict the time of peak heat of hydration for any new Class F fly ash. However, with a small data available for Class F ashes, some extreme observations as was observed in the case of Class C ashes might have been missed.

Figure 5.13 shows the plot of the observed and predicted time of peak heat of hydration for all the Class F ashes. It can be observed that all the points have been predicted accurately.

5.3.2.2.4 Model verification. Two fly ashes (NIP 1 – Class F ash and NIP 1A – Class C ash) not included in the set of fly ashes utilized for development of the above models were used to test their accuracy. The specific surface (spsurface), mean particle size (meansize) and the MgO (mgo) content of the fly ashes are given in Table 5.24. The observed and predicted values of time of peak heat of hydration for these test ashes are shown in Table 5.25.

From Table 5.23, it is clear that the prediction of the Class F model is not similar to the observed values as the difference between the observed and predicted peak heat of hydration is more than 30 minutes. This was expected even though the p-value of the model was smaller than 0.1, as the observation did not belong to the range of observations used in the prediction. The value for predicted timepeak for Class C ash (NIP 1A) could not be calculated as the value for spsurface of NIP 1A was unavailable. It was

TABLE 5.23
Observed and predicted time of peak heat of hydration of Class F ashes.

ID	Observed Timepeak (min)	Predicted Timepeak (min)	Residual (min)	Squared Residual (min^2)
Miami 8	440	447.5	-7.509	56.38
Miami 7	477	460	16.814	282.72
Petersburg	487.5	525.5	-38.23	1461.8
Elmersmith	521.5	516	5.6526	31.95
Millcreek	560	547	13.174	173.55
Trimble	562	552.5	9.4543	89.38
Zimmer	587	586	0.6478	0.42

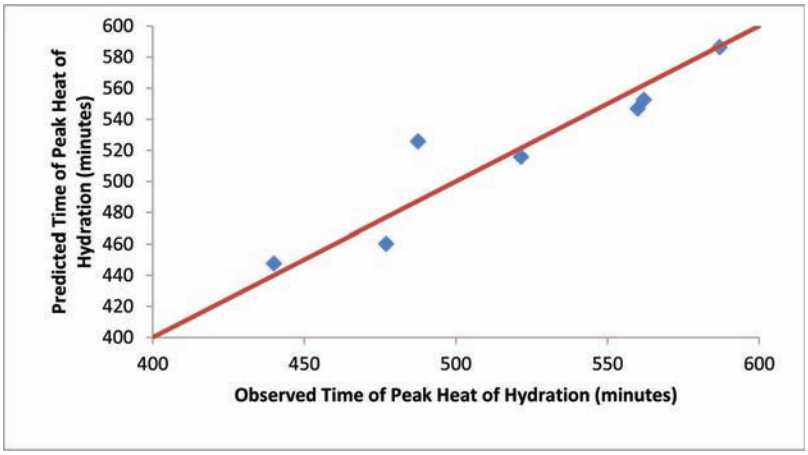

Figure 5.13 Plot showing the variations in the predicted and observed time of peak heat of hydration for all the Class F ashes.

TABLE 5.24
Characteristics of the test fly ashes used for model verification.

Fly Ash	Spsurface (cm^2/cm^3)	Meansize (μm)	Mgo (%)
NIP 1	20978	3	2.84
NIP 1A	—	15	3.63

expected that the residual for this model would have been relatively large as well, as the p-value for the model was higher than 0.1.

5.3.2.3 Total heat of hydration (totalheat). The values of total heat of hydration measured for three days, for binary binder systems are shown in the Table 5.26. All the values are in J/kg. The values of the total heat of hydration for the binary paste systems were noted directly from their respective calorimeter curves.

The total heat of hydration for the plain cement paste was found to be 242.79 J/kg. Figure 5.14 shows a comparison of the total heat of hydration for all the fly ashes and the plain cement paste. In Figure 5.14, the first 13 bars represent the total heat of hydration for the binary binder systems containing Class C ashes. The next seven bars represent Class F ashes and the last bar represents the same data for a paste containing plain cement paste.

It is clear from Figure 5.14 that all the ashes tend to reduce the total heat of hydration as compared to plain cement paste except for one Class F ash, Miami 8. Most of the Class C ashes had a very similar total heat of hydration. The total heat of hydration in Class C ashes ranges from 207 J/kg to 233 J/kg and the total heat in Class F ashes had a wider range from 194 J/kg to 256 J/kg. The highest value of total heat was 256.88 J/kg and was obtained for a Class F ash, Miami 8. It is however interesting to note that this fly ash was the only fly ash which had advanced the occurrence of the peak heat of hydration. No correlations were seen between total heat of hydration and time of peak heat of hydration, peak heat of hydration or the setting time for all the ashes.

5.3.2.3.1 Selection of variables for statistical modeling. Statistical linear regression models were built for the total heat of hydration of the binary paste systems using all data points given in Table 5.26. The independent variables considered when constructing the regression models are mentioned in Table 5.1.

A SAS code was written which investigated all the possible combinations of independent variables to construct the regression models. A template of the code is given in Appendix B. The program uses all independent variables and the dependent variable (totalheat). The output of the program consists of a table containing the list of combinations of independent

TABLE 5.25
Observed and predicted time of peak heat of hydration (minutes) for the test ashes.

Fly Ash	Class	Observed Timepeak	Predicted Timepeak	Residual	Squared Residual
NIP 1	F	332	707.4662	375.4662	140974.9
NIP1A	C	632.5	—	—	—

TABLE 5.26
Total heat of hydration for all the fly ashes.

Fly Ash	Class	Total Heat (J/kg)	Fly Ash	Class	Total Heat (J/kg)
Edwards	C	207.38	Baldwin	C	225.62
Joppa	C	208.65	Miller	C	233.5
Hennepin	C	209.31	Rush Island	C	233.85
Vermilion	C	210.4	Petersburg	F	194.14
Rockport	C	211.36	Miami 7	F	217.74
Kenosha	C	212.61	Trimble	F	218.48
Will County	C	212.99	Mill Creek	F	220.77
Labadie	C	215.79	Elmer smith	F	230.07
Schahfer	C	218.66	Moscow	F	230.66
Joliet	C	221.83	Miami 8	F	256.88

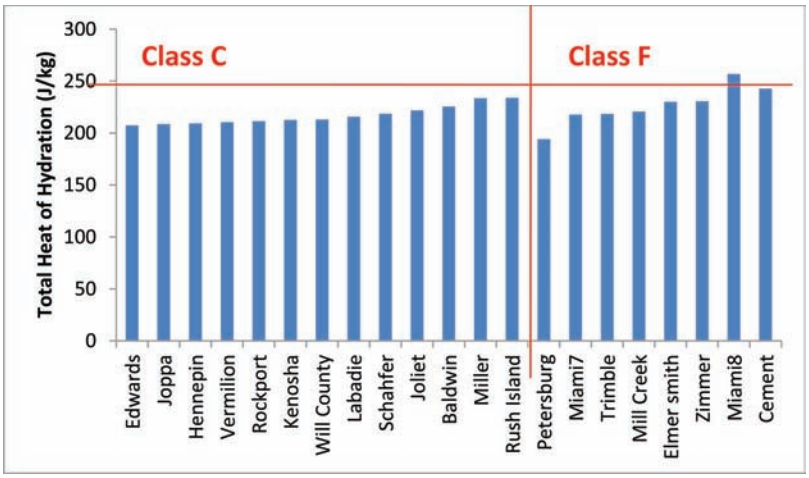

Figure 5.14 Comparison of total heat of hydration for all the paste systems.

variables forming linear regression models, sorted according to the adj-R^2 values. The values of the R^2 are also listed in the table for each model.

The best ten regression models are listed in Table 5.27.

From the Table 5.27, it can be inferred that both physical and chemical characteristics of fly ashes affect the total heat of hydration, the most important variables being blaines, meansize, carbon, SAF and cao (listed in Model 1).

The R^2 and adj-R^2 for the model were relatively higher than for peak heat of hydration. The ranges of the total heat of hydration for both the classes were significantly different.

The variables chosen to build the linear regression models for Class C and Class F ashes were meansize, carbon, SAF and cao. This was the four variables set which had the best adj-R^2 of 0.3948 and R^2 of 0.5222. The reason for choosing four variables set over a three variables set for linear regression analysis was that, none of the three variables sets produced a significant model even for at least one of the classes of ashes with a good adj-R^2. The best model with three variables was found to contain carbon, SAF and mgo. A regression analysis on the two classes of ashes using these variables rendered an extremely poor fit (adj-R^2 = 0.0042 for Class C ashes and adj-R^2 = 0.0104 for Class F ashes), combined with a non-significant model for both the classes.

From the chosen best model with four variables, it is clear that both physical and chemical characteristics of fly ash influence the total heat of hydration.

5.3.2.3.2 Linear regression models for binary pastes containing class C ashes. Linear regression analysis was performed on the total heat of hydration of binary paste systems containing Class C ashes, using the four

chosen dependent variables meansize, carbon, SAF and cao. The ANOVA table along with the regression coefficients and the p-values are shown in Table 5.28 shows the results of the model (R^2, adj-R^2 and parameter estimate values along with the p values for the model and the variables) ANOVA analysis.

The sign of the coefficients in the parameter estimate column indicates the effect of the variables on the dependent variable. The sign of the coefficient of the variable, meansize was positive indicating that the increase in the mean size of the fly ashes leads to an increase in the total heat of hydration of the binder. This definitely is not the case as the increase in the mean particle size reduces the specific surface area of the binders, thus increasing the rate of hydration. However, the increase in the rate of hydration was seen only in the early stages of the reaction, in the first peak according to Hasset and Eylands (*38*). This part of the calorimeter curve was not captured in the present modeling process for reason mentioned in Section 3.3.3.3. It was found that the total heat released after the deduction of the initial peak, remains constant with the addition of the fly ash (*38*). This was also observed in the comparison bar chart in Figure 5.14.

The effect of loss on ignition seems to be justified as the increase in the LOI leads to an increase in the carbon content of the fly ash, which in turn leads to withholding of more water in its pores. Thus, a reduction in the rate of reaction will be observed. However the p-value of this variable was higher than 0.1, and hence was not significant.

The p-values of the variables SAF and cao were also greater than 0.1, which implies that these variables were no significant either, when compared to the mean particle size. However, the inclusion of these variables implies that there was a considerable difference in the performance of Class C and F ashes.

The R^2 and the adj-R^2 for the model for Class C ashes was better than for the model including both the classes, thus giving better predictions. In addition, the p-value for the model was also less than 0.1, which means that the predictions were reliable.

Table 5.29 shows the observed and predicted total heat of hydration of all the Class C ashes. The residuals and the squared residuals of the model are also included.

It can be seen from Table 5.29 that most the values have been predicted within ± 5 J/kg (which was observed as the standard deviation for multiple tests on similar samples).

Figure 5.15 shows the plot of the observed and predicted total heat of hydration for all the Class C ashes. It can be observed that the few points not predicted well lie at lower extreme of the set of points.

TABLE 5.27
Best ten regression models for total heat of hydration.

Model Number	Number of Variables in the Model	Adjusted R^2	R^2	Variables in the Model
1	5	0.4052	0.5618	blaines, meansize, carbon, SAF, cao
2	4	0.3948	0.5222	meansize, carbon, SAF, cao
3	4	0.3870	0.5161	meansize, carbon, SAF, mgo
4	4	0.3846	0.5142	blaines, meansize, carbon, mgo
5	5	0.3808	0.5438	blaines, meansize, carbon, SAF, mgo
6	5	0.3777	0.5414	blaines, meansize, carbon, mgo, glass
7	5	0.3732	0.5381	blaines, meansize, carbon, mgo, alumina
8	4	0.3731	0.5051	meansize, carbon, cao, mgo
9	5	0.3678	0.5342	blaines, meansize, carbon, cao, mgo
10	6	0.3677	0.5673	blaines, meansize, carbon, SAF, cao, mgo

TABLE 5.28
Regression analysis for total heat of hydration of binary pastes with Class C ashes.

Source	DF	Sum of Squares	Mean Square	Model F Value	Model p-Value
Model	4	639.783	159.9458	3.652021	0.0562
Error	8	350.372	43.7965		
Total	12	990.155			
		R^2	0.6461		
		adj-R^2	0.4692		
Variable	**DF**	**Parameter Estimate**	**Standard Error**	**Variable t-Value**	**Variable p-Value**
Intercept	1	559.8252	306.728	1.825152	0.1054
meansize	1	1.43925	0.4671	3.081246	0.0151
carbon	1	-37.928	22.447	-1.68967	0.1296
SAF	1	-3.8206	2.9122	-1.31193	0.2259
cao	1	-4.764	4.9528	-0.96188	0.3643

TABLE 5.29
Observed and predicted total heat of hydration of Class C ashes.

ID	Observed Totalheat (J/kg)	Predicted Totalheat (J/kg)	Residual (J/kg)	Squared Residual (J^2/kg^2)
Edwards	207.4	210.9	-3.4939	12.208
Joppa	208.7	218.3	-9.6913	93.921
Hennepin	209.3	206.3	3.003	9.0182
Vermilion	210.4	204.6	5.7689	33.28
Rockport	211.4	216.1	-4.7403	22.47
Kenosha	212.6	215.5	-2.9356	8.6177
Will County	213	220.4	-7.4561	55.594
Labadie	215.8	219	-3.185	10.145
Schahfer	218.7	213.9	4.745	22.515
Joliet	221.8	218	3.8005	14.444
Baldwin	225.6	220.8	4.8396	23.421
Miller	233.5	228.1	5.4052	29.216
Rush Island	233.9	229.9	3.94	15.524

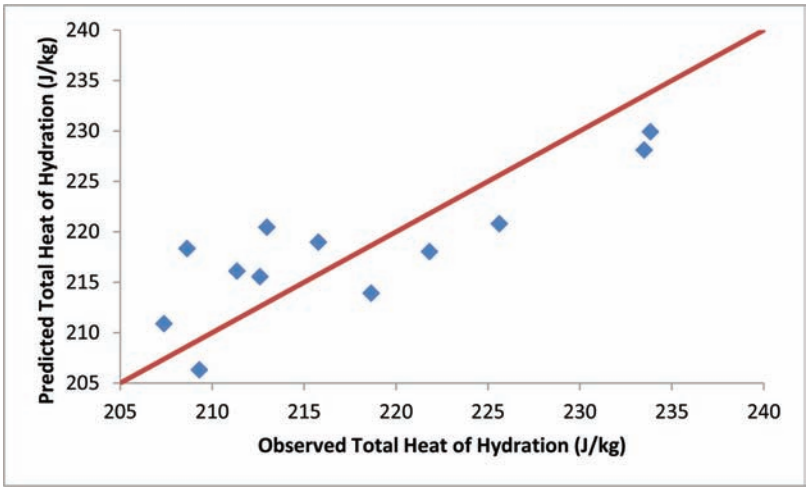

Figure 5.15 Plot showing the variations in the predicted and observed total heat of hydration for all the Class C ashes.

5.3.2.3.3 Linear regression models for binary pastes containing class F ashes. Linear regression analysis was performed on the total heat of hydration of binary paste systems containing Class F ashes, using the model with the three chosen dependent variables spsurface, meansize and mgo. Table 5.30 shows the results of the model (R^2, adj-R^2 and parameter estimate values along with the p values for the model and the variables) ANOVA analysis.

The sign of the coefficients in the parameter estimate column indicates the effect of the variables on the dependent variable. The sign of the coefficient of meansize was negative, indicating that the increase in the surface area of the fly ashes leads to a decrease in the total heat of hydration of the binder. However, this is not a reliable result as the p-values for the variable and the model were much larger than 0.1.

The R^2 and adj-R^2 for the model were very low and hence the predictions were very inaccurate. The p-value of the model was greater than 0.1 indicating that the model produces very unreliable predictions. The p-values for all the variables were much larger than 0.1 indicating that the regression model was highly unreliable in predicting the total heat of hydration.

Table 5.31 shows the observed and predicted total heat of hydrations of all the Class F ashes. The residuals and the squared residuals of the model are also included.

It can be seen from Table 5.31 that none of the seven ashes have been predicted accurately. This model cannot be used to predict the total heat of hydration for any new Class F fly ash.

Figure 5.16 shows the plot of the observed and predicted total heat of hydration for all the Class F ashes.

5.3.2.3.4 Model verification. Two fly ashes (NIP 1 – Class C ash and NIP 1A – Class F ash) not included in the set of fly ashes utilized for development of the above models were used to test their accuracy. The specific surface (spsurface, mean particle size (meansize) and the MgO (mgo) content of the fly ashes are given in Table 5.32. The observed and predicted set times for the test ashes are shown in Table 5.33.

TABLE 5.30
Regression analysis for total heat of hydration of binary pastes with Class F ashes.

Source	DF	Sum of Squares	Mean Square	Model F Value	Model p-Value
Model	4	1493.51	373.3775	1.17	0.5101
Error	2	640.2966	320.1483		
Total	6	2133.807			
		R^2	0.6999		
		adj-R^2	0.0998		
Variable	**DF**	**Parameter Estimate**	**Standard Error**	**Variable t-Value**	**Variable p-Value**
Intercept	1	659.605	506.0852	1.303348	0.3223
meansize	1	-2.2513	8.5489	-0.26334	0.8169
carbon	1	32.8216	42.9733	0.763767	0.5248
SAF	1	-4.8452	6.683	-0.725	0.5438
cao	1	-3.2055	6.6765	-0.48012	0.7719

TABLE 5.31
Observed and predicted total heat of hydration of Class F ashes.

ID	Observed Totalheat (J/kg)	Predicted Totalheat (J/kg)	Residual (J/kg)	Squared Residual (J^2/kg^2)
Petersburg	194.1	195.2	-1.067	1.138
Miami 7	217.7	225.4	-7.694	59.196
Trimble	218.5	226.2	-7.733	59.791
Millcreek	220.8	211.6	9.2007	84.652
Elmersmith	230.1	238.5	-8.439	71.223
Zimmer	230.7	233.8	-3.101	9.617
Miami 8	256.9	238	18.833	354.68

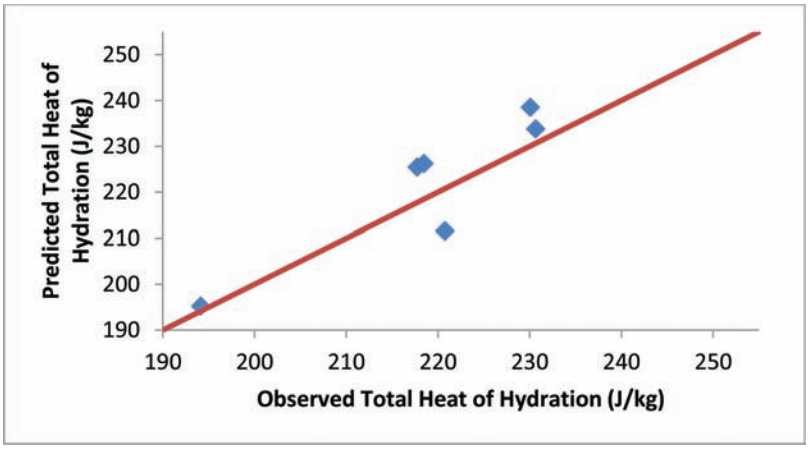

Figure 5.16 Plot showing the variations in the predicted and observed total heat of hydration for all the Class F ashes.

TABLE 5.32
Characteristics of the test fly ashes used for model verification.

Fly Ash	Spsurface (cm^2/cm^3)	Meansize (μm)	Mgo (%)
NIP 1	20978	3	2.84
NIP 1A	—	15	3.63

From Table 5.33, it was clear that the predictions of the class F model were not accurate. This was expected, as the p-value for the model for Class F ashes was much larger than 0.1 and R^2 for the model was extremely small. A better prediction for the Class C ash could be expected as the model was significant. However, the error of the intercept was high, which again might lead to erroneous predictions. Hence, these models cannot

be used for predicting the total heat of hydration for binders with either of the classes of ashes.

5.3.3 Thermo-Gravimetric Analysis

Thermo-gravimetric analysis was performed on all the binary paste systems. The data points for calcium hydroxide content, the non-evaporable water content and the loss on ignition were compared and modeled. The values of the calcium hydroxide content and the non-evaporable water content were read-off from the weight loss curve, with a correction applied, due to carbonation of the paste. The non-evaporable water content was calculated by the method described by Barneyback, 1983 (*36*). The results for calcium hydroxide content and non-evaporable water are shown in this section, while it was seen that the data for loss on ignition had a high correlation with the calcium hydroxide content.

5.3.3.1 Calcium hydroxide content. The values of the calcium hydroxide contents measured at four different ages (1 day, 3 day, 7 day and 28 day) for binary paste systems and cement paste are shown in the Table 5.34. All the values are in percentage of the weight of the sample.

TABLE 5.33
Observed and predicted total heat of hydration (J/kg) for the test ashes.

Fly Ash	Class	Observed Totalheat (J/kg)	Predicted Totalheat (J/kg)	Residual (J/kg)	Squared Residual (J^2/kg^2)
NIP 1	F	200.33	296.37	96.04656	9224.942
NIP1A	C	205.79	—	—	—

TABLE 5.34
Calcium hydroxide contents (% of sample weight) at four ages for all the fly ashes.

Fly Ash	Class	1 Day	3 Day	7 Day	28 Day
Baldwin	C	2.886	3.703	4.784	5.537
Edwards	C	3.405	3.619	4.285	5.148
Hennepin	C	2.824	3.533	5.861	6.308
Joliet	C	2.622	3.489	4.577	6.771
Joppa	C	2.688	3.371	4.848	6.625
Kenosha	C	2.805	3.482	5.094	6.336
Labadie	C	2.707	4.6	4.843	5.683
Miller	C	2.684	4.143	4.549	5.641
Rush Island	C	2.975	3.779	4.348	5.706
Schahfer	C	3.109	3.602	4.251	5.412
Vermilion	C	2.937	3.651	3.848	5.628
Will County	C	2.914	3.737	4.109	5.843
Elmer Smith	F	3.493	3.929	5.093	5.799
Miami 7	F	3.138	3.787	4.974	6.321
Mill Creek	F	3.065	3.903	4.917	5.997
Petersburg	F	2.977	3.814	4.292	6.501
Trimble	F	3.247	4.137	4.331	5.959
Zimmer	F	3.05	3.973	4.299	6.715
Cement		3.157	4.51	4.724	5.688

Figure 5.17 to Figure 5.20 show a comparison of the calcium hydroxide content for all the fly ashes at four ages. In all these figures, the first 12 bars represent the total heat of hydration for the binary paste systems containing Class C ashes. The next 6 bars denote Class F ashes and the last bar represents the same data for a paste containing plain cement paste.

It is clear from Figure 5.17 that most of the ashes tend to reduce the formation of calcium hydroxide at 1 day as compared to plain cement paste except for one Class C ash, Edwards and two Class F ashes, Trimble and Elmersmith. The calcium hydroxide content at 1 day in Class C ashes ranged from 2.62% to 3.41% and the calcium hydroxide content in Class F ashes had a narrower range from 3.05% to 3.5%. The highest value of the observed calcium hydroxide content at 1 day was 3.5%. This was observed for a Class F ash, Elmersmith. The lowest value of the calcium hydroxide content at 1 day was observed in a Class C ash (2.62%), Joliet.

From Figure 5.18, it can be seen that all of the ashes but one (Class C ash, Labadie) tend to reduce the formation of calcium hydroxide at 3 days as compared to plain cement paste. This fly ash had a very low content at 1 day and had showed a remarkable increase in the calcium hydroxide content. The reduction in the amount of calcium hydroxide at earlier ages is understandable as fly ash is inert both in terms of hydration reaction or pozzolanic reaction in the early ages.

The calcium hydroxide content at 3 days in Class C ashes ranges from 3.37% to 4.6% and the calcium hydroxide content in Class F ashes has a narrower range from 3.79% to 4.14%. The highest value of calcium hydroxide content at 3 days, 4.51%, was observed for Labadie, which is a Class C ash, and the lowest was observed in a Class C ash with 3.37%, Joppa.

It is clear from Figure 5.19 that the fly ashes start to assist in the hydration reaction leading to a small increase in the formation of calcium hydroxide at 7 days in a few fly ashes when compared to plain cement paste. This increase in the rate of formation of calcium hydroxide can be attributed to an increase in the rate of the hydration reaction in cements due to the presence of fly ash particles. It was observed by Wang et al. (*39*), that the reaction rates of cement in fly ash-cement pastes depend on the amount of fly ash present in the paste system. Apart from the fly ash content in the paste systems, other properties of fly ash might also contribute significantly to the reaction rates. This can be inferred from the variables, which affect this process, in the following sections.

The calcium hydroxide content at 7 days in Class C ashes ranged from 2.62% to 3.41% and the calcium hydroxide content in Class F ashes had a narrower range from 3.05% to 3.5%. The highest value amongst all the ashes was 3.5%, which was a Class F ash, Elmersmith, and the lowest was a Class C ash with 2.62%, Joliet.

From the Figure 5.20 it can be seen that most of the ashes have caused an increase in the formation

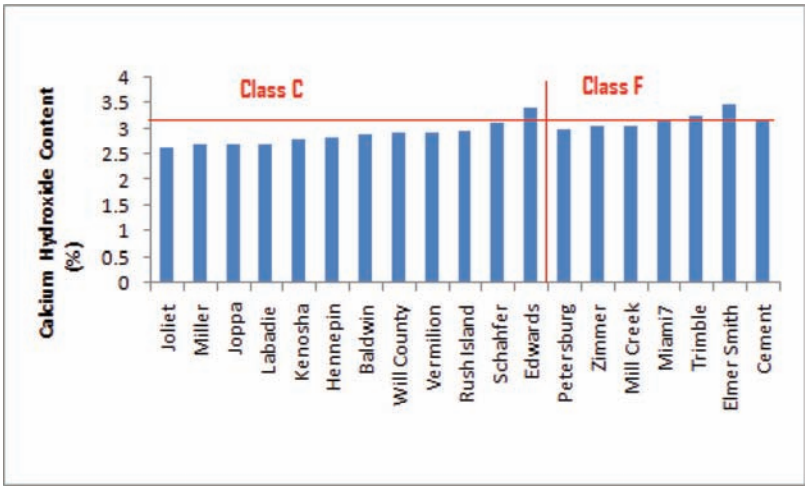

Figure 5.17 Comparison of calcium hydroxide content at 1 day for all the paste systems.

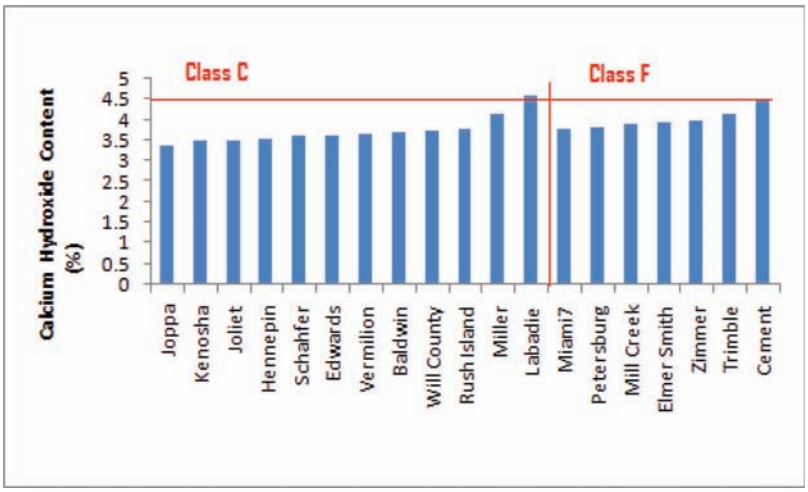

Figure 5.18 Comparison of calcium hydroxide content at 3 day for all the paste systems.

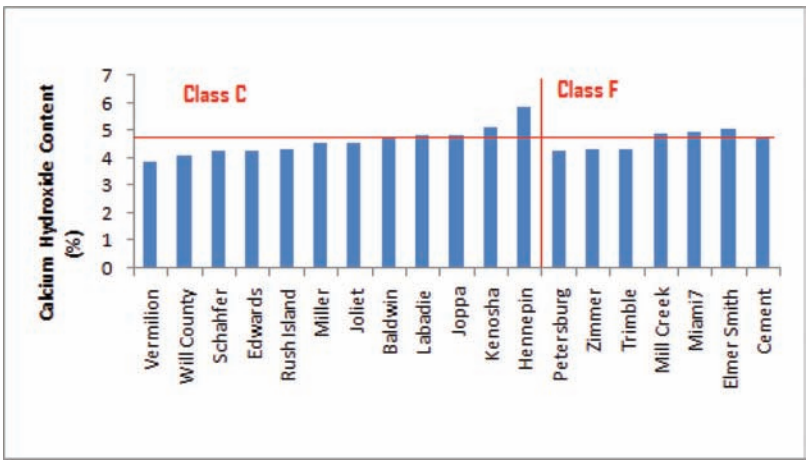

Figure 5.19 Comparison of calcium hydroxide content at 7 day for all the paste systems.

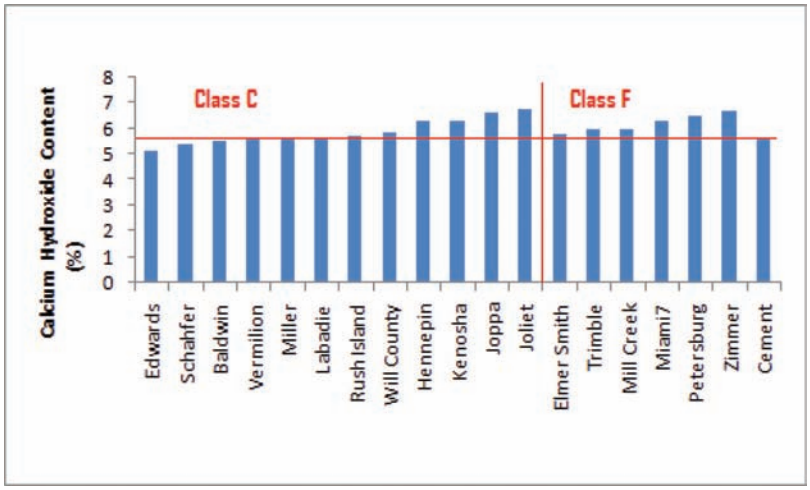

Figure 5.20 Comparison of calcium hydroxide content at 28 day for all the paste systems.

of calcium hydroxide content at the age of 28 days compared to plain cement paste. This certainly implies that the rate of hydration reaction of fly ash at this stage dominates over the rate of pozzolanic reaction for quite a few ashes. In addition, the amount of alkalis released by the presence of fly ash in the system could have had an effect on the rate of reaction of the cement in the fly ash-cement binder systems. This complies with the findings of Marsh and Day (*40*), who pointed out that the pozzolanic reaction takes into effect only at much later ages, around 56 days.

The calcium hydroxide content at 28 days in Class C ashes ranged from 5.15% to 6.77% and the calcium hydroxide content in Class F ashes had a narrower range from 5.79% to 6.71%. The highest value of the calcium hydroxide content at 28 days was 6.77%. This was observed for a Class C ash, Joliet, which incidentally had the lowest percentage at 1 day. It is interesting to note how the percentage of calcium hydroxide in Joliet fly ash paste system progressed from the lowest in the group of ashes at 1 day to the highest at 28 days. The lowest percentage of calcium hydroxide content observed within all the ashes was 5.15%. This was observed in a Class C ash, Edwards, which coincidentally had the highest amount of calcium hydroxide at 1 day. Again, the percentage of calcium hydroxide in Edwards' fly ash paste system gradually reduced from the highest of the group of class C ashes at 1 day to the lowest of the group by 28 days.

5.3.3.1.1 Selection of variables for statistical modeling. Statistical linear regression models were built for the amount of calcium hydroxide formed at 1, 3, 7 and 28 days in the binary paste systems using all data points given in Table 5.34. The independent variables considered when constructing the regression models are mentioned Table 5.1.

A SAS code was written, which investigated all the possible combinations of independent variables to construct the regression models. A template of the code is given in Appendix B. The program uses all independent variables and the dependent variable (calcium hydroxide content). The output of the program consists of a table containing the list of combinations of independent variables forming linear regression models, sorted according to the adj-R^2 values. The values of the R^2 are also listed in the table for each model.

TABLE 5.35
Chosen three variable models for calcium hydroxide content at all the ages.

Age (Days)	Variables	Adjusted R^2	R^2
1	blaines, carbon, alumina	0.7527	0.8022
3	blaines, meansize, sulfate	0.2222	0.3594
7	blaines, cao, glass	0.4073	0.5119
28	blaines, spsurface, sulfate	0.6104	0.6791

Instead of the table with the best ten regression models (as was the case with time of set and heat of hydration), a table with the chosen best model containing three variables at each age is shown along with the adj-R^2 for the models in Table 5.35.

From the Table 5.35 it can be inferred that both physical and chemical characteristics of fly ashes affect the amount of calcium hydroxide content formed at various ages, the most important variables being blaines, meansize, spsurface, carbon, cao, glass and sulfate. The specific surface area of fly ash using Blaine's apparatus was the common variable at all the ages.

The R^2 and adj-R^2 for the model were relatively higher than all the previous dependent variables (heat of hydration and time of set). Hence, the fit of the model was better than the other models. However, the p-values for the models and the individual variables comprising these models would indicate the reliability of the models to predict the properties for any new fly ashes. The presence of the variables SAF and cao indicates the difference in the behavior of both the classes of ashes.

The linear regression models for the amount of calcium hydroxide formed at various ages are shown in the following sections.

5.3.3.1.2 Linear regression models for binary pastes containing class C ashes. Linear regression analysis was performed on the amount of calcium hydroxide formed at various ages of binary pasta systems containing Class C ashes, using the model with the three chosen dependent variables based in adj-R^2 as shown in Table 5.35. Table 5.36, Table 5.38, Table 5.39 and Table 5.41 show the results of the model (R^2, adj-R^2 and parameter estimate values along with the p values for the model and the variables) ANOVA analysis.

The sign of the coefficients in the parameter estimate column indicates the effect of the variables on the dependent variable. The sign of the coefficient of blaines was positive, indicating that the increase in the surface area of the fly ashes leads to an increase in the calcium hydroxide content of the paste. This is justified as the increase in the specific surface area increases the rate of reaction and thus increasing the rate of formation of calcium hydroxide. In addition, this was the only significant variable of the three selected ones.

The effect of Loss on ignition (carbon content in the fly ash) does not seem to be justified as the increase in the carbon content leads to withholding of more water in its pores, thus leading to a reduction of the rate of reaction. Here, we have a positive sign for the coefficient of the variable, carbon, which suggests the opposite. However the p-value of this variable was much higher than 0.1, and hence is not significant.

The p-value of the variable alumina was also much greater than 0.1, which implies that these variables were not significant either.

The absence of the variables cao or SAF leads to a conclusion that at early ages, the class of the ash relatively does not influence the performance of the binder system in terms of the formation of calcium hydroxide content at early ages.

The R^2 and the adj-R^2 for the model for Class C ashes was better than for the model that includes both the classes, thus giving better predictions. In addition, the p-value for the model was also less than 0.1, which means that the predictions are reliable.

Table 5.37 shows the observed and predicted calcium hydroxide content at the age 1 day, for all the Class C ashes. The residuals and the squared residuals of the model are also included.

Figure 5.21 shows the plot of the observed and predicted calcium hydroxide content at 1 day, for all the Class C ashes. It can be observed that the three points not predicted well lie at either extremes of the set of points.

Table 5.38 shows the results of the model (R^2, adj-R^2 and parameter estimate values along with the p values for the model and the variables) ANOVA analysis.

The p-values for the model and all the variables were much greater than 0.1 suggesting that this model cannot be used for predicting the calcium hydroxide content at 3 days. Hence, there cannot be a three variable model, which can predict the amount of calcium hydroxide formed at 3 days. The predictions for this model were not reliable and hence not shown.

The regression analysis of calcium hydroxide formed at the age of 7 days is shown in Table 5.39.

The sign of the coefficients in the parameter estimate column indicates the effect of the variables on the dependent variable. The sign of the coefficient of blaines was positive, indicating that the increase in the surface area of the fly ashes leads to an increase in the calcium hydroxide content of the binder. This is justified as the increase in the specific surface area increases the rate of reaction and thus increasing the rate of formation of calcium hydroxide. The variable had a p-value smaller than 0.1 and hence was significant.

The p-value of the variable, cao was large, which implies that this variable was not significant. The error for the parameter estimate of this variable was very large as well.

The p-value of the variable glass was also smaller than 0.1, which implies that this variable was significant. The sign of the coefficient was positive, which means that the increase in the glass content leads to a faster rate of formation of calcium hydroxide at the age of 7 days.

The presence of the variable cao leads to a conclusion that at the age of 7 days, the class of the ash does have an influence on the performance of the paste system in terms of the formation of calcium hydroxide.

TABLE 5.36
Regression analysis for the amount of calcium hydroxide formed at 1 day in binary paste systems with Class C ashes.

Source	DF	Sum of Squares	Mean Square	Model F Value	Model p-Value
Model	3	0.3087	0.1029	3.852309	0.0565
Error	8	0.21369	0.02671125		
Total	11	0.52239			
		R^2	0.5909		
		adj-R^2	0.4375		
Variable	**DF**	**Parameter Estimate**	**Standard Error**	**Variable t-Value**	**Variable p-Value**
Intercept	1	1.31376	1.15436	1.138085	0.288
blaines	1	0.0001918	0.00005818	3.296494	0.0109
carbon	1	0.07257	0.49086	0.147843	0.8861
alumina	1	0.02428	0.06525	0.372107	0.7195

TABLE 5.37
Observed and predicted calcium hydroxide content at 1 day of Class C ashes.

Fly Ash	Observed $Ca(OH)_2$ %	Predicted $Ca(OH)_2$ %	Residual %	Squared Residual
Joliet	2.622	2.81	-0.189	0.0356
Miller	2.684	2.731	-0.046	0.0021
Joppa	2.688	2.614	0.0739	0.0055
Labadie	2.707	3.002	-0.295	0.0872
Kenosha	2.805	2.683	0.1224	0.015
Hennepin	2.824	2.811	0.0129	0.0002
Baldwin	2.886	2.99	-0.104	0.0109
Will County	2.914	2.922	-0.008	6E-05
Vermilion	2.937	2.862	0.0754	0.0057
Rush Island	2.975	2.873	0.1024	0.0105
Schahfer	3.109	3.047	0.0618	0.0038
Edwards	3.405	3.212	0.1932	0.0373

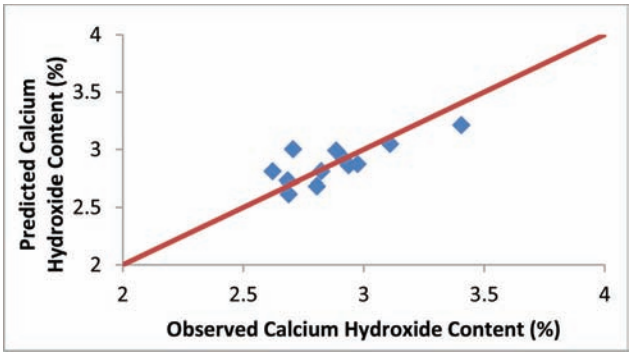

Figure 5.21 Plot showing the variations in the predicted and observed calcium hydroxide content for all the Class C ashes at 1 day.

The R^2 and the adj-R^2 for the model for Class C ashes were high, thus giving rise to a better fit of the data. In addition, the p-value for the model was also less than 0.1, which means that the predictions are reliable.

Table 5.40 shows the observed and predicted calcium hydroxide content at the age 7 days, for all the Class C ashes. The residuals and the squared residuals of the model are also included.

Figure 5.22 shows the plot of the observed and predicted calcium hydroxide content at 7 days, for all Class C ashes. It can be observed that the two points not predicted well lie at lower extreme of the set of points.

Table 5.41 shows the ANOVA analysis for the calcium hydroxide content formed at 28 days.

The sign of the coefficients in the parameter estimate column indicates the effect of the variables on the dependent variable. The sign of the coefficient of blaines was positive, indicating that the increase in the surface area of the fly ashes leads to an increase in the calcium hydroxide content of the binder. This is justified as the increase in the specific surface area increases the rate of reaction and thus increasing the rate of formation of calcium hydroxide. In addition, this was the only significant variable of the three selected ones.

The effect of spsurface is also justified as described above. However, the variable was not significant as the p-value was greater than 0.1.

The p-value of the variable sulfate was also greater than 0.1, which implies that this variable was not significant either. However, the coefficient suggests that the increase in the amount of sulfate, leads to an increase in the amount of calcium hydroxide formed at later ages.

The R^2 and the adj-R^2 for the model for Class C ashes was better than for the model that includes both the classes, thus giving a better fit. In addition, the p-value for the model was also less than 0.1, which means that the predictions were reliable.

Table 5.42 shows the observed and predicted calcium hydroxide content at the age 28 days, for all the Class C ashes. The residuals and the squared residuals of the model are also included.

Figure 5.23 shows the plot of the observed and predicted calcium hydroxide content at 28 days, for all the Class C ashes. It can be seen that most of the points are predicted accurately.

5.3.3.1.3 Linear regression models for binary pastes containing class F ashes. Linear regression analysis was performed on the calcium hydroxide content of binary paste systems containing Class F ashes, using the model with the three chosen dependent variables blaines, spsurface, and sulfate. Table 5.43, Table 5.45, Table 5.46 and Table 5.47 show the results of the model (R^2, adj-R^2 and parameter estimate values along with the p values for the model and the variables) ANOVA analysis.

The sign of the coefficients in the parameter estimate column indicates the effect of the variables on the dependent variable. The sign of the coefficient of blaines was negative, indicating that the increase in the surface area of the fly ashes leads to a decrease in the calcium hydroxide content of the hydrated binder. The opposite of the above result is expected, as the increase in the

TABLE 5.38
Regression analysis for the amount of calcium hydroxide formed at 3 days in binary paste systems with Class C ashes.

Source	DF	Sum of Squares	Mean Square	Model F Value	Model p-Value
Model	3	0.47456	0.15818667	1.62524	0.2589
Error	8	0.77865	0.09733125		
Total	11	1.25321			
		R^2	0.3787		
		adj-R^2	0.1457		
Variable	**DF**	**Parameter Estimate**	**Standard Error**	**Variable t-Value**	**Variable p-Value**
Intercept	1	2.1004	0.90655	2.316916	0.0492
blaines	1	0.0000958	0.0001139	0.841089	0.4248
meansize	1	0.0488	0.03012	1.620186	0.1436
sulfate	1	0.4231	0.26678	1.585951	0.1514

TABLE 5.39
Regression analysis for the amount of calcium hydroxide formed at 7 days in binary paste systems with Class C ashes.

Source	DF	Sum of Squares	Mean Square	F Value	p-Value
Model	3	2.15889	0.71963	6.260646	0.0171
Error	8	0.91956	0.114945		
Total	11	3.07845			
		R^2	0.7013		
		adj-R^2	0.5893		
Variable	**DF**	**Parameter Estimate**	**Standard Error**	**t-Value**	**p-Value**
Intercept	1	3.47894	2.01361	1.727713	0.1223
blaines	1	0.000324	0.0001198	-2.70659	0.0268
cao	1	0.05958	0.06349	0.938415	0.3755
glass	1	1.03531	0.31541	3.282426	0.0111

TABLE 5.40
Observed and predicted calcium hydroxide content (%) at 7 days of Class C ashes.

Fly Ash	Observed $Ca(OH)_2$	Predicted $Ca(OH)_2$	Residual	Squared Residual
Vermilion	3.848	4.453	-0.604	0.3653
Will County	4.109	4.508	-0.399	0.1588
Schahfer	4.251	4.318	-0.067	0.0045
Edwards	4.285	4.31	-0.247	0.0006
Rush Island	4.348	4.321	0.0278	0.0008
Miller	4.549	4.541	0.0079	6E-05
Joliet	4.578	4.385	0.1929	0.0372
Baldwin	4.784	4.33	0.4546	0.2067
Labadie	4.843	4.59	0.2531	0.0641
Joppa	4.848	4.955	-0.107	0.0115
Kenosha	5.094	4.829	0.2647	0.0701
Hennepin	5.861	5.86	0.0006	0

surface area leads to an increase in the rate of reaction, as was observed in Class C ashes. However, this was not a reliable result as the p-values for the variable and the model were much larger than 0.1.

The variables carbon and alumina have negative and positive signs for their coefficients, respectively, indicating an increase in the carbon content leads to a decrease in the formation of calcium hydroxide and vice versa in the case of alumina. Both these variables had p-values of less than 0.1 indicating that these were the significant variables.

The R^2 and adj-R^2 for the model were very high and hence the predictions were accurate. The p-value of the model was less than 0.1 indicating that the model

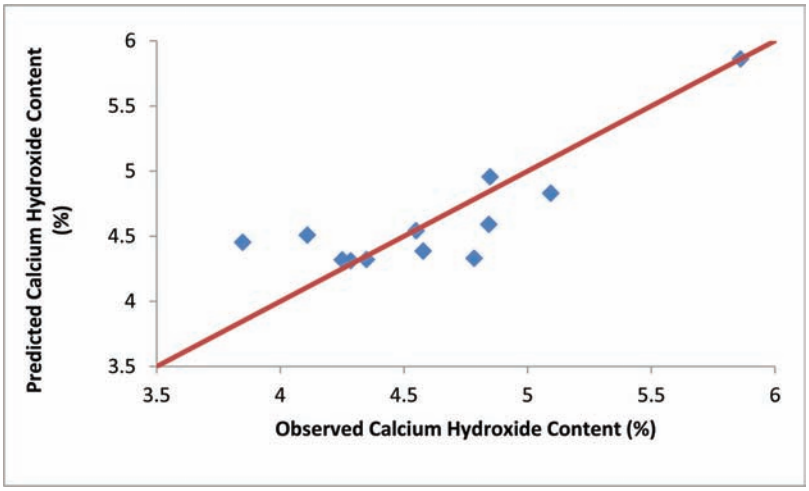

Figure 5.22 Plot showing the variations in the predicted and observed calcium hydroxide content at 7 days for all the Class C ashes.

TABLE 5.41
Regression analysis for the amount of calcium hydroxide formed at 28 days in binary pastes with Class C ashes.

Source	DF	Sum of Squares	Mean Square	Model F Value	Model p-Value
Model	3	2.01449	0.6715	6.8228	0.0135
Error	8	0.78737	0.09842		
Total	11	2.80186			
		R^2	0.719		
		adj-R^2	0.6136		
Variable	**DF**	**Parameter Estimate**	**Standard Error**	**Variable t-Value**	**Variable p-Value**
Intercept	1	7.90358	0.93598	8.444176	<0.0001
blaines	1	0.0005233	0.00011679	4.48061	0.0021
spsurface	1	0.00004188	0.00004984	0.840289	0.4252
sulfate	1	0.38429	0.26282	1.462179	0.1818

TABLE 5.42
Observed and predicted calcium hydroxide content (%) at 28 days of Class C ashes.

Fly Ash	Observed $Ca(OH)_2$	Predicted $Ca(OH)_2$	Residual	Squared Residual
Edwards	5.148	5.293	-0.1441	0.02076
Schahfer	5.412	5.34	0.07227	0.00522
Baldwin	5.536	5.465	0.07109	0.00505
Vermilion	5.628	5.842	-0.2138	0.04572
Miller	5.642	6.281	-0.6394	0.40882
Labadie	5.683	5.752	-0.0687	0.00472
Rush Island	5.706	5.555	0.15108	0.02283
Will County	5.843	5.799	0.04466	0.00199
Hennepin	6.308	6.044	0.26387	0.06962
Kenosha	6.336	6.471	-0.1351	0.01825
Joppa	6.625	6.378	0.24651	0.06077
Joliet	6.771	6.419	0.3516	0.12362

produces reliable predictions. The p-values for all the variables except blaines were smaller than 0.1 indicating that the regression model is reliable in predicting the amount of calcium hydroxide at
1 day.

Table 5.44 shows the observed and predicted calcium hydroxide content at 1 day for all the Class F ashes. The residuals and the squared residuals of the model are also included.

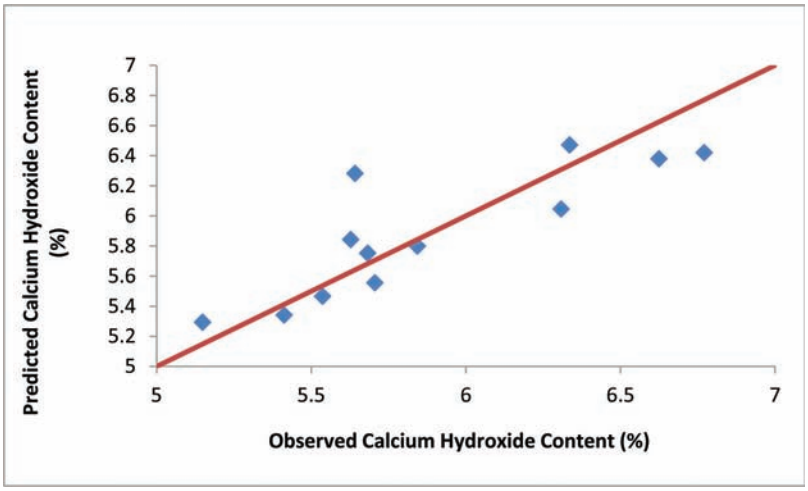

Figure 5.23 Plot showing the variations in the predicted and observed calcium hydroxide content at 28 days for all the Class C ashes.

TABLE 5.43
Regression analysis for calcium hydroxide content at 1 day for binary paste systems with Class F ashes.

Source	DF	Sum of Squares	Mean Square	Model F Value	Model p-Value
Model	3	0.16838	0.05613	21.02	0.0458
Error	2	0.00534	0.00267		
Total	5	0.17372			
		R^2	0.9692		
		adj-R^2	0.9231		
Variable	**DF**	**Parameter Estimate**	**Standard Error**	**Variable t-Value**	**Variable p-Value**
Intercept	1	3.03427	0.15684	19.34628	0.0027
blaines	1	-0.000006	0.00004131	-0.14234	0.8998
carbon	1	0.41087	0.05419	7.582026	0.017
alumina	1	-0.0276	0.0063	-4.38095	0.0484

TABLE 5.44
Observed and predicted calcium hydroxide content (%) at 1 day for Class F ashes.

Fly Ash	Observed $Ca(OH)_2$	Predicted $Ca(OH)_2$	Residual	Squared Residual
Petersburg	2.97742	2.99139	-0.01398	0.0002
Zimmer	3.0502	3.0969	-0.0467	0.00218
Millcreek	3.06588	3.02765	0.038234	0.00146
Miami 7	3.1383	3.14665	-0.00835	6.97E-05
Trimble	3.24728	3.20997	0.037311	0.00139
Elmersmith	3.49378	3.5003	-0.00652	4.25E-05

It can be seen from Table 5.44 that all of the seven ashes have been predicted well. This model can be used to predict the calcium hydroxide content for any new Class F fly ash.

Figure 5.24 shows the plot of the observed and predicted calcium hydroxide content for all the Class F ashes at 1 day.

Table 5.45 shows the regression analysis of the amount of calcium hydroxide formed at the age at 3 days for all class F ashes.

As was the case with Class C ashes, the predictions for the class F ashes using a three variable model are not possible as the p-value was very high and the R^2 and adj-R^2 values were very low. It was also seen that the best model with four variables also yielded a p-value of greater than 0.1 and hence cannot be used for predictions.

Table 5.46 shows the regression analysis for calcium hydroxide content at 7 days for class F ashes.

None of the variables or the model had a p-value less than 0.1, leading to a conclusion that the model cannot be used for predicting the calcium hydroxide content of class F ashes. Hence, the table and plot for the predictions are not shown.

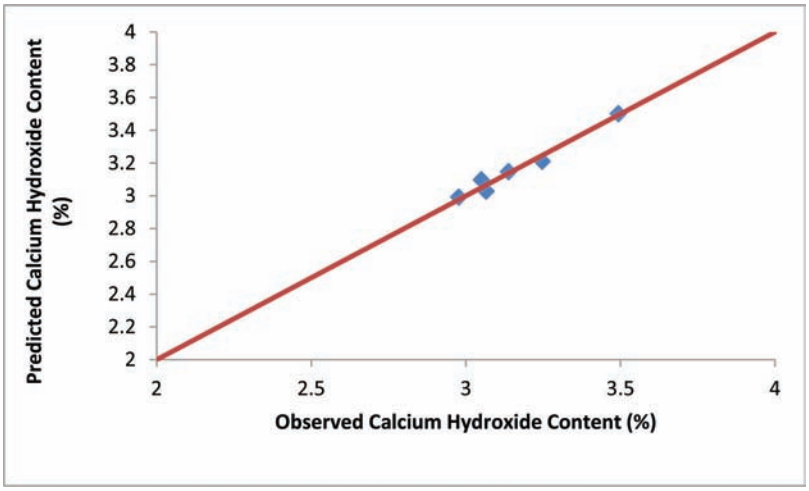

Figure 5.24 Plot showing the variations in the predicted and observed calcium hydroxide content at 1 day for all the Class F ashes.

TABLE 5.45
Regression analysis for calcium hydroxide content at 3 day for binary paste systems with Class F ashes.

Source	DF	Sum of Squares	Mean Square	Model F Value	Model p-Value
Model	3	0.01685	0.005616667	0.18	0.902
Error	2	0.0624	0.0312		
Total	5	0.07925			
		R^2	0.2126		
		adj-R^2	-0.9685		
Variable	**DF**	**Parameter Estimate**	**Standard Error**	**Variable t-Value**	**Variable p-Value**
Intercept	1	3.972	1.30082	3.053459	0.0926
blaines	1	-0.000012	0.000013136	-0.90743	0.936
meansize	1	-0.00321	0.0367	-0.08747	0.9383
sulfate	1	0.0881	0.16693	0.527766	0.6504

TABLE 5.46
Regression analysis for calcium hydroxide content at 7 days for binary paste systems with Class F ashes.

Source	DF	Sum of Squares	Mean Square	Model F Value	Model p-Value
Model	3	0.4977	0.1659	1.46	0.4321
Error	2	0.22802	0.11401		
Total	6	0.72572			
		R^2	0.6858		
		adj-R^2	0.2145		
Variable	**DF**	**Parameter Estimate**	**Standard Error**	**Variable t-Value**	**Variable p-Value**
Intercept	1	3.1044	0.93671	3.314153	0.0802
blaines	1	0.00001234	0.00030301	0.040725	0.9712
cao	1	0.12454	0.06776	1.837957	0.2075
glass	1	0.53989	0.39579	1.364082	0.3058

However, this was quite contrary to the model for class C ashes, which was found reliable. This could be due to the number of available points for class C, which was much larger than those were available for class F ashes.

Table 5.47 shows the regression analysis for calcium hydroxide content at 28 days for class F ashes.

The sign of the coefficients in the parameter estimate column indicates the effect of the variables on the

dependent variable. The sign of the coefficient of blaines was negative, indicating that the increase in the surface area of the fly ashes leads to a decrease in the calcium hydroxide content of the binder. The opposite of the above result is expected, as the increase in the surface area leads to an increase in the rate of reaction, as was observed in Class C ashes. However, this is not a reliable result as the p-values for the variable and the model were much larger than 0.1.

Similarly, the variable, sulfate was also not reliable as the p-value was greater than 0.1. The sign of this variable indicates that the increase in the amount of sulfate leads to an increase in the amount of calcium hydroxide formed at later ages, which was a similar observation at age 3 as well. However, both these results are not reliable as the coefficients are negative.

The variable spsurface has a positive sign, which was as expected. In addition, the p-value of the variable was also less than 0.1.

The R^2 and adj-R^2 for the model were high and hence the predictions were very accurate. The p-value of the model was less than 0.1 indicating that the model produces reliable predictions. However, the p-values for all the variables except spsurface were smaller than 0.1 indicating that the regression model was not very reliable in predicting the amount of calcium hydroxide at 28 days.

Table 5.48 shows the observed and predicted calcium hydroxide contents at 28 days for all the Class F ashes. The residuals and the squared residuals of the model are also included.

It can be seen from Table 5.48 that calcium hydroxide content of all six fly ashes have been predicted well. This model can be used to predict the calcium hydroxide content at 28 days for any new Class F fly ash.

Figure 5.25 shows the plot of the observed and predicted calcium hydroxide content at 28 days for all the Class F ashes.

5.3.3.1.4 Model verification. Two fly ashes (NIP 1 – Class C ash and NIP 1A – Class F ash) not included in the set of fly ashes utilized for development of the above models were used to test their accuracy. The specific surface (spsurface, blaines) respectively, lime content (cao), sulfate content (sulfate), mean particle size (meansize), loss on ignition (carbon), alumina content (alumina) and the glass content of the fly ashes are given in Table 5.49. The observed and predicted calcium hydroxide contents for the significant models at different ages for the test ashes are shown in Table 5.50.

From Table 5.50, it can be seen that the prediction of both the Class C and Class F model at the age of 1 day is close to the observed values as the difference between the observed and predicted peak heat of hydration is only 0.2%. This was expected, as the p-value for the models were smaller than 0.1 and the intercept error is extremely small. Most of the variables also had very small p-values and hence the model is excellent for predictions. The predictions for Class C ash at 7 days were not accurate. This was also quite expected as the intercept, which the highest contribution in the model had a large error associated with it. Hence, even though

TABLE 5.47
Regression analysis for calcium hydroxide content at 28 day for binary paste systems with Class F ashes.

Source	DF	Sum of Squares	Mean Square	Model F Value	Model p-Value
Model	3	0.56119	0.187063333	5.40	0.1602
Error	2	0.06929	0.034645		
Total	5	0.63048			
		R^2	0.8901		
		adj-R^2	0.7253		
Variable	**DF**	**Parameter Estimate**	**Standard Error**	**Variable t-Value**	**Variable p-Value**
Intercept	1	5.45955	0.494	11.05172	0.0081
blaines	1	-0.0002886	0.00016748	-1.72313	0.227
spsurface	1	0.00014693	0.00004825	3.045181	0.093
sulfate	1	0.29562	0.14197	2.082271	0.1728

TABLE 5.48
Observed and predicted calcium hydroxide content (%) at 28 days for Class F ashes.

Fly Ash	Observed $Ca(OH)_2$	Predicted $Ca(OH)_2$	Residual	Squared Residual
Elmersmith	5.799	5.678	0.12102	0.01465
Trimble	5.959	6.144	-0.18515	0.03428
Millcreek	5.997	6.098	-0.10095	0.01019
Miami 7	6.321	6.254	0.06683	0.00447
Petersburg	6.502	6.474	0.02821	0.0008
Zimmer	6.716	6.646	0.07005	0.00491

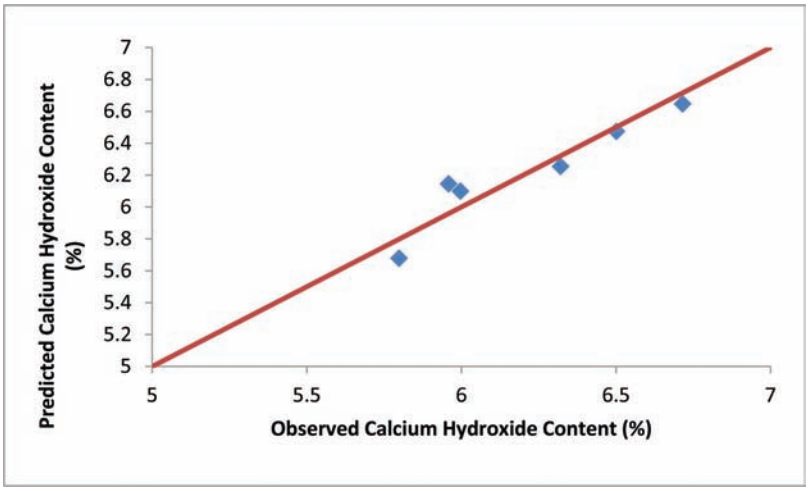

Figure 5.25 Plot showing the variations in the predicted and observed calcium hydroxide content at 28 days for all the Class F ashes.

TABLE 5.49
Characteristics of the test fly ashes used for model verification.

Fly Ash	spsurface (cm^2/cm^3)	blaines (cm^2/g)	meansize (μm)	carbon (%)	sulfate (%)	alumina (%)	glass	cao (%)
NIP 1	20978	7100	3	2.24	87	23	2.5545	2.64
NIP 1A	—	5200	15	9.3	58.1	15.2	0.9239	31

TABLE 5.50
Observed and predicted calcium hydroxide content (%) at all ages for the test ashes.

Fly Ash	Class	Age (Days)	Observed $Ca(OH)_2$	Predicted $Ca(OH)_2$	Residual	Squared Residual
NIP1A	C	1	3.591	3.363	-0.22792	0.051947
NIP1A	C	7	4.510	4.598	0.088143	0.007769
NIP1A	C	28	6.236	—	—	—
NIP 1	F	1	3.513	3.277	-0.23554	0.05548
NIP 1	F	28	5.426	5.949	0.523178	0.273715

the model was significant, the error in intercept lead to the poor prediction. Hence, this model is incapable of predicting the calcium hydroxide content at 7 days.

The model for Class F ash at 28 days resulted in an accurate prediction, however the larger residuals, than compared to the 1 day predictions maybe due to the p-value of the model being slightly larger than 0.1. Nevertheless, the intercept of the model had a very low error (low p-value) which means that the model can be successfully used to predict the calcium hydroxide content at 28 days. The same can be expected out of the Class C model for calcium hydroxide at 28 days as it has a very similar p-values and error in the variables; however, it could not be shown here due to the unavailability of the value for spsurface.

5.3.3.2 Non-evaporable water content. The values of the non-evaporable water contents measured at four different ages (1 day, 3 days, 7 days and 28 days) for binary paste systems and cement paste are shown in the Table 5.51. All the values are in percentage weight of the sample.

Figure 5.26, Figure 5.27, Figure 5.28 and Figure 5.29 show a comparison of the non-evaporable water content for all the fly ashes at four ages (1 day, 3 days, 7 days and 28 days). In all these figures, the first 12 bars represent the non-evaporable water content for the binary paste systems containing Class C ashes. The next 6 bars represent the non-evaporable water content in Class F ashes and the last bar represents the paste containing plain cement paste.

It is clear from Figure 5.26 that most of the ashes tend to reduce the amount of non-evaporable water at 1 day as compared to plain cement paste except for two Class C ashes, Edwards and Rush Island and two Class F ashes, Zimmer and Elmersmith. The non-evaporable water content at 1 day in Class C ashes ranged from 2.181% to 2.777% and the non-evaporable water

content in Class F ashes had a wider range from 2.09% to 2.78%. The highest value of the non-evaporable water content at 1 day was 2.78%. This was observed in a Class F ash, Zimmer and the lowest value of the non-evaporable water content at 1 day, 2.09%, was observed in a Class F ash, Petersburg.

From Figure 5.27, it can be seen that all of the ashes tend to reduce the amount of non-evaporable water at 3 days as compared to plain cement paste except for one Class C ash, Labadie. This fly ash had a low content at 1 day and has showed a remarkable increase in the non-evaporable content at 3 days. The reduction in the amount of non-evaporable at earlier ages is understandable as fly ash is inert both in terms of hydration reaction or pozzolanic reaction in the early ages. The degree of hydration in cement paste was higher than all the fly ash-cement systems except for one.

TABLE 5.51
Non-evaporable water contents (%) at four ages for all the fly ashes.

Fly Ash	Class	1 Day	3 Days	7 Days	28 Days
Baldwin	C	2.246	3.581	5.015	5.851
Edwards	C	2.683	3.701	4.746	5.954
Hennepin	C	2.459	3.683	4.623	6.107
Joliet	C	2.181	3.956	4.689	6.111
Joppa	C	2.322	3.39	4.721	6.836
Kenosha	C	2.319	3.638	4.921	6.226
Labadie	C	2.513	4.031	4.79	5.747
Miller	C	2.232	3.816	4.58	6.093
Rush Island	C	2.777	3.799	4.537	5.554
Schahfer	C	2.612	3.503	4.23	6.122
Vermilion	C	2.479	3.554	3.761	6.098
Will County	C	2.606	3.828	4.319	5.857
Elmer Smith	F	2.712	3.237	4.445	5.065
Miami 7	F	2.494	3.325	4.099	5.703
Mill Creek	F	2.383	3.196	4.447	6.183
Petersburg	F	2.091	3.641	3.907	5.855
Trimble	F	2.373	3.949	3.883	5.756
Zimmer	F	2.782	3.511	4.446	5.557
Cement		2.605	4.03	4.772	6.18

The non-evaporable water content at 3 days in Class C ashes ranged from 3.39% to 4.03% and the non-evaporable water content in Class F ashes had a range from 3.19% to 3.94%. The highest value of non-evaporable water content at 3 days was 4.03%. This was observed in Labadie, a Class C ash. The lowest non-evaporable water content at 3 days was observed in a Class F ash Mill Creek, 3.19%.

It is clear from Figure 5.28 that the fly ashes start to assist in the hydration reaction leading to a small increase in the non-evaporable water content at 7 days in a few fly ashes when compared to plain cement paste. Most of the Class C ashes had non-evaporable water content very similar to the plain cement paste at this age. This increase in the rate of formation of non-evaporable water content can be attributed to an acceleration of the hydration reaction in the fly ash-cement pastes due to the presence of the fly ash particles. This is also proved by the amount of calcium hydroxide, which increases by a significant amount at this age. An increase in both the amount of calcium hydroxide and the non-evaporable water content suggests that there is an increased hydration reaction in the cement present in the binder systems. It was observed by Wang et al. (*39*) that the reaction rates of cement in fly ash-cement pastes depend on the amount of fly ash present in the binder system. It might be possible that, apart from the fly ash content in the binder systems, other properties of fly ash might also contribute to the reaction rates. This can be inferred from the variables, which affect this process, in the following sections.

The non-evaporable water content at 7 days in Class C ashes ranged from 3.76% to 5.01% and the non-evaporable water content in Class F ashes had a narrower range from 3.88% to 4.45%. The highest value of non-evaporable water content was 5.01%. This was observed in a Class C ash, Baldwin. The lowest value of non-evaporable water content was also a Class C ash Vermilion, 3.76%.

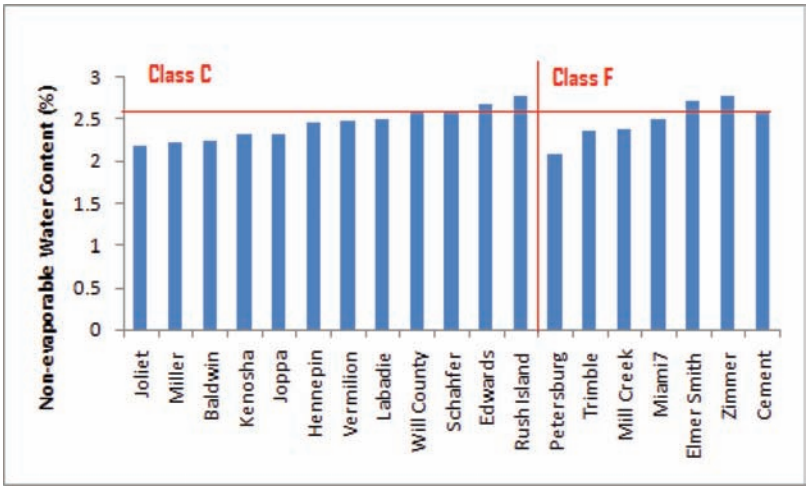

Figure 5.26 Comparison of non-evaporable water content at 1 day for all the paste systems.

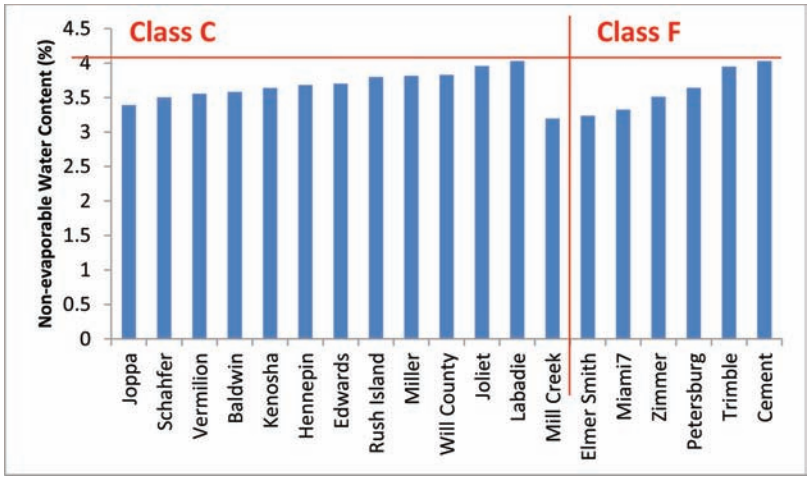

Figure 5.27 Comparison of non-evaporable water content at 3 days for all the paste systems.

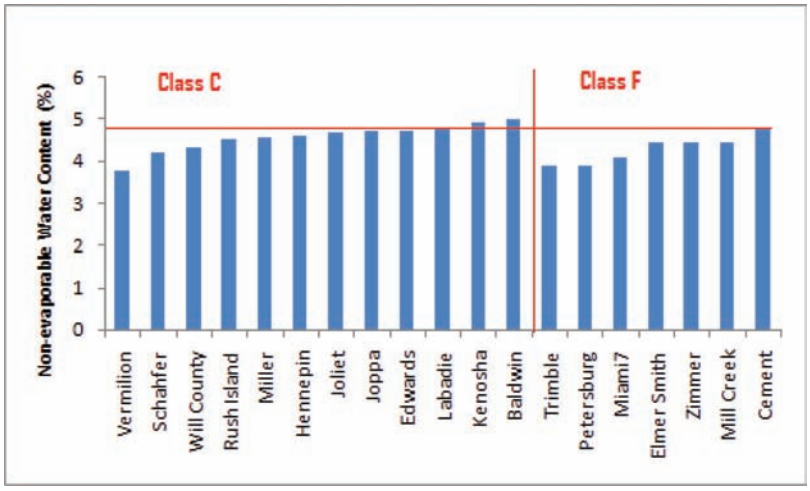

Figure 5.28 Comparison of non-evaporable water content at 7 days for all the paste systems.

From the Figure 5.29 it can be seen that all of the ashes have a lower non-evaporable water content at the age of 28 days than plain cement paste. A few of the ashes (Baldwin, Labadie, Will county) had a drastic reduction the rate of increase of non-evaporable water content. While, quite a few ashes, which had a lower amount of non-evaporable water, now have a higher rate of increase in the non-evaporable water content. This means that the inception of pozzolanic reaction in the ashes differs within the class. Pozzolanic reaction in some ashes occurs at earlier ages, while the reaction starts at a later age in other ashes. In the case of Class F ashes, except for the ash Mill Creek, no other ash shows any indication of a hydration reaction as the amount of non-evaporable water was consistently below the value of the plain cement paste.

These results comply with Marsh and Day (*40*), who pointed out that the pozzolanic reaction takes into effect only at much later ages, around 56 days.

The non-evaporable water content at 28 days in Class C ashes ranged from 5.55% to 6.84% and the non-evaporable water content in Class F ashes had a narrower range from 5.06% to 6.18%. The highest value of non-evaporable water content at 28 days was 6.84%, which was observed in a Class C ash, Joppa. This fly ash had low percentages at 1 and 3 days compared to the rest of the fly ashes. The lowest percentage of all the ashes was observed in a Class F ash Elmersmith with 5.06%. This fly ash had a high amount of non-evaporable water at 1 day when compared to the non-evaporable water content in rest of the ashes.

5.3.3.2.1 Selection of variables for statistical modeling. Statistical linear regression models were built for the amount of non-evaporable water at 1, 3, 7 and 28 days in the binary paste systems using all data points given in Table 5.51. The independent variables considered when constructing the regression models are mentioned in Table 5.1. A SAS code was written, which investigated all the possible combinations of independent variables to construct the regression models. A template of the code is given in

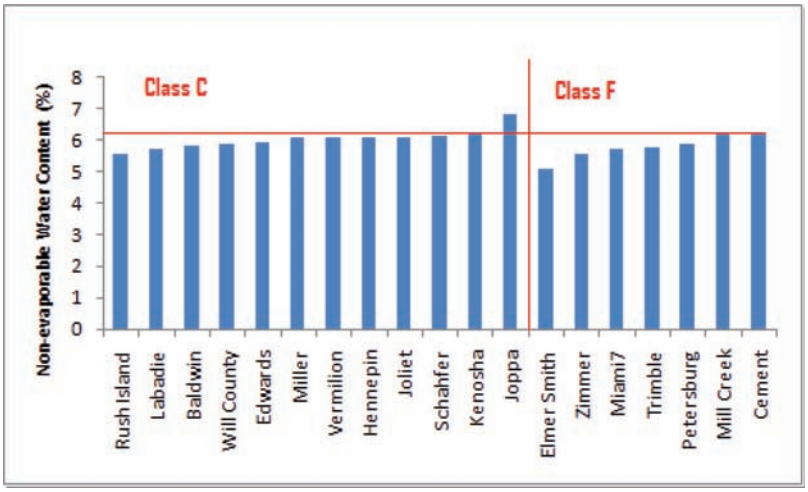

Figure 5.29 Comparison of non-evaporable water content at 28 days for all the paste systems.

Appendix B. The program uses all independent variables and the dependent variable (non-evaporable water content). The output of the program consists of a table containing the list of combinations of independent variables forming linear regression models, sorted according to the adj-R^2 values. The values of the R^2 are also listed in the table for each model.

Instead of the table with the best ten regression models (as was the case with time of set and heat of hydration), a table with the chosen best model containing three variables at each age is shown along with the adj-R^2 for the models.

From the Table 5.52 it can be inferred that both physical and chemical characteristics of fly ashes affect the non-evaporable water content at various ages, the most important variables being blaines, meansize, carbon, SAF, cao, mgo, alumina and sulfate.

The R^2 and adj-R^2 for the model were relatively slightly lower than the dependent variables, calcium hydroxide content at various ages. Hence, the fit of the model was slightly worse when compared to the models for calcium hydroxide. However, the p-values for the models and the individual variables comprising these models would indicate the reliability of the models to predict the properties for any new fly ashes. The presence of the variables SAF and cao indicates the difference in the behavior of both the classes of ashes in terms of the amount of non-evaporable water content at various ages.

The linear regression models for the amount of non-evaporable water formed at various ages is shown in the following sections.

5.3.3.2.2 Linear regression models for binary pastes containing class C ashes. Linear regression analysis was performed on the non-evaporable water content at various ages of binary paste systems containing Class C ashes, using the chosen dependent variables based in adj-R^2 as shown in Table 5.52. In the case of the model for 7 days, four variables were chosen as the best three variable model could not explain the variation

TABLE 5.52
Chosen three or four variable models for non-evaporable water content at all the ages.

Age (Days)	Variables	Adjusted R^2	R^2
1	blaines, carbon, alumina	0.3517	0.4661
3	sulfate, SAF, mgo	0.2222	0.3594
7	meansize, sulfate, cao, mgo	0.3416	0.4965
28	blaines, carbon, alumina	0.43	0.5306

in the non-evaporable content using the three variables. Table 5.53, Table 5.55, Table 5.57 and Table 5.58 show the results of the model (R^2, adj-R^2 and parameter estimate values along with the p values for the model and the variables) ANOVA analysis.

The sign of the coefficients in the parameter estimate column indicates the effect of the variables on the dependent variable. The sign of the coefficient of blaines was positive, indicating that the increase in the surface area of the fly ashes leads to an increase in the non-evaporable water content of the binder. This is justified as the increase in the specific surface area increases the rate of reaction. In addition, this was the only significant variable of the three selected ones.

The effect of Loss on ignition is justified as the increase in the LOI leads to an increase in the carbon content, which in turn leads to withholding of more water in its pores. Thus the rate of reaction is reduced. Here, we have a negative sign for the coefficient of the variable, carbon, which confirms the hypothesis. However the p-value of this variable was larger than 0.1, and hence was not significant.

The p-value of the variable alumina was also much greater than 0.1, which implies that these variables are not significant either.

The R^2 and the adj-R^2 for the model for Class C ashes were similar to the model that includes both the classes, thus giving a better fit. In addition, the p-value

TABLE 5.53
Regression analysis for the amount of non-evaporable water at 1 day in binary pastes with Class C ashes.

Source	DF	Sum of Squares	Mean Square	F Value	p-Value
Model	3	0.23463	0.07821	3.525554	0.0684
Error	8	0.17747	0.02218375		
Total	11	0.4121			
		R^2	0.5694		
		adj-R^2	0.4079		
Variable	**DF**	**Parameter Estimate**	**Standard Error**	**t-Value**	**p-Value**
Intercept	1	2.22771	1.05198	2.117635	0.0671
blaines	1	0.000132	0.00005302	2.494908	0.0372
carbon	1	-0.64483	0.44733	-1.44151	0.1874
alumina	1	-0.01391	0.05946	-0.23394	0.8209

TABLE 5.54
Observed and predicted non-evaporable water content (%) at 1 day of Class C ashes.

Fly Ash	Observed W_n	Predicted W_n	Residual	Squared Residual
Joliet	2.181	2.371	-0.19039	0.036249
Miller	2.231	2.325	-0.09351	0.008744
Baldwin	2.245	2.449	-0.20339	0.041369
Kenosha	2.318	2.291	0.02666	0.000711
Joppa	2.321	2.329	-0.00813	0.000066
Hennepin	2.458	2.242	0.21577	0.046557
Vermilion	2.478	2.421	0.0571	0.00326
Labadie	2.512	2.627	-0.11509	0.013246
Will County	2.606	2.525	0.08073	0.006518
Schahfer	2.611	2.525	0.08614	0.00742
Edwards	2.683	2.649	0.03368	0.001135
Rush Island	2.776	2.666	0.11044	0.012196

for the model was also less than 0.1, which means that the predictions are reliable.

Table 5.54 shows the observed and predicted non-evaporable water content at the age 1 day, for all the Class C ashes. The residuals and the squared residuals of the model are also included.

Figure 5.30 shows the plot of the observed and predicted non-evaporable water content at 1 day, for all the Class C ashes.

Table 5.55 shows the results of the model (R^2, adj-R^2 and parameter estimate values along with the p values for the model and the variables) ANOVA analysis.

The p-value for the model was smaller than 0.1 suggesting that this model can be used for predicting the non-evaporable water content at 3 days. Of the three variables sulfate, SAF and mgo, only sulfate had a p-value smaller than 0.1, which means that this was the only significant variable. The sign of this variable was positive, indicating an increase in the amount of sulfate increases the amount of non-evaporable water. The variable sulfate was seen only in the set of variables for the amount of calcium hydroxide at 28 days, and its coefficient was positive as well.

Table 5.56 shows the observed and predicted non-evaporable water content at the age 3 days, for all the Class C ashes. The residuals and the squared residuals of the model are also included.

Figure 5.31 shows the plot of the observed and predicted non-evaporable water content at 3 day, for all the Class C ashes.

The regression analysis of non-evaporable water formed at the age of 7 days is shown in Table 5.57.

It was found that there was no model containing three variables, with a p-value less than 0.1. Hence, the best four variable model was chosen for predictions. However, none of the variables including the model had a p-value less than 0.1, which means that even this model cannot be used for predictions. Nevertheless, it will be seen in the later section that the model can be used to predict the values for Class F ashes.

The presence of the variable cao leads to a conclusion that at the age of 7 days, the class of the ash does have an influence on the performance of the binder system in terms of the non-evaporable water content.

The R^2 and the adj-R^2 for the model for Class C ashes were very low, thus giving a poor fit of the data. As the model cannot be used for predictions, the table with observed and predicted values is not shown here.

Table 5.58 shows the ANOVA table for the amount of non-evaporable water formed at 28 days.

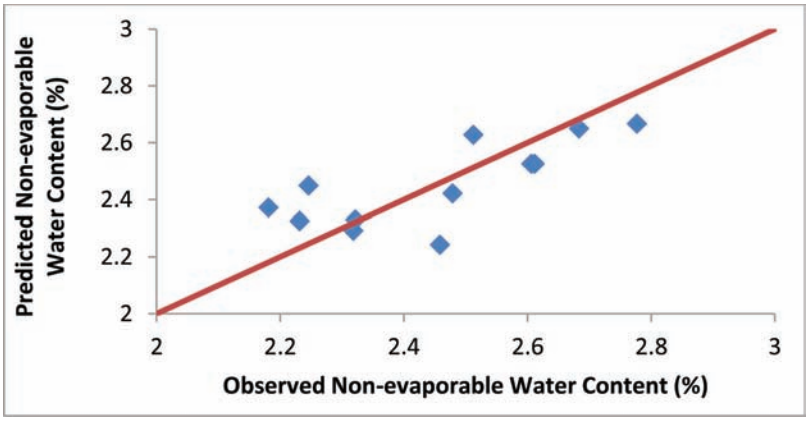

Figure 5.30 Plot showing the variations in the predicted and observed non-evaporable water content for all the Class C ashes at 1 day.

TABLE 5.55
Regression analysis for the amount of non-evaporable water formed at 3 days in binary pastes with Class C ashes.

Source	DF	Sum of Squares	Mean Square	Model F Value	Model p-Value
Model	3	0.25026	0.08342	4.831041	0.0333
Error	8	0.13814	0.0172675		
Total	11	0.3884			
		R^2	0.6443		
		adj-R^2	0.511		
Variable	**DF**	**Parameter Estimate**	**Standard Error**	**Variable t-Value**	**Variable p-Value**
Intercept	1	4.2187	1.66837	2.528636	0.0353
sulfate	1	0.32747	0.10387	3.152691	0.0135
SAF	1	-0.01468	0.01841	-0.79739	0.4483
mgo	1	0.04352	0.11843	0.367474	0.7228

TABLE 5.56
Observed and predicted non-evaporable water content (%) at 3 days of Class C ashes.

Fly Ash	Observed W_n	Predicted W_n	Residual	Squared Residual
Joppa	3.39	3.575	-0.185	0.0344
Schahfer	3.502	3.565	-0.063	0.004
Vermilion	3.553	3.547	0.006	4.00E-05
Baldwin	3.58	3.675	-0.094	0.0089
Kenosha	3.637	3.695	-0.058	0.0034
Hennepin	3.682	3.583	0.0993	0.0099
Edwards	3.7	3.761	-0.06	0.0036
Rush Island	3.798	3.623	0.1751	0.0307
Miller	3.815	3.737	0.0786	0.0062
Will County	3.827	3.767	0.0599	0.0036
Joliet	3.955	4.062	-0.107	0.0114
Labadie	4.03	3.881	0.149	0.0222

The sign of the coefficients in the parameter estimate column indicates the effect of the variables on the dependent variable. The sign of the coefficient of blaines was positive, indicating that the increase in the surface area of the fly ashes leads to an increase in the non-evaporable water content of the paste at 28 days. This was justified as the increase in the specific surface area increases the rate of reaction. In addition, this was the only significant variable of the three selected ones.

The p-value of the variables carbon and alumina were greater than 0.1, which implies that these variables were not significant. However, the coefficients suggest that the increase in the amount of carbon and alumina,

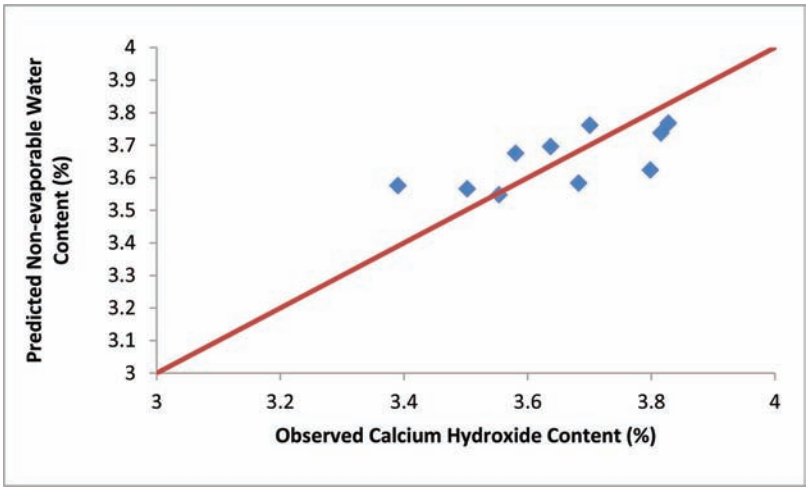

Figure 5.31 Plot showing the variations in the predicted and observed non-evaporable water content for all the Class C ashes at 3 days.

TABLE 5.57
Regression analysis for the amount of non-evaporable water formed at 7 days in binary paste systems with Class C ashes.

Source	DF	Sum of Squares	Mean Square	Model F Value	Model p-Value
Model	3	0.51844	0.17281333	1.83128	0.3891
Error	8	0.75494	0.0943675		
Total	11	1.27338			
		R^2	0.4071		
		adj-R^2	0.0684		
Variable	**DF**	**Parameter Estimate**	**Standard Error**	**Variable t-Value**	**Variable p-Value**
Intercept	1	2.88891	1.28958	2.240194	0.0601
meansize	1	0.02928	0.03617	0.809511	0.4448
sulfate	1	0.27884	0.29138	0.956963	0.3705
cao	1	-0.02739	0.06794	-0.40315	0.6989
mgo	1	0.32504	0.29657	1.095998	0.3094

TABLE 5.58
Regression analysis for the amount of non-evaporable water formed at 28 days in binary paste systems with Class C ashes.

Source	DF	Sum of Squares	Mean Square	Model F Value	Model p-Value
Model	3	0.48995	0.6715	6.8228	0.1618
Error	8	0.58509	0.09842		
Total	11	1.07504			
		R^2	0.719		
		adj-R^2	0.6136		
Variable	**DF**	**Parameter Estimate**	**Standard Error**	**Variable t-Value**	**Variable p-Value**
Intercept	1	6.83573	1.9101	3.578729	0.0072
blaines	1	0.00022	0.00009628	2.26703	0.0531
carbon	1	0.63946	0.81222	0.787299	0.4538
alumina	1	0.00992	0.10796	0.091886	0.929

leads to an increase in the amount of non-evaporable water at later ages.

The R^2 and the adj-R^2 for the model for Class C ashes were better than for the model that includes both the classes, thus giving a better fit. In addition, the p-value for the model was slightly greater than 0.1, which means that the predictions are not reliable at 90% confidence level.

Table 5.59 shows the observed and predicted non-evaporable water content at the age 28 days, for all the Class C ashes. The residuals and the squared residuals of the model are also included.

Figure 5.32 shows the plot of the observed and predicted non-evaporable water content at 28 days, for all the Class C ashes. It can be seen that many points are not predicted very well, as the model was not significant.

5.3.3.2.3 Linear regression models for binary pastes containing class F ashes. Linear regression analysis was performed on the non-evaporable water content of binary paste systems containing Class F ashes, using the three or four chosen dependent variables. Table 5.60, Table 5.62, Table 5.64 and Table 5.66 show the results of the model (R^2, adj-R^2 and parameter estimate values along with the p-values for the model and the variables) ANOVA analysis.

The sign of the coefficients in the parameter estimate column indicates the effect of the variables on the dependent variable. The sign of the coefficient of blaines was positive, indicating that the increase in the surface area of the fly ashes leads to an increase in the non-evaporable water content of the binder. This was expected as the surface area increases the rate of hydration reaction increases. However, this is not a reliable result as the p-values for the variable and the model were larger than 0.1.

The variables carbon and alumina have positive and negative signs for their coefficients, respectively, indicating an increase in the carbon content leads to an increase in the non-evaporable water content and vice versa in the case of alumina. Both these variables had p-values of less than 0.1 indicating that these are the significant variables.

The R^2 and adj-R^2 for the model were high and hence the fit of the model was very accurate. The p-value of the model was greater than 0.1 indicating that the model does not produce reliable predictions. The p-values for all the variables were smaller than 0.1 indicating that the regression model was not reliable in predicting the amount of non-evaporable water at 1 day.

Table 5.61 shows the observed and predicted non-evaporable water content at 1 day for all the Class F

TABLE 5.59
Observed and predicted non-evaporable water content at 28 days of Class C ashes.

Fly Ash	Observed W_n	Predicted W_n	Residual	Squared Residual
Rush Island	5.553	5.819	-0.26542	0.07045
Labadie	5.747	5.818	-0.07153	0.00512
Baldwin	5.851	6.009	-0.15831	0.02506
Will County	5.896	5.954	-0.05733	0.00329
Edwards	5.953	5.706	0.24695	0.06098
Miller	6.092	6.244	-0.15166	0.023
Vermilion	6.098	6.088	0.00958	0.00009
Hennepin	6.106	6.299	-0.19288	0.0372
Joliet	6.11	6.157	-0.04661	0.00217
Schahfer	6.121	5.905	0.21622	0.04675
Kenosha	6.225	6.306	-0.08079	0.00653
Joppa	6.835	6.284	0.55177	0.30445

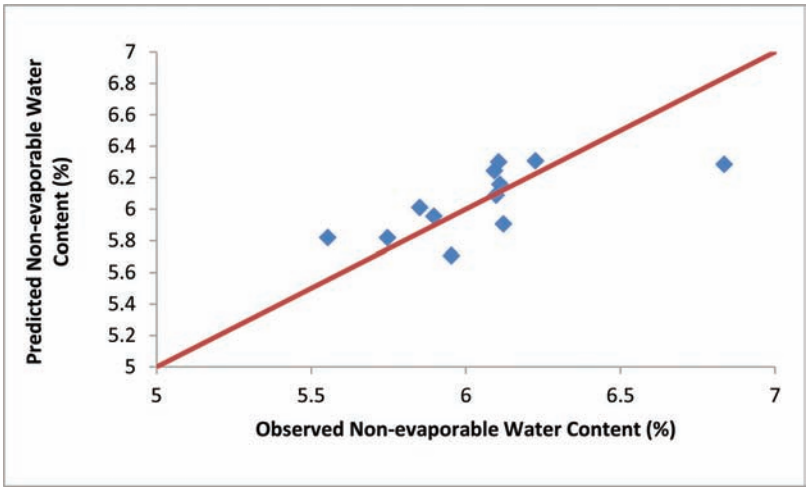

Figure 5.32 Plot showing the variations in the predicted and observed non-evaporable water content at 28 days for all the Class C ashes.

TABLE 5.60
Regression analysis for non-evaporable water content at 1 day for binary paste systems with Class F ashes.

Source	DF	Sum of Squares	Mean Square	Model F Value	Model p-Value
Model	3	0.255	0.085	2.74	0.2786
Error	2	0.06202	0.03101		
Total	5	0.31702			
		R^2	0.8044		
		adj-R^2	0.5109		
Variable	**DF**	**Parameter Estimate**	**Standard Error**	**Variable t-Value**	**Variable p-Value**
Intercept	1	1.90824	0.53436	3.571076	0.0703
blaines	1	0.00030095	0.000141	2.13834	0.1659
carbon	1	0.27098	0.18464	1.467613	0.2799
alumina	1	-0.04396	0.02146	-2.04846	0.1771

ashes. The residuals and the squared residuals of the model are also included.

It can be seen from Table 5.61 that all of the seven ashes have been predicted well. However, this model cannot be used to predict the non-evaporable water content for any new Class F fly ash as the p-value for the model is greater than 0.1.

Figure 5.33 shows the plot of the observed and predicted non-evaporable water content for all the Class F ashes at 1 day.

Table 5.62 shows the regression analysis of the amount of non-evaporable water at the age at 3 days for all class F ashes.

The p-value for the model was slightly larger than 0.1 suggesting that this model cannot be used for predicting the non-evaporable water at 3 days. Of the three variables sulfate, SAF and mgo, only sulfate had a p-value smaller than 0.1, which means that this was the only significant variable. This was the case even with Class C ashes. The sign of this variable was positive, indicating an increase in the amount of sulfate increases the amount of non-evaporable water. The other two variables had a p-value larger than 0.1 and hence were not significant in affecting the prediction of the results as compared to the variable sulfate.

Table 5.63 shows the observed and predicted non-evaporable water content at the age 3 days, for all the Class F ashes. The residuals and the squared residuals of the model are also included.

Figure 5.34 shows the plot of the observed and predicted non-evaporable water content at 3 day, for all the Class F ashes.

Table 5.64 shows the regression analysis for non-evaporable water content at 7 days for class F ashes.

All the variables in the model and the model itself, had p-values less than 0.1, leading to a conclusion that the model can be used for predicting the non-evaporable water content of class F ashes.

However, this was quite contrary to the model for class C ashes, which was found completely unreliable. The coefficient of the variable meansize was negative indicating that the reduction in the meansize increases the non-evaporable water content which was justified as the reduction in the particle size of the fly ash leads to an increase in the surface area of the particles.

TABLE 5.61
Observed and predicted non-evaporable water content (%) at 1 day for Class F ashes.

Fly Ash	Observed W_n	Predicted W_n	Residual	Squared Residual
Petersburg	2.091	2.048	0.04244	0.0018
Trimble	2.372	2.472	-0.09984	0.00997
Millcreek	2.382	2.528	-0.14605	0.02133
Miami 7	2.494	2.469	0.02455	0.0006
Elmersmith	2.712	2.701	0.01098	0.00012
Zimmer	2.781	2.614	0.16792	0.0282

The coefficients of cao and mgo were also positive indicating an increase in the content of cao and mgo leads to an increase in the non-evaporable water content.

Table 5.65 shows the observed and predicted non-evaporable water content at the age 7 days, for all the Class F ashes. The residuals and the squared residuals of the model are also included.

Figure 5.35 shows the plot of the observed and predicted non-evaporable water content at 7 days, for all the Class F ashes. It can be seen that all of the points were predicted very accurately.

Table 5.66 shows the regression analysis for non-evaporable water content at 28 days for class F ashes.

None of the variables or the model had a p-value less than 0.1. This means that this model cannot be used for predicting the non-evaporable water content at 28 days. However, the p-value of the intercept was less than 0.1 indicating that, the non-evaporable water content for all the paste systems are similar and close to 5.7395. The results obtained for Class F ashes are quite opposite to what was observed in Class C ashes.

Now, since this model cannot be used for predictions, the table and figure containing the predicted and observed values is not shown.

5.3.3.2.4 Model verification. Two fly ashes (NIP 1 – Class C ash and NIP 1A – Class F ash) not included in the set of fly ashes utilized for development of the

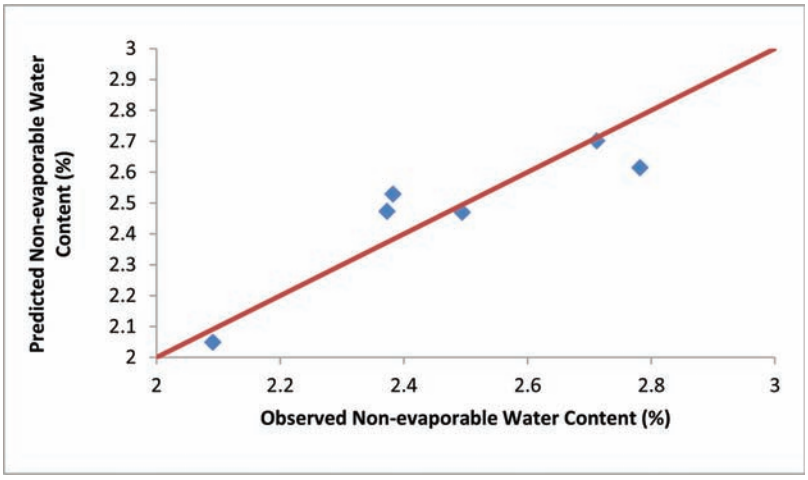

Figure 5.33 Plot showing the variations in the predicted and observed non-evaporable water content at 1 day for all the Class F ashes.

TABLE 5.62
Regression analysis for non-evaporable water content at 3 day for binary paste systems with Class F ashes.

Source	DF	Sum of Squares	Mean Square	F Value	p-Value
Model	3	0.36622	0.122073	5.50	0.1576
Error	2	0.04436	0.02218		
Total	5	0.41058			
		R^2	0.892		
		adj-R^2	0.7299		
Variable	**DF**	**Parameter Estimate**	**Standard Error**	**t-Value**	**p-Value**
Intercept	1	0.89762	1.74365	0.514794	0.6579
sulfate	1	1.04884	0.29146	3.598573	0.0693
SAF	1	0.02403	0.01989	1.208145	0.3505
mgo	1	-0.32493	0.11549	-2.81349	0.1065

TABLE 5.63
Observed and predicted non-evaporable water content (%) at 3 days for Class F ashes.

Fly Ash	Observed W_n	Predicted W_n	Residual	Squared Residual
Zimmer	3.511	3.503	0.00755	6.00E-05
Millcreek	3.195	3.35	-0.15424	0.0238
Elmersmith	3.236	3.193	0.04323	0.0019
Miami 7	3.324	3.232	0.09259	0.0086
Petersburg	3.641	3.706	-0.06532	0.0043
Trimble	3.949	3.872	0.07619	0.0058

above models were used to test their accuracy. The specific surface (blaines), lime content (cao), sulfate content (sulfate), mean particle size (meansize), loss on ignition (carbon), alumina content (alumina), MgO content (mgo) and SAF content of
the fly ashes are given in Table 5.67. The observed and predicted non-evaporable water contents for the significant models at different ages for the test ashes are shown in Table 5.68.

From Table 5.68, it can be seen that the predictions for both the Class C and Class F models at early ages of 1 and 3 days were not very accurate as the difference between the observed and predicted non-evaporable water content was at least 0.4%. This was expected, as the p-value for most of the models at early ages were larger than 0.1 and the intercept error was comparable to the coefficient (except in the case of the model for Class F ashes at 7 days). Quite a few variables in all the models also had very larger p-values than 0.1 and hence the models were not good for predictions. The prediction for Class C ash at 28 days was extremely poor as the model itself was not so significant. The most surprising result was that of the prediction of the model for Class F ash at 7 days. The only reason could be that the non-evaporable water content of the paste at 7 days did not lie within the range of the values, which were used to build the model.

5.3.4 Rate of Strength Gain

Experiments were performed on mortar cubes made of neat cement and binary paste systems as mentioned

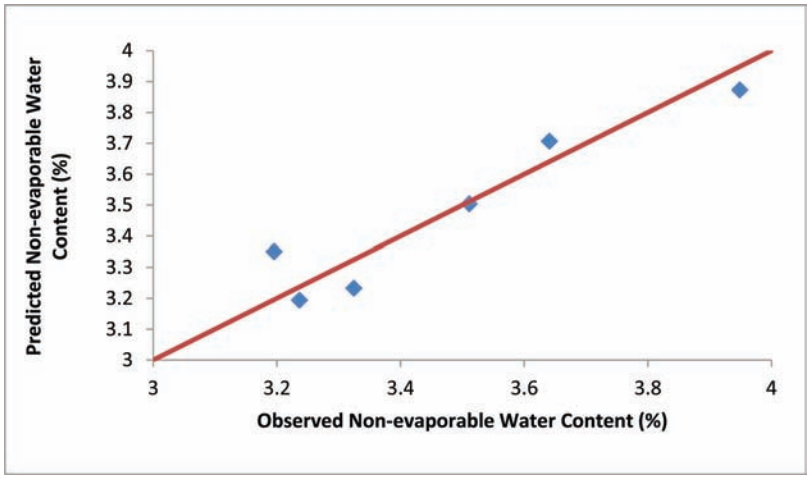

Figure 5.34 Plot showing the variations in the predicted and observed non-evaporable water content for all the Class F ashes at 3 days.

TABLE 5.64
Regression analysis for non-evaporable water content at 7 days for binary paste systems with Class F ashes.

Source	DF	Sum of Squares	Mean Square	F Value	p-Value
Model	3	0.37653	0.12551	307.54	0.0697
Error	2	0.00081622	0.000408		
Total	6	0.37735			
		R^2	0.9978		
		adj-R^2	0.9892		
Variable	**DF**	**Parameter Estimate**	**Standard Error**	**t-Value**	**p-Value**
Intercept	1	5.44319	0.21546	25.26311	0.0252
meansize	1	-0.04532	0.00699	-6.48355	0.0975
sulfate	1	-0.68088	0.06398	-10.6421	0.0596
cao	1	0.07384	0.00506	14.59289	0.0435
mgo	1	0.25769	0.02178	11.8315	0.0537

TABLE 5.65
Observed and predicted non-evaporable water content (%) at 7 days of Class F ashes.

Fly Ash	Observed W_n	Predicted W_n	Residual	Squared Residual
Trimble	3.883	3.868	0.01516	0.0002
Petersburg	3.907	3.929	-0.02272	0.0005
Miami 7	4.098	4.09	0.00834	7.00E-05
Zimmer	4.445	4.445	0.00017	3.00E-08
Elmersmith	4.445	4.445	-0.00045	2.00E-07
Millcreek	4.447	4.447	-0.0005	3.00E-07

in Section 3.3.2. The strength activity index (%) of all the binary binder systems and the reference cement mortar at ages 1 day, 3 days, 7 days and 28 days is mentioned in Table 5.69. The data shown is the average strength of three cubes prepared from the same mix as a proportion of the strength of plain cement cubes at 7 days. All the strength activity index values shown are in percentages.

Figure 5.36 to Figure 5.39 show a comparison of the strength for all the fly ashes at four ages (1 day, 3 days, 7 days and 28 days). In all these figures, the first 12 bars represent the strength activity index for the binary paste systems containing Class C ashes. The next 6 bars denote Class F ashes and the last bar represents the same data for a paste containing plain cement paste.

It is clear from Figure 5.36 that most of the ashes have a reduction in the strength activity index at 1 day as compared to plain cement paste except for three Class C ashes, Edwards, Labadie and Will County and one Class F ash, Mill Creek. The strength activity index at 1 day in Class C ashes ranged from 39.9% to 45.5% and the strength activity index in Class F ashes had a wider range from 38.2% to 53.6%. However, most Class F ashes had a range of around 38% to 40%, with one exception of Mill Creek, 53.6%. The highest value amongst all the ashes was 53.%, which was a Class F ash, Mill Creek and the lowest was again a Class F ash with 38.2%, Elmersmith. It was clear

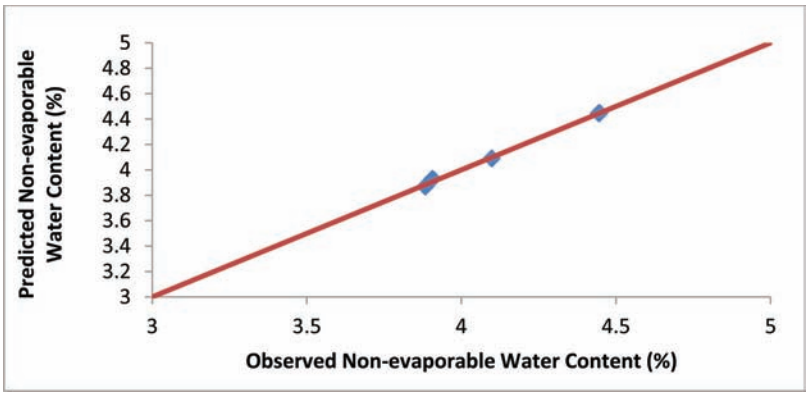

Figure 5.35 Plot showing the variations in the predicted and observed non-evaporable water content at 7 days for all the Class F ashes.

TABLE 5.66
Regression analysis for non-evaporable water content at 28 day for binary paste systems with Class F ashes.

Source	DF	Sum of Squares	Mean Square	F Value	p-Value
Model	3	0.52055	0.173517	2.13	0.3356
Error	2	0.16311	0.081555		
Total	5	0.63048			
		R^2	0.7614		
		adj-R^2	0.4036		
Variable	**DF**	**Parameter Estimate**	**Standard Error**	**t-Value**	**p-Value**
Intercept	1	5.73953	0.86658	6.623197	0.022
blaines	1	0.00007164	0.000228	0.313866	0.7833
carbon	1	-0.71966	0.29943	-2.40343	0.1381
alumina	1	0.04661	0.03481	1.338983	0.3125

TABLE 5.67
Characteristics of the test fly ashes used for model verification.

Fly Ash	blaines cm^2/g	meansize µm	carbon %	sulfate %	mgo %	SAF %	cao %	alumina %
NIP 1	7100	3	2.24	3.13	2.84	87	2.64	23
NIP 1A	5200	15	9.3	5.98	3.63	58.1	31	15.2

TABLE 5.68
Observed and predicted non-evaporable water content (%) at all ages for the test ashes.

Fly Ash	Class	Age (days)	Observed W_n	Predicted W_n	Residual	Squared Residual
NIP1A	C	1	3.803	3.292	-0.51112	0.261239
NIP1A	C	3	5.031	5.482	0.45054	0.202986
NIP1A	C	28	6.457	11.798	5.341388	28.53043
NIP1	F	1	3.838	3.640	-0.1977	0.039085
NIP 1	F	3	4.581	5.348	0.767098	0.588439
NIP 1	F	7	4.850	2.053	-2.79691	7.82269

from the plot that all the Class F fly ashes have a detrimental effect on the strength, while some of the Class C ashes have higher strength than plain cement mortars. Even though there was not much correlation between strength and non-evaporable water content or calcium hydroxide content, we can observe that the fly ashes displaying higher strength have a higher amount of non-evaporable water contents. However, this was not entirely true as there were exceptions seen, as in the case of the fly ash Rush Island, it had the highest amount of non-evaporable water and the lowest strength.

From Figure 5.37, it can be seen that most of the ashes tend to reduce the strength activity index at 3 days as compared to plain cement paste except for two Class C ashes, Edwards and Schahfer, and one Class F ash, Trimble. The fly ash, Schahfer had a low strength at 1 day and has showed a good improvement at 3 days. The reduction in the strength at earlier ages is understandable as fly ash is inert in terms of both hydration reaction or pozzolanic reaction in the early ages. We can already observe a wide variety of rates of increase in strength for all various ashes. This kind of variation in rate of strength gain trends will be more apparent in the results of 7 and 28 days.

The strength activity index at 3 days in Class C ashes ranged from 50% to 80.6% and the strength activity index in Class F ashes had a range from 56.6% to 73.6%. The highest value amongst all the ashes was 80.6%, which was a Class C ash, Edwards and the lowest was again a Class C ash with 50%, Baldwin.

It is clear from Figure 5.38 that Class C fly ashes start to assist in the hydration reaction leading to a small increase in the strength activity index at 7 days in a few fly ashes when compared to plain cement paste. This was what was observed even in the case of non-evaporable water content. Most of the Class C ashes had a strength activity index close to the plain cement paste (100%) at this age. This increase in the rate of strength gain can be attributed to an inception of the hydration reaction in the fly ashes. This is also proved by the amount of calcium hydroxide, which increases by a significant amount at this age. An increase in both the amount of calcium hydroxide and the non-evaporable water content suggests that there is an accelerated hydration reaction in the paste systems. On the other hand, all of the Class F ashes had a strength value smaller than the plain cement mortar, which is also justified as the rate of hydration reaction is slightly lower in pastes containing Class F ashes.

The strength activity index at 7 days in Class C ashes ranged from 77.6% to 115.8% and the strength activity index in Class F ashes had a narrower range from 72% to 90.8%. Most of the Class C ashes had a strength of either greater or equal to all the Class F ashes. The highest value amongst all the ashes was 115.9%, which was a Class C ash, Hennepin and the lowest was a Class F ash with 72%, Zimmer.

The strength of fly ash mortars and plain cement paste at 28 days are compared with the strength of the 7 days specimen of plain cement mortar cubes.

From the Figure 5.39 it can be seen that all the Class C ashes had a higher strength activity index at the age of 28 days than plain cement paste, while most of the Class F ashes had a 28 day strength, either less than or equal to the strength of plain cement paste at 7 days. This clearly suggests that the rate of hydration of Class C fly ash pastes dominates at this age over the pozzolanic reaction of Class C ashes. However, in the case of Class F ashes, the rate of hydration reaction

TABLE 5.69
Strength (psi) at four ages of all the binary paste systems.

Fly ash	Class	1 Day	3 Day	7 Day	28 Day
Baldwin	C	39.9	50.1	98.5	105.9
Cement		42.3	72.6	100.0	105.0
Edwards	C	43.6	80.6	111.4	111.0
Elmer Smith	F	38.2	56.6	90.8	98.2
Hennepin	C	41.3	68.4	115.9	121.4
Joliet	C	42.0	62.8	77.6	99.5
Joppa	C	42.5	55.5	101.3	114.3
Kenosha	C	35.9	59.1	95.9	102.7
Labadie	C	44.3	67.9	97.0	101.9
Miami#7	F	38.2	58.5	77.6	100.6
Mill Creek	F	53.6	58.9	89.5	101.8
Miller	C	41.1	60.4	99.4	104.6
Moscow	F	39.9	63.9	72.0	88.7
Petersburg	F	38.3	59.8	84.8	99.6
Rush Island	C	32.6	66.8	87.0	105.4
Schahfer	C	40.7	73.7	85.1	100.8
Trimble	F	39.2	73.6	82.5	97.4
Vermilion	C	38.1	62.9	102.7	122.9
Will County	C	45.5	61.0	82.1	118.1

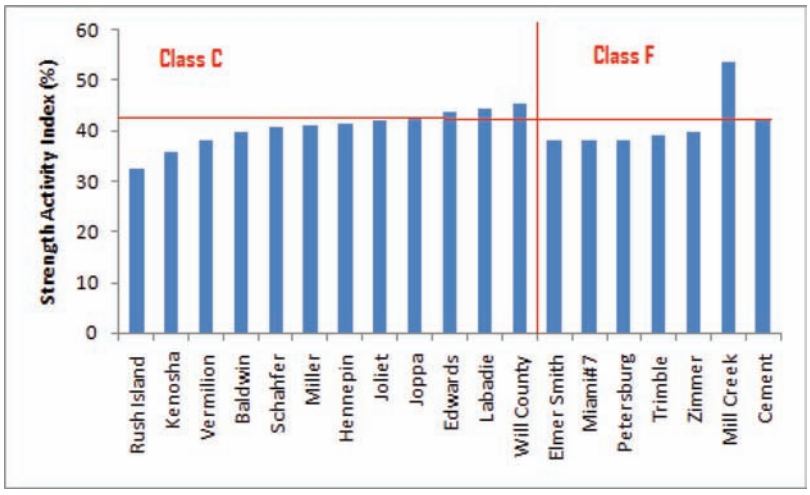

Figure 5.36 Comparison of strength activity index at 1 day for all the paste systems.

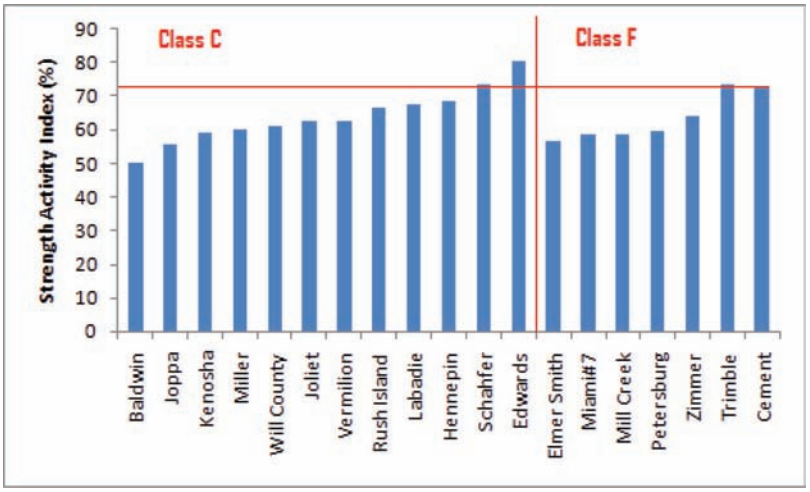

Figure 5.37 Comparison of strength activity index at 3 day for all the paste systems.

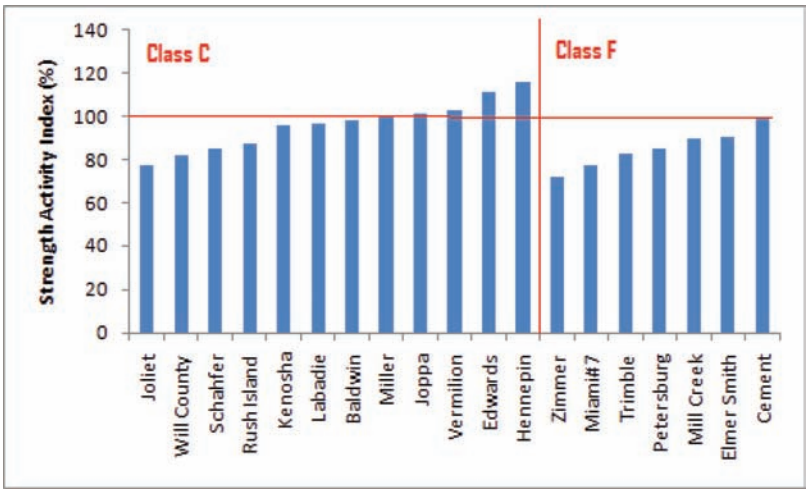

Figure 5.38 Comparison of strength activity index content at 7 day for all the paste systems.

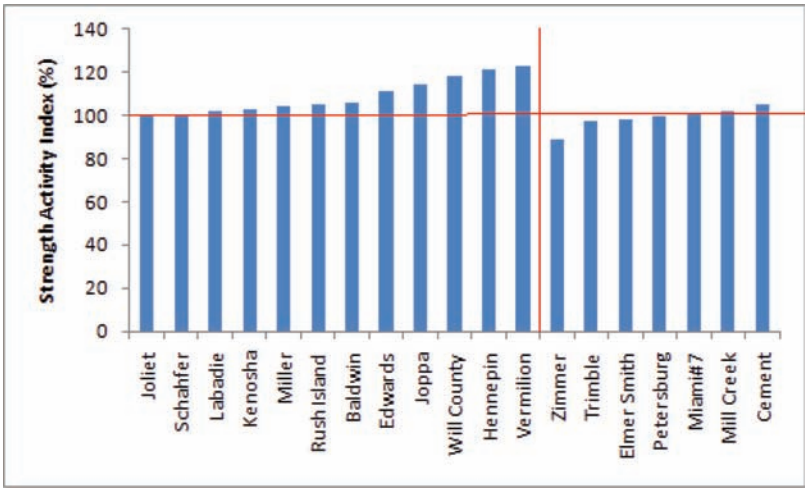

Figure 5.39 Comparison of strength activity index content at 28 day for all the paste systems.

could have slightly increased, while there could also be a small increase in the rate of pozzolanic reaction. This is evident as there is not much increase in the strength gain, however we could observe a small increase in non-evaporable water contents in Class F ashes. This could be resolved by looking at the calcium hydroxide contents at 28 days, which also show a small increase. This essentially means that there is a significant hydration reaction and not much pozzolanic reaction.

The strength activity index at 28 days in Class C ashes ranged from 99.5% to 122.9% and the strength activity index in Class F ashes had a range from 88.7% to 104.9%. The highest value amongst all the ashes was 122.9%, which was a Class C ash, Vermilion, which initially had low percentages at 1 and 3 days. The lowest percentage of all the ashes was that of a Class F ash with 88.7%, Zimmer, which had a high amount of non-evaporable water at 1 day, which showed a remarkably high percentage of calcium hydroxide at 28 days and a significantly low percentage of non-evaporable water content at the same age.

5.3.4.1 Selection of variables for statistical modeling. Statistical linear regression models were built for the strength activity index at 1, 3, 7 and 28 days in the binary paste systems using all data points given in Table 5.69. The independent variables considered when constructing the regression models are mentioned in Table 5.1.

A SAS code was written, which investigated all the possible combinations of independent variables to construct the regression models. A template of the code is given in Appendix B. The program uses all independent variables and the dependent variable (strength activity index). The output of the program consists of a table containing the list of combinations of independent variables forming linear regression models, sorted according to the adj-R^2 values. The values of the R^2 are also listed in the table for each model.

Instead of the table with the best ten regression models (as was the case with time of set and heat of hydration), a table with the chosen best model containing three variables at each age is shown along with the adj-R^2 for the models.

From the Table 5.70 it can be inferred that both physical and chemical characteristics of fly ashes affect the strength activity index at various ages, the most important variables being meansize, SAF, alumina, glass and sulfate.

TABLE 5.70
Chosen two or three variable models for strength activity index at all the ages.

Age (Days)	Variables	Adjusted R^2	R^2
1	meansize, mgo	-0.0158	0.1037
3	SAF, alumina, glass	0.2601	0.3988
7	SAF, cao, glass	0.5375	0.6191
28	meansize, sulfate, SAF	07047	0.7568

The R^2 and adj-R^2 for the models at early ages (1 and 3 days) are extremely poor. Hence, there cannot be a valid statistical model to predict the early age strength. However, the R^2 and adj-R^2 for the models at later ages (7 and 28 days) are high and might lead to a good model for predictions. The presence of the variables SAF indicates the difference in the behavior of both the classes of ashes.

The linear regression models for the strength activity index at various ages are shown in the following sections.

5.3.4.2 Linear regression models for binary pastes containing class C ashes. Linear regression analysis was performed on the strength activity index at various ages of binary paste systems containing Class C ashes, using the chosen dependent variables based in adj-R^2 as shown in Table 5.70. In this case, only the regression models at later ages (7 and 28 days) are shown, as the other two are deemed unreliable. The ANOVA table along with the regression coefficients and the p-values for the ages 7 and 28 days are shown in Table 5.71 and Table 5.73.

The sign of the coefficients in the parameter estimate column indicates the effect of the variables on the dependent variable. The sign of the coefficients of all the variables (SAF, cao, and glass) was positive indicating that the increase in the contents of any of the variables leads to an increase in the strength activity index of the binder.

The effect of SAF (or cao content in the fly ash) is not justified as the increase in the cao content leads to its direct reaction with water producing calcium hydroxide and thus having a detrimental effect on the strength. In this case, even though the p-values for both the variables is less than 0.1 and are significant, the result would not be reliable as there is a very high correlation between SAF and cao. The presence of two highly correlated variables in the model leads to a multi-collinearity in the regression model. The predictions using this model would not be reliable as the confidence intervals would be extremely large. In addition, the coefficients and their signs could be highly misleading. It is also to be noted that the error in the intercept is large, which might also lead to erroneous predictions.

Nevertheless, the presence of the variables SAF leads to a conclusion that at later ages, the class of the ash influences the performance of the binder system in terms of the strength gain of the mortar.

Table 5.72 shows the observed and predicted strength activity index (%) at the age 7 days, for all the Class C ashes. The residuals and the squared residuals of the model are also included.

Figure 5.40 shows the plot of the observed and predicted strength activity index at 7 days, for all the Class C ashes. Most of the points (except two) are predicted within a variation of 10.3% (the variation acceptable between two measurements as mentioned in ASTM C 311 (*6*)). Even as the model and all the

TABLE 5.71
Regression analysis for the strength activity index at 7 days in binary paste systems with Class C ashes.

Source	DF	Sum of Squares	Mean Square	F Value	p-Value
Model	3	873.541	291.180337	4.017362	0.0514
Error	8	579.8439	72.480485		
Total	11	1453.385			
		R^2	0.601		
		adj-R^2	0.4514		
Variable	**DF**	**Parameter Estimate**	**Standard Error**	**t-Value**	**p-Value**
Intercept	1	-521.432	308.59493	-1.6897	0.1296
SAF	1	5.86739	3.05711	1.91926	0.0912
cao	1	9.32163	4.97522	1.873612	0.0979
glass	1	17.94111	7.88917	2.274144	0.0525

TABLE 5.72
Observed and predicted strength activity index (%) at 7 days of Class C ashes.

Fly Ash	Observed SAI	Predicted SAI	Residual	Squared Residual
Joliet	77.65	78.98	-1.3364	1.786
Will County	82.08	89.47	-7.3913	54.631
Schahfer	85.07	96.28	-11.2098	125.659
Rush Island	87.04	96.03	-8.9957	80.923
Kenosha	95.95	94.64	1.3067	1.707
Labadie	97.01	102.44	-5.4384	29.576
Baldwin	98.49	92.88	5.6039	31.404
Miller	99.43	87.11	12.3168	151.704
Joppa	101.31	98.89	2.4157	5.835
Vermilion	102.71	100.87	1.8398	3.385
Edwards	111.39	101.82	9.5645	91.48
Hennepin	115.86	114.53	1.3242	1.753

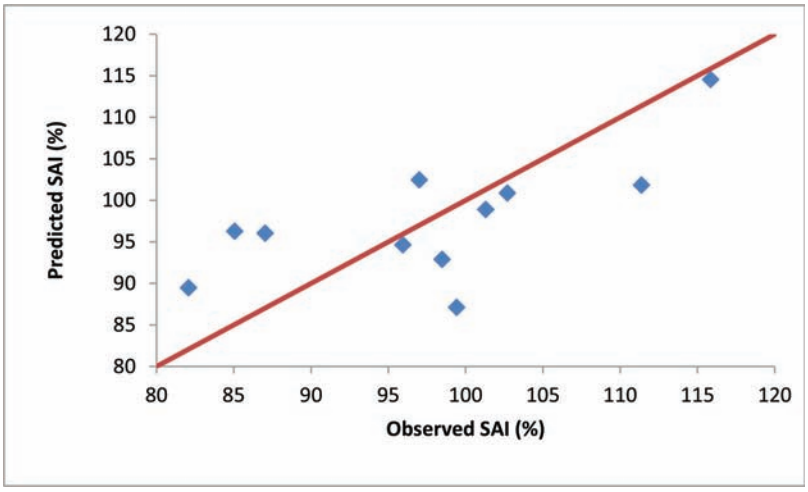

Figure 5.40 Plot showing the variations in the predicted and observed strength activity index for all the Class C ashes at 7 day.

variables are significant, the predictions for a couple of points, even for the data points used in the modeling process were poor, indicating the unreliability of the model.

Table 5.73 shows the results of the model (R^2, adj-R^2 and parameter estimate values along with the p values for the model and the variables) ANOVA analysis.

The sign of the coefficients in the parameter estimate column indicates the effect of the variables on the dependent variable. The sign of the coefficient of meansize was negative, indicating that the increase in the mean particle size of the fly ashes leads to a decrease in the strength activity index of the binder. This is justified as the decrease in the particle size results in an

TABLE 5.73
Regression analysis for the strength activity index at 28 days in binary paste systems with Class C ashes.

Source	DF	Sum of Squares	Mean Square	Model F Value	Model p-Value
Model	3	470.0203	156.67343	4.444977	0.0407
Error	8	281.9784	35.2472975		
Total	11	751.9987			
		R^2	0.625		
		adj-R^2	0.4844		
Variable	**DF**	**Parameter Estimate**	**Standard Error**	**Variable t-Value**	**Variable p-Value**
Intercept	1	142.0434	1.66837	85.13902	0.0036
meansize	1	-1.573	0.10387	-15.1439	0.0246
sulfate	1	-15.7847	0.01841	-857.398	0.0135
SAF	1	0.0496	0.11843	0.418813	0.9266

TABLE 5.74
Observed and predicted strength activity index (%) at 28 days for Class C ashes.

Fly Ash	Observed SAI	Predicted SAI	Residual	Squared Residual
Joliet	99.49	101.91	-2.41957	5.8543
Schahfer	100.81	108.1	-7.29151	53.1662
Labadie	101.91	100.93	0.97992	0.9602
Kenosha	102.66	109.57	-6.91883	47.8702
Miller	104.57	97.62	6.94708	48.2619
Rush Island	105.36	111.44	-6.08937	37.0804
Baldwin	105.93	106.09	-0.16011	0.0256
Edwards	111	109.59	1.40728	1.9804
Joppa	114.26	115.08	-0.82839	0.6862
Will County	118.09	114.81	3.27489	10.7249
Hennepin	121.43	113.25	8.17402	66.8145
Vermilion	122.89	119.96	2.9246	8.5533

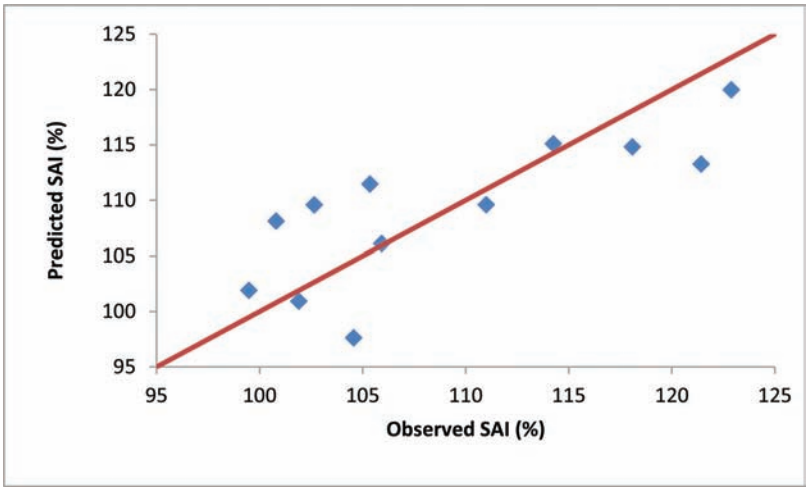

Figure 5.41 Plot showing the variations in the predicted and observed strength activity index for all the Class C ashes at 28 days.

increase in the specific surface area, which in turn increases the rate of hydration reaction. In addition, lower the particle size, the better they seal up the voids in between the cement grains and thus improving the strength.

The coefficient of the variable, sulfate also has a negative sign indicating the increase in the sulfate content reduces the strength of the mortar. This is also justified as the increase in the sulfate content leads to an excessive expansion at later ages due to the late formation of ettringite.

The effect of SAF (CaO content in the fly ash) is not justified as the increase in the CaO content leads to its direct reaction with water producing calcium hydroxide

TABLE 5.75
Regression analysis for strength activity index (%) at 7 days for binary paste systems with Class F ashes.

Source	DF	Sum of Squares	Mean Square	Model F Value	Model p-Value
Model	3	229.16838	76.38946	5.55	0.1565
Error	2	27.53575	13.76788		
Total	5	256.70413			
		R^2	0.8927		
		adj-R^2	0.7318		
Variable	**DF**	**Parameter Estimate**	**Standard Error**	**Variable t-Value**	**Variable p-Value**
Intercept	1	-234.5254	89.77232	-2.61245	0.1206
SAF	1	3.44957	0.98377	3.50648	0.0726
cao	1	5.08465	1.32791	3.829062	0.0619
glass	1	-1.29999	3.55845	-0.36532	0.7499

TABLE 5.76
Observed and predicted strength activity index (%) at 7 days for Class F ashes.

Fly Ash	Observed SAI	Predicted SAI	Residual	Squared Residual
Zimmer	71.98	73.43	-1.45139	2.1065
Miami 7	77.63	79.58	-1.95154	3.8085
Trimble	82.51	78.6	3.91509	15.3279
Petersburg	84.83	86.39	-1.56119	2.4373
Mill Creek	89.5	87.69	1.81006	3.2763
Elmersmith	90.79	91.55	-0.76102	0.5792

and thus having a detrimental effect on the strength. However the p-value of this variable is greater than 0.1, and hence is not significant and will not affect the strength gain relative to the other two variables.

Nevertheless, the presence of the variables SAF leads to a conclusion that at later ages, the class of the ash influences the performance of the paste system in terms of the strength gain of the mortar.

The R^2 and the adj-R^2 for the model for Class C ashes are similar to the model that includes both the classes, which are both relatively high, thus giving a better fit. In addition, the p-value for the model is also less than 0.1, which means that the predictions are reliable.

Table 5.74 shows the observed and predicted strength activity index at the age 28 days, for all the Class C ashes. The residuals and the squared residuals of the model are also included.

Figure 5.41 shows the plot of the observed and predicted non-evaporable water content at 3 day, for all the Class C ashes.

5.3.4.3 Linear regression models for binary pastes containing class F ashes. Linear regression analysis was performed on the strength activity index of binary paste systems containing Class F ashes, using the three or four chosen dependent variables. Table 5.75 and Table 5.77 show the results of the model (R^2, adj-R^2 and parameter estimate values along with the p values for the model and the variables) ANOVA analysis.

The sign of the coefficients in the parameter estimate column indicates the effect of the variables on the dependent variable. The same reasoning as mentioned in Class C ashes for the 7 days strength activity index holds true for Class F ashes as well.

Table 5.76 shows the observed and predicted non-evaporable water content at 7 days for all the Class F ashes. The residuals and the squared residuals of the model are also included.

It can be seen from Table 5.76 that all of the seven ashes have been predicted well. However, this model cannot be used to predict the strength activity index for any new Class F fly ash as we have multi-collinearity in the regression model.

Figure 5.42 shows the plot of the observed and predicted strength activity index for all the Class F ashes at 7 days.

Table 5.77 shows the regression analysis of the strength activity index at the age at 28 days for all class F ashes.

The sign of the coefficients in the parameter estimate column indicates the effect of the variables on the dependent variable. The signs of the coefficients of the variables meansize and sulfate was similar to the Class C ashes.

The sign of the coefficient of meansize was negative, indicating that the increase in the mean particle size of

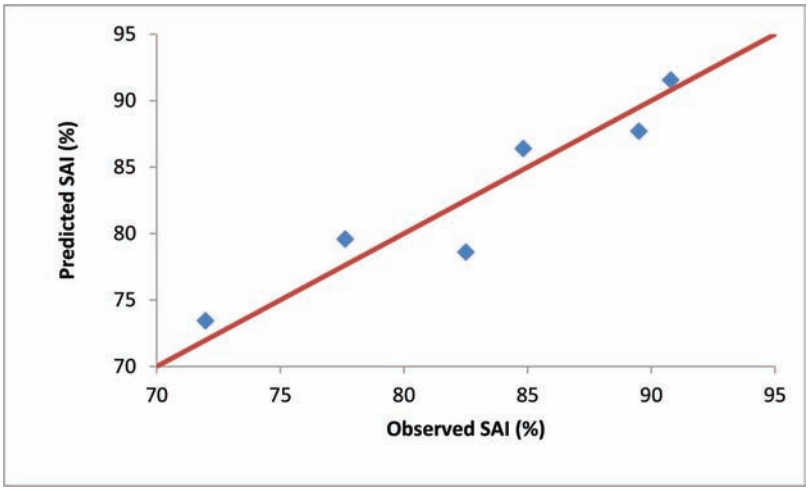

Figure 5.42 Plot showing the variations in the predicted and observed strength activity index at 7 day for all the Class F ashes.

TABLE 5.77
Regression analysis for strength activity index at 28 days for binary paste systems with Class F ashes.

Source	DF	Sum of Squares	Mean Square	Model F Value	Model p-Value
Model	3	107.65676	35.88559	40.13	0.0244
Error	2	1.78839	0.894195		
Total	5	109.44515			
		R^2	0.9837		
		adj-R^2	0.9591		
Variable	**DF**	**Parameter Estimate**	**Standard Error**	**Variable t-Value**	**Variable p-Value**
Intercept	1	126.13758	17.78975	7.090464	0.0193
meansize	1	-0.67193	0.23397	-2.87186	0.1029
sulfate	1	-9.27674	1.16409	-7.96909	0.0154
SAF	1	-0.00329	0.1415	-0.02325	0.9835

the fly ashes leads to a decrease in the strength activity index of the binder.

The coefficient of the variable, sulfate also has a negative sign indicating the increase in the sulfate content reduces the strength of the mortar.

The sign of the coefficient of SAF (CaO content in the fly ash) is justified as the increase in the CaO content leads to its direct reaction with water producing calcium hydroxide and thus having a detrimental effect on the strength. However the p-value of this variable is greater than 0.1, and hence is not significant and will not affect the strength gain relative to the other two variables.

Nevertheless, the presence of the variables SAF leads to a conclusion that at later ages, the class of the ash influences the performance of the binder system in terms of the strength gain of the mortar.

The R^2 and the adj-R^2 for the model for Class C ashes are very high and thus giving a good fit. In addition, the p-value for the model is also less than 0.1, which means that the predictions are reliable.

Table 5.78 shows the observed and predicted strength activity index at the age 28 days, for all the Class C ashes. The residuals and the squared residuals of the model are also included.

Figure 5.43 shows the plot of the observed and predicted strength activity index at 28 day, for all the Class F ashes. The strength activity index for all the fly ashes has been predicted accurately with a residual of less than 1% for all the predictions. This model can be used in the prediction for the 28 days strength for any new fly ashes.

5.3.4.4 Model verification. Two fly ashes (NIP 1 – Class C ash and NIP 1A – Class F ash) not included in the set of fly ashes utilized for development of the above models were used to test their accuracy. The mean particle size (meansize), lime content (cao), sulfate content (sulfate), glass ratio and SAF content of the fly ashes are provided in Table 5.79. The observed and predicted strength activity index for the significant models at ages 7 and 28 days for the test ashes are shown in Table 5.72.

From Table 5.80, it can be seen that the prediction of both the Class C and Class F model the 7 and 28 day predictions were close to the observed values as the maximum difference between the observed and predicted

TABLE 5.78
Observed and predicted strength activity index at 28 days of Class F ashes.

Fly Ash	Observed SAI	Predicted SAI	Residual	Squared Residual
Zimmer	88.71	88.99	-0.28189	0.07946
Trimble	97.39	97.36	0.02323	0.00054
Elmersmith	98.21	97.93	0.27657	0.07649
Petersburg	99.59	98.71	0.87663	0.76848
Miami 7	100.58	101.51	-0.92858	0.86226
Millcreek	101.75	101.71	0.03404	0.00116

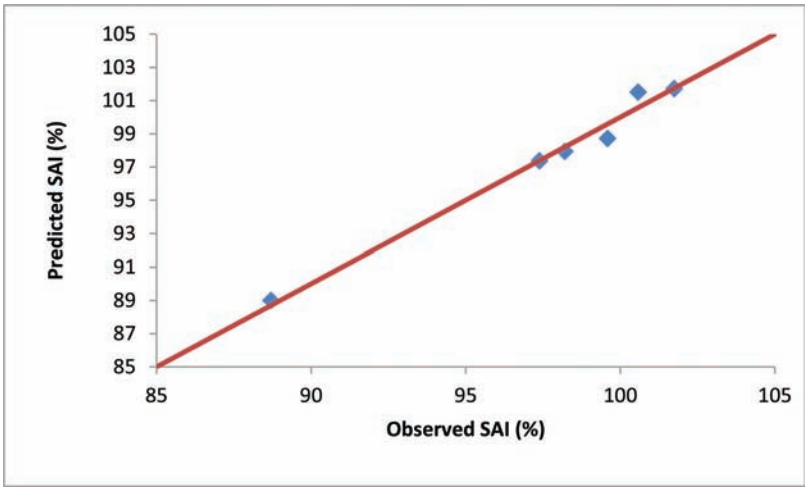

Figure 5.43 Plot showing the variations in the predicted and observed strength activity index for all the Class F ashes at 28 days.

TABLE 5.79
Characteristics of the test fly ashes used for model verification.

Fly Ash	Class	meansize (μm)	sulfate (%)	SAF (%)	cao (%)	glass
NIP 1	F	3	3.13	87	2.64	2.555
NIP 1A	C	15	5.98	58.1	31	0.924

TABLE 5.80
Observed and predicted strength activity index (%) at ages 7 and 28 days for the test ashes.

Fly Ash	Class	Age (Days)	Observed SAI	Predicted SAI	Residual	Squared Residual
NIP1A	C	7	84.11	91.85	7.748636	60.04136
NIP1A	C	28	108.7	106.93	-1.7624	3.106054
NIP1	F	7	77.38	75.48	-1.89106	3.576096
NIP 1	F	28	96.15	94.80	-1.35064	1.824218

peak heat of hydration is only 7.7%. This was expected, as the p-value for the models were smaller than 0.1 and the intercept error was significantly smaller than the coefficient. Most of the variables also had very small p-values and hence the model is good for predictions. These models can be used to predict the strength activity index at ages 7 and 28 days. However, the models can predict only within the ranges of the strength activity indices of the data points used in the modeling process.

6. LABORATORY RESULTS AND STATISTICAL ANALYSIS OF TERNARY PASTE SYSTEMS

The objectives of performing statistical analysis on ternary paste systems (cement + two different fly ashes) are:

1. To ascertain the additivity of the dependent variables (time of set, heat of hydration, amount of calcium hydroxide at 28 days, the amount of non-evaporable water content at 28 days and the strength activity index at 28 days) when two different fly ashes (could be from either of the Classes) were added to the cement binder system.
2. To identify the percentage influence of each of the variables (which were chosen from the statistical analysis of binary paste systems) on the dependent variables and to estimate the error percentage.

6.1 Testing of Ternary Paste Systems and Statistical Analysis Procedure

This section describes the testing and analysis procedures for the properties of ternary paste systems comprising of Type I portland cement and two different fly ashes.

Cement + fly ash (FA1) + fly ash (FA2) pastes were prepared using two fly ashes chosen from the available thirteen Class C ashes and seven Class F ashes and mixed in specific proportions. In the ternary pastes, 20% by weight of the cement is replaced by a mixture of the two fly ashes. These ternary pastes were tested for various properties as mentioned above. The details of the procedures used for testing have been described in Chapter 3.

The two ashes to be used in the ternary system can be selected in 180 different ways (full factorial design) and the ratio in which they can be any number between 0 and 1. However, it is practically not feasible to perform as many tests to evaluate the behavior of the ternary paste systems. Hence, an experimental design, which can reduce the number of experiments to be performed without compromising on the quality of the output data, was employed. In other words, the data obtained from the reduced experimental design was a representative data from the full factorial design.

An experimental design technique named orthogonal array technique was followed in the current study (see Section 6.1.1), which would drastically reduce the number of experiments to be performed from 180 to 9, which would take into account the averages and extremities of the available data set. Fly ash pairs (FA1 and FA2) were chosen based on this experimental design and the experiments were run on the ternary paste systems containing the chosen fly ash pairs.

ANOVA procedure was then performed on this data set of nine points to investigate the effect of all the chosen independent variables (factors) on the dependent variable (see Section 6.1.3). This would give information about, which factor (independent variable) has the most influence on the dependent variable. It would also give information about how much of the variation in the dependent variable is explained by each of the chosen variables.

To realize the objectives of evaluating the additivity of ternary binder systems, the following statistical procedure was followed.

The additivity of the models when two different fly ashes were added to the binder system was ascertained in a straightforward technique. Tests were performed on the nine different binder systems, comprising of two different ashes mixed in specific ratios, chosen according to the test matrix developed using the orthogonal array technique (see Section 6.1.1) to experimentally observe the dependent variables. The theoretical values were estimated by adding the predictions from the binary binder models in the same ratios as the mixture of fly ashes (weighted summation). The observed and the estimated values would then be compared. If the observed and the estimated values are similar, it means that the binary binder models can be added to evaluate any ternary system.

Three different binary binder models were used to estimate the values for the dependent variable of the ternary binder system. The three models are explained below.

- **Model Set 1** – The two models obtained for Class C and Class F ashes from the binary binder, with the chosen independent variables (factors) were used to predict the properties (dependent variables) for both the Classes of ashes separately. The two predicted values were then added in the proportions of the added fly ashes to obtain the final value of prediction for the ternary binder system. This value was compared with the experimentally observed values.
- **Model Set 2** – The best models obtained for Class C, Class F ashes individually were used to predict the properties of the ashes in the mixture separately, and the predicted values of the properties were added in the proportion of the ashes to obtain the final value of the predicted properties of the ternary binder systems.
- **Model Set 3** – The model obtained for the entire set of Class C and Class F ashes together using all the 20 data points, containing the best three chosen independent variables was used to predict the properties of Class C and Class F ashes separately.

6.1.1 Orthogonal Array Technique

This technique is a form of experimental design, which is used when the available data set is enormous and when it is not practical to test every available data point. This design of experiments helps in studying many variables simultaneously and most economically.

A study of the effect of the individual variables cannot be done by testing one variable at a time as usually all the other variables are also in action in any application. The only way to study their real behavior is when the influences of all the variables have an equal opportunity to be present. Only designed experiments can capture such effects. Orthogonal array technique is a technique to design such experiments. An orthogonal array is a row-column layout of experiments, where

each of the columns represents a factor (variable) level at which the test is performed and each of the rows represents a combination of the factors (variables) at their factor levels to be used in each experiment. The word orthogonal has a different meaning in the current context when compared to geometry or matrix algebra. It means that in the experimental design, each of the columns is balanced within itself (meaning, all the factor levels are repeated in equal number of experiments). This can be explained by considering the orthogonal array in Table 6.1. The designation of this orthogonal array is L-4 (2^3) which denotes that there are four rows or experiments (L-4) to be performed, and there are three variables, each at two factor levels. Thus, we have a total set of 2^3 or 8 different possible combinations of variables out of which we perform four experiments.

In the current statistical analysis, an L-9 (3^3) orthogonal array was used and in the case where this is not possible, an L-9 (3^4) orthogonal array was used. The number of variables in the L-9 array was three. In case if none of the three variable models predict the properties of the two classes of ashes, an L-9 array with four variables was used. The templates of both the orthogonal arrays are shown in Table 6.2 and Table 6.3.

6.1.2 Fly Ash Pairing

The factors (independent variables) A, B and C (D in some cases) were chosen from the models built for the binary binder systems as the most influencing of all the set of variables. Out of the three variables chosen, the one that mostly affects the properties (dependent variables) of ternary binder systems can be found out using the analysis of variance of the experiments performed according to the orthogonal array.

TABLE 6.1
Table showing an L-4 (2^3) orthogonal array.

	Factors		
Exp. No.	**A**	**B**	**C**
1	1	1	1
2	1	2	2
3	2	1	2
4	2	2	1

TABLE 6.2
Table showing an L-9 (3^3) orthogonal array.

	Factors		
Exp. No.	**A**	**B**	**C**
1	1	1	1
2	1	2	2
3	1	3	2
4	2	1	2
5	2	2	3
6	2	3	1
7	3	1	3
8	3	2	1
9	3	3	2

TABLE 6.3
Table showing an L-9 (3^4) orthogonal array.

	Factors			
Exp. No.	**A**	**B**	**C**	**D**
1	1	1	1	1
2	1	2	2	2
3	1	3	3	3
4	2	1	2	3
5	2	2	3	1
6	2	3	1	2
7	3	1	3	2
8	3	2	1	3
9	3	3	2	1

The levels of the factors (1, 2 and 3) were chosen to be 33.33, 50, and 66.67 percentile values of the available data set as the fly ash pairing for any percentiles lower than those listed would not yield an accurate required composition of all the three variables.

Two different fly ashes were chosen to be mixed at a specific ratio in the ternary bindery system, to meet the required composition obtained according to the array (experimental design). However, the composition of the binder system containing any two ashes mixed at a specific percentage would certainly not yield a 100% match of the required factor levels for all the experimental designs. For example, experiment 1 of table requires a 33.33 percentile value of the independent variable (factor) from the data set available for all the fly ashes of factor A, factor B and factor C. However, such pairing is not achievable by pairing of random fly ashes. Therefore, an attempt was made to obtain the best combination of ashes, i.e. a combination which would be closest to the required combination.

A code in C++ Language was written, which examines all the possible combinations of all the fly ashes at 1% increments. The input of the code is the required combination of the chosen factors (variables) and the output would contain the best possible combination chosen in terms of the best "Scaled Standard Deviation" (SSD) for the combination defined as below. For example, if the variables chosen from the binary model are Factor A, Factor B and Factor C at a specific percentile levels for the three variables, the value of SSD is defined as

$$\mathrm{SSD} = \frac{\left|\left[\text{Required Factor level } A - \left[\begin{array}{c}\alpha FlyAsh_i(\text{Factor } A)\\ +(1-\alpha)FlyAsh_j(\text{Factor } A)\end{array}\right]\right]\right|}{StdDev(\text{FFactor } A)} + \frac{\left|\left[\text{Required Factor level } B - \left[\begin{array}{c}\alpha FlyAsh_i(\text{Factor } B)\\ +(1-\alpha)FlyAsh_j(\text{Factor } B)\end{array}\right]\right]\right|}{StdDev(\text{FFactor } B)} + \frac{\left|\left[\text{Required Factor level } C - \left[\begin{array}{c}\alpha FlyAsh_i(\text{Factor } C)\\ +(1-\alpha)FlyAsh_j(\text{Factor } C)\end{array}\right]\right]\right|}{StdDev(\text{FFactor } C)} + \tag{14}$$

where, i and j are the number of available fly ashes and $i \neq j$; $\alpha \varepsilon (0,1)$ at increments of 0.01

The combination, which yields the lowest SSD is used for the experiment.

The output of the C++ code would give the best possible combination, the two fly ashes, the percentage of the two fly ashes and the SSD of the combination.

The standardization of the value of SSD is required as few of the experiments yield an unusually large SSD values. A series of tests on time of set were performed to standardize the value of SSD. Time of setting was performed on various combinations of fly ashes at different SSD levels to find out the cap on SSD for different mixtures, which would obtain the same value of the time of set. It was found that, until an SSD value of 0.3, the mixtures would practically yield the same time of set. The variation of the time of set for different mixture with different SSD is shown in Figure 6.1. Hence, a value of 0.3 SSD was fixed as a cap, which would yield practically the same values of the dependent variable for the experiments.

6.1.3 Analysis of Variance (ANOVA)

The main objective of performing ANOVA is to determine what percentage of total variation observed in the results is caused by the variation of any individual factor. The ANOVA calculation procedure is shown below.

For a data set comprising of results, X_1, X_2, X_3, ..., X_N the total variation (total sum of squares) S_T can be calculated by

$$S_T = \sum_{i=1}^{N} (X_i - \bar{X})^2 \tag{15}$$

which can be reduced to

$$S_T = \sum_{i=1}^{N} X_i^2 - \frac{T^2}{N} \tag{16}$$

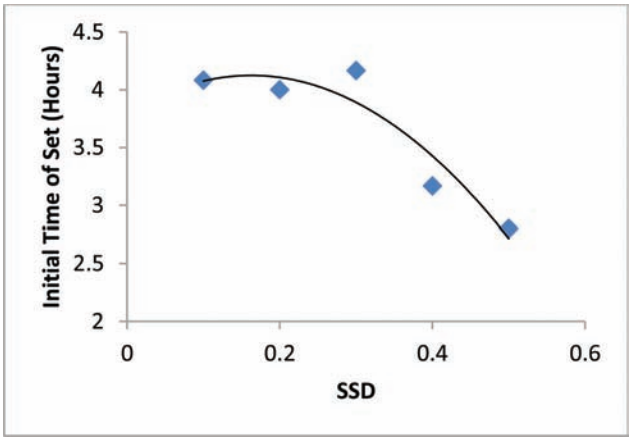

Figure 6.1 Variation of initial time of set with SSD.

where, T is sum of the results (X_i) and N is total number of results

The variation caused by a single factor (say A) can be estimated by the following calculation (using factor sum of squares),

$$S_A = \frac{A_1 2}{N_{A_1}} + \frac{A_2 2}{N_{A_2}} - \frac{T^2}{N} \tag{17}$$

where, N_{A1} is the total number of experiments in which level 1 of factor A is present and A_1 is the sum of the results of level 1 of factor A (X_i)

From the above calculates total and factor sum of sum of squares, the percent influence of each factor can be calculates as follows,

Mean squares (Variance): $V_A = \frac{S_A}{f_A}$

F-ratio: $F_A = \frac{V_A}{V_e}$

Pure sum of squares: $S_A' = S_A(V_e x f_A)$

Percent Influence: $P_A = \frac{S'_A}{S_T}$

where, f_A is the degrees of freedom for factor A

V_e is the variance for the error term, which is calculated as $\frac{S_e}{f_e}$

S_e is the error sum of squares defined as the difference between total sum of squares and factor sum of squares

f_e is the error degrees of freedom defines as the difference between the total degrees of freedom and sum of factor degrees of freedom

6.2 Analysis of the Results for the Dependent Variables

6.2.1 Initial Time of Set

Regression analysis was performed on the binary paste systems for initial time of set and the chosen models containing three variables were also used for the analysis of ternary paste systems.

An orthogonal array was constructed using these three variables (factors) and is shown in Table 6.4.

The factor levels were fixed at 33.33 percentile (level 1), 50 percentile (level 2) and 66.67 percentile (level 3) values of their respective data sets. The

TABLE 6.4
Experimental design using orthogonal array for initial time of set.

Exp. No.	sulfate	alumina	glass
1	1	1	1
2	1	2	2
3	1	3	3
4	2	1	2
5	2	2	3
6	2	3	1
7	3	1	3
8	3	2	1
9	3	3	2

corresponding values of the factor levels are shown in Table 6.5.

The C++ code mentioned in Section 6.1.2 was used to obtain the closest combination of fly ashes with the least SSD for all the experiments shown in Table 6.4. The corresponding fly ash combinations and their SSD values are shown in Table 6.6.

The time of set experiments were performed according to the above-mentioned experimental design and subsequently the analysis for ascertaining the additivity of the properties and the analysis to identify the most influencing variable was performed.

The analysis for the additivity of ashes was performed according to the model analyses mentioned in Section 6.1.3. Regression analysis was performed on the binary paste systems to obtain the model coefficients for all the models (model 1, model 2 and model 3). The variables in each of the models and their corresponding coefficients are shown in the Table 6.7.

The estimated initial time of set was obtained by calculating the weighted sum of the results of the model predictions (for model 1, 2 and 3 separately) for each of the fly ashes.

Table 6.8 shows the observed data of initial time of set (in minutes) from the experiments and the predicted values of the initial time of set from all the above-mentioned models. The residuals (predicted – observed) are listed in Table 6.9.

From Table 6.9, it can be clearly seen that none of the models predict the value of the initial setting time accurately, with residuals of more than 30 minutes. The best model was found to be Model 2; however, even this model has a very high value of the residuals.

The SSD values for two of the combinations of fly ashes were closer to the values of what was found to be a reasonable approximation as 0.3 (estimated by extensive experimentation for set times at various SSD

TABLE 6.5
Factor levels for initial time of set.

Factors/Levels	1	2	3
sulfate (%)	0.4347	0.5281	0.7593
alumina (%)	18.75	19.28	20.07
glass	1.294	1.476	1.513

TABLE 6.6
Fly ash combinations for the experiments and their SSD values.

SSD	FA1	FA2	FA1(%)
0.0219	Kenosha	Will County	12
0.0284	Baldwin	Zimmer	86
0.0543	Baldwin	Moscow	73
0.062	Vermilion	Trimble	78
0.129794	Kenosha	Schahfer	60
0.0921	Labadie	Will County	47
0.291153	Baldwin	Schahfer	13
0.0369	Schahfer	Elmersmith	64
0.0255	Schahfer	Moscow	83

TABLE 6.8
Observed and predicted data for initial time of set (minutes).

Exp. No.	Observed	Model 1 Predicted	Model 2 Predicted	Model 3 Predicted
1	120	157.4	157.5	128
2	155	150.2	162.4	210.8
3	160	156.8	168.872	210.2
4	195	151.5	153.8465	147.2
5	125	152.9	165.2368	26
6	230	173.6	168.3	177.9
7	170	144.7	152.4	119.2
8	225	151.5	151.6	129.3
9	190	153.2	161	122.7

TABLE 6.7
Models and the coefficients for initial time of set.

Model 1

	Intercept	sulfate	alumina	glass
Class C	4.45631	1.178	-0.0851	-0.5834
Class F	1.26093	0.4695	0.07325	-0.0845

Model 2

	Intercept	blaines	spsurface	sulfate	carbon	cao	mgo	glass
Class C	-16.4936	0.0009	-0.00056	1.6638	7.86274	1.1979	-2.0174	0.54108

	Intercept	blaines	meansize	carbon	cao	mgo
Class F	2.90193	-0.0003	0.02711	0.4052	-0.1113	0.2291

Model 3

	Intercept	sulfate	alumina	glass
Classes C & F	0.50206	0.78973	0.13384	-0.5654

values). The poor match of the SSD values could be a reason for the mismatch of the observed and predicted values. However, no apparent relation was found between the SSD values and the residuals of any model. Nevertheless, since all the SSD values were within the approximation cap, the difference in SSD values could not have caused a significant distortion in the observed data points.

It can hence be stated that the property, initial time of set, is not a linearly additive property.

To estimate the percent influence of each of the three chosen variables and the unexplained variation, analysis was performed according to Section 6.1.3.

Table 6.10 shows the percent influence of each of the variables and the error percentage.

Sulfate was found to be the most influencing variable than compared to alumina and glass. However, more than 50% of the variation in the initial time of set was not explained by these three variables. This leads to a conclusion that the number of variables influencing the initial time of set is not constrained to the three chosen variables and not constrained to the properties of fly ash alone. Small variations in other factors might lead to changes that are comparable to the changes caused by the variation in fly ash composition, in the initial time of set.

6.2.2 Peak Heat of Hydration

Regression analysis was performed on the binary paste systems for the peak heat of hydration and the model containing the three chosen variables were chosen for the analysis of ternary paste systems.

In this case, the variables in the best model obtained using the entire data set containing three variables were spsurface, SAF and glass. The best model with any number of variables using the entire data set contained variables namely, spsurface, SAF, cao and alumina. The best models for each of the classes of ashes individually contained blaines, spsurface, meansize, SAF, cao, mgo, alumina and glass for Class C ashes and blaines, spsurface, meansize, carbon and alumina for Class F ashes.

An orthogonal array was constructed using the three chosen variables (factors) and is shown in Table 6.11.

The factor levels were fixed at 33.33 percentile (level 1), 50 percentile (level 2) and 66.67 percentile (level 3) values of their respective data sets. The corresponding values of the factor levels are shown in Table 6.12.

The corresponding fly ash combinations and their SSD values are shown in Table 6.13.

Heat of hydration experiments were performed according to the above-mentioned experimental design and subsequently the analysis for ascertaining the additivity of the properties and the analysis to identify the most influencing variable was performed.

The analysis for the additivity of ashes was performed according to the above-mentioned model analyses (See

TABLE 6.9
Model residuals for intial time of set (minutes).

Exp. No.	Model 1 Residual	Model 2 Residual	Model 3 Residual
1	37.4	37.5	8
2	-4.8	7.4	55.9
3	-3.2	8.9	50.3
4	-43.5	-41.2	-47.8
5	27.9	40.2	-99
6	-56.4	-61.6	-52.1
7	-25.3	-17.5	-50.7
8	-73.5	-73.3	-95.7
9	-36.8	-29	-67.3

TABLE 6.10
Percentage influence of each of the factors.

	sulfate	alumina	glass	Error
F-Value	5.124827	2.087379	3.169209	—
Percent Influence	26.81695	7.069432	14.1028	52.01082

TABLE 6.11
Experimental design using orthogonal array for peak heat of hydration.

Exp. No.	spsurface	SAF	glass
1	1	1	1
2	1	2	2
3	1	3	3
4	2	1	2
5	2	2	3
6	2	3	1
7	3	1	3
8	3	2	1
9	3	3	2

TABLE 6.12
Factor levels for peak heat of hydration.

Factors/Levels	1	2	3
spsurface (cm^2/g)	12173.1	15492	17347.4
SAF (%)	61.59	64.09	82.13
glass	1.294	1.476	1.513

TABLE 6.13
Fly ash combinations for the experiments and their SSD values.

SSD	FA1	FA2	FA1(%)
0.6432	Baldwin	Elmersmith	64
0.0668	RushIsland	Trimble	79
0.0654	Baldwin	Vermilion	24
0.5625	Baldwin	Rockport	25
0.571	Edwards	Petersburg	46
0.0425	Joliet	Labadie	26
0.13928	Edwards	Millcreek	16
0.2773	Labadie	Elmersmith	90
0.1975	Edwards	Labadie	15

Section 6.3). The model coefficients for all the variables and for all the models are shown in Table 6.14.

Table 6.15 shows the observed data of peak heat of hydration (W/kg) from the experiments and the expected values of the peak heat of hydration from all the above models.

The residuals (predicted – observed) are listed in Table 6.16.

In this case, the best model with three variables contained three variables namely, spsurface, SAF and glass using the entire data set was found to be the best model (model 3).

From Table 6.16, it can be clearly seen that none of the models predict the value of the peak heat of hydration accurately, with residuals of more than 0.1 W/kg.

Three of the nine combinations have an SSD value greater than 0.3, which might have caused a significant distortion in the observed values of peak heat of hydration. However, no apparent relation was found between the SSD values and the residuals of any model.

It can be stated that the property, peak heat of hydration, is not a linearly additive property and cannot be predicted accurately by any of the above linear regression models.

To estimate the percent influence of each of the three chosen variables and the unexplained variation, analysis was performed according to the Section 6.2.3.

Table 6.17 shows the percent influence of each of the variables and the error percentage.

Spsurface and SAF were found to be the most influencing variables than compared to glass. More than 80% of the variation in the peak heat of hydration was explained by these three variables. The error percentage is less than 20%, which means that the effects of unexplained variation is much smaller than compared to the unexplained variations in the initial time of set.

6.2.3 Time of Peak Heat of Hydration

Regression analysis was performed on the binary paste systems for the time of peak heat of hydration and the best models using the entire data set according to the adj-R^2 were chosen for the analysis of ternary binder systems.

TABLE 6.15
Observed and predicted data for peak heat of hydration (W/kg).

Exp. No.	Observed	Model 1 Predicted	Model 2 Predicted	Model 3 Predicted
1	3.427	3.936	3.748	3.613
2	3.169	3.641	3.346	3.924
3	3.133	2.921	3.128	2.497
4	3.765	3.362	3.669	3.224
5	3.435	2.518	2.986	2.373
6	3.689	3.404	3.298	3.3134
7	3.875	3.243	3.296	3.252
8	3.457	3.542	3.517	3.649
9	3.223	3.257	3.322	3.391

TABLE 6.16
Model residuals (W/kg).

Exp. No.	Model 1	Model 2	Model 3
1	0.5089	0.3206	0.1853
2	0.4716	0.1764	0.7545
3	-0.2117	-0.0052	-0.6364
4	-0.402	-0.0953	-0.5406
5	-0.9168	-0.4488	-1.0627
6	-0.2851	-0.3917	-0.3758
7	-0.6313	-0.5788	-0.6229
8	0.084	0.0598	0.1914
9	0.034	0.0985	0.1675

TABLE 6.14
Models and the coefficients for peak heat of hydration.

Model 1

	Intercept	spsurface	SAF	glass
Class C	17.71747	-0.00029	-0.1681	0.68174
Class F	11.39065	-2.6E-05	-0.0995	0.61193

Model 2

	Intercept	blaines	spsurface	meansize	SAF	cao	mgo	alumina	glass
Class C	12.43867	0.00025721	-0.0003407	0.07023	-0.2379	0.32793	-1.11003	0.23043	1.20276
	Intercept	**blaines**	**spsurface**	**meansize**	**carbon**	**alumina**			
Class F	11.09964	-0.0001063	0.00003604	-0.35316	2.53082	-0.0881			

Model 3

	Intercept	spsurface	SAF	glass
Classes C & F	7.60065	-0.00015	-0.0389	0.48463

TABLE 6.17
Percentage influence of each of the factors.

	spsurface	SAF	Glass	Error
F-Value	16.82508	16.14431	2.137662	
Percent	39.4571	37.75972	2.836563	19.94661

TABLE 6.18
Experimental design using orthogonal array for time of peak heat of hydration.

Exp. No.	spsurface	meansize	mgo
1	1	1	1
2	1	2	2
3	1	3	3
4	2	1	2
5	2	2	3
6	2	3	1
7	3	1	3
8	3	2	1
9	3	3	2

TABLE 6.19
Factor levels for time of peak heat of hydration.

Factors/Levels	1	2	3
spsurface (cm^2/g)	12173.1	15492	17347.4
meansize (μm)	17.69	21.99	27.02
mgo	2.15	4.81	5.343

TABLE 6.20
Fly ash combinations for the experiments and their SSD values.

SSD	FA1	FA2	FA1(%)
0.7526	Vermilion	Trimble	37
0.3461	Labadie	Zimmer	43
0.2262	Miller	Zimmer	15
0.1038	RushIsland	Zimmer	68
0.05	Miller	Miami 8	83
0.1394	Edwards	Miami 8	27
0.1016	Joppa	Kenosha	35
0.4802	Edwards	Miami 7	50
0.3764	Miller	Miami 8	80

In this case, the variables in the best model obtained using the entire data set containing three variables were spsurface, meansize and mgo. The best model with any number of variables using the entire data set contained six variables namely, blaines, spsurface, meansize, sulfate, mgo and alumina . The best models for each of the classes of ashes individually contained blaines, spsurface, meansize, sulfate, carbon, mgo and alumina for Class C ashes and blaines, spsurface, meansize, carbon and mgo for Class F ashes.

An orthogonal array was constructed using the three chosen variables (factors) and is shown in Table 6.18.

The factor levels were fixed at 33.33 percentile (level 1), 50 percentile (level 2) and 66.67 percentile (level 3) values of their respective data sets. The corresponding values of the factor levels are shown in Table 6.19.

The corresponding fly ash combinations and their SSD values are shown in Table 6.20.

Heat of hydration experiments were performed according to the above-mentioned experimental design and subsequently the analysis for ascertaining the additivity of the properties and the analysis to identify the most influencing variable was performed.

The analysis for the additivity of ashes was performed according to the above-mentioned model analyses (Section 6.3). The model coefficients for all the variables and for all the models are shown in the Table 6.21.

Table 6.22 shows the observed data for time of peak heat of hydration (minutes) from the experiments and the expected values of the time of peak heat of hydration from all the above models. The residuals (predicted – observed) are listed in Table 6.23.

In this case, the best model with three variables contained three variables namely, spsurface, meansize and mgo using the entire data set was found to be the best model. However, the residuals for all the ternary paste systems were high.

From Table 6.23, it can be clearly seen that none of the models predict the value of the time of peak heat of hydration accurately, as they contain very high residuals.

It can hence be stated that the property, time of peak heat of hydration, is not a linearly additive property and cannot be predicted accurately by any of the above linear regression models.

To estimate the percent influence of each of the three chosen variables and the unexplained variation, analysis was performed according to the Section 6.2.3.

Table 6.24 shows the percent influence of each of the variables and the error percentage.

The variable spsurface was found to be the most influencing variable than compared to meansize and mgo. More than 68% of the variation in the time of peak heat of hydration was explained by these three variables. The error percentage was more than 30%, which means that the effects of unexplained variation is much smaller than compared to the unexplained variations in the initial time of set but larger than the unexplained error in peak heat of hydration.

6.2.4 Non-evaporable Water Content

Regression analysis was performed on the binary paste systems for the non-evaporable water content and the best models using the entire data set according to the adj-R^2 were chosen for the analysis of ternary binder systems.

In this case, the variables in the best model obtained using the entire data set containing three variables were blaines, carbon and alumina. The best models for each of the classes of ashes individually contained

TABLE 6.21
Models and the coefficients for time of peak heat of hydration.

	Model 1							
	Intercept	**spsurface**	**meansize**	**mgo**				
Class C	967.7839	-0.03014	-10.1287	63.35305				
Class F	1010.562	-0.01446	-12.49137	13.57689				
	Model 2							
	Intercept	**blaines**	**spsurface**	**meansize**	**sulfate**	**carbon**	**mgo**	**alumina**
Class C	-6.04545	-0.0406	-0.01356	-6.76153	-48.3605	-479.530	44.45672	62.15536
	Intercept	**blaines**	**spsurface**	**meansize**	**carbon**	**mgo**		
Class F	1011.787	0.03587	-0.01982	-15.7633	16.47141	10.52289		
	Model 3							
	Intercept	**spsurface**	**meansize**	**mgo**				
Classes C & F	939.7103	-0.02042	-8.78838	30.93357				

TABLE 6.22
Observed and predicted data for time of peak heat of hydration (minutes).

Observed	Model 1 Predicted	Model 2 Predicted	Model 3 Predicted
583.0	561.0	562.7	570.2
604.5	596.2	618.8	695.4
639.5	582.0	615.9	711.8
688.0	581.8	589.1	635.1
652.5	538.8	528.3	552.7
660.5	451.2	459.3	447.3
578.5	616.4	603.5	723.4
618.5	460.8	475.1	471.2
620.5	535.5	525.1	548.7

TABLE 6.23
Model residuals.

Model 1 Residual	Model 2 Residual	Model 3 Residual
-22.0	-20.3	-12.8
-8.3	14.3	90.9
-57.5	-23.6	72.3
-106.2	-98.9	-52.9
-113.7	-124.2	-99.8
-209.3	-201.2	-213.2
37.9	25.0	144.9
-157.7	-143.4	-147.3
-85.0	-95.4	-71.8

blaines, meansize, carbon, SAF, mgo and alumina for Class C ashes and carbon, cao, mgo and glass for Class F ashes.

An orthogonal array was constructed using the three chosen variables (factors) and is shown in Table 6.25.

The factor levels were fixed at 33.33 percentile (level 1), 50 percentile (level 2) and 66.67 percentile (level 3) values

TABLE 6.24
Percentage influence of each of the factors.

	spsurface	meansize	mgo	Error
F-Value	17.06556	2.063158	1.193738	
Percent	63.44392	4.198479	0.765082	31.59252

TABLE 6.25
Experimental design using orthogonal array for non-evaporable water content.

Exp. No.	blaines	carbon	alumina
1	1	1	1
2	1	2	2
3	1	3	3
4	2	1	2
5	2	2	3
6	2	3	1
7	3	1	3
8	3	2	1
9	3	3	2

of their respective data sets. The corresponding values of the factor levels are shown in Table 6.26.

The corresponding fly ash combinations and their SSD values are shown in Table 6.27.

Thermo-gravimetric analysis was performed according to the above-mentioned experimental design and subsequently the analysis for ascertaining the additivity of the properties and the analysis to identify the most influencing variable was performed.

The analysis for the additivity of ashes was performed according to the above-mentioned model analyses (Section 6.1.3). The model coefficients for all the variables and for all the models are shown in the Table 6.28.

Table 6.29 shows the observed data for non-evaporable water content (%) from the experiments and the values of the non-evaporable water content (%) predicted by all of the above models. The residuals (predicted – observed) are listed in Table 6.30.

In this case, the model with the least residual values was found to be the best models (model 1) with three variables for each of the Classes. However, the residuals for all the ternary binder systems were high. Most of the predictions were higher than the observed values.

From Table 6.30, it can be clearly seen that none of the models predict the value of the non-evaporable water content accurately, as they contain very high residuals.

TABLE 6.26
Factor levels for non-evaporable water content.

Factors/Levels	1	2	3
blaines (cm^2/g)	3884.2	4452	5783.09
carbon (%)	0.43	0.49	1.383
alumina (%)	18.75	19.28	20.07

TABLE 6.27
Fly ash combinations for the experiments and their SSD values.

SSD	FA1	FA2	FA1(%)
0.6432	Joppa	Petersburg	80
0.0668	Joppa	Petersburg	75
0.0654	Rockport	Zimmer	16
0.5625	Joppa	Petersburg	39
0.571	Kenosha	Millcreek	89
0.0425	Edwards	Zimmer	19
0.13928	Labadie	Rockport	73
0.2773	Baldwin	Joliet	57
0.1975	Edwards	Elmersmith	64

It can hence be stated that the property, non-evaporable water content at 28 days, is not a linearly additive property and cannot be predicted accurately by linear addition of any binary paste models.

To estimate the percent influence of each of the three chosen variables and the unexplained variation, analysis was performed according to the Section 6.1.3.

Table 6.31 shows the percent influence of each of the variables and the error percentage.

Blaine's specific surface area was found to be the most influencing variable than compared to carbon and alumina. More than 75% of the variation in the non-evaporable water content was explained by these three variables. The error percentage was close to 25%, which means that the effects of unexplained variation in the sample were relatively high.

6.2.5 Strength Activity Index at 28 Days

Regression analysis was performed on the binary paste systems for the strength activity index at 28 days and the best models using the entire data set according to the adj-R^2 were chosen for the analysis of ternary paste systems.

In this case, the variables in the best model obtained using the entire data set containing three variables were meansize, sulfate and SAF. The best models for each of the classes of ashes individually contained spsurface, meansize, sulfate, and glass for Class C ashes and meansize, SAF, cao, and glass for Class F ashes.

An orthogonal array was constructed using the three chosen variables (factors) from the binary paste models and is shown in Table 6.32.

The factor levels were fixed at 33.33 percentile (level 1), 50 percentile (level 2) and 66.67 percentile (level 3) values of their respective data sets. The corresponding values of the factor levels are shown in Table 6.33.

TABLE 6.28
Models and the coefficients for non-evaporable water content for all three models.

				Model 1			
	Intercept	**blaines**	**carbon**	**alumina**			
Class C	6.83573	-0.0002183	0.63946	0.00992			
Class F	5.73953	0.00007164	-0.71966	0.04661			
				Model 2			
	Intercept	**blaines**	**meansize**	**carbon**	**SAF**	**mgo**	**alumina**
Class C	17.02077	-0.0003	0.03759	1.22719	-0.1751	-1.0625	0.31264
	Intercept	**carbon**	**cao**	**mgo**	**glass**		
Class F	6.47239	-1.4420	0.0853	-0.0899	-0.8785		
				Model 3			
	Intercept	**blaines**	**carbon**	**alumina**			
Classes C & F	6.18952	-0.0002	-0.632	0.05751			

TABLE 6.29
Observed and predicted data for non-evaporable water content.

Exp. No.	Observed	Model 1 Predicted	Model 2 Predicted	Model 3 Predicted
1	6.8	6.2	6.0	6.2
2	6.49	6.2	5.8	6.2
3	6.41	6.0	4.0	5.8
4	6.44	6.1	4.6	6.2
5	6.58	6.1	5.8	6.5
6	6.38	5.8	3.7	5.7
7	6.77	6.1	4.8	6.1
8	6.26	6.1	5.4	6.0
9	6.19	5.5	5.4	5.6

TABLE 6.30
Model residuals.

Model 1 Residual	Model 2 Residual	Model 3 Residual
0.6	0.6	0.6
0.29	0.29	0.29
0.41	0.41	0.61
0.34	1.84	0.22
0.48	1.78	0.08
0.58	0.88	0.68
0.67	1.97	0.67
0.16	0.86	0.26
0.69	0.79	0.59

TABLE 6.31
Percentage influence of each of the factors.

	blaines	carbon	alumina	Error
F-Value	17.055	4.511755	5.617818	
Percent	49.884	10.9114	14.34805	24.85685

The corresponding fly ash combinations and their SSD values are shown in Table 6.34.

Strength activity index test was performed according to the above-mentioned experimental design and subsequently the analysis for ascertaining the additivity of the properties and the analysis to identify the most influencing variable was performed.

The analysis for the additivity of ashes was performed according to the above-mentioned model analyses (Section 6.1.3). The model coefficients for all the variables and for all the models are shown in the Table 6.35.

Table 6.36 shows the observed data for strength activity index at 28 days (%) from the experiments and the values of the strength activity index at 28 days (%) predicted by all of the above models. The residuals (predicted – observed) are listed in Table 6.37.

In this case, the models with containing the three chosen variables from binary paste models (model 1) for each of the Classes were found to have the least residuals. The residuals for all the ternary paste systems were within the specified variation of 10.3% according to ASTM C 311 (*6*). Most of the predictions for the other models (model 2 and model 3) were higher than 10.3%.

From Table 6.37, it can be clearly seen that none of the models predict the value of the strength activity index at 28 days accurately, as they contain very high residuals.

TABLE 6.32
Experimental design using orthogonal array for strength activity index at 28 days.

Exp. No.	meansize	sulfate	SAF
1	1	1	1
2	1	2	2
3	1	3	3
4	2	1	2
5	2	2	3
6	2	3	1
7	3	1	3
8	3	2	1
9	3	3	2

TABLE 6.33
Factor levels for time of strength activity index.

Factors/Levels	1	2	3
meansize (μm)	17.69	21.99	27.02
sulfate (%)	0.4347	0.5281	0.7593
SAF (%)	61.59	64.09	82.13

TABLE 6.34
Fly ash combinations for the experiments and their SSD values.

SSD	FA1	FA2	FA1(%)
0.6432	Joppa	Labadie	66
0.0668	Kenosha	Elmersmith	98
0.0654	Joliet	Schahfer	34
0.5625	Rockport	Willcounty	41
0.571	Vermilion	Millcreek	35
0.0425	Labadie	Miller	36
0.13928	Willcounty	Miami 7	24
0.2773	Miller	Rockport	72
0.1975	Miller	Zimmer	85

TABLE 6.35
Models and the coefficients for strength activity index for all three model.

			Model 1		
	Intercept	**meansize**	**sulfate**	**SAF**	
Class C	142.0434	-1.573	-15.784	0.0496	
Class F	126.1376	-0.67193	-9.2767	-0.0032	
			Model 2		
	Intercept	**spsurface**	**meansize**	**sulfate**	**glass**
Class C	102.3113	0.00127	-0.98192	-15.937	6.83886
	Intercept	**meansize**	**SAF**	**cao**	**glass**
Class F	-169.891	-0.83883	3.05858	4.26668	5.02163
			Model 3		
	Intercept	**meansize**	**sulfate**	**SAF**	
Classes C & F	120.9835	-1.15994	-11.77	-0.24	

TABLE 6.36
Observed and predicted data for strength activity index at 28 days.

Exp. No.	Observed	Model 1 Predicted	Model 2 Predicted	Model 3 Predicted
1	125.3265	110.3	104.9	80.5
2	123.0756	109.3	104.2	78.8
3	119.3986	106.0	103.6	76.5
4	118.0756	103.7	102.6	75.1
5	118.5395	108.1	101.7	70.4
6	115.6357	98.8	96.1	61.9
7	113.4192	104.7	104.0	65.2
8	117.354	94.9	90.4	57.1
9	112.2337	96.3	90.2	54.3

TABLE 6.37
Model residuals.

Model 1 Residual	Model 2 Residual	Model 3 Residual
-15.1	-20.4	-44.8
-13.7	-18.8	-44.3
-13.4	-15.8	-42.9
-14.3	-15.4	-43.0
-10.4	-16.8	-48.2
-16.8	-19.6	-53.7
-8.7	-9.4	-48.2
-22.5	-27.0	-60.2
-15.9	-22.1	-58.0

It can hence be stated that the property, strength activity index at 28 days, is a linearly additive property and can be predicted accurately by linear addition of the binary paste models.

To estimate the percent influence of each of the three chosen variables and the unexplained variation, analysis was performed according to the Section 6.1.3. Table 6.38 shows the percent influence of each of the variables and the error percentage.

TABLE 6.38
Percentage influence of each of the factors.

	meansize	**sulfate**	**SAF**	**Error**
F-Value	37.71579	9.320701	3.077081	
Percent	66.61842	15.09737	3.768729	14.51548

Mean particle size was found to be the most influencing variable than sulfate and SAF. More than 85% of the variation in the strength activity index at 28 days was explained by these three variables. The error percentage was less than 15%, which means that the effects of unexplained variations in the sample were very low and most of the variation in the property was well explained by the three variables.

7. SUMMARY AND CONCLUSIONS

7.1 Fly Ash Characterization

Twenty fly ashes, mostly from INDOT's list of approved pozzolanic materials, have been studied and characterized for the purpose of updating the information on their basic physical and chemical characteristics. The obtained data were used in the statistical analysis and modeling of binary paste systems (comprising of portland cement and a fly ash), and ternary paste systems (comprising of portland cement and two different fly ashes).

The following conclusions are drawn from examinations performed during this study:

1. In terms of the availability of the fly ashes for use in Indiana, the number of the available Class C fly ashes is currently much higher than Class F ashes (13 to 7).
2. With a few exceptions, ashes from the same class show relatively consistent chemical compositions as summarized below.

   Typically, for Class C fly ashes, the compositional parameters were as follows:

   a. A combined silicon, aluminum and iron oxide content ranged from 56% to 65%.
   b. Iron oxide content varied very little from the typical content of 6%, except for one ash.
   c. The typical calcium oxide content for the majority of the fly ashes ranged from 22% to 26%.
   d. Moderate total alkali contents of around 2% were observed for most fly ashes; almost none of the alkalis were soluble.
   e. Sulfate contents were all below 2.7%.
   f. With two exceptions, loss on ignition (LOI) values ranged from 0.17% to 0.49%.

   Similarly, the chemical composition characteristics for Class F fly ashes could be summarized as follows:

   a. A combined silicon, aluminum and iron oxides contents ranged from 81% to 91%.
   b. The iron oxide contents ranged from 18% to 25%. In two fly ashes (both from the same plant) the values of iron oxide were much lower (close to 5%).
   c. Typical CaO contents for all ashes were below 5% (with one exception).
   d. Consistent alkalis contents of around 2.3% were found.
   e. Sulfate contents varied in a broad range from negligible (0.2%) to 3.1%.
   f. Loss on ignition (LOI) levels were higher than those for Class C ashes and ranged from 1.3% to 2.4%.

3. The particle size distribution results seem consistent within each of the Class C ash and Class F ash groups. The percentage of particles smaller than 1 μm found in Class C fly ashes was typically 5% but only about 2% for Class F fly ashes. The difference in the mean size between the groups was highly significant and suggests that the Class F ashes were coarser than Class C ashes.
4. The area under the glass hump (glass content) for all Class F fly ashes was higher than that for most of the Class C ashes. About three out of thirteen Class C ashes' had glass content coinciding with the lower end of the range for Class F ashes.

7.2 Binary Paste Systems

This section summarizes the statistical analysis of the properties of binary paste systems. These properties included: (a) initial time of set, (b) peak heat of hydration, (c) time of peak heat of hydration, (d) total heat of hydration (measured over a period of three days), (e) calcium hydroxide content at various ages (f) non-evaporable water content at various ages and (g) rate of strength gain (strength activity index at 1, 3, 7 and 28 days). It was seen that a few of the above-mentioned variables were predicted well, while the rest had relatively poor predictions. Most of the models had a very large value of the intercept, while the effect of the variables was relatively smaller. This suggested that the variations in the properties of the binders containing various fly ashes, were marginal. The most common reasons for the poor predictions of the models can be summarized as follows,

1. In some cases, either the models or the variables were not found significant, even if the fit was good.
2. In some other cases both the variables and the model had a good significance, but the fit was poor (low R^2).
3. Even if both the model and the variables were significant and the model itself had a good fit, the intercept had a very high degree of error associated with it, thus introducing a large degree of error in the model itself.

7.2.1 Initial Time of Set

Significant differences were observed between the performance of Class C and Class F ashes with respect to the initial time of set. Pastes with Class F ashes exhibited in general, a higher initial time of set when compared to the time of set for plain cement. On the other hand, most of the pastes with Class C ashes had a lower time of set than plain cement pastes.

The chemical characteristics of fly ashes were found to have a stronger influence on the set time than their physical characteristics. Sulfate content, alumina content and glass content were found to be the most influencing variables affecting the initial time of set. However, none of them was statistically significant and the statistical model using these three variables could not explain a relatively large variation in the observed time of set using the three variables.

Sulfate content was found to be the variable with the maximum effect in comparison with alumina content and glass content. The sign of the coefficient associated with sulfate suggested that an increase in the amount of sulfate leads to a delay in the setting time. A sulfate content of more than 1% definitely leads to a set time much greater than that of binders containing fly ashes with sulfate content less than 1%.

7.2.2 Peak Heat of Hydration

Significant differences were seen in the peak heat of hydration between pastes containing Class C and Class F ashes. Most of the Class C ashes reduced the peak heat of hydration compared to that obtained from plain cement. In contrast, most of the Class F ashes acted the other way, with a few exceptions. A slight indication of an increase in the set time with the peak heat of hydration was observed. The only fly ash which exhibited a flash set, Kenosha, had a very low peak heat of hydration.

Specific surface, the sum of the silicon, aluminum and iron oxides and the glass content were found to be the most influencing variables affecting the peak heat of hydration. The model predictions for Class C ashes were accurate, with the specific surface and the sum of oxides variables being highly significant. Hence, the model predictions were reliable. The only insignificant variable in the model was the glass content. The model for Class F fly ashes was not significant and hence the model predictions were considered to be not reliable.

A weak correlation between the specific surface area and peak heat of hydration could be observed. An increase in the specific surface area leads to a decrease in the peak heat of hydration, with a few exceptions. However, the amount of calcium oxide also plays a major role in the peak heat of hydration. Most of the variation in the peak heat of hydration of the binder systems containing Class C ashes could be explained using these two variables.

7.2.3 Time of Peak Heat of Hydration

With the exception of one, all ashes delayed the occurrence of the peak heat of hydration. Class C ashes had marginally higher time of the peak than Class F ashes. Slight correlation was seen between time of peak heat and initial time of set. However, no correlation was seen between the time of peak heat of hydration and the value of the peak heat of hydration itself.

The physical characteristics of fly ashes were found to affect the delay of peak of hydration more than their chemical characteristics. The specific surface, the mean particle size and the magnesium oxide content were the most influencing variables. However, specific surface was more significant the other two. The sign of the specific surface variable indicated that an increase in the specific surface leads to a delay in the occurrence of the peak heat of hydration. The model predictions for all of the twenty available ashes seemed reasonable. However, the predictions for the ashes which were not used in the model were poor. This was because of the error seen in the intercept of the model, which had a major effect when compared to the rest of the variables.

7.2.4 Total Heat of Hydration

All fly ash pastes (except for one) had a lower total heat of hydration compared to the total heat of hydration of plain cement paste. Most of the ashes had a very comparable total heat of hydration, with Class F ashes showing a marginally higher total heat of hydration than Class C ashes.

The best of the three variables model could not explain the variations for either of classes of ashes and thus, a four variable model was chosen. The four variables chosen were: mean particle size, loss on ignition, sum of the oxides of silicon, aluminum and iron, and calcium oxide content. The model for Class F fly ash was poor, while the model for Class C ashes was significant. Of all the variables used in the model for Class C ashes, only mean particle size was significant. The predictions for the ashes used for building the model were not reasonable. The model is not reliable as the error for intercept was comparable to the intercept itself. No correlations were observed between total heat of hydration and any of the previously evaluated variables.

7.2.5 Calcium Hydroxide Content

Most of the ashes tended to reduce the amount of calcium hydroxide (CH) produced in the hydration reaction at very early ages (1 and 3 days). However, there was a significant rise in the CH contents at the age of 7 days and 28 days for quite a few of the ashes. This was attributed to the hydration reaction in the Class C ashes. However, some of the ashes have shown a reduction in the rate of formation of calcium hydroxide from 7 to 28 days, leading to a conclusion that there was an inception of pozzolanic reaction in the binders systems. A conclusion that the rate of hydration and pozzolanic reactions in these binder systems varies even within the same Class of fly ashes can thus be made.

The variables chosen for statistical modeling at all ages included both physical and chemical characteristics. The Blaine's specific surface was the common variable in the models for all ages. This variable was also significant at all the ages. However, only the models at 1,7 and 28 days for Class C ashes, and 1 and 28 days for Class F ashes were significant and were therefore tested with new ashes (verification) for their accuracy. All these models proved very accurate in estimating the calcium hydroxide content at the respective ages for the new ashes. These models are all significant and have a good fit as well. Hence, these models can be used for predicting the calcium hydroxide contents.

7.2.6 Non-evaporable Water Content

The results of the non-evaporable water content suggested that the rates of the hydration reaction in the fly ash pastes varied (as expected) with the type of fly ashes. These conclusions also agreed well with the amount of calcium hydroxide observed at various ages. A good correlation was also seen between the calcium hydroxide content and the non-evaporable water content at all ages. However, the R^2 values for these

TABLE 7.1
Most influencing variable for the properties of tern'ary binders.

Property of the binder	Most influencing independent variables
Initial time of set	sulfate
Peak heat of hydration	spsurface, SAF
Time of peak heat	spsurface, meansize
Non-evaporable water content at 28 days	blaines, carbon
Strength activity index at 28 days	meansize, sulfate

correlations reduced with age, as the fly ashes started undergoing reactions. The above correlation was relatively poorer at the later ages with the inception of pozzolanic reaction in the fly ashes.

Blaine's specific surface area was found to be the most significant variable at both early and later ages. However, some chemical characteristics of fly ashes were also present in the models. Contrary to the models for calcium hydroxide contents, non-evaporable water content models predicted better at early ages than at later ages. The models at 1 day can be used to predict the amount of non-evaporable water contents for fly ash-cement binary binders.

7.2.7 Rate of Strength Gain

Pastes with Class C ashes developed comparatively higher strength than pastes from Class F ashes at all the ages. The rate of strength gain varied a lot for different ashes. Class C ashes, which had a lower strength at earlier ages, generally showed higher strengths at later ages and vice versa, with a few exceptions.

The models for strength at early ages (1 day and 3 days) were practically unreliable. This was attributed to the very high initial of strength gain. However, the prediction models for 7 and 28 days were reliable. The models were all significant and had a very good fit. The only drawback in the models for 7 days was that two highly correlated variables (cao and SAF) were also present in the model. This causes multicollinearity in the system, which tends to deflate the p-value of the model. However, the predictions for the new ashes were found agreeable. These models can be used to predict the strength activity index for fly ashes at later ages.

Mean particle and sulfate content were found to be major contributors to strength at 28 days, while the glass content and SAF content were found to be the most influencing variables at 7 days for both classes of ashes.

7.3 Ternary Paste Systems

This section summarizes the statistical analysis of the properties of ternary paste systems for initial time of set, peak heat of hydration, time of peak heat of hydration, the non-evaporable water content at various ages and the strength activity index at 28 days.

It was observed that none of the above-mentioned properties of ternary paste systems were found to be linearly additive (as a weighted summation of the individual binary models), except for strength activity index at 28 days. The possible reasons for the non-linearity are listed below,

1. The variables chosen in the binary paste models, which were used for testing the linearity of ternary paste models, could not explain the variations in the dependent variables to a large extent. This was observed in most of the dependent variables in the form of the error percentage, which was higher than 20%.
2. A few of the binary paste models, which were used in estimating the properties of ternary paste systems, were not significant and the predictions were not accurate. The error in the binary models carried into the estimation of the properties of ternary systems when the models were used.
3. The chosen variables might not be linearly related to the properties of the binary binder systems and also some interactions between the chosen variables might have played a role in the poor predictions of the binary binder systems. This non-linearity causes an error in the prediction for the ternary model, when the binary models are added as a weighted summation.

Only the weighted linear combination of the binary paste models (individual Class C and Class F models, model 1) used for predicting the strength activity index at 28 days were found to satisfactorily predict the strength activity index of the ternary paste systems.

In this study of ternary paste systems, there were several independent variable(s), which have the maximum effect on each of the properties of the ternary paste systems. Table 7.1 summarizes these variables.

7.4 Conclusions

The statistical studies resulted in a conclusion that both the physical and the chemical characteristics of fly ash affect the properties of the pastes containing ashes at all ages. The sets of variables affecting various binder properties were unique for each of the properties evaluated. However, the variable which was found to have the most significant effect on almost all the binder properties was the specific surface area of the fly ash grains.

The statistical analysis for the properties of the binary paste systems allow us to draw inferences about which of the characteristics of fly ash holds the most significance on the effect of the properties. The sign of the coefficients of the significant variables indicates the type of effect the variables has on the property.

For most of the properties evaluated, the variables that affect the property the most could be easily

identified. However, some of the properties evaluated had a high degree of variation, which could not be explained by any sets of characteristics of the fly ash.

The statistical analysis of the properties evaluated for ternary paste systems (using the orthogonal array technique) indicated that the properties of the ternary binder systems are not a weighted linear combination of the properties of binary pastes prepared from the individual fly ashes. However, the most significant variables, along with their relative percent influence on the ternary systems, could be identified and were summarized in Section 7.3.

REFERENCES

1. Barroso, J., J. Ballester, L. M. Ferrer, and S. Jimenez. Study of Coal Ash Deposition in an Air Entrained Flow Reactor: Influence of Coal Type, Blend Composition and Operating Conditions. *Fuel Processing Technology,* Vol. 87, 2006, pp. 737–752.
2. ASTM C618. *Standard Specification for Coal Fly Ash and Raw or Calcined Natural Pozzolan for Use in Concrete.* American Society for Testing and Materials, West Conshohocken, Pennsylvania.
3. Jiang, L., Z. Liu, and Y. Ye. Durability of Concrete Incorporating Large Volumes of Low-Quality Fly Ash. *Cement and Concrete Research,* Vol. 34, 2004, pp. 1467–1469.
4. Affolter, R. H., M. E. Brownfield, and J. D. Cathcart. *Chemical Variation of Feed Coal and Coal Combustion Products from an Indiana Power Plant Utilizing Low sulfur Powder River Basin Coal*. International Ash Utilization Symposium. University of Kentucky, 1999.
5. Ural, S. Comparison of Fly Ash Properties from Afsin-Elbistan Coal Basin, Turkey. *Journal of Hazardous Materials*, Vol. B119, 2005, pp. 85–92.
6. ASTM C311. *Standard Test Methods for Sampling and Testing Fly Ash or Natural Pozzolans for Use in Portland-Cement Concrete.* American Society for Testing and Materials, West Conshohocken, Pennsylvania.
7. ASTM C204. *Standard Test Methods for Fineness of Hydraulic Cement by Air-Permeability Apparatus.* American Society for Testing and Materials, West Conshohocken, Pennsylvania.
8. Malhotra, V. M., and P. K. Mehta. *High-Performance, High-Volume Fly Ash Concrete: Materials, Mixture Proportioning, Properties, Construction Practice, and Case Histories.* Supplementary Cementing Materials for Sustainable Development Inc., Ottawa, Canada, 2002.
9. Diamond, S. Rapid Particle Size Analysis of Fly Ash with a Commercial Laser Diffraction Instrument. *Materials Research Society,* Vol. 113, 1988, pp. 119–127.
10. Kulaots, I., R. H. Hurt, and E. M. Suuberg. Size Distribution of Unburned Carbon in Coal Fly Ash and its Implications. *Fuel,* Vol. 83, 2004, pp. 223–230.
11. Frias, M., M. I. Sanchez de Rojas, M. P. Luxan, and N. Garcia. Determination of Specific Surface Area by the Laser Diffraction Technique. Comparison with the Blaines Permeability Method. *Cement and Concrete Research,* Vol. 21, 1991, 709–717.
12. Diamond, S. Particle Morphologies in Fly Ash. *Cement and Concrete Research*, Vol. 16, 1986, pp. 569–579.
13. Lopez-Flores, F. *Flyash and Effects of Partial Cement Replacement by Flyash: Informational Report*. Publication FHWA/IN/JHRP-82/11. Joint Highway Research Project, Indiana Department of Transportation and Purdue University, West Lafayette, Indiana, 1982. doi: 10.5703/1288284314049.
14. Hubbard, F. H., R. K. Dhir, and M. S. Ellis. Pulverized-Fuel Ash for Concrete: Compositional Characterization of United Kingdom PFA. *Cement and Concrete Research,* Vol. 15, 1985, pp. 185–198.
15. Roode, M. V., E. Douglas, and R. T. Hemmings. X-ray Diffraction Measurement of Glass Content in Fly Ashes and Slags. *Cement and Concrete Research,* Vol. 17, 1987, pp. 183–197.
16. Hemmings, R. T., and E. E. Berry. On the Glass in Coal Fly Ashes: Recent Advances. *Material Research Society,* Vol. 113, 1987, pp. 3–38.
17. Diamond, S. On the Glass Present in Low-Calcium and in High-Calcium Flyashes. *Cement and Concrete Research,* Vol. 13, 1983, pp. 459–464.
18. Simons, H. S., and J. W. Jeffery. An X-ray Study of Pulverized Fuel Ash. *Journal of Applied Chemistry,* Vol. 10, 1960, pp. 328–336.
19. Kiattikomol, K., C. Jaturapitakkul, S. Songpiriyakij, and S. Chutubtim. A Study of Ground Coarse Fly Ashes with Different Finenesses from Various Sources as Pozzolanic Materials. *Cement and Concrete Composites,* Vol. 23, 2001, pp. 335–343.
20. ASTM C150. *Standard Specification for Portland Cement.* American Society for Testing and Materials, West Conshohocken, Pennsylvania.
21. Sybertz F., and U. Wiens. Effect of Fly Ash Fineness on Hydration Characteristics and Strength Development. In *Proceedings of the International Conference on Blended Cements in Construction.* University of Sheffield, UK, 1991, pp. 152–165.
22. Fajun, W., M. W. Grutzeck, and D. M. Roy. The Retarding Effects of Fly Ash upon the Hydration of Cement Pastes: The First 24 Hours. *Cement and Concrete Research,* Vol. 15, 1985, pp. 174–184.
23. Ma, W., and P. W. Brown. Hydrothermal Reactions of Fly Ash with $Ca(OH)_2$ and CaSO4.2H2O. *Cement and Concrete Research,* Vol. 27, 1997, pp. 1237–1248.
24. Smith, M. A., and J. D. Matthews. Conduction Calorimetric Studies of the Effect of Sulfate on the Hydration Reactions of Portland Cement. *Cement and Concrete Research,* Vol. 4, 1974, pp. 45–55.
25. ACI Committee 232. *Use of Fly Ash in Concrete (ACI-232.2R-96)*. American Concrete Institute, Farmington Hills, Michigan, 1996.
26. Zheng, L., C. Xuehua, and T. Mingshu. Hydration and Setting Time of MgO-Type Expansive Cement. *Cement and Concrete Research,* Vol. 22, 1992, pp. 1–5.
27. Atis, C. D. Strength Properties of High-Volume Fly Ash Roller Compacted and Workable Concrete, and Influence of Curing Condition. *Cement and Concrete Research,* Vol. 35, 2005, pp. 1112–1121.
28. Langan, B. W., and K. Weng. Effect of Silica Fume and Fly Ash on Heat of Hydration of Portland Cement. *Cement and Concrete Research,* Vol. 32, 2002, pp. 1045–1051.
29. Antiohos, S. K., V. G. Papadakis, E. Chaniotakis, and S. Tsimas. Improving the Performance of Ternary Blended Cements by Mixing Different Types of Fly Ashes. *Cement and Concrete Research*, Vol. 37, 2007, 877–885.

30. Srinivasan, C. B., N. Lakshmi Narasimhan, and S. V. Ilango. Development of Rapid-Set High-Strength Cement Using Statistical Experimental Design. *Cement and Concrete Research,* Vol. 33, 2003, pp. 1287–1292.
31. ASTM C778. *Standard Specification for Standard Sand*. American Society for Testing and Materials, West Conshohocken, Pennsylvania.
32. ASTM C191. *Standard Test Methods for Time of Setting of Hydraulic Cement by Vicat Needle*. American Society for Testing and Materials, West Conshohocken, Pennsylvania.
33. ASTM C187. *Standard Test Method for Amount of Water Required for Normal Consistency of Hydraulic Cement Paste*. American Society for Testing and Materials, West Conshohocken, Pennsylvania.
34. ASTM C1437. *Standard Test Method for Flow of Hydraulic Cement Mortar*. American Society for Testing and Materials, West Conshohocken, Pennsylvania.
35. Wexham Developments. *JAF Calorimeter Operating Manual* (ed. 5). Wexham Developments, Reading Berks, UK, November 1998.
36. Barneyback, R. S., Jr. *Alkali-Silica Reactions in Portland Cement Concrete.* Ph.D. Thesis, Purdue University, West Lafayette, Indiana, 1983.
37. Wikipedia. *P-value*. http://en.wikipedia.org/wiki/P-value
38. Hassett, D. J., and K. E. Eylands. Heat of Hydration of Fly Ash as a Predictive Tool. *Fuel*, Vol. 76, Issue 8, June 1997, pp. 807–809.
39. Wang, A., C. Zhangb, and W. Suna. Fly Ash Effects: II. The Active Effect of Fly Ash. *Cement and Concrete Research*, Vol. 34, 2004, pp. 2057–2060.
40. Marsh, B. K., and R. L. Day. Pozzolanic and Cementitious Reactions of Fly Ash in Blended Cement Pastes. *Cement and Concrete Research,* Vol. 18, 1988, pp. 301–310.

APPENDIX A. FLY ASH DATA SHEETS

This section contains the example of the data sheet supplied by the fly ash manufacturer. The data sheet in Figure A.1 contains the physical and chemical properties of fly ash determined by the laboratory contracted by the fly ash supplier.

Similar data were collected for all but three of the remaining fly ashes and can be found in the supplemental document (titled *Fly Ash Handbook*) that accompanies this report and is available for download at https://doi.org/10.5703/1288284315213. This solution was implemented in order to reduce the overall size of the report. The easiest way to navigate the Fly Ash Handbook is to open the Excel worksheet titled

Analytical Testing Service Laboratories, Inc.
P.O. Box 1118, Joplin, Missouri 64802
(417) 782-6573

Headwaters Resourses, Inc
4043 N. Euclid Ave.
Bay City, MI 48706
1-989-671-1500

July 5, 2006

Attn: Donna

Re: 5988 - Baldwin Unit 3 Fly Ash Sample 2000 Ton Composite - 05/22-26/06

	ASTM C-618 Class "C" Requirements	Actual
Fineness (+325 Mesh)	34% Max	10.80%
Moisture Content	3% Max	0.06%
Specific Gravity	****	2.59
Specific Gravity Variation	5% Max	0.93%
Loss on Ignition	6% Max	0.67%
Soundness	0.8% Max	0.01%
S.A.I., 7 Days	75% Min	98.20%
S.A.I., 28 Days	75% Min	101.40%
Water Req. % Control	105% Max	93.00%
Silica SiO_2	****	36.34%
Aluminum Oxide Al_2O_3	****	22.71%
Ferric Oxide Fe_2O_3	****	7.44%
Total	50% Min	66.49%
Sulfur Trioxide SO_3	5% Max	1.76%
Calcium Oxide CaO	****	22.02%
Magnesium Oxide MgO	****	4.73%
Available Alkalies as Na_2O	****	1.18%

We certify the above was tested in accordance with ASTM C-618.

Analytical Testing Service Laboratories, Inc.

John K. Cupp, Manager

Figure A.1 Analytical Testing Service Laboratories fly ash data sheet.

"Fly Ash Information" which contains two series of clickable links.

Table A.1 provides the overall summary of the selected physical and chemical characteristics of all fly ashes used in the study and includes information about the source of the fly ash, data on the percentages of the main oxides present in the fly as, loss on ignition (LOI) values as well as the values of the strength activity index (SAI) at both 7 and 28 days.

TABLE A.1
Physical and chemical characteristics of Class C and Class F fly ashes.

CLASS C FLY ASHES													
	Source (Plant)												
Properties	**Baldwin**	**Edwards**	**Hennepin**	**Joliet**	**Joppa**	**Kenosha**	**Labadie**	**Miller**	**Rush Island**	**Rockport**	**Schahfer**	**Vermilion**	**Will County**
SiO_2, %	35.06	33.15	40.36	32.12	35.75	37.78	37.03	36.38	34.23	43.65	41.90	39.13	32.30
Al_2O_3, %	19.39	19.21	19.38	17.88	18.01	20.11	19.28	18.74	16.91	21.76	19.32	18.77	18.55
Fe_2O_3, %	6.25	10.11	5.91	6.41	6.36	5.87	6.46	6.03	6.86	6.58	6.76	6.19	6.47
CaO, %	25.23	24.28	21.80	26.98	26.23	23.35	24.26	24.62	27.66	16.98	20.29	23.92	26.97
MgO, %	5.90	4.92	4.93	5.83	5.01	5.52	4.86	5.64	5.51	3.55	4.29	4.55	5.78
SO_3, %	1.55	2.73	1.43	2.45	1.72	1.11	2.13	1.97	2.40	0.98	1.42	1.40	2.61
(Na_2Oeq), %	2.24	1.63	1.99	3.92	2.31	2.18	1.94	2.08	2.26	2.08	1.83	1.91	3.06
LOI, %	0.49	0.43	0.61	0.49	0.35	0.38	0.25	0.44	0.17	0.90	0.44	0.43	0.35
7d SAI (%)	98.5	111	116	78	101	96	97	99.5	87		85	103	82
28d SAI (%)	106	111	121	99.5	114	103	102	104.6	105.4		101	123	118

CLASS C FLY ASHES							
Properties	**Elmersmith**	**Miami 7**	**Miami 8**	**Mill Creek**	**Petersburg**	**Trimble**	**Zimmer**
SiO_2, %	41.60	55.89	55.52	47.48	43.82	46.91	38.66
Al_2O_3, %	17.74	29.45	26.02	19.99	21.74	21.08	18.96
Fe_2O_3, %	22.02	4.96	4.62	18.52	25.29	19.90	24.90
CaO, %	9.31	1.25	3.98	5.42	1.86	2.50	4.94
MgO, %	0.90	0.85	1.44	1.05	0.88	0.86	4.81
SO_3, %	1.71	0.21	0.45	1.12	0.54	0.99	3.07
(Na_2Oeq), %	2.32	2.20	2.55	2.55	2.29	2.03	1.44
LOI, %	2.37	2.31	2.43	1.38	1.39	1.89	1.48
7d SAI (%)	91	78		89.5	85	82.5	72
28d SAI (%)	98	100.6		101.8	99.6	97	89

APPENDIX B. TEMPLATE FOR THE SAS CODE FOR STATISTICAL ANALYSIS

This appendix provides the template of the SAS code, which was used in the modeling process of this study

```
DATA full;
 INPUT blaines spsurface meansize sai sulfate carbon SAF cao mgo alumina Totalheat Timepeak glass
(independent and dependent variables);
CARDS;
6102    15492    21.99    105.93  0.2771…
.
.(data points)
;
RUN;
PROC REG DATA = full;
  TITLE "Model for all Fly Ashes";
  MODEL sai(dependent variable) = meansize sulfate SAF (chosen independent variables);
  OUTPUT OUT = saiPredictions_full P = Predict R = Residual;
RUN;

DATA saiPredictions_full;
  SET saiPredictions_full;
  SquaredResidual = Residual**2;
RUN;
PROC SORT DATA = saiPredictions_full;
  BY SquaredResidual;
RUN;
AXIS1 LABEL = (ANGLE = 90 "Predicted Value of sai") ORDER = (50 TO 150 BY 10);
AXIS2 LABEL = ("Timepeak") ORDER = (50 TO 150 BY 10);
PROC GPLOT DATA = saiPredictions_full;
  TITLE "Plot of Predicted sai vs. Observed sai for all Fly Ashes";
  PLOT Predict * sai / ANNO = ANNOTATE VAXIS = AXIS HAXIS = AXIS2;
RUN;
PROC PRINT DATA = saiPredictions_full NOOBS LABEL;
  TITLE "Predicted sai Time and Observed sai Time for all Fly Ashes";
  VAR sai Predict meansize sulfate SAF glass Residual SquaredResidual;
RUN;
```

APPENDIX C. FLY ASH CHARACTERISTICS

This section provides an example of the summaries of the physical and chemical characteristics of two fly ashes (Baldwin – Class C and Mill Creek – Class F). In addition, the X-ray diffraction patterns and the morphological characteristics of all these fly ashes are also provided.

Similar data were collected for all remaining fly ashes and can be found in the *Fly Ash Handbook* (FAH), which accompanies this document and is available for download at https://doi.org/10.5703/1288284315213. This solution was implemented in order to reduce the overall size of the report.

The description of each of the fly ashes is divided into four different sections. The first section comprises of the results of total chemical analysis along with a brief interpretation of the observed chemical characteristics of the fly ash. The second section contains the particle size distribution (PSD) curve, which includes a comparison of the PSD of this fly ash with the PSD of the typical Class C fly ash, Miller (chosen as typical in terms of it means particle size). This section also provides details about the other physical characteristics of the fly ash. The third section gives a description of the X-ray diffraction curve of the fly ash, along with a brief description of its mineralogical composition. The final section describes a set of four representative SEM micrographs obtained for the fly ash. A summary of all the characteristics of the fly ash is provided at the end.

C.1 BALDWIN

Headwaters Resources, Baldwin Power Plant, Baldwin, Illinois.

C.1.1 Chemical Analysis

C.1.1.1 Results of Total Chemical Analysis

The results of the total chemical analysis results from experiments for the Baldwin fly ash are shown in Table C.1.1.

The results of the analyses were used to calculate the "Derived Parameters" values shown in Table C.1.2. Other pertinent information for this fly ash is shown in Table C.1.3.

TABLE C.1.1
Total chemical analysis—Baldwin fly ash.

CaO, %	25.23
SiO_2, %	35.06
Al_2O_3, %	19.39
Fe_2O_3, %	6.25
Na_2O, %	1.93
K_2O, %	0.47
SO_3, %	1.55
MgO, %	5.90
Total	**95.78**

TABLE C.1.2
Derived parameters—Baldwin fly ash.

Total SiO_2+ Al_2O_3+ Fe_2O_3, %	60.70
Total alkalies, as equivalent Na_2O, %	2.24

TABLE C.1.3
Results of analyses—Baldwin fly ash.

Loss on ignition, %	0.49
Total SO_3, %	1.55
Soluble SO_3, %	0.28
Percentage of the total SO_3 that is soluble	18%
Soluble Na_2O, %	0.05
Soluble K_2O, %	0.01
Total alkalies, as equivalent Na_2O, %	2.24
Soluble alkalies, as equivalent Na_2O, %	0.06
Percentage of the alkalies that are soluble	2.7%

C.1.1.2 Chemical Analysis Interpretations

This fly ash is classified as a Class C fly ash based on its composition, with a total SiO_2+Al_2O_3+Fe_2O_3 content of 60% (<70%, in ASTM C 618 specification). The CaO content was found to be 25%. The MgO content (5.90%) was rather high as compared to the other Class C fly ashes presented in this report. The contents of other elements are not unusual and the loss on ignition value was similar to the results obtained for other Class C fly ashes tested here. The alkali content was about 2% and all of it was insoluble.

C.1.2 Physical Characteristics

C.1.2.1 Results from Experiments

This section contains the results of the physical characteristics determined for Baldwin fly ash. The particle size distribution of this fly ash is presented in Figure C.1.1; a comparison of particle size distribution between this fly ash and the "typical" (Miller) Class C fly ash is given in Figure C.1.2. Parameters related to particle size for this fly ash are shown in Table C.1.4.

C.1.2.2 Particle Size Distribution Interpretation

This is a typical particle size distribution, similar to the "typical" (Miller) fly ash used as the reference on the bar chart, especially for the particles smaller than 5 μm. The mean particle size of 22 μm was close to that of Miller fly ash (~25 μm). It was observed that the amount of particles in the range of 5 to 26 μm was higher compared to the amount of particles in the range of 26 to 100 μm, while the percentage of particles >45 μm (about 16%) is smaller (~19% of Miller fly ash). As a result, this fly ash appears finer than the "typical" fly ash.

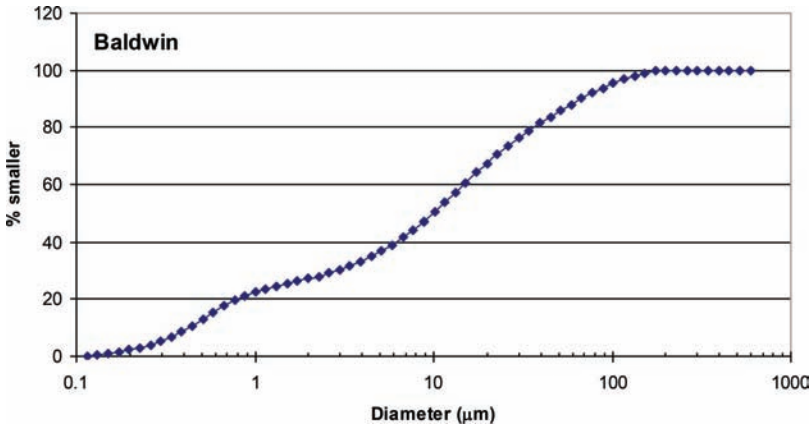

Figure C.1.1 Particle size distribution—Baldwin fly ash.

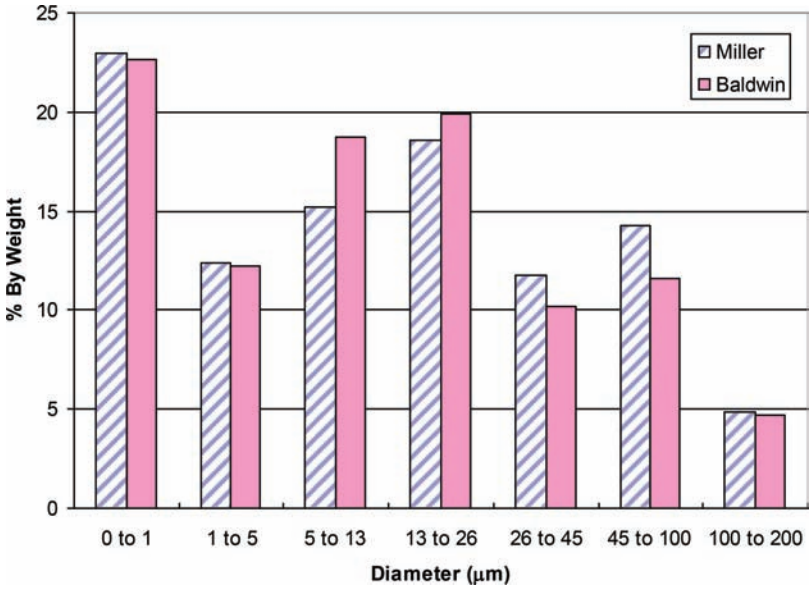

Figure C.1.2 Relative particle size distribution—Baldwin fly ash.

TABLE C.1.4
Particle size parameters - Baldwin fly ash.

% > No.325 sieve (Supplier Certificate), %	10.30
% > 45 μm (LPSD), %	16.28
Mean particle size (LPSD), μm	21.99
Specific area (LPSD), cm^2/g	15492
Blaine fineness, cm^2/g	6102

C.1.3 Measurements of Physicochemical Parameters

This section contains X-ray diffraction (XRD) analysis and the test results for content for magnetic particles found in Baldwin fly ash.

The X-ray diffraction pattern obtained for this fly ash is presented in Figure C.1.3. The crystalline components detected included: lime (CaO), quartz (SiO_2), periclase (MgO), anhydrite ($CaSO_4$), and merwinite ($Ca_3Mg(SiO_4)_2$). These components are normally found in Class C fly ashes. A hump, representing a calcium-aluminate type of glass with a maximum near $2\theta = \sim 32^\circ$ is visible.

No magnetic particles were found in this fly ash.

C.1.4 Scanning Electron Micrographs

The four micrographs chosen as a representative of the larger set obtained for this fly ash are described below.

Figure C.1.4 (a) shows a micrograph of the Baldwin fly ash taken at a magnification of 600×, and showing the great disparity in sizes of the individual particles in this fly ash. There are two large spheres seen here, about 40 μm in size. Both the particles show smooth surface. Both spheres have very small particles deposited on their surfaces. Many smaller fly ash particles are also present in the area depicted in the micrograph.

A different field of the Baldwin fly ash taken at a slightly lower magnification (400×) is shown in

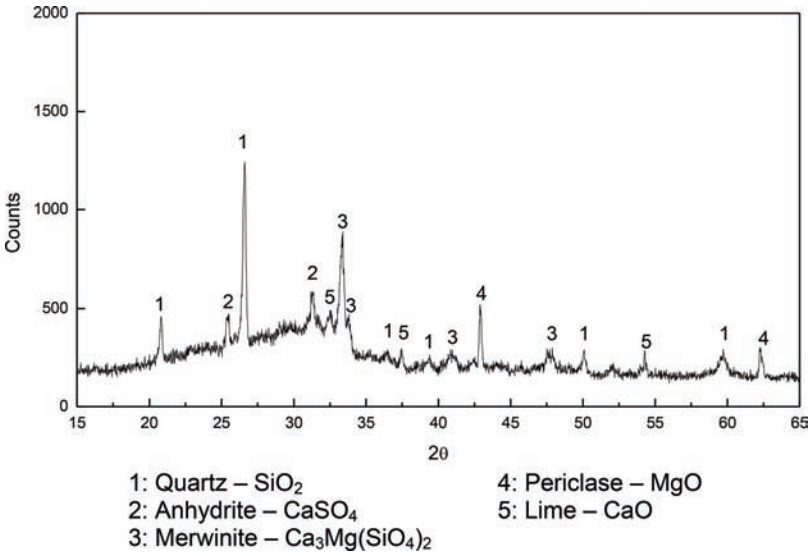

Figure C.1.3 X-ray diffraction results—Baldwin fly ash.

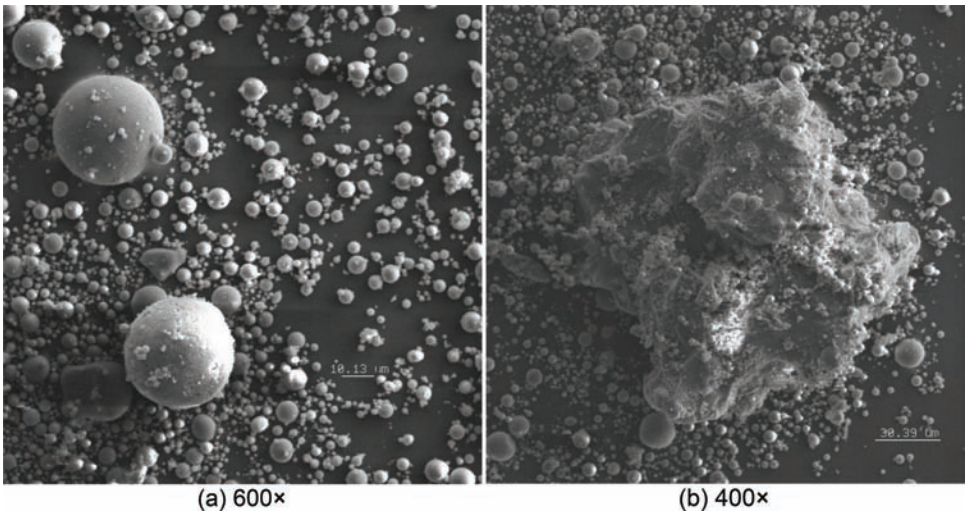

Figure C.1.4 SEM Micrographs of Baldwin fly ash as magnification of (a) 600×, (b) 400×.

Figure C.1.4 (b). A large irregular grain (almost 200 μm in size) is present in the center of this micrograph. Similar large irregular grains were found in most of the other micrographs (not shown here) obtained for this fly ash.

Figure C.1.5 (c) shows an incompletely spherical plenosphere about 40μm in size. Most of the smaller particles inside the plenosphere are clean spheres with smooth surfaces.

An unusually thin and long carbon residue grain (confirmed using EDX examination) is shown in Figure C.1.5 (d). This carbon particle is longer than 200 μm, but its width is less than 20 μm.

C.1.5 Summary

This fly ash is a high-calcium fly ash of typical chemical composition, except for a little higher content of magnesium. Occasionally, extremely large grains (around 200 μm in size) are common in this fly ash, and quite a few oversized carbon particles are also present. They are probably responsible for the relatively (relative to other Class C ashes) large mean particle size of this fly ash.

C.2 MILL CREEK

Mineral Resource Technologies, Mill Creek Station, Louisville, Kentucy.

C.2.1 Chemical Analysis

C.2.1.1 Results of Total Chemical Analysis

The results of the total chemical analysis for the Mill Creek fly ash are shown in Table C.2.1. The results of

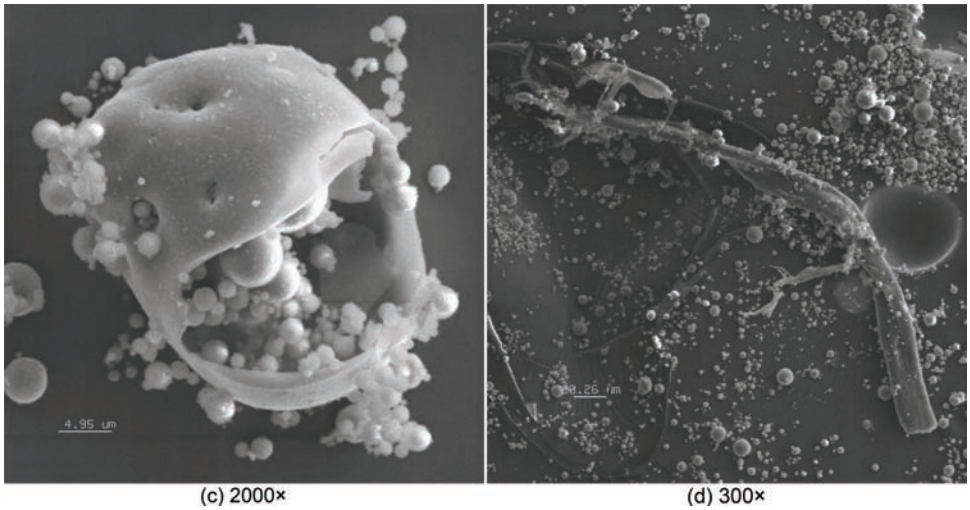

Figure C.1.5 SEM Micrographs of Baldwin fly ash as magnification of (c) 2000×, (d) 300×.

TABLE C.2.1
Total chemical analysis—Mill Creek fly ash.

CaO, %	5.42
SiO_2, %	47.48
Al_2O_3, %	19.99
Fe_2O_3, %	18.52
Na_2O, %	0.60
K_2O, %	2.97
SO_3, %	1.12
MgO, %	1.05
Total	97.15

this analysis were used to calculate the "Derived Parameters" values shown in Table C.2.2. Other pertinent information for this fly ash is shown in Table C.2.3 under the heading "Other Analysis."

C.2.1.2 Chemical Analysis Interpretations

This fly ash would be properly classified as Class F fly ash, since the total SiO_2+Al_2O_3+Fe_2O_3 content was 86%, meeting the requirement given in ASTM C 618 (>70%). The SiO_2 content (47.48%) is a little high while the CaO content (5.42%) is moderate. The loss on ignition of this fly ash is the lowest when compared to other Class F fly ashes tested in this study.

C.2.2 Physical Characteristics

C.2.2.1 Results from Experiments

This section contains the results of the physical characteristics evaluations of the Mill Creek fly ash. Particle size distribution of this fly ash is presented in Figure C.2.1, while the comparison of particle size distribution between this fly ash and the "typical" (Miller) Class C fly ash is given in Figure C.2.2. Parameters related to particle size for this fly ash are shown in Table C.2.4.

TABLE C.2.2
Derived parameters—Mill Creek fly ash.

Total SiO_2+ Al_2O_3+ Fe_2O_3, %	85.99
Total alkalies, as equivalent Na_2O, %	2.55

TABLE C.2.3
Other analysis—Mill Creek fly ash.

Loss on ignition, %	1.38
Total SO_3, %	1.12
Soluble SO_3, %	0.69
Percentage of the total SO_3 that is soluble	62%
Soluble Na_2O, %	0.04
Soluble K_2O, %	0.06
Total alkalies, as equivalent Na_2O, %	2.55
Soluble alkalies, as equivalent Na_2O, %	0.08
Total alkalies, as equivalent Na_2O, %	3.1%

TABLE C.2.4
Particle size parameters—Mill Creek fly ash.

% > No.325 sieve (Supplier Certificate), %	16.80
% > 45 μm (LPSD), %	19.03
Mean particle size (LPSD), μm	26.35
Specific area (LPSD), cm^2/g	10295
Blaine fineness, cm^2/g	3739

C.2.2.2 Particle Size Distribution Interpretation

This is a very different particle size distribution from that of all the previous fly ashes described before. However, it is typical for the Class F fly ashes studied in this project. The main difference for Class F fly ashes from Class C fly ashes is the deficiency of particles in the finer categories (0 to 5 μm) and a substantially higher content of coarser particles. The mean particle size of this fly ash is 26 μm, which is not so difference from that of the "typical" (Miller) fly ash (25 μm). The

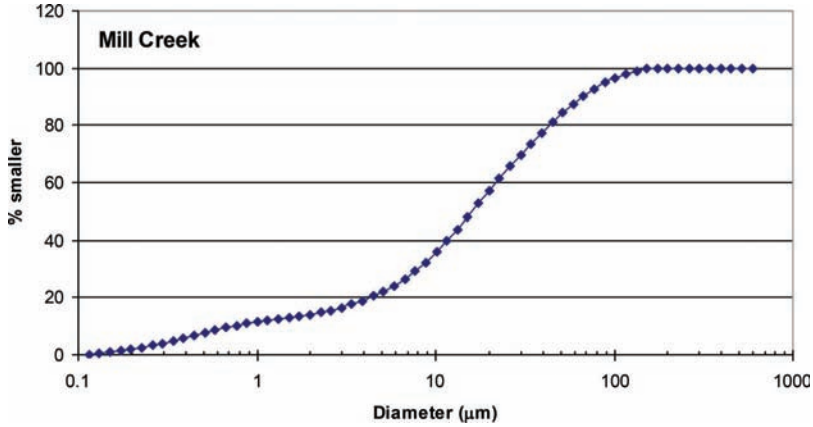

Figure C.2.1 Particle size distribution—Mill Creek fly ash.

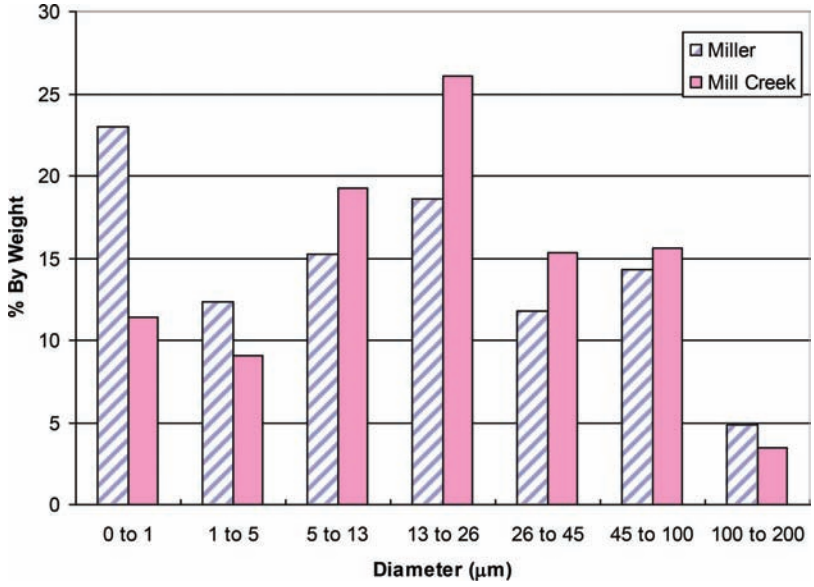

Figure C.2.2 Relative particle size distribution—Mill Creek fly ash.

percentage of particles larger than 45 μm, (about 20%) is also close to that of the Miller fly ash. However, it should be noticed that the content of particles larger than 100 μm in this fly ash is less than that of the typical fly ash.

C.2.3 Measurements of Physicochemical Parameters

This section contains the test results of content of magnetic particles and X-Ray Diffraction (XRD) analysis for the Mill Creek fly ash.

The measured weight content of magnetic particles of this fly ash was 24.90%.

X-ray diffraction analysis results for this fly ash are given in Figure C.2.3. The crystalline components detected in this fly ash include: quartz (SiO_2), anhydrite ($CaSO_4$), mullite ($Al_6Si_2O_{13}$), hematite (Fe_2O_3), and magnetite (Fe_3O_4). A hump, representing a silica type of glass with a maximum at $2\theta = \sim 24^\circ$ is visible.

C.2.4 Scanning Electron Micrographs

A set of four of the micrographs obtained for this fly ash were chosen as the representative, and are described below.

Figure C.2.4 (a) shows an area of mostly spherical fly ash particles, some of which are with rough surface, while others are smooth. The particles in this area range from less than 1 μm to almost 20μm.

Figure C.2.4 (b) was taken at a relatively low magnification to show a variety of particles present in this fly ash. In addition to the spherical solid particles, there are some hollow and incomplete spheres as well as some irregular particles. The particle with rough surface is presumable magnetic particle and it is typical in this fly ash.

Large piece of carbon residue is shown in Figure C.2.5 (c). It is more than 100 μm in size, and is probably responsible for the coarse fineness results.

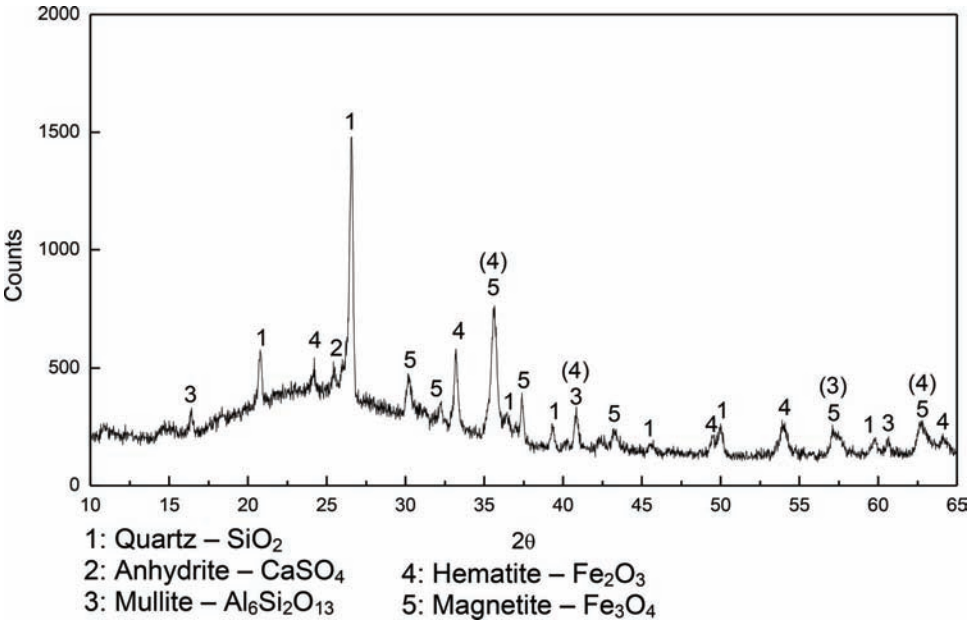

Figure C.2.3 X-ray diffraction results—Mill Creek fly ash.

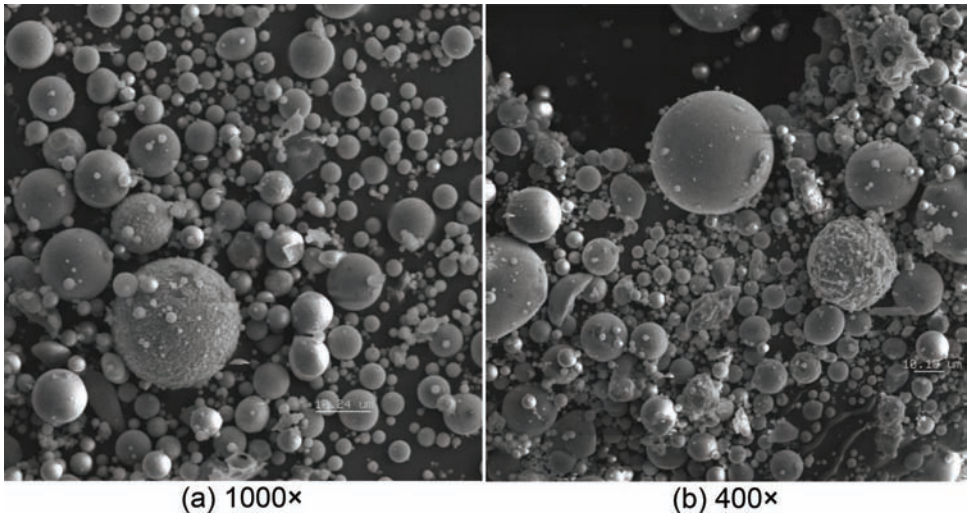

Figure C.2.4 SEM Micrographs of Mill Creek Fly Ash as Magnification of (a) 1000× (b) 400×.

Figure C.2.5 (d) shows one of the larger grains, an incompletely spherical partly hollow particle about 20 μm. The particles inside are smaller spherical particles and some irregular grains.

Mill Creek being a Class F fly ash, the results for strength activity index of this fly ash is surprising high, as being 95% at the age of 7 days and being 126% at the age of 28 days, especially for the early age. The result of 7 days age appears to be the highest when compared to those of all other Class F fly ashes, even higher than most of the Class C fly ashes. At the same time, the result of 28 days age still remains to be the highest among those of all Class F fly ashes, yet becomes lower than most of the Class C fly ashes. This fact indicates that this fly ash works better when the early strength of mortar is important, as compared to other Class F fly ashes. However, this fly ash still has a limited potential reactivity as it is a Class F fly ash.

C.2.5 Summary

This is a Class F fly ash with a slightly elevated content of SiO_2 and the lowest loss on ignition among all the Class F fly ashes tested in this study. The reactive crystalline compounds and a silica type of glass structure detected in XRD are found to be normal as to Class F fly ash. This fly ash is rather coarse with a very different particle size distribution pattern from that of the typical (Miller) fly ash. Large

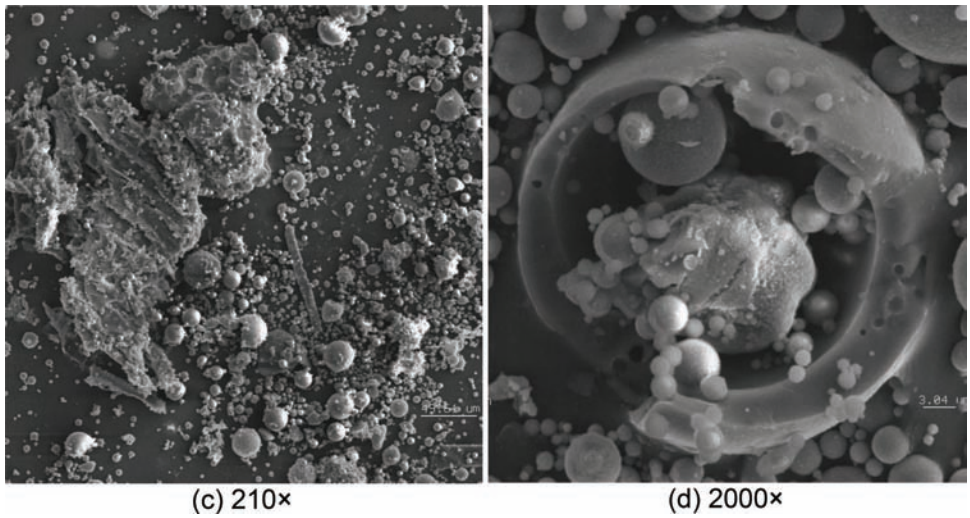

Figure C.2.5 SEM Micrographs of Mill Creek Fly Ash as Magnification of (c) 210× (d) 2000×.

pieces of carbon residue are easily found in this fly ash using SEM, which may be responsible for the relatively coarse particle size distribution. The strength activity index test shows that this fly ash has very less negative effect on the strength of mortar at early age and a surprisingly good potential reactivity with cement at the late age. That is not common for a Class F fly ash.

About the Joint Transportation Research Program (JTRP)

On March 11, 1937, the Indiana Legislature passed an act which authorized the Indiana State Highway Commission to cooperate with and assist Purdue University in developing the best methods of improving and maintaining the highways of the state and the respective counties thereof. That collaborative effort was called the Joint Highway Research Project (JHRP). In 1997 the collaborative venture was renamed as the Joint Transportation Research Program (JTRP) to reflect the state and national efforts to integrate the management and operation of various transportation modes.

The first studies of JHRP were concerned with Test Road No. 1—evaluation of the weathering characteristics of stabilized materials. After World War II, the JHRP program grew substantially and was regularly producing technical reports. Over 1,500 technical reports are now available, published as part of the JHRP and subsequently JTRP collaborative venture between Purdue University and what is now the Indiana Department of Transportation.

Free online access to all reports is provided through a unique collaboration between JTRP and Purdue Libraries. These are available at: http://docs.lib.purdue.edu/jtrp

Further information about JTRP and its current research program is available at: http://www.purdue.edu/jtrp

About This Report

An open access version of this publication is available online. This can be most easily located using the Digital Object Identifier (doi) listed below. Pre-2011 publications that include color illustrations are available online in color but are printed only in grayscale.

The recommended citation for this publication is:

Tanikella, P., & Olek, J. (2017). *Updating physical and chemical characteristics of fly ash for use in concrete* (Joint Transportation Research Program Publication No. FHWA/IN/JTRP-2017/11). West Lafayette, IN: Purdue University. https://doi.org/10.5703/1288284315213